Validierung einer dialysebasierten Apparatur zur Untersuchung der Wirkstofffreisetzung aus kolloidalen Arzneistoffträgern mit Fokus auf Datenauswertung und halbfesten Formulierungen

Dissertation

zur Erlangung des Doktorgrades

der Naturwissenschaften

vorgelegt beim Fachbereich Biochemie, Chemie und Pharmazie

der Johann Wolfgang Goethe-Universität

in Frankfurt am Main

von

Marc-Phillip Mast

aus Nagold

Frankfurt am Main (2023)

(D30)

Vom Fachbereich Biochemie, Chemie und Pharmazie der
Johann Wolfgang Goethe – Universität als Dissertation angenommen.

Dekan/in:	Prof. Dr. Clemens Glaubitz
1. Gutachter/in:	Prof. Dr. Jochen Klein
2. Gutachter/in:	Prof. Dr. Matthias G. Wacker

Datum der Disputation: 14. Juli 2023

Danksagung

- entfernt -

Inhaltsverzeichnis

Abkürzungsverzeichnis

A4D	*Adapter for Dialysis*
AAFE	*Absolute Average Fold Error*
ANOVA	*Analysis of variance*, Varianzanalyse
AUC	*Area under the curve*, Fläche unter der Kurve
BSA	Bovines Serumalbumin
C	Cholesterin
Caco-2	Humane Colonkarzinom-Zelllinie
CaSki	Humane Zelllinie des Zervixkarzinoms
CC_{50}	Mittlere zytotoxische Konzentration
CE	Celluloseester
COX	Cyclooxygenase
DiMeC	*Dialysis Membrane Permeation Calculator*, Programm zur Berechnung der Permeationsrate einer Dialysemembran
DLin-MC3-DMA	*(6Z,9Z,28Z,31Z)-heptatriacont-6,9,28,31-tetraene-19-yl-4-(dimethyla-mino)butanoate*
DLS	Dynamische Lichtstreuung
DMPC	Dimyristoylphosphatidylcholin
DMPG	Dimyristoylphosphatidylglycerol
DR	*Dispersion Releaser*
DSC	Dynamische Differenzkalorimetrie
DSPC	Distearolyphosphatidylcholin
DSPE	Distearylphosphatidylethanolamin
DSPG	Distearoylphosphatidylglycerol
EE%	Verkapselungseffizienz
EMA	*European Medicines Agency*, Europäische Arzneimittel-Agentur
EPC	Ei-Phosphatidylcholin
EPG	Ei-Phosphatidylglycerol
f1	*Difference factor,* Unterschiedsfaktor
f2	*Similarity factor*, Ähnlichkeitsfaktor
HBSS	Salzlösung nach Hanks
HC	Hycdrocortison
HEC-1-A	Humane Zelllinie des Endometriumkarzinoms
HIV	Humanes Immundefizienz-Virus
HPLC	Hochdruckflüssigkeitschromatographie
HSPC	Hydriertes Soja-Phosphatidylcholin
IVIVC	*In vitro-in vivo* Korrelation
$mPEG_{2000}$-DSPE	Methoxy-Polyethylenglycol-Distearoylphosphatidylethanolamin
MWCO	Molekularer Größenausschluss
NTA	*Nanoparticle Tracking Analysis*

P_{app}	Scheinbare Permeabilitätskonstante
PBS	*Phosphate-buffered Saline*, Phosphatgepufferte Salzlösung
PC	Phosphatidylcholin
PDI	Polydispersitätsindex
PEG	Polyethylenglycol
PEG_{2000}-DMG	1,2-dimyristoyl-rac-glycero-3-methoxy-polyethylenglycol-2000
PER	*Permeability enhancement ratio*
Ph. Eur.	Europäisches Arzneibuch
PTDR	Pharma Test *Dispersion Releaser*
PTDR ReNo	PTDR *Release Normalizer,* Programm zur Normalisierung von Freisetzungsprofilen im PTDR
RC	Regenerierte Cellulose
SD	Standardabweichung
SE	Standardfehler
SEC	*Size exclusion chromatography*, Größenausschlusschromatgraphie
SPC	Soja-Phosphatidylcholin
sVSF	*Simple vaginal fluid simulant*, simples, simuliertes Vaginalfluid
TEER	Transepithelialer elektrischer Widerstand
TEM	Transmissionselektronenmikroskopie
UPM	Umdrehungen pro Minute
USA	Vereinigte Staaten von Amerika
US-FDA	*U.S. Food and Drug Administration*, amerikanische Behörde für Lebens- und Arzneimittel
USP	*U.S. Pharmacopeia,* Amerikanisches Arzneibuch
UV	Ultraviolettes Licht
Vis	Sichtbares Licht

1 Einleitung

1.1 Nanomedizin

Nanomedizin hat in Wissenschaft und pharmazeutischer Industrie in den letzten Jahrzehnten stark an Bedeutung gewonnen. Der Begriff Nanomedizin bezieht sich auf spezielle Therapien mit verschiedenen (Nano-)Materialien, von denen - mit Hilfe von hochspezifischen Technologien - mindestens eine Dimension im Nanometermaßstab (1-1000 nm) liegt. Darunter fallen auch die nanopartikulären Arzneistoffträger, die in Liposomen [1], *Solid Lipid Nanopartikel* [2], polymerbasierte Nanopartikel [3], *Nanocrystals* [4], Nanoemulsionen, Mizellen [5] und Dendrimere eingeteilt werden.

Die Relevanz des Themas spiegelt sich auch im Bereich der Arzneimittelzulassung wider, wobei das amerikanische Arzneibuch (USP) diesem Themenkomplex ein eigenes Kapitel widmet <1153> *Drug Products Containing Nanomaterials*. Die verschiedenen Arzneiformen ermöglichen die Anwendung von schwerlöslichen Arzneistoffen durch Verbesserung der Wasserlöslichkeit, erhöhen die Verträglichkeit für den Patienten durch verminderte systemische Nebenwirkungen und können die Bioverfügbarkeit von Arzneistoffen durch Schutz vor Abbau oder durch eine verbesserte Auflösungsgeschwindigkeit, beispielsweise im Darm, erhöhen. Des Weiteren kontrolliert der Arzneistoffträger zum einen die Freisetzung des Arzneistoffes und zum anderen verändert er die Verteilung des Arzneistoffes im Körper. Dabei reichert sich der Träger in Zielgeweben an, wodurch eine zielgerichtete Therapie ermöglicht wird. Die Anreicherung kann dabei passiv oder aktiv erfolgen [6]. Beim passiven *Targeting* reichern sich die Partikel aufgrund ihrer Größe in fenestrietem Gewebe wie Tumoren an, die zusätzlich hypervaskularisiert sind und ein gestörtes lymphatisches System aufweisen. Beim aktiven *Targeting* werden Liganden wie Antikörper an die Trägersysteme gekoppelt, um Zellen mit entsprechenden Zielstrukturen zu erreichen. Neben klassischen, chemischen Molekülen können Peptide, Proteine oder Nukleotid-Stränge eingesetzt werden. Klassischerweise werden nanopartikuläre Arzneistoffträger intravenös verabreicht. Mittlerweile sind aber auch perorale, dermale, inhalative, ophthalmische, intramuskuläre und vaginale Anwendungen in neu übermittelten Zulassungsanträgen an die amerikanische *Food and Drug Administration* (US-FDA) zu finden [7].

Die größte Relevanz von Nanoarzneimitteln liegt bei onkologischen Behandlungen. Der Einsatz von Nanomaterialien wird auch zur Behandlung von Infektionen, Anämien sowie

kardiovaskulären und endokrinen Erkrankungen untersucht. Zusätzlich können Nanoarzneimittel zu diagnostischen Zwecken eingesetzt werden [7]. Eine Übersicht über zugelassene nanopartikuläre Arzneimittel, die parenteral angewendet werden, liefert Tabelle 1.

Tabelle 1: *Übersicht von ausgewählten, zugelassenen nanoskaligen Arzneistoffträgern. Die Tabelle wurde modifiziert nach [8]. Weitere zugelassene Arzneimittel sind dort gelistet.*

Handelsname	Beschreibung	Wirkstoff	Zulassung	Ref.
Doxil® (Johnson & Johnson, USA)	**Zusammensetzung** - HSPC - Cholesterin - $mPEG_{2000}$-DSPE Molares Verhältnis: 56:39:5 **Indikation** - HIV-assoziiertes Kaposi-Sarkom - Ovarialkarzinom - Multiples Myelom	Doxorubicin	1995 (US-FDA)	[9]
DaunoXome® (Gilead Sciences, USA)	**Zusammensetzung** - DSPC - Cholesterol - Cholesterin Molares Verhätlnis: 2:1 **Indikation** HIV-assoziiertes Kaposi-Sarkom	Daunorubicin	1996 (US-FDA)	[10]
AmBisome® (Astellas Pharma, USA)	**Zusammensetzung** - HSPC - Cholesterol - Cholesterin - DSPG Molare Verhältnis: 26:13:10 **Indikation** Systemische Mykosen	Amphotericin B	1997 (US-FDA)	[11]
Myocet® (Teva B.V., Niederlande)	**Zusammensetzung** - EPC - Cholesterol - Cholesterin Molares Verhältnis: 55:45 **Indikation** Metastierendes Mammakarzinom	Doxorubicin	2000 (EMA)	[12]
Visudyne® (Novartis Pharmaceuticals, USA)	**Zusammensetzung** - DMPC - EPG Molares Verhältnis: unbekannt **Indikation** Altersbezogene Makuladegeneration	Verteporfin	2000 (US-FDA)	[13]

Marqibo™ (Talon Therapeutics, USA)	**Zusammensetzung** - SM - Cholesterol - Cholesterin Molares Verhältnis 58:42 **Indikation** Philadelphia-Chromosom negative akute lymphatische Leukämie	Vincristin	2012 (US-FDA)	[14]
Onivyde™ (Merrimack Pharmaceuticals, USA)	**Zusammensetzung** - DSPC - Cholesterol - Cholesterin - mPEG2000-DSPE Molares Verhältnis 3:2:0.015 **Indikation** Metastasierendes Pankreaskarzinom	Irinotecan	2015 (US-FDA)	[15]
Vyxeos® (Jazz Pharmaceuticals, USA)	**Zusammensetzung** - DSPC - DSPG - Cholesterol - Cholesterin Molares Verhältnis 7:2:1 **Indikation** Metastierendes Mammakarzinom	Cytarabin: Daunorubicin (1:5 molares Verhältnis)	2017 (US-FDA)	[16]
Abraxane™ (Bristol-Myers Squibb, USA)	**Zusammensetzung** Humanalbumin Stoffmengenverhältnis Wirkstoff:Protein 9:1 **Indikation** Metastierendes Mammakarzinom	Paclitaxel	2005 (US-FDA)	[17]
Feraheme™ (AMAG Pharmaceuticals, USA)	**Zusammensetzung** Polyglucose-Sorbitolcarboxymethylether Verhältnis Eisenoxid:Kohlenhydrat 6:4 **Indikation** Anämie	Eisenoxid	2009 (US-FDA)	[18]
Onpattro™ (Alnylam Pharmaceuticals, USA)	**Zusammensetzung** - DLin-MC3-DMA - PEG_{2000}-DMG - DSPC - Cholesterol - Cholesterin Molares Verhältnis49:2:10:39 **Indikation** Hereditäre Transthyretin-Amyloidose bei Patienten mit Polyneuropathie	siRNA	2018 (US-FDA)	[19, 20]

Abkürzungen:

DLin-MC3-DMA, *(6Z,9Z,28Z,31Z)-heptatriacont-6,9,28,31-tetraene-19-yl 4-(dimethylamino)butanoate*; DMPC, Dimyristoylphosphatidylcholin; DMPG, Dimyristoyl phosphatidylglycerol; DSPC, Distearolyphosphatidylcholin; DSPE, Distearyl phosphatidylethanolamin; DSPG, Distearoylphosphatidylglycerol; EPC, Ei-Phosphytidylcholin; EPG, Ei-Phosphatidylglycerol; HSPC, hydriertes Soja-Phosphatidylcholin; $mPEG_{2000}$-DSPE, Methoxy-Polyethylenglycol-Distearoylphosphatidylethanolamin; PEG, Polyethylenglycol; PEG_{2000}-DMG, *α-(3´-{[1,2-di(myristyloxy)propanoxy] carbonylamino}propyl)-ω-methoxypolyoxyethylene*

1.2 Liposomen

Liposomen werden, im Vergleich zu anderen Arzneistoffträgern, bereits seit langem innerhalb und außerhalb der Medizin eingesetzt. Vor der Zulassung des ersten liposomalen Arzneimittels Doxil® 1995 in den USA, wurden Liposomen in der Kosmetikindustrie genutzt [21]. Liposomen sind sphärische Vesikel, deren Membran aus einer Lipiddoppelschicht besteht. Die Lipide bestehen aus einer hydrophilen Kopfgruppe und zwei lipophilen Fettsäureketten, weshalb sie amphiphile Eigenschaften aufweisen. Gibt man sie in Wasser, formen sich spontan Liposomen, um die Grenzflächenspannung zu minimieren. Die hydrophilen Kopfgruppen zeigen dabei in die hydrophile Wasserphase und schirmen die Fettsäureketten in einer lipophilen Doppelmembran von außen ab. Liposomen können daher sowohl hydrophile Arzneimittel in ihrem wässrigen Innenraum als auch lipophile Substanzen in ihrer lipophilen Doppelmembran einschließen [22]. Sie können in einem breiten Größenbereich gezielt hergestellt werden und eignen sich daher als Arzneistoffträgersysteme [23]. Je nach Größe der Vesikel und Anzahl der Lipid-Doppelschichten können Liposomen unterschiedlich klassifiziert werden. Unilamellare Vesikel haben eine Lipiddoppelmembran, wohingegen multilamellare Liposomen mehrere Membranschichten aufweisen. Bei multivesikulären Liposomen sind mehrere kleine Vesikel in einem größeren Liposom eingeschlossen. In der Regel werden unilamellare Liposomen als Arzneistoffträgersysteme eingesetzt, da sie am besten zu reproduzieren und charakterisieren sind. Liegt der Durchmesser unter 100 nm spricht man von kleinen unilamellaren Liposomen, sonst von großen unilamellaren Liposomen [24].

Synthetische und natürliche Lipide können zur Ausbildung der Lipiddoppelschicht eingesetzt werden. Am häufigsten werden Phospholipide verwendet. Charakteristisch für Phospholipide ist die Phosphodiesterbindung, die den hydrophoben und hydrophilen Molekülteil miteinander verbindet. Phospholipide werden je nach enthaltenem Alkohol zwischen Glyerophospholipiden mit Glycerin im Grundgerüst und Sphingomyelinen mit Sphingosin unterschieden. Sphingosin ist ein langkettiger Aminoalkohol. Bei Glycerophospholipiden sind zwei Fettsäuren mit dem Glycerin verestert und bilden den lipophilen Anteil im Molekül. Über eine Amid-Bindung am C2-Atom des Sphingosins sitzt bei Sphingomyelinen eine Fettsäure und bildet zusammen mit dem Sphingosin den hydrophoben Anteil. Phospholipide werden auch anhand ihrer verschiedenen polaren Kopfgruppen unterteilt, wobei die wichtigsten Vertreter Cholin, Serin, Inositol und Ethanolamin sind. Das am häufigste verwendete Phospholipid ist Phosphatidylcholin (PC), das sogenannte Lecithin, das aus Eidotter oder pflanzlichen Samen wie Soja gewonnen werden kann. Ein großer Vorteil von Phospholipiden ist die fehlende Immunogenität bei der

medizinischen oder kosmetischen Anwendung [25]. Cholesterin (C) ist ein gängiger Zusatzstoff bei der Herstellung von Liposomen, der Einfluss auf die Fluidität der Liposomenmembran nimmt und kann mit einem Stoffmengenanteil von bis zu 50 % in die Membran integriert werden. Dabei wird die Rigidität und Flexibilität der Lipiddoppelschicht beeinflusst [24].

Zur Herstellung von Liposomen sind verschiedene Methoden etabliert. Die Filmmethode ist eine der am häufigsten genutzten Methoden. Dabei wird zuerst eine organische Lösung der Lipidbestandteile hergestellt. Anschließend wird ein dünner Lipidfilm unter Vakuumtrocknung erstellt, der im letzten Schritt mit Wasser oder Pufferlösungen unter spontaner Ausbildung von Liposomen hydratisiert wird. Die gewünschte Größe und die Anzahl der Lipiddoppelschichten kann mit Hilfe verschiedener Verfahren in einem weiteren Schritt individuell eingestellt werden. Dazu eignen sich beispielsweise Ultraschall, Extrusion und Filtration. Lipophile Wirkstoffe werden der organischen Lösung hinzugefügt und während der Vakuumtrocknung in den Lipidfilm integriert. Wasserlösliche Wirkstoffe werden während der Hydratation des Films in die liposomalen Vesikel eingeschlossen.
Um die verkapselte Wirkstoffmenge (EE%) zu bestimmen, können Zentrifugation, Filtration oder Größenausschlussverfahren eingesetzt werden. Um liposomale Arzneimittel industriell herzustellen, werden Methoden benötigt, bei denen größere Ansätze hergestellt werden oder ein kontinuierlicher Herstellprozess genutzt wird. Zusätzlich muss vor allem bei der parenteralen Anwendung die Sterilität der liposomalen Formulierung gewährleistet sein.
Eine neue Methode von wachsendem Interesse, auch für die pharmazeutische Industrie, basiert auf Mikrofluidik [26, 27]. Bei dieser Herstellmethode werden die Lipide in wassermischbaren, polaren Lösungsmitteln gelöst und mit Puffer in einem mikrofluidischen Chip vermischt. Dabei ist die laminare Strömung sowie die kontrollierte Durchmischung charakteristisch und führt zu einem abrupten Abfall der Lipidlöslichkeit, wobei sich spontan Vesikel bilden. Die Liposomengröße kann präzise durch den Fluss, die Mischrate und das Mischverhältnis zwischen Lipidlösung und Puffer kontrolliert werden [27].

Liposomen zeigen neben ihren zahlreichen Vorteilen als Arzneistoffträgersystem auch einige Nachteile. Die physikochemischen Eigenschaften der liposomalen Trägersysteme verändern sich mit dem Einschluss von Wirkstoffen und Stabilitätsprobleme (Agglomeration, frühzeitige Freisetzung des Wirkstoffs) können die Folge sein. In wässriger Dispersion zeigen Liposomen des Weiteren physikalische und chemische Instabilitäten, worunter die Aggregation von Liposomen, die Hydrolyse und Oxidation von Phospholipiden und das frühzeitige Austreten von verkapseltem Wirkstoff in die äußere Trägerphase mit

der Folge einer reduzierten EE% fallen [28-30]. Eine Möglichkeit die Stabilität zu erhöhen, ist die Gefriertrocknung von Liposomen. Dabei muss allerdings darauf geachtet werden, sowohl die Membranintegrität als auch die ursprünglichen Eigenschaften der Liposomen (Partikelgröße und Größenverteilung, *in vitro* Wirkstofffreisetzung) nach Rekonstitution zu erhalten [31]. Um die Trocknung als weiteren Herstellungsschritt zu umgehen, können Proliposomen verwendet werden [32]. Hierbei werden die Liposomen über ein Trägersystem *in situ* bei beziehungsweise vor der Applikation erzeugt, wodurch Stabilitätsprobleme in der wässrigen Dispersion während der Lagerung vermieden werden können. Als Trägersysteme werden in der Regel inerte Materialien wie Mannitol, Sorbitol oder Cellulosederivate verwendet, die mit einem Lipidfilm überzogen werden [32, 33]. Final bildet sich ein frei fließendes Pulver, dessen enthaltenes Trägermaterial sich bei Zugabe von Wasser rasch unter Vesikelbildung auflöst. Proliposome können im Sprühtrocknungsverfahren [34, 35], in Verfahren basierend auf superkritischem Kohlendioxid [36, 37], im Wirbelschichtverfahren [38-40] und mit einer modifizierten Film-auf-Träger-Methode [41] hergestellt werden. Letztere wurde im Rahmen dieser Arbeit verwendet. Proliposomen wurden in der peroralen [42], transdermalen [43], pulmonalen [44] und vaginalen Anwendung [45] untersucht.

1.3 Anwendungsort Vagina

Die Vagina ist Teil des weiblichen Geschlechtsorgans und ist ein etwa zehn cm langer Muskelschlauch [46]. Die vaginale Anwendung von Arzneistoffen war schon bei den antiken Ägyptern gängige Praxis [47]. Heutzutage ist die lokale und systemische Arzneimitteltherapie in der Vagina gut etabliert. Die Vagina besitzt eine große und gut durchblutete Oberfläche, wodurch viele Wirkstoffe mit unterschiedlichen Molekülmassen eine hohe Permeabilität und damit einhergehende gute Bioverfügbarkeit zeigen. Zusätzlich wird die erste Leberpassage von Arzneistoffen (*first pass effect*) im Vergleich zur klassischen, oralen Therapie umgangen und gastrointestinale Nebenwirkungen vermieden. Allerdings beeinflussen Faktoren wie der Menstruationszyklus und das Alter das vaginale Milieu und die Dicke des vaginalen Epithels, wodurch sich das Permeationsverhalten von Wirkstoffen verändern kann. Zusätzlich können eingebrachte Wirkstoffe durch vaginalen Ausfluss, vor allem im Rahmen der vaginalen Selbstreinigung, ausgespült werden, wodurch sich ihre Bioverfügbarkeit verringert. Einen Einfluss auf die Wirkstoffverfügbarkeit spielt auch die individuell praktizierte Vaginalhygiene. Ferner kann die vaginale Arzneimittelanwendung je nach kulturellem Hintergrund in der Bevölkerung durch fehlende Akzeptanz limitiert sein.

Im Allgemeinen werden Antiinfektiva zur Behandlung von Vaginalmykosen oder bakteriellen Vaginosen lokal angewendet. Eine weitere Indikation mit explizit lokaler Anwendung ist die Kontrazeption mit vaginal aufzutragenden Spermiziden. Demgegenüber werden Hormontherapien zur Kontrazeption oder zur Linderung menopausaler Beschwerden in der Regel systemisch angewendet.

Herkömmliche Arzneiformen zur vaginalen Anwendung können fest (Tabletten, Suppositorien, Vaginalringe), flüssig (Lösungen, Emulsionen, Suspensionen) oder halbfest (Salben, Cremes, Gele, Schäume) sein. Sie lassen sich leicht in größerem Maßstab herstellen und haben oft eine lange Haltbarkeit und Stabilität. Allerdings beeinträchtigen das Auslaufen der Arzneiform und die kurze Verweildauer am Wirk- beziehungsweise Resorptionsort die Wirksamkeit der Arzneistoffe und die Compliance der Patientin [48].

Neuartige, arzneistoffträgerbasierte vaginale Arzneiformen wie Nanopartikel, Liposomen oder Niosomen wurden daher eigens entwickelt, um diese Probleme zu umgehen [49, 50]. Durch ihre Interaktion mit dem vaginalen Mucin zeigen sie eine verbesserte Verteilung und eine verlängerte Verweildauer in der Vagina als die genannten herkömmlichen Arzneiformen. Die anpassbaren Freisetzungseigenschaften der vaginalen Nanoarzneimittel können die lokalen und systemischen Arzneistoffkonzentrationen im Gleichgewicht halten und so das Nutzen-Risiko-Verhältnis optimieren [51, 52]. Dies kann besonders bei der Behandlung von entzündlichen Erkrankungen vorteilhaft sein, um systemische Nebenwirkungen zu reduzieren.

Wie bei der oralen Administration gilt auch für die vaginale Anwendung, dass sich der Wirkstoff im Vaginalfluid auflösen und durch die Epithelschicht permeieren muss, um seine Wirkung auszuüben. Demzufolge haben alle Änderungen der Vaginalphysiologie (zum Beispiel bei Schwangerschaft, je nach Menstruationszyklus oder Alter) einen Einfluss auf den Therapieerfolg der eingesetzten Arzneiform. Um die Wirkstofffreisetzung aus den verschiedenen Arzneiformen zu untersuchen, sind biorelevante Medien, die die Physiologie des Anwendungsortes simulieren, ein geeignetes Mittel der Wahl. Diese können auch zur *in vivo* Vorhersage genutzt werden. Alternativ werden simplere, arzneibuchkonforme Puffer, vor allem im Bereich der Qualitätskontrolle, verwendet. Dabei ist zu beachten, dass es für die vaginale Anwendung kein Standardmedium in den Arzneibüchern gibt. In den letzten Jahrzehnten wurden deshalb verschiedene Untersuchungen zur Charakterisierung des humanen Vaginalfluids durchgeführt. Dabei wurde entweder mit Tampons oder Glaspipetten das Vaginalfluid gesammelt und analysiert. Physiologisch befinden sich etwa 0,5 mL Fluid in der Vagina, wobei täglich je nach Quelle zwischen 1-8 g/d Vaginalfluid produziert werden [46, 53]. Der vaginale pH-Wert von gesun-

den, prämenopausalen Frauen ist aufgrund einer physiologischen Besiedelung mit *Lactobacilli,* die Glucose zu Milchsäure umsetzen, schwach sauer. Elektrodengestützte pH-Messungen in der Vagina ergeben pH-Werte im Bereich 3,4 bis 8,0, wobei ein pH von 4,2 als typischer Wert angenommen wird [53]. Neben etwa 2 g/L Milchsäure sind im simulierten Vaginalfluid nach Owen und Katz Proteine (Albumin), Essigsäure, Glycerin, Urea und Glucose sowie Calcium-, Natrium-, Kalium- und Chloridionen enthalten [53]. Um die komplexe und schwierige Herstellung des biorelevanten Vaginalfluids zu vereinfachen und die physikochemische Stabilität (mehrwertige Ionen wie Calcium tendieren dazu auszufallen) zu erhöhen, haben Rastogi et al. aufbauend auf der bestehenden Literaturgrundlage ein simples, simuliertes Vaginalfluid (*simple vaginal fluid simulant*, sVSF) entwickelt [54]. Es simuliert den pH-Wert, die Osmolarität und die Pufferkapazität der Vaginalflüssigkeit und ist über einen Zeitraum von einem Monat im Kühlschrank stabil. Die Zusammensetzung von sVSF (pH 4,2) ist in Tabelle 2 zusammengefasst. In der vorliegenden Arbeit wurde die Wirkstofffreisetzung aus einem proliposomalen Gel in sVSF untersucht.

Tabelle 2: *Zusammensetzung des simplen, simulierten Vaginalfluids. Die Angaben sind zur Herstellung von 1 L.*

Inhaltsstoff	Masse [g]	Molare Konzentration [mM]
Natriumchlorid	5,25	90,6
Milchsäure	0,61	8
Essigsäure	0,79	13,2
Natriumlactat-Lösung (50 %)	2,02	18
Natriumacetat	0,31	3,8

Um resorbiert werden zu können, muss der Wirkstoff nach der Auflösung im Vaginalfluid über die Zellmembran permeieren. Die Resorption kann passiv, transzellulär oder parazellulär sowie aktiv über Transporter stattfinden [55]. Untersuchungen haben gezeigt, dass die meisten Substanzen eine passive Diffusion zeigen [56]. Lipophilere Substanzen wie Steroide werden in der Regel über den transzellulären Weg aufgenommen [57]. Im Gegensatz dazu diffundieren hydrophilere Substanzen bevorzugt über die parazelluläre Route [56].

Es wurden verschiedene *in vitro* und *ex vivo* Methoden entwickelt, um die Permeabilität von Wirkstoffen und Formulierungen zu untersuchen. Darunter fallen verschiedene Zell-, Gewebe- und Tiermodelle. Sie unterscheiden sich in ihrer technischen Komplexität, ethischen Fragestellungen und Kosten [58]. Zur Untersuchung der Permeabilität von Substanzen über die Vagina wurden verschiedene *in vitro* Zellkulturmethoden etabliert. Sie zeichnen sich durch einen einfachen, günstigen und robusten Aufbau im Vergleich zu Tiermodellen aus und werden häufig in der frühen Phase der pharmazeutischen Ent-

wicklung eingesetzt. Außerdem können Bedingungen in der Zellkultur schnell und einfach angepasst werden, weshalb sich diese *in vitro* Zellsysteme zur Beurteilung der Permeabilität eignen [58]. In der Regel werden dabei immortalisierte Zellen oder Primärzellen eingesetzt, die eine Zellmonoschicht ausbilden. Diese simuliert strukturell und funktionell die zu überwindende Epithelzellbarriere und trennt ein Donorkompartiment (apikal) vom Akzeptorkompartiment (basolateral). Dennoch können die Vaginalphysiologie beeinflussende Faktoren wie Erkrankungen, Alter und Umweltfaktoren nicht abgebildet werden [58].

In der vorliegenden Arbeit wurde eine humane Zervixkarzinomzelllinie (CaSki) [59] und eine humane Endometriumkarzinomzelllinie (HEC-1-A) [60] verwendet. Beide Zelllinien sind zur Charakterisierung der Permeabilität von Wirkstoffen unter Einfluss verschiedener Formulierungen sowie zur Untersuchung der Assoziation mit der Zellschicht etabliert [61, 62]. Um die Permeabilität von verschiedenen Formulierungen und Wirkstoffen zu vergleichen, kann ein scheinbarer Permeabilitätskoeffizient P_{app} berechnet werden (Gleichung 1) [62]. Hierbei ist *Q* die gesamte permeierte Wirkstoffmenge zum Zeitpunkt *t.* Die Permeationsoberfläche *A* und die initiale Wirkstoffkonzentration *C* gehen in die Gleichung mit ein.

$$P_{app} = \frac{Q}{A \cdot C \cdot t} \quad (1)$$

1.4 Methoden zur Bestimmung der Wirkstofffreisetzung

Untersuchungen zur Wirkstofffreisetzung sind essentieller Bestandteil der Qualitätskontrolle und werden von regulatorischen Behörden gefordert. Jedoch gibt es bis heute keine einheitliche Methode, die behördlich empfohlen wird, um die Wirkstofffreisetzung aus Nanoarzneiformen zu untersuchen. Um eine Korrelationen zwischen der *in vitro* Wirkstofffreisetzung und Parameter der humanen Pharmakokinetik einer Testformulierung zu erhalten, sollten die Testbedingungen so gewählt werden, dass sie die *in vivo* Freisetzungsbedingungen geeignet simulieren. Im Bestfall kann eine mathematische *in vivo-in vitro*-Korrelation (IVIVC) etabliert werden. Alternativ eignet sich die Wirkstofffreisetzung zur Untersuchung von kritischen Material- und Formulierungseigenschaften oder dazu Prozessparameter zu untersuchen. Demnach können auch verschiedene Herstellchargen im Rahmen der Qualitätskontrolle auf diese Weise überprüft werden. Wichtige Hinweise zur Auswahl relevanter Testbedingungen für parenterale Produkte wie Doxil® liefert ein Dokument der US-FDA mit dem Titel *Liposome Drug Products - Chemistry, Manufacturing, and Controls; Human Pharmacokinetics and Bioavailability; and Labeling*

Documentation [63] und ein Reflexionspapier von der Europäischen Arzneimittel-Agentur (EMA) [64]. Hier werden beispielsweise biorelevante Medien mit humanen Plasma für Freisetzungs- und Stabilitätstests vorgeschrieben, um Arzneiformen für die parenterale Anwendung zu charakterisieren. Die zu untersuchenden Parameter können für Arzneiformen mit anderen Anwendungsgebieten angepasst werden. Zusätzlich müssen alle Methoden von Nanoarzneimitteln in der Lage sein, die gelöste Wirkstofffraktion von der ungelösten, mit dem Träger assoziierten Fraktion zuverlässig zu trennen. Dies geht bei klassischen Wirkstofffreisetzungsmethoden wie Filtration oft mit einem Verlust der Sensitivität einher, weshalb verschiedene neue Separationsmethoden Gegenstand aktueller Forschung sind. Dazu gehören *sample and separate*-Verfahren wie Filtration und Zentrifugation, Verfahren mittels Dialyse und Online-Messsysteme [65-67]. Eine Expertengruppe der USP hat kürzlich eine Übersicht über die verschiedenen Methoden veröffentlicht und wichtige Hinweise zur Methodenvalidierung zusammengefasst [68].

1.4.1 Sample and separate-Methoden

Bei s*ample and separate*-Methoden wird die freie Wirkstofffraktion nach dem Probenzug ermittelt und die Trennung von Wirkstoff und Arzneistoffträger erfolgt als Schritt der Probenaufarbeitung. Es können dabei verschiedene Filtrations- oder Zentrifugationsmethoden und die Festphasenextraktion zum Einsatz kommen. Die Methoden kommen mit wenig präparativen Aufwand aus und können mit Apparaturen aus den Pharmakopöen, aber auch mit Gefäßen mit kleineren Volumina für geringere Formulierungsmengen kombiniert werden [69]. Da bei den Methoden jedoch oft starke Scherkräfte auf die Arzneistoffträger wirken, können sensible Formulierungen wie Mizellen oder Liposomen nur bedingt mit *sample and separate*-Methoden untersucht werden. Zudem muss die Abtrennung aufgrund weiterer Wirkstofffreisetzung aus dem Arzneistoffträger zeitnah erfolgen. Der Einsatz der richtigen Methode richtet sich nach den Eigenschaften der jeweiligen Formulierung. In jedem Fall ist eine zuverlässige und vollständige Abtrennung der nano- oder mikroskaligen Arzneiform im Rahmen einer Methodenvalidierung nachzuweisen [67].

Die Filtration ist die klassische Methode zur Abtrennung von ungelösten Wirk- und Hilfsstoffen und wird üblicherweise bei festen Arzneiformen eingesetzt. Im Bereich der nanoskaligen Arzneiformen eignet sich die Filtration vor allem für orale *Nanocrystals*. Man kann zwischen Spritzenvorsatz- [70, 71] und Zentrifugalfiltern [72] unterscheiden. Die Auswahl des richtigen Filtermaterials, der richtigen Porengröße und Filterfläche erfolgt in Abhängigkeit der Arzneiformeigenschaften und des Freisetzungsmediums (pH-Wert,

Ionenstärke, Viskosität). Die Verstopfung der Filter ist neben der unzureichenden Abtrennung des Trägers bzw. forcierten Wirkstofffreisetzung durch Scherkräfte zu beachten.

Um die Filtrationsleistung zu überprüfen, können Methoden zur Partikelgrößenbestimmung des Filtrats wie die *nanoparticle tracking analysis* (NTA) oder die dynamische Lichtstreuung (DLS) eingesetzt werden. Hierbei sollte darauf geachtet werden, dass das Dispersionsmittel die Nanokristalle nicht auflöst [68, 71]. Eine ausreichende Filtrationsleistung ist in der Regel gewährleistet, wenn die Porengröße des Filters kleiner als 90 % der Arzneiform ist [68]. Beispielsweise zeigten die von Weng et al. durchgeführten Untersuchungen mit verschiedenen Filterporengrößen, dass Filtergrößen mit 0,45 µm und 0,2 µm nicht geeignet waren, die untersuchten, circa 100 nm großen Partikel sicher abzutrennen. Darüber hinaus konnte ein starker Burst-Effekt nachgewiesen werden [73]. Demgegenüber können unter Einsatz von Zentrifugalfiltern zuverlässigere Ergebnisse erzielt werden. Fenofibrat-Nanokristallen konnten mit Zentrifugalfiltern mit einer Porengröße von 0,1 µm erfolgreich abgetrennt werden [74].

Eine weitere Möglichkeit zur Abtrennung der Arzneistoffträger ist die präparative Ultrazentrifugation. Hierbei werden durch sehr große Zentrifugalkräfte über einen langen Zeitraum die feinen Partikel im Freisetzungsmedium sedimentiert. In Untersuchungen wurde jedoch gezeigt, dass Liposomen im Größenbereich von 100 nm nur schwer abzutrennen waren [75]. Die Auswahl der richtigen Parameter richtet sich nach der Dichte und Größe der Partikel, sowie den Eigenschaften des Freisetzungsmediums. Durch die sehr lange Zentrifugationsdauer wird die präparative Ultrazentrifugation seltener als andere Methoden angewendet [67]. Im Vergleich dazu beträgt der Zeitaufwand beim Einsatz von Zentrifugalfiltern nur wenige Minuten und die Zentrifugalkräfte sind wesentlich geringer.

Für sensitive Arzneiformen wie Liposomen kann zur Probenaufbereitung die Festphasenextraktion eingesetzt werden, da hierbei im Gegensatz zu den oben vorgestellten Methoden keine Scherkräfte auftreten, die einen Einfluss auf die Integrität der Arzneiform haben [76]. Die Trennung erfolgt bei der Festphasenextraktion durch Affinitätsunterschiede des Arzneistoffträgers und des Wirkstoffs mit der stationären Phase. Diese Methode eignet sich vor allem zur Auftrennung in komplexen Matrices wie biologischen Proben, wobei ein interner Standard genutzt werden muss [77, 78]. Auch beim Einsatz dieser Methode muss darauf geachtet werden, dass das Trägermaterial der stationären Phase keinen Einfluss auf die Nanopartikel und ihre Stabilität hat [79]. Andernfalls könnten so falsch-erhöhte Konzentrationen der freien Wirkstofffraktion gemessen werden. Solche Effekte können durch Auswahl eines geeigneten Materials der stationären Phase

sowie durch die passend gewählte Porengröße reduziert werden. Die Festphasenextraktion konnte beispielsweise erfolgreich für Doxorubicin-Liposomen [80] und *Solid Lipid Nanoparticles* mit Cyclosporin A angewendet werden [81].

1.4.2 Wirkstofffreisetzung mittels Dialyse

Im Gegensatz zu den *sample and separate*-Methoden findet die Trennung des gelösten vom am Arzneistoffträger gebundenen Wirkstoff mit Hilfe einer Dialysemembran statt. Hierbei handelt es sich um eine semipermeable Membran, die ein Donorkompartiment von einem Akzeptorkompartiment trennt, wobei gelöste Moleküle entlang eines Konzentrationsgefälles die Membran vom Donor- ins Akzeptorkompartiment durchqueren können. Große Moleküle und Kleinstpartikel werden aber zurückgehalten. Die Permeation von Molekülen durch die Dialysemembran kann mit dem Fick'schen Diffusionsgesetz beschrieben werden (Gleichung 2) [82]. Dabei ändert sich die Konzentration einer Substanz im Akzeptorkompartiment (C_a) in Abhängigkeit von der Zeit proportional zum Kozentrationsgefälle (ΔC) zwischen Donor- (C_d) und Akzeptorkonzentration. Die Permeation erfolgt schneller, je größer die Oberfläche der Diffusionsschicht beziehungsweise Dialysemembran (A) und je kleiner die Dicke der Dialysemembran (δ) ist. Zusätzlich hat das Volumen des Akzeptorkompartiments (V_a) und die Membranpermeationskonstante (k_M) einen Einfluss auf die Diffusion.

$$\frac{dC_a}{dt} = \left[\frac{k_M \cdot A}{\delta \cdot V_a}\right] * [\Delta C] \qquad (2)$$

Die Membranpermeationskonstante ist abhängig vom diffundierenden Stoff und der Temperatur. Einen weiteren Einfluss auf k_M hat der molekulare Größenauschluss (*molecular weight cut off,* MWCO) und das Membranmaterial [83]. Die gängigsten Materialien sind regenerierte Cellulose (RC) und Cellulosederivate wie Celluloseester (CE). Der MWCO in Dalton beschreibt diejenige Molekülgröße, die im ermittelten Zeitraum zu mindestens 90 % von der Dialysemembran zurückgehalten wird. Diese beträgt bei den Dialyseschläuchen von Repligen® (ehemals SpectrumLabs®, Waltham, Massachusetts, USA) 17 Stunden [84]. Um eine freie Permeation zu ermöglichen und damit eine maximale k_M zu haben, sollte der MWCO einhundertfach größer sein als das Molekulargewicht des Arzneistoffs [85]. Gängige MWCO liegen zwischen 1 und 1000 kDa. Zusätzlich gewährleistet ein großer Diffusionsgradient eine gute Permeationsrate, was durch ein großes Volumen des Akzeptor- und ein kleines Volumen des Donorkompartiments unterstützt werden kann [66].

Dialysemethoden bieten den Vorteil des einfachen Probenzuges. Zusätzlich werden keine starken Scherkräfte auf die Formulierung ausgeübt, wodurch dialysebasierte Verfahren im Vergleich zu Filtrations- und Zentrifugationsverfahren schonender und für sensible Formulierungen wie Liposomen vorzuziehen sind [66]. Bei Methoden mit statischer Dialyse können je nach Arzneiform Sedimentationseffekte auftreten. Diese verfälschen das Ergebnis, da durch zusätzliche Diffusionsbarrieren die Freisetzung im ungünstigsten Fall zum Erliegen kommen kann [65]. Des Weiteren müssen Adsorptionseffekte des Wirkstoffs an der Dialysemembran untersucht werden. Die Verwendung von Hilfsstoffen wie Fette können die Dialysemembran verstopfen. Zudem können Wirkstofffreisetzungen durch die begrenzte Löslichkeit im kleineren Volumen der Donorkammer verlangsamt erscheinen. Um diese Effekte zu umgehen, kann die sogenannte reverse Dialyse [85] eingesetzt werden, bei der die Kompartimente im Vergleich zur klassischen Dialyse mit Dialysesack umgekehrt werden. Der geringere Konzentrationsunterschied kann die Dialyse jedoch auch verlangsamen.

Der Dialysesack ist die häufigste und einfachste dialysebasierte Methode. Hierbei wird ein Dialyseschlauch wie bei der Aufreinigung von Proteinen beispielsweise mit Klemmen verschlossen. Als Akzeptorkompartiment kann ein simples Becherglas dienen, aber auch eine Kopplung mit der Blattrührerapparatur ist möglich. Neben der fehlenden Agitation im Dialysesack ist die nicht vorhandene Standardisierung der Methode ein Problem, wodurch die Vergleichbarkeit zwischen einzelnen Messungen erschwert wird. So ist beispielsweise die Größe und die Befüllung des Dialysesacks nicht einheitlich und auch das Einhängen in den Vessel kann variieren. Kommerzielle Dialysekammern wie der *Float-A-Lyzer*® von Repligen® bieten die Möglichkeit, einheitliche Dialysekammern zu verwenden, und reduzieren den präparativen Aufwand. Der *Float-A-Lyzer*® wurde zur Untersuchung der Wirkstofffreisetzung von nanoskaligen Formulierungen mit der Blattrührerapparatur (USP Apparatur II) und der Durchflusszelle (USP Apparatur IV) gekoppelt. Zum Beispiel konnte so für multivesikuläre Liposomen mit Bupivacain eine dreiphasige Freisetzung mit der Blattrührerapparatur ermittelt werden [86]. In einer anderen Untersuchung konnten Formulierungsparameter, die zur Aggregation von Nanokristallen führen, ermittelt werden [87].

Die Dialysekammer kann alternativ auch in die Durchflusszelle der USP Apparatur IV eingeklemmt werden. Neben dem Einsatz des *Float-A-Lyzers*® gab es den sogenannten *Adapter for Dialysis* (A4D), der speziell zum Einbau in die Durchflusszelle von Burgess et al. an der Universität von Connecticut entwickelt und von der Sotax AG (Aesch, Schweiz) vertrieben wurde [88]. Der Vertrieb des Adapters wurde mittlerweile allerdings eingestellt und die Apparatur wurde im Wesentlichen durch den *Float-A-Lyzer*® ersetzt

[67]. Es konnten mit dem *Float-A-Lyzer*® erfolgreich die Wirkstoffuntersuchung von Liposomen mit Doxorubicin [89] und Amphotericin B [90-92] untersucht werden. Die Freisetzung von Amphotericin B aus den Liposomen wurde in Medien mit unterschiedlichen Konzentrationen an Albumin charakterisiert. Dies ermöglichte die Untersuchung des Einflusses des Plasmaproteins Albumin auf die Freisetzung und mit Hilfe eines physiologiebasierten pharmakokinetischen Modells konnte die *in vivo* Performance der Amphotericin B-Liposomen für Patienten mit Hypoalbuminurie vorhergesagt werden [93].

Um die fehlende Agitation in der Dialysekammer zu umgehen und damit die Ausbildung von statischen Diffusionsschichten zu reduzieren, wurde zwischen 2011 und 2013 an der Goethe Universität, Frankfurt am Main, der *Dispersion Releaser* (DR) entwickelt [94]. Das System kann mit dem standardisierten Antriebsmotor der USP Apparatur I/II gekoppelt werden und wird inzwischen von der Pharma Test Apparatebau AG (Hainburg, Deutschland) vertrieben (Abbildung 1). Als Donorkompartiment dient ein standardisierter Käfig, über dem ein Dialyseschlauch mit zwei O-Ringen befestigt wird. Der so präparierte Käfig wird in den Käfighalter der Apparatur gesteckt und verbleibt während des Experiments an einer exakten Position im Vessel. Ein Rührer im Donorkompartiment (Innenrührer) gewährleistet eine stetige Durchmischung der Probe und sorgt zusätzlich für einen zielgerichteten Druck nach außen ins Akzeptorkompartiment. Dieses wird mit einem Außenrührer ebenfalls, in derselben Geschwindigkeit wie das Donorkompartiment, gerührt. Die Kopplung der beiden Rührer erfolgt mit zwei Magneten, sodass beide Kompartimente während der Wirkstofffreisetzung stets gleichmäßig durchmischt und Sedimentation oder unbewegte Flüssigkeitsschichten vermieden werden. In einer ersten Validierungsuntersuchung wurden reproduzierbare Ergebnisse mit geringer Standardabweichung im Dispersion Releaser erzielt [82]. Dabei war, im direkten Vergleich mit dem Dialysesack, die Membranpermeation einer Flurbiprofen-Lösung im DR unter gleichen Bedingungen wesentlich schneller, wodurch Formulierungsunterschiede mit Letzterem sensitiver detektiert werden konnten [82]. Inzwischen wurde der DR erfolgreich zur Untersuchung der Wirkstofffreisetzung aus Liposomen [95-97], Nanopartikeln [70, 82, 98] und Mikropartikeln [99, 100] eingesetzt. Des Weiteren konnte für viele Anwendungen, nach Normalisierung des Permeationsprofils, ein Zusammenhang zwischen der *in vitro*- und *in vivo*-Freisetzung gefunden werden [8, 70, 95, 96, 98-100].

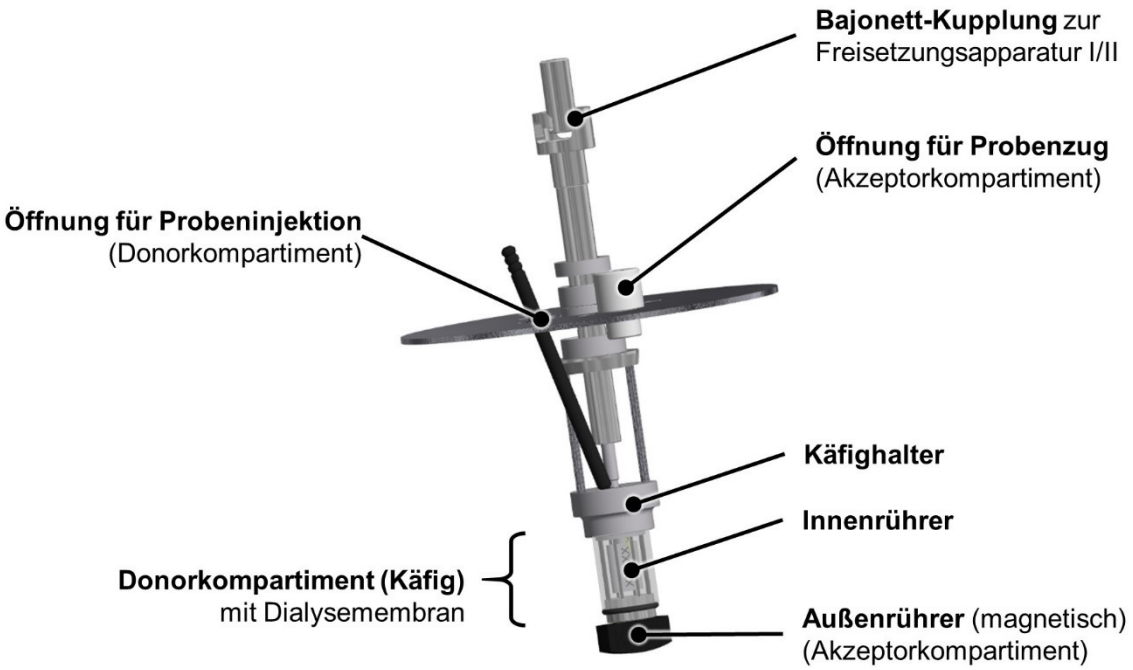

Abbildung 1: *Schematische Darstellung der im Rahmen dieser Arbeit erfolgreich angepassten Konstruktion des Pharma Test Dispersion Releasers (PTDR). Abbildung modifiziert nach [101].*

Unter der Normalisierung des Freisetzungsprofils wird die Berechnung des tatsächlichen Freisetzungsprofils des Arzneistoffträgers ohne den Einfluss der Dialysemembran verstanden. Während des Freisetzungsexperiments wird der Wirkstoff in der Donorkammer freigesetzt (k_{rel}). Der freie Wirkstoff muss im Anschluss durch die Dialysemembran in das Akzeptorkompartiment permeieren, um dort nach Probenzug quantifiziert werden zu können. Hierbei spielt die Membranpermationskonstante k_M eine entscheidende Rolle. Um die tatsächliche Freisetzung richtig zu interpretieren, muss die Permeation schneller erfolgen als die Wirkstofffreisetzung, andernfalls können Übersättigungsphänomene in der Donorkammer zu falschen Rückschlüssen führen. Die Prozesse während der Dialyse sind in Abbildung 2 dargestellt.

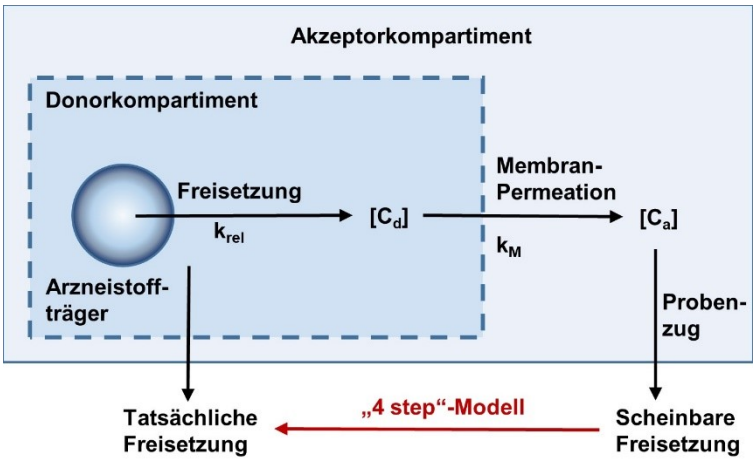

Abbildung 2: *Schematische Darstellung der verschiedenen Prozesse während einer Freisetzungsuntersuchung in dialysebasierten Apparaturen inklusive Verknüpfung mit dem mathematischen 4-step-Modell.*

Grundlage für die mathematische Normalisierung des Freisetzungsprofils ist das *4-step*-Modell von Xie et al [83]. Dabei wird mit Hilfe eines Referenzexperiments (Permeationsuntersuchung einer Wirkstofflösung) zuerst k_M ermittelt. Unter Annahme einer konstanten Wirkstoffmenge Q_0, die am Anfang des Experiments in die Donorkammer injiziert wird, kann die Wirkstoffkonzentration im Donorkompartiment C_d unter Einbezug der Volumina des Donorkompartiments V_d und Akzeptorkompartiments V_a berechnet werden (Gleichung 3).

$$C_d(t) = \frac{[Q_0 - C_a(t) \cdot V_a]}{V_d} \tag{3}$$

Wird C_d in Gleichung 2 nun durch Gleichung 3 ersetzt, erhält man Gleichung 4:

$$\frac{dC_a}{dt} = \left[\frac{k_M \cdot A}{\delta \cdot V_a}\right] \cdot \left[\frac{Q_0 - C_a(t) \cdot V_a}{V_d} - C_a(t)\right] \tag{4}$$

Gleichung 4 kann analytisch gelöst werden und man erhält Gleichung 5:

$$C_a(t) = \left[\frac{Q_0}{V_a(t) + V_d}\right] \cdot \left\{1 - exp\left[\frac{A \cdot k_M \cdot (V_a + V_d) \cdot t}{\delta \cdot V_a \cdot V_d}\right]\right\} \tag{5}$$

In geschlossenen Dialyseexperimenten strebt das System zur Konzentration im Equilibrium C_{eq} mit $C_{eq} = Q_0 / (V_a + V_d)$. Fasst man die Konstanten im Exponenten von Gleichung 5 zusammen und führt die totale Membranpermeationskonstante k_T *ein*, kann diese mit Gleichung 6 dargestellt werden:

$$k_T = \left[\frac{A \cdot k_M \cdot (V_a + V_d)}{\delta \cdot V_a \cdot V_d}\right] \tag{6}$$

Damit kann Gleichung 5 zu Gleichung 7 vereinfacht werden.

$$C_a(t) = C_{eq} \cdot [1 - exp(k_T \cdot t)] \quad (7)$$

Die ermittelte Wirkstoffpermeation einer Wirkstofflösung kann dann genutzt werden, um mittels nichtlinearer Regression k_T zu ermitteln. Die Membranpermeationskonstante k_M kann anschließend mit Gleichung 6 berechnet werden. Bei der Durchführung des Referenzexperiments sollte auf eine ausreichende Löslichkeit des Wirkstoffs im Volumen der Donorkammer geachtet werden, damit die Membranpermeation nicht durch Artefakte in der Auflösung verfälscht wird. Das Einhalten der sogenannten *sink*-Bedingung hat sich dabei bewährt, wobei die Konzentration im Donorkompartiment maximal ein Drittel der Sättigungslöslichkeit des Wirkstoffs beträgt. Lösungsvermittler wie Cyclodextrine können bei schlechtlöslichen Wirkstoffen notwendig sein.

Nachdem mit Hilfe einer geeigneten Referenzmessung k_M ermittelt wurde, kann aus dem Permeationsprofil der Formulierung, unter Annahme einer Pseudolinearität zwischen den ermittelten Datenpunkten, die Konzentrationszunahme im Akzeptorkompartiment mit Gleichung 8 ausgedrückt werden.

$$\frac{dC_a}{dt} \approx \frac{\Delta C_a}{\Delta t} = \left[\frac{k_M \cdot A}{\delta \cdot V_a}\right] \cdot [C_d(t) - C_a(t)] \quad (8)$$

Durch Umstellen von Gleichung 8 erhält man zur Berechnung der freien Wirkstoffkonzentration im Donorkompartiment in Abhängigkeit von C_a Gleichung 9:

$$C_d(t) = \left(\frac{\Delta C_a}{\Delta t}\right) \cdot \left[\frac{\delta \cdot V_a}{k_M \cdot A}\right] + C_a(t) \quad (9)$$

Im letzten Schritt kann die totale Wirkstoffkonzentration Q_t aus den Konzentrationen im Donor- und Akzeptorkompartiment und damit das normalisierte Freisetzungsprofil ermittelt werden (Gleichung 10).

$$Q_t(t) = C_d(t) \cdot V_d + C_a(t) \cdot V_a \quad (10)$$

Zur weiteren Auswertung der Wirkstofffreisetzung kann das normalisierte Profil mit Hilfe von Modellen weiter beschrieben werden. Damit können wiederum Profile unter Zuhilfenahme modellspezifischer Parameter verglichen oder *in silico* Modelle zur Berechnung der Pharmakokinetik eingesetzt werden. Dafür eignet sich beispielsweise das *reciprocal powered time*-Modell, das die Freisetzung aus nanoskaligen Arzneistoffträgern aus einer Kombination von Diffusions- und Auflösungsprozessen beschreibt [102].

1.5 Die verwendeten Modellarzneistoffe

1.5.1 Diclofenac

Diclofenac (Abbildung 3) ist ein häufig verwendetes, nichtsteroidales Antiphlogistikum. Der Wirkstoff ist eine schwache Säure mit einem pK_s-Wert von 3,80 [103]. Damit zeigt Diclofenac eine pH-Wert-abhängige Löslichkeit im Bereich des Magen-Darm-Traktes, die mit steigendem pH-Wert zunimmt [103]. Durch die Hemmung der Cyclooxygenase (COX), mit einer Präferenz für die Isoform COX-2, wirkt Diclofenac analgetisch, antipyretisch und antiphlogistisch. Diclofenac wird im Darm sehr gut resorbiert und zeigt eine hohe Plasmaproteinbindung von 99 %, vorwiegend an Albumin [104-106]. Aufgrund seiner Pharmakodynamik ist es bei leichten bis mittleren Schmerzen und Entzündungen, wie auch bei Zerrungen, Prellungen und rheumatoider Arthritis indiziert. Typische Nebenwirkungen sind gastrointestinale Störungen (zum Beispiel Übelkeit, Erbrechen, Ulzerationen) und lokale Hautreaktionen. Im Markt sind neben Film-, Trink- und Retardtabletten auch topische Formulierungen wie Gele, Sprays und Schmerzpflaster sowie Suppositorien zu finden. Verschiedene zugelassene halbfeste Formulierungen eigenen sich zur Untersuchung des Einflusses von Hilfsstoffen aufgrund ihrer Standardisierung besonders, um eine Methode hinsichtlich ihres Potentials zur Detektion von Formulierungsunterschieden zu bewerten. In verfügbaren Fertigarzneimitteln liegt Diclofenac als Salz vor, wobei das Natrium-Salz das häufigste ist. Aber auch Kalium- und Diethylamin-Salze können verwendet werden [103]. Die Salze unterscheiden sich in ihren Löslichkeits- und Permeationseigenschaften, weshalb beispielsweise in Voltaren® Emulgel (GlaxoSmithKline Consumer Healthcare GmbH & Co. KG, München, Deutschland) das Diethylamin-Salz aufgrund der besseren Penetrationseigenschaften verwendet wird.

1.5.2 Hydrocortison

Hydrocortison (Abbildung 3) gehört zur Gruppe der Glucocorticoide und entspricht dem physiologischen Cortisol. Glucocorticoide entfalten ihre Wirkung über intrazelluläre Rezeptoren, die Einfluss auf die Transkription von Genen haben. Sie beeinflussen den Kohlenhydrat-, Fett- und Eiweißstoffwechsel und halten die Homöostase aufrecht. Therapeutisch wird Cortisol vor allem zur Substitution bei Nebennierenrindeninsuffizienz eingesetzt. Aber auch seine antiphlogistische, antiallergische und immunsuppressive Wirkung wird genutzt. Eine systemische oder topische Therapie mit Hydrocortison kann zur Behandlung von Hauterkrankungen, rheumatischen Beschwerden, allergischen Reaktionen, Lungenerkrankungen und chronisch entzündlichen Darmerkrankungen erfolgen.

Die vaginale Anwendung von Hydrocortison ist beispielsweise bei vulvovaginalem *Lichen planus* oder zur Reduktion perinealer Schmerzen nach der Geburt in klinischen Studien untersucht worden [107, 108].

Hydrocortison zeigt eine schlechte Wasserlöslichkeit und eine gute Darmresorption [109]. Demgegenüber ist die Resorption von Hydrocortison in der Vagina nicht gut erfasst. Allerdings konnte in Tierstudien eine hohe systemische Hydrocortison-Exposition nach vaginaler Anwendung festgestellt werden [110]. Hydrocortison lässt sich leicht in Liposomen verkapseln und kann deshalb gut als Modellsubstanz für die Entwicklung eines topischen Arzneistoffträgersystems verwendet werden, um die kritischen Formulierungsparameter zu erfassen.

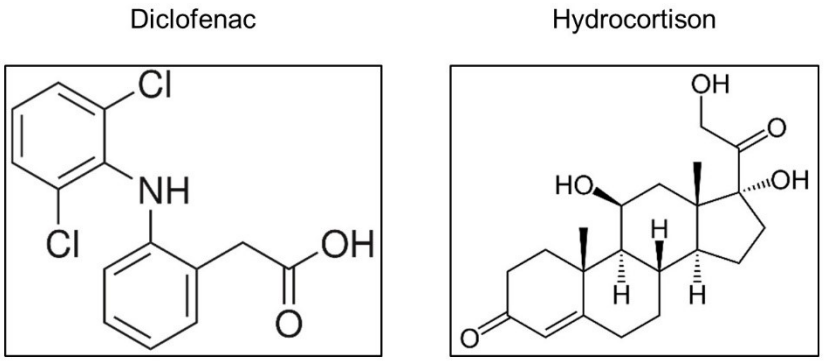

Abbildung 3:*Strukturformeln von Diclofenac [111] und Hydrocortison [112].*

2 Ziele der vorliegenden Forschungsarbeit

In den letzten Jahrzehnten haben Nanoarzneimittel immer mehr an Bedeutung gewonnen. Dies ist insbesondere auch in der Zunahme der Zulassungsanträge, die Nanoarzneimittel enthalten, zu erkennen. Infolgedessen kamen in den letzten Jahren Wirkstoffe auf den Markt, die an Arzneistoffträger wie Liposomen gebunden sind (Tabelle 1). Neben der Wirksamkeit und Unbedenklichkeit der neuen Arzneimittel, muss für die Zulassung auch die Qualität gewährleistet sein. Dabei spielen verschiedene Eigenschaften der Nanoarzneimittel eine wichtige Rolle, die im Rahmen der Qualitätskontrolle überwacht werden müssen. Neben der Partikelgröße und der Partikelgrößenverteilung, der Oberflächenladung und Hydrophilie des Arzneiträgersystems, spielt die (Rest-)Kristallinität des Wirkstoffs und die Wirkstofffreisetzung eine wesentliche Rolle für die erfolgreiche *in vivo* Performance von Nanoarzneimitteln. Zur Bestimmung der Wirkstofffreisetzung aus kolloidalen Arzneistoffträgern wie Liposomen, Nanopartikeln oder Mizellen gibt es bis heute keine Standardmethode. In der Wissenschaft und der pharmazeutischen Industrie werden verschiedene Wirkstofffreisetzungsmethoden verwendet, um die Konzentration des freien Wirkstoffs zu ermitteln. Dabei ist die Wahl der Separationsmethode auf die Eigenschaften der verschiedenen Arzneistoffträger abzustimmen.

In der vorliegenden Arbeit wurde eine dialysebasierte Apparatur, der *Dispersion Releaser* (DR), verwendet. Sie kann direkt in die Apparaturen I/II der Arzneibücher der Europäischen Union (Ph. Eur.) und der Vereinigten Staaten (USP) eingesetzt werden. Die Entwicklung und Patentierung eines funktionsfähigen Prototyps erfolgte an der Goethe Universität und wurde im Rahmen dieser Arbeit gemeinsam mit der Pharma Test Apparatebau AG (Hainburg, Deutschland) weiterentwickelt zu einer kommerziell erwerbbaren Apparatur (*Pharma Test Dispersion Releaser*, PTDR) weiterentwickelt. Darunter fällt die Rekonstruktion des Prototyps unter Einbezug der Anforderungen der pharmazeutischen Industrie, sowie die Erleichterung der Anwendung für den Anwender. Die finale Apparatur wurde zuletzt einer ausgiebigen Validierung unterzogen. Neben Untersuchungen zur Hydrodynamik und dem Einfluss der Umdrehungszahl auf die Membranpermeationsrate k_M wurde eine Methode mit Goldpartikeln zur Bestimmung der Dichtigkeit des Systems entwickelt. Der Einfluss von Proteinen im Freisetzungsmedium auf die Permeation wurde ebenfalls untersucht. Diclofenac diente dabei als Modellarzneistoff für die Validierungsuntersuchungen. Der DR wurde ursprünglich zur Untersuchung von parenteralen Nanoformulierungen entwickelt. Die Wirkstofffreisetzungsuntersuchung von halbfesten Zubereitungen ist noch nicht erfolgt und soll im Rahmen dieser Forschungsarbeit für zwei verschiedene Diclofenac-Gele unter verschiedenen Bedingungen evaluiert werden.

Des Weiteren wurde Hydrocortison als Modellsubstanz in vier verschiedene Proliposomen zur vaginalen Anwendung formuliert und das nach Rekonstitution entstandene liposomale Gel untersucht. Die Wirkstofffreisetzung des Hydrocortisons, sowie die Permeabilität über eine Zellmonoschicht wurde vergleichend untersucht und die verschiedenen Formulierungen bewertet. Eine kommerziell erhältliche Hydrcortison-Creme wurde als Referenz verwendet.

Die eingesetzte Dialysemembran hat einen Einfluss auf die Rate, mit der Wirkstoffe im Akzeptorkompartiment gemessen werden. Dabei ist eine langsamere Freisetzungsrate im Vergleich zur Membranpermeationrate entscheidend für eine gute Auswertung. Eine Auswertung ist mit dem vorgestellten *4-step*-Modell möglich, aber es fehlt an einer Standardisierung, die im Rahmen der Validierung des kommerziellen PTDR etabliert und die Auswertung in einem mathematischen Modell in Stella Architect® (iseesystems, Lebanon, New Hempshire, USA) eingebettet wurde. Zusätzlich sollte ein webbasiertes Interface mit Stella Architect® erstellt werden.

3 Ergebnisse und Diskussion

3.1 Anpassung der Konstruktion des Dispersion Releasers

Das erste Ziel der vorliegenden Arbeit ist die an den Anforderungen der pharmazeutischen Industrie ausgerichtete Weiterentwicklung des DRs. Dabei sollte ergänzend die Anwenderfreundlichkeit verbessert werden. Der vorliegende Prototyp der Goethe Universität besteht aus sehr vielen Einzelteilen und ist spezifisch für Freisetzungsapparaturen der Firma ERWEKA GmbH (Langen, Deutschland) mit einem keiner offiziellen Norm entsprechenden Minivessel entwickelt worden. Dadurch sind Freisetzungstests mit dem DR - neben extensiven Schulungen der Anwender - zum einen mit einem erheblichen Zeitaufwand beim Zusammenbauen, Abbauen und Reinigen der verschiedenen Einzelteile verbunden. Zum anderen ist der Prototyp weder mit arzneibuchkonformen Vessel noch mit automatisierten Probenzugsystemen kompatibel. Eine weitere Schwäche des Prototyps ist das versehentliche Entkoppeln des Käfigs oder des Rührers von der Freisetzungsapparatur während eines laufenden Experiments, das die Untersuchung ungültig macht. Bei der Rekonstruktion sind deshalb folgende Ziele festgesetzt worden:

- Reduktion der Anzahl an Bauteilen für den Anwender
- Schnelles Einstecken der Dialysekammer in den Käfighalter statt Einsetzen und Festziehen einer kleinen Schraube
- Schnelles Einhängen in die Freisetzungsapparatur durch eine simple Kupplung statt Einschrauben
- Verschluss der Probeninjektionsöffnung mit einem Metallstift von außen statt mit Pinzette durch die Probenzugöffnung
- Anpassung des Prototyps an arzneibuchkonforme Vessel statt Sonderfertigung
- Anpassungen sollen ohne Minimierung der Membranpermeationskonstante k_M erfolgen

Gemeinsam mit dem Kooperationspartner Pharma Test Apparatebau AG (Hainburg, Deutschland) wurden verschiedene Konstruktionen einem Belastungstest unterzogen. Dabei wurden die Freisetzungsapparatur für sieben Tage bei 150 UPM betrieben mit den verschiedenen Konstruktionsänderungen betrieben und das Ergebnis verglichen. Es wurden unterschiedliche Varianten zur Kopplung des PTDRs mit der Freisetzungsapparatur, Kugellager und Edelstahlqualitäten getestet. Dabei erwiesen sich die Bajonett-Kupplung für die Kopplung mit dem Freisetzungstester und das offene Kugellager

als am robustesten und wurden für die Rekonstruktion ausgewählt, wodurch eine stabile Apparatur erhalten wurde. Feine Partikel traten bei längerer Anwendung allerdings weiterhin auf, die durch weitere Anpassungen, insbesondere durch die Auswahl der Dichtungen um das Kugellager, minimiert wurden. Die Auswahl des richtigen Edelstahls, sowie eines wasserdichten Verschlusses an den Neodym-Magneten im Innenrührer löste die Probleme von Rost im Donorkäfig (Abbildung 4a). Ein sehr präziser Zusammenbau der Einzelteile ist notwendig, damit kein reibender Kontakt zwischen verschiedenen Konstruktionsteilen entsteht. Dies wurde zum Beispiel zwischen dem Innenrührer und dem Käfighalter beobachtet (Abbildung 4b). Der Durchmesser des Käfighalters und die Einkerbungen im Käfig müssen genau ausgemessen sein, um die O-Ringe am richtigen Platz zu halten. Andernfalls kann der Käfig nicht ordnungsgemäß in den Käfighalter eingesetzt werden und Verletzungen der Membran sind die Folge (Abbildung 4c).

Die vor der Rekonstruktion festgesetzten Ziele konnten erreicht und die Arbeitszeit zum Vorbereiten des PTDRs reduziert werden. Das Einführen der Probe in das Donorkompartiment und der Probenzug während des laufenden Experimentes daraus wurden optimiert und können fortan durch eine weitere Öffnung unabhängig vom Probenzug aus dem Akzeptorkompartment erfolgen. Dies war beim Prototypen der Goethe Universität nicht möglich. Die Öffnung des Probenzugs für das Akzeptorkompartiment wurde ebenfalls angepasst. Der Probenzug beim PTDR kann nun entweder manuell mit einer Mikropipette oder über ein automatisiertes System erfolgen. Der Prototyp der Goethe Universität war auf einen manuellen Probenzug beschränkt. Die Verknüpfung mit einem automatisierten Probenzugsystem konnte im Rahmen der vorliegenden Arbeit erfolgreich innerhalb des Projektes *Dispersify* gezeigt werden. Die nun durch den Umbau mögliche Kombination des PTDRs mit verschiedenen arzneibuchkonformen Vessel ermöglicht eine internationale Vergleichbarkeit der Freisetzungsuntersuchungen.

Abbildung 4: *Probleme, die bei den ersten Prototypen der Rekonstruktion des PTDRs während des Stresstests auftraten: Rost im Donorkompartiment (a), nicht exakte Ausrichtung des Käfighalters zum Innenrührer (b),Verletzung der Membran und Deformation des oberen O-Rings (c).*

Während der Anpassung der Konstruktion an die Anforderungen der pharmazeutischen Industrie, wurde festgestellt, dass einige der Dialyseschläuche einen für das DR-System zu geringen Innendurchmesser aufwiesen. Auf Anfrage beim Membranhersteller Repligen® wurden nicht frei zugängliche Spezifikationen zur Verfügung gestellt. Prozessbedingte Fertigungsunterschiede führen chargenabhängig zu einer Abweichung im Membranschlauchdurchmesser von 17,2 mm bis 20,4 mm. Der nominelle Durchmesser wird jedoch im Produktkatalog mit 20 mm angegeben. Da der Käfigdurchmesser 19,2 mm beträgt, soll daher im Zuge der laufenden Rekonstruktion eine Anpassung des Käfigdurchmessers erfolgen, um Kompatibilität mit möglichst vielen im Markt befindlichen Membrantypen sicherzustellen.

Der angepasste Käfigdurchmesser wird bei der finalen Konstruktion 17,0 mm betragen, wobei die Länge des Käfigs angepasst wurde, um dasselbe Probenvolumen applizieren zu können. Die dadurch entstandenen Veränderungen am Innenrührer, Außenrührer und der Käfighalterung sowie die entsprechend geänderte Positionierung der Probenöffnungen des Akzeptor- und Donorkompartiments wurden in neuen Konstruktionsteilskizzen angepasst und der Pharma Test Apparatebau AG zur Verfügung gestellt.

Im Anschluss fertigte die Pharma Test Apparatebau AG die entsprechenden Konstruktionsteile für die finale Version des PTDRs. Durch die Änderung des Käfigdurchmessers

musste auch der obere O-Ring angepasst werden. Schließlich mussten zwei unterschiedliche O-Ringe für die beiden Membranmaterialien trotz umfassender Testung verschiedener Größen und Dicken von O-Ringen eingesetzt werden, weil die verschiedenen Membranmaterialien unterschiedlich dick sind und ein unterschiedlich großer Falz beim Beziehen des Käfigs entsteht. Letzteres beruht auf dem angepassten Käfigdurchmesser und der großen Streuung des Membrandurchmessers. Um den Käfig ohne Verletzen der Membran in die Halterung einbringen zu können, wird die dickere Dialysemembran aus CE mit einem dünneren O-Ring verschlossen. Im Gegensatz dazu wird für dünnere Membranen aus RC ein dickerer O-Ring benötigt, damit der Käfig nicht aus der Halterung fällt. Dies ist ein Manko, das im Zug der Weiterentwicklung außerhalb der vorliegenden Arbeit behoben werden kann.

Um zu überprüfen, ob eine Verlangsamung der Membranpermeation durch die geänderten Käfigdimensionen der finalen Konstruktion stattfand, wurde eine Flurbiprofen-Wirkstofflösung unter typischen Bedingungen dialysiert [82]. Die Membranpermeationskonstante k_M in dieser Version betrug $2{,}98 \pm 0{,}12 \times 10^{-3}$ cm²/h im Vergleich zu $2{,}14 \pm 0{,}06 \times 10^{-3}$ cm²/h im Prototypen der Goethe Universität. Die Konstante ist im neuen System größer als im Alten, was einer schnelleren Permeation des Flurbiprofens durch die Dialysemembran entsprach. Die Konstruktion wurde somit nicht nur hinsichtlich der Nutzerfreundlichkeit, sondern auch hinsichtlich der Dialysegeschwindigkeit (als Maß für die Messsensitivität) verbessert. Einzig die Nutzung der O-Ringe, unabhängig von der verwendeten Membran, sollte bei zukünftigen Anpassungen der Apparatur weiter optimiert werden.

Damit die Fertigung jedes weiteren DRs identisch ist, wurden folgende Größen als kritisch festgelegt und die erlaubten Abweichungen sehr eng spezifiziert:

- Länge und Durchmesser des Donorkäfigs
- Länge und Durchmesser des Käfighalters
- Dimensionen der Einkerbung im Donorkäfig für die O-Ringe
- Gewährleistung des orthogonalen Einbaus des Schafts zum Kugellager, um Pendeln / Ausschlagen um die eigentliche Soll-Achse der Schäfte zu minimieren

Die Kontrolle dieser gerätespezifischen Größen dient der Vergleichbarkeit zwischen jedem PTDR. Zusätzlich wird damit sichergestellt, dass das Käfigvolumen und die Oberfläche konstant und vergleichbar bleiben. Das Einstecken des Donorkäfigs in den Käfighalter ist weiterhin mit jeder Membranart und Dicke möglich. Allerdings können kleine Veränderungen des Durchmessers oder der Tiefe der Einkerbung für die O-Ringe zu Schwierigkeiten (Abbildung 4c) führen. Außerdem sollte das Ausschlagen um die eigene

Achse des Innenrührers wie bei der Qualifizierung von Freisetzungsapparaturen überprüft werden, damit er weder den Käfighalter noch die Streben des Donorkompartiments berührt.

3.2 Validierung der aktualisierten Konstruktion des Dispersion Releasers

Nach der erfolgreichen Anpassung des PTDRs an die Anforderungen der pharmazeutischen Industrie wurde im Folgenden überprüft, ob das Gerät korrekt funktioniert. Dabei wurden verschiedene Versuche durchgeführt, die die Funktion und Leistung des Gerätes dokumentieren sollten. Dabei wurde der Fokus vor allem auf die Dialysemembran gelegt, die für die Trennung der verschiedenen Fraktionen des Arzneistoffes (frei im Medium gelöst, gebunden am Arzneistoffträger oder proteingebunden) verantwortlich ist. Des Weiteren wurde der Einfluss der Umdrehungsgeschwindigkeit auf die Membranpermeation und die Homogenität des Außenkompartiments überprüft. Der Einfluss verschiedener Hilfsstoffe wie Proteine und Löslichkeitsvermittler auf die Membran und Membranpermeation wurde untersucht.

3.2.1 Funktionsqualifizierung des Dispersion Releasers

3.2.1.1 Überprüfung der Dichtigkeit des Dispersion Releasers

Die einwandfreie Integrität der Dialysemembran ist eine wesentliche Voraussetzung für den ordnungsgemäßen Betrieb des PTDRs. Bei der klassischen Verwendung der Dialysemembranen zur Aufreinigung von verschiedenen Proteinfraktionen oder zum Austauschen der Puffersalze werden in der Regel speziell angefertigte Klammern eingesetzt, die den optimalen Verschluss des Dialyseschlauchs gewährleisten. Beim PTDR werden O-Ringe anstelle von Klammern verwendet, um den Dialyseschlauch zu verschließen und damit die beiden Kompartimente voneinander zu trennen. Durch die konstruktionsbedingte Verkleinerung des Donorkompartiments, die der breiten Variation des Durchmessers der Dialysemembran entgegenwirkt, kann sich bei größeren Durchmessern des Dialyseschlauchs ein Falz bilden. In diesem Fall gilt es besonders sicherzustellen, dass keine Fraktion des am Arzneistoffträger gebundenen Wirkstoffs durch den Falz oder durch unzureichenden Verschluss der Membran in das Akzeptorkompartiment gelangt.

Dies kann zu falschen Rückschlüssen auf die Wirkstofffreisetzungsrate aus dem Arzneistoffträger führen.

Die Anforderungen an ein geeignetes Partikelsystem als Standard zur Bestimmung der Dichtigkeit des PTDRs waren eine monodisperse Größenverteilung, eine ausreichende Stabilität bei 37 °C und dass gegebenenfalls verwendete Fluoreszenz-Farbstoffe nicht aus dem Trägersystem austreten durften. Gold-Nanopartikel erschienen dabei das geeignete Partikelsystem zu sein, da sie ohne Tenside und Stabilisatoren bei 37 °C ausreichend stabil sind und in den geforderten Partikeldurchmessern präzise synthetisiert werden können. Zusätzlich absorbieren sie in Abhängigkeit ihrer Größe Licht und können neben DLS mittels UV/Vis-Spektroskopie untersucht werden. Der vorliegende Versuch wurde mit drei Testvessel, sowie je eine Positiv- und Negativkontrolle durchgeführt. Bei der Negativkontrolle wurde das Hintergrundrauschen für die DLS-Messung ermittelt. Die Positivkontrolle wies im Vergleich zu den Testvessel von Beginn des Versuches an eine Inzision in der Membran auf, wodurch zu allen Probenzeitpunkten ein typisches UV/Vis-Absorptionsspektrum beobachtet wurde (Abbildung 5e). Dies konnte in den Messungen mittels DLS bestätigten werden (Abbildung 5f). Im Vergleich dazu war die Negativkontrolle ohne Befund und auch in der DLS wurden keine Partikel festgestellt (< 1000 kcps). Innerhalb von 24 h Untersuchungszeit wurde bei den Testvessel weder ein Absorptionsmaximum bei 534 nm noch eine signifikante Partikelanzahl (mittlere abgeleitete Zählrate als Surrogat) festgestellt (Abbildung 5a) [113, 114]. Erst nach Inzision der Membran, um eine Verletzung zu simulieren, wurden die Goldpartikel im Akzeptorkompartiment nachgewiesen (Abbildung 5, b-d). Damit wurde die Gewährleistung einer Trennung zwischen den beiden Kompartimenten über eine Dialysemembran für Partikel bis 50 nm für 24 h nachgewiesen.

Alternativ kann die Abwesenheit von Partikeln im Akzeptorkompartiment für jedes Partikelsystem durch Vermessungen von Proben am Ende des Freisetzungsversuches mittels DLS oder NTA ermittelt werden, sollte die Versuchsdauer 24 h überschreiten. Dies ist jedoch mit erheblichem Zeit- und Validierungsaufwand verbunden. Zusätzlich kann eine erfolgreiche Vermessung mittels DLS durch komplexe Medien mit Tensiden oder Proteinen erschwert sein.

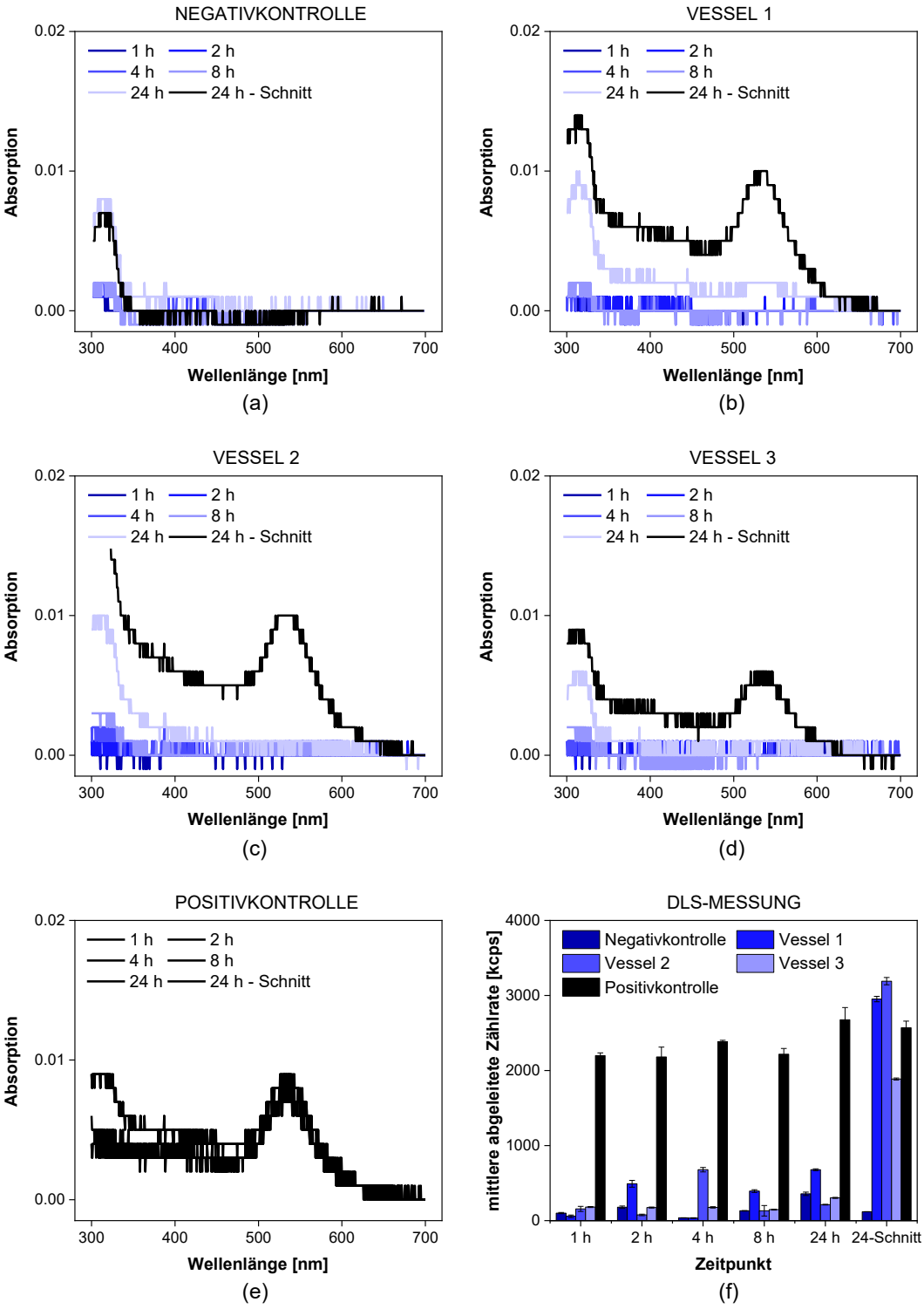

Abbildung 5: *Überprüfung der Membranintegrität mit 50 nm Gold-Nanopartikeln (λ_{max} = 535 nm). Die Proben aus dem Akzeptorkompartiment wurden mit UV/Vis-Spektroskopie im Bereich von 300-700 nm analysiert. Die Negativkontrolle wurde ohne Zugabe von Gold-Nanopartikeln gemessen (a), während bei der Positivkontrolle die Dialysemembran vor Beginn des Experiments eingeschnitten wurde (e). Bei allen anderen Proben (b-d) wurden die Gold-Nanopartikel in das Donorkompartiment gegeben. Nach 24 h wurde die Membran punktiert (Schnitt, schwarze Kurve b-d). Zusätzlich wurden DLS-Messungen durchgeführt (f). Auch hier wurde erst nach dem Einschnitt ein Signal (> 1000 kcps) erhalten. Die Abbildung wurde modifiziert nach [101].*

3.2.1.2 Überprüfung der Retention von Makromolekülen im Dispersion Releaser

Albumin ist das meistvertretene Protein im Blut und spielt beim Transport von hydrophoben Molekülen eine wichtige Rolle. Zusätzlich bindet es an Arzneistoffträgersystemen und kann deren Freisetzung beeinflussen. Das Retentionsverhalten des Albumins in der Dialyse ermöglicht daher Aufschluss über die Dichtigkeit der Dialysemembran und kann genutzt werden, um Einflüsse auf die Wirkstofffreisetzung zu untersuchen. Im Falle der eingesetzten 50 kDa Dialysemembran aus RC hat der Hersteller als Spezifikation festgelegt, dass maximal 10 % des Albumins nach 17 h die Dialysemembran passieren [82].

Eine Lösung von bovinem Serumalbumin (BSA) wurde in das Donorkompartiment injiziert und die permeierte Menge im Akzeptorkompartiment über einen Zeitraum von 24 h ermittelt. Diese wurde einerseits mit Größenauschlusschromatographie (SEC, *size exclusion chromatography*) und andererseits mit einer UV/Vis-Sonde, die eine kontinuierliche Messung ermöglichte, quantifiziert (Abbildung 6). Während der ersten 6 h wurde weder über die SEC noch über die Sonde BSA im Akzeptorkompartiment detektiert. Die Messung mit der UV/Vis-Sonde zeigte erst nach 8 h eine Überschreibung der Konzentrationsgrenze zur Quantifizierung. Danach stieg die BSA-Konzentration kontinuierlich an. Bei der vom Hersteller festgelegten Zeit von 17 h wurde im Schnitt 10 ± 8 % BSA chromatographisch ermittelt. Die Messung mit der Sonde bestätigte dieses Ergebnis. Damit wurde die Spezifikation vom Hersteller überschritten. Dies liegt daran, dass die Dialyse im Regelfall bei Raumtemperatur (25 °C) unter moderatem Rühren des Akzeptorkompartiments stattfindet. Die Experimente im PTDR wurden bei Körpertemperatur (37 °C) und unter Rühren des Donorkompartiments durchgeführt, was zur beschleunigten Permeation des BSA führte. Zusätzlich zeigte die Permeation von BSA eine breite Streuung, weshalb die Verwendung des Proteins zur Dichtigkeitsbestimmung nicht geeignet war.

Bei der Untersuchung der freien Wirkstofffraktion unter Einfluss von Albumin sollte der Versuch nach spätestens 15 h beendet sein, da ab diesem Zeitpunkt BSA in das Akzeptorkompartiment übergeht. Jedoch ist auch bei einer vorzeitigen Permeation des BSAs unter Berücksichtigung des Verhältnisses zwischen BSA und Wirkstoff von keinem relevanten Fehler bei der Bestimmung auszugehen. Trotzdem sollten kinetische Untersuchungen mit Albumin kurz (am besten maximal 8 h) oder unter Verwendung eines kleineren MWCO wie 30 kDa durchgeführt werden, um den analytischen Fehler gering zu halten.

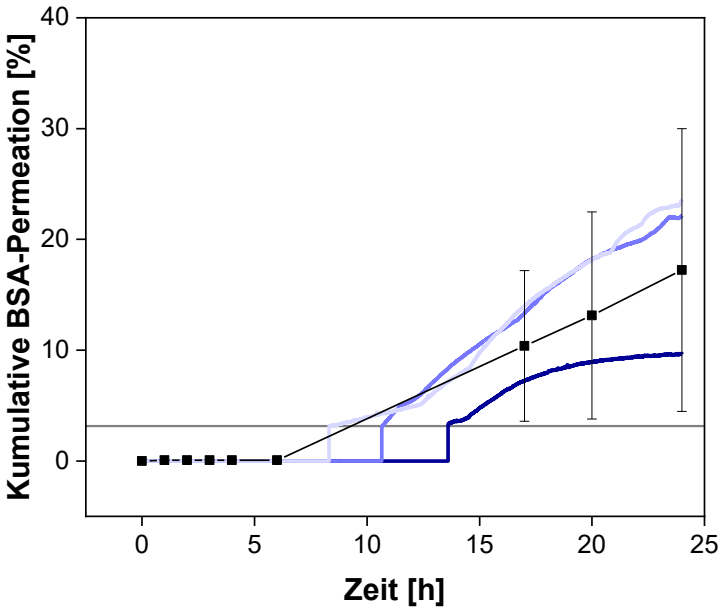

Abbildung 6: *Kumulative Permeation von bovinem Serumalbumin (BSA) bei 37 °C, 50 UPM und einer 50 kDa Dialysemembran aus regenerierter Cellulose. Die Konzentrationsbestimmung erfolgte mit einer SEC-HPLC-Methode (schwarze Quadrate, Mittelwert ± SD, n = 3) und einer in situ-UV/Vis-Sonde (blaue Linien). Die graue Horizontale stellt das Quantifizierungslimit für die UV/Vis-Sonde dar. Abbildung modifiziert nach [101].*

3.2.1.3 Überprüfung der Hydrodynamik im Akzeptorkompartiment

Vorrausetzung für die zuverlässige Quantifizierung der Wirkstoffkonzentration im Akzeptorkompartiment ist eine gleichmäßige, schnelle Verteilung des Wirkstoffs im Vessel während des Freisetzungsexperiments. Zusätzlich bleibt der Konzentrationsgradient als treibende Kraft der Permeation bei einer schnellen und gleichmäßigen Verteilung hoch, wodurch eine rapide und konstante Permeationsrate erreicht wird.

Da die Drehbewegung des äußeren Rührers nur indirekt über Magnete vom Rührer im Donorkompartiment übertragen wird, wurde die gleichmäßige Verteilung des Wirkstoffs mit einer farbigen Lösung nachgestellt und überprüft. Dazu wurde eine Messsonde im Akzeptorkompartiment eingebracht, die die Absorption im Wellenlängenbereich des eingebrachten Farbstoffs kontinuierlich misst. Die Umdrehungszahl wurde im Bereich von 0 bis 100 UPM variiert. Die Ergebnisse sind in Abbildung 7 dargestellt. Bei den Umdrehungsgeschwindigkeiten von 50 und 100 UPM wurde ein Plateau der Absorption innerhalb weniger Sekunden erreicht, was für eine schnelle Verteilung der farbigen Lösung spricht. Im Gegensatz dazu konnten bei 25 UPM Schwankungen der Absorption festgestellt werden, die erst nach einer Minute in ein Plateau übergingen. Blieb das Rühren

aus, konnte keine konstante Absorption innerhalb von 15 min festgestellt werden und die Verteilung des farbigen Wirkstoffs im Akzeptorkompartment blieb inhomogen. Daraus ließ sich schließen, dass das Rühren wichtig ist, um eine gleichmäßige Verteilung für eine repräsentative Stichprobe aus dem Vessel zu erhalten. Dies wird bei Umdrehungsgeschwindigkeiten zwischen 50 und 100 UPM stets gewährleistet. Auch eine Drehzahl von 25 UPM kann eingestellt werden, da Probenzüge in der Regel in Abständen von mehr als 5 min stattfinden und in dieser Zeit eine homogene Verteilung gewährleistet ist.

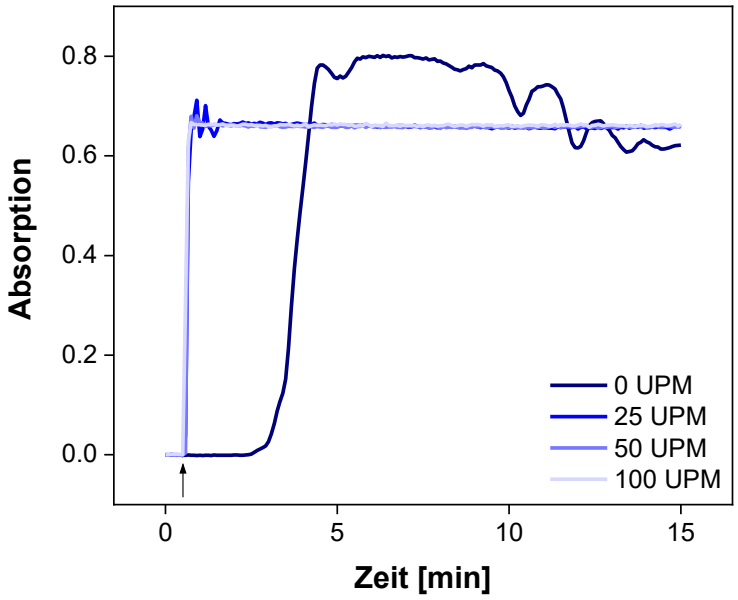

Abbildung 7: *Messungen im Akzeptorkompartiment mit einer in situ UV/Vis-Sonde bei 283 nm bei unterschiedlichen Rührgeschwindigkeiten. Der Pfeil markiert die Zugabe einer farbigen Lösung in das Akzeptorkompartiment. Abbildung modifiziert nach [101].*

3.2.1.4 Einfluss der Drehzahl auf die Membranpermeationsrate

Das Rühren des Donorkompartments ist eine einzigartige Funktion des PTDRs, die sich von konventionellen Dialysemethoden wie dem Dialysesack unterscheidet. Fehlendes Rühren kann im Dialysesack zu Aufschwimmen, Sedimentation oder Agglomeration des nanodispersen Systems führen und ist ein typischer Nachteil konventioneller Systeme [67, 82]. In der Regel spiegelt die Umdrehungsgeschwindigkeit nicht die physiologische Hydrodynamik am Ort der Administration wieder, jedoch werden die zuvor bereits beschriebenen Effekte vermieden und die Reproduzierbarkeit der Messung ist gewährleistet. Zusätzlich wird die Membranpermeation durch das Rühren erhöht und vom Beginn

des Experiments an konstant gehalten. Dies führt zu sensitiveren Messungen der verschiedenen kinetischen Prozesse im PTDR und ermöglicht die mathematische Berechnung der Freisetzung von Wirkstoffen aus verschiedenen Arzneistoffträgern unter Annahme einer konstanten Membranpermeation [5, 82]. Zusätzlich ist die Bestimmung der Freisetzungsrate nur unter der Voraussetzung möglich, dass die Membranpermeation schneller ist als die Freisetzung selbst. Um den Effekt der Umdrehungsgeschwindigkeit auf die Membranpermeation zu untersuchen, wurde die diese von 0 bis100 UPM variiert.

Ohne Rühren zeigte die Permeation von Diclofenac eine Verzögerung (*lag time*), bis eine konstante Diffusionsrate (*steady state)* erreicht wurde (Abbildung 8). Dies ist für Diffusionsprozesse typisch. Im Vergleich zu den unter Rühren ermittelten Permeationskurven zeigte das Permeationsprofil ohne Rühren eine Verzögerung am Anfang des Experimentes. Dabei betrug die kumulative Freisetzung nach 15 min nur 5 %. Im Vergleich dazu wurden unter Rühren nach 7,5 min schon 10 % der eingesetzten Dosis im Akzeptorkompartiment wiedergefunden. Dieser Unterschied von circa 10-20 % blieb über die ganze Permeation der ersten 4 h bestehen und verdeutlicht den großen beschleunigenden Einfluss der Drehzahl auf die Membranpermeation (Abbildung 8). Der Unterschied in der Dialyserate (permeierter Wirkstoff pro Zeiteinheit) spiegelte sich auch in der Zeit bis zum Erreichen eines Equilibriums wider (Plateauphase). Diese wurde ohne Rühren nach 6 h erreicht und unter Rühren bereits nach 4 h (Abbildung 8). Eine Erhöhung der Drehzahl von 25 UPM auf 50 UPM führte zu einer beschleunigten Permeation. Dies zeigte sich auch in einer erhöhten Membranpermeationskonstante k_M (Tabelle 4). Eine weitere Erhöhung der Drehzahl auf 100 UPM veränderte die Permeationsrate nicht.

Da weitere Parameter wie die physikochemischen Eigenschaften des Wirkstoffs, das Membranmaterial und der MWCO auch einen Einfluss auf k_M haben, können keine allgemeingültigen Empfehlungen für einen Freisetzungstest gegeben werden. Trotzdem zeigte die Untersuchung, dass Umdrehungsgeschwindigkeiten über 50 UPM die Permeation nicht unbedingt verbessern. Zusätzlich können hohe Umdrehungszahlen zu erhöhten Scherkräften im Donorkompartiment führen, die die Freisetzungsmechanismen der Formulierung negativ beeinflussen können (Disruption einer Liposomenmembran). Deshalb sollte eine geeignete Umdrehungsgeschwindigkeit als Kompromiss zwischen Stabilität der Formulierung unter Scherkräften und einer ausreichend hohen und konstanten Membranpermeation getroffen werden. Dabei kann diese zwischen 25 und 100 UPM liegen, wobei 50 UPM empfohlen werden.

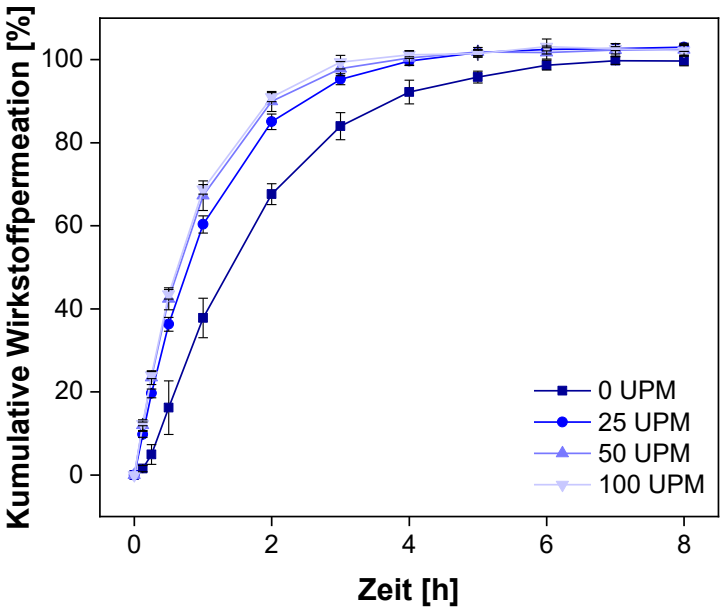

Abbildung 8: *Mittelwertsprofile einer Permeation einer Diclofenac-Lösung bei 37 °C mit einer Dialysemembran aus regenerierter Cellulose (MWCO 50 kDa). Die Umdrehungszahlen wurden zwischen 0 bis100 UPM variiert (n = 6). Abbildung modifiziert nach [101].*

3.2.1.5 Untersuchung der Selektivität von verschiedenen Größenfraktionen im Dispersion Releaser

Schwerlösliche Stoffe werden im Körper häufig proteingebunden oder in Form von Komplexen aus Proteinen und Lipiden (Lipoproteine) im Blutkreislauf transportiert. Dadurch verbessert sich ihre Löslichkeit. Für die Bindung von Arzneistoffen spielt dabei vor allem das humane Serumalbumin eine wichtige Rolle. Arzneistoffe interagieren mit diesem Protein an verschiedenen unspezifischen Bindungsstellen über ionische oder hydrophobe Interaktionen [105]. Diese Interaktion wird mit der Plasmaproteinbindung charakterisiert.

Aufgrund einfacherer Verfügbarkeit wurde in den hier beschriebenen Untersuchungen auf das bovine Serumalbumin (BSA) zurückgegriffen. Nachgewiesenermaßen sind die Unterschiede zwischen dem vom Menschen und dem vom Rind stammenden Albumin nur gering [104]. Laut Literatur verfügt Diclofenac über eine Plasmaproteinbindung von mindestens 99 %, wobei das stöchiometrisches Verhältnis von Wirkstoff zu Protein 2:1 beträgt [105, 115]. Im Folgenden wurden verschiedene Proteinkonzentration dem Medium zugesetzt, um die Trennung der verschiedenen Wirkstofffraktionen im PTDR zu untersuchen. Da BSA ein Molekulargewicht von 66,5 kDa hat, wird es von der 50 kDa

RC-Dialysemembran zurückgehalten. Dabei kann die frei gelöste Fraktion des Diclofenacs die Membran passieren, wobei die Permeation des an BSA gebundenen Diclofenacs innerhalb der ersten 8 h nicht möglich ist und im Donorkompertiment zurückgehalten wird (vgl. Kapitel 3.2.1.2).

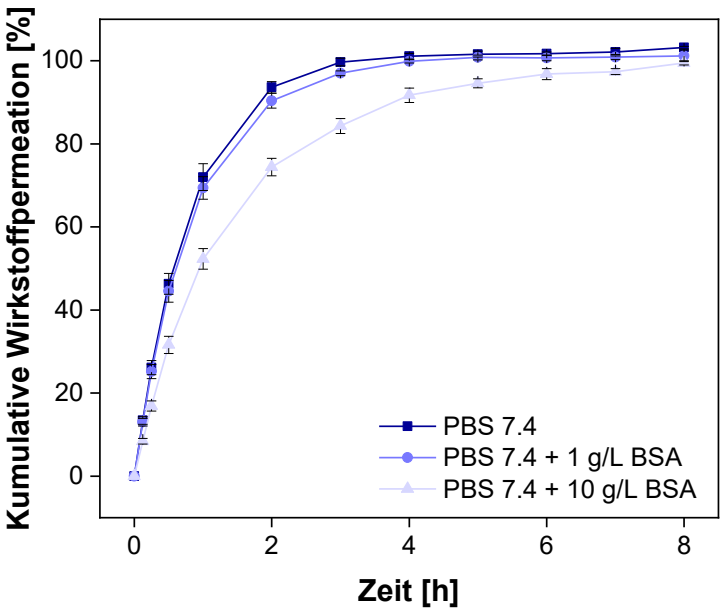

Abbildung 9: *Kumulative Permeation einer Diclofenac-Lösung mit verschiedenen BSA-Konzentrationen in PBS 7,4. Die Permeation erfolgte bei 37 °C, 100 UPM und mit einer Dialysemembran aus regenerierter Cellulose (MWCO 50 kDa). Mittelwerte ± SD sind dargestellt (n = 6). Abbildung modifiziert nach [101].*

Es wurden zwei verschiedene BSA-Konzentrationen (1 g/L und 10 g/L) auf Basis des Ph. Eur. ausgewählt und in phosphatgepufferter Salzlösung (PBS) mit einem pH von 7,4 gelöst. Beide Konzentrationen liegen unterhalb der physiologischen Albuminkonzentration von ungefähr 40 g/L. Nachdem Diclofenac-Natrium in den verschiedenen Puffern gelöst wurde, wurden die Permeationsprofile bei 100 UPM ermittelt. Diese sind in Abbildung 9 dargestellt. Um eine quantitative Auswertung zu erhalten, wurde zusätzlich die Fläche unter den verschiedenen Permeationskurven (AUC) berechnet (Tabelle 3). Das Permeationsprofil mit der geringeren BSA-Konzentration zeigte keinen signifikanten Unterschied im Vergleich zum proteinfreien Permeationsprofil. Die beiden AUC waren identisch. Unter Berücksichtigung des stöchiometrischen Verhältnisses zwischen BSA und Diclofenac werden etwa 0,7 % des Diclofenacs am Protein innerhalb des Donorkompartiments gebunden. Da Diclofenac nicht kovalent am BSA gebunden ist, ist die Retention nicht groß genug, um einen Unterschied festzustellen. Bei der Verwendung von 10 g/L BSA können 7 % des Diclofenacs im Donorkompartiment an Albumin gebunden und zurückgehalten werden. Dies spiegelte sich im Permeationsverlauf wider. Das Profil zeigte eine deutlich verlangsamte Permeation und das Equilibrium lag unterhalb von 100 %.

Vergleicht man die Flächen unter den Permeationsprofilen, ergab sich ein Verhältnis zwischen 10 g/L und 0 g/L BSA von 0,91 ± 0,02. Das ermittelte Verhältnis stimmte somit, im Rahmen des analytischen Fehlers, in etwa mit dem theoretischen Verhältnis von 0,93 überein. Damit erlaubt der PTDR eine Unterscheidung zwischen freiem und an Protein gebundenem Wirkstoff.

Tabelle 3: *Berechnete Flächen unter der Kurve (AUC) für Permeationsprofile von Diclofenac-Natrium in PBS 7,4 mit verschiedenen BSA-Konzentrationen (n = 6).*

Medium	AUC (0-8 h) [µg h/mL]	SD [µg h/mL]	Verhältnis
PBS 7,4 + 0 g/L BSA	292	2	-
PBS 7,4 + 1 g/L BSA	292	2	1,00 ± 0,01
PBS 7,4 + 10 g/L BSA	265	4	0,91 ± 0,02

Um die Möglichkeit des Unterschiedes zwischen den beiden Wirkstofffraktionen sicher unterscheiden zu können, muss die Untersuchungszeitraum beachtet werden. Wie in Kapitel 3.2.1.2 diskutiert, zeigte sich nach einigen Stunden eine erhöhte Permeation von BSA durch die Dialysemembran, weshalb die Experimente zur Untersuchung von verschiedenen Größenfraktionen von Wirkstoffen mit BSA-haltigen Medien nicht über 15 h andauern sollten. Eine Möglichkeit den analytischen Fehler zu reduzieren, kann die Auswahl einer Membran mit verringertem MWCO, wie 20 kDa, sein. Die freie Permeation des Diclofenacs wird dadurch nicht wesentlich behindert und erlaubt eine verbesserte Unterscheidung zwischen freiem und proteingebundenem Wirkstoff.

3.2.2 Analyse der Membranpermeationskonstante mit Hilfe eines mathematischen Modells

Die Bestimmung der Permeationsrate einer Wirkstofflösung wird benötigt, um die Membranpermationskonstante k_M zu berechnen. Die Konstante ist ein Maß für die Sensitivität einer dialysebasierten Methode und beschreibt den analytischen Fehler, der durch die Membran verursacht wird. Zusätzlich wird k_M zur Normalisierung eingesetzt, um die Membranpermeation bei der Freisetzungsuntersuchung aus kleinstpartikulären Arzneistoffträgersystems abzuziehen und damit die tatsächliche Wirkstofffreisetzung zu berechnen. Die Normalisierung eines Permeationsprofils ist für die Vergleichbarkeit vor allem bei der Verwendung von Dialysemembranen von verschiedenen Herstellern relevant. Dazu ist das setzen einer Spezifikation für k_M hilfreich, um den Austausch verschiedener Hersteller zu überwachen.

Ein Ziel dieser Dissertation war die Integration des mathematischen Modells zur Berechnung der Wirkstofffreisetzung im PTDR in Stella Architect®, um die *in vitro* Freisetzung in bestehende pharmakokinetische Modelle zu integrieren und IVIVC zu ermöglichen [116]. Die Berechnung der Membranpermationskonstanten k_M erfolgt über Gleichung 11 auf Basis der Bestimmung der totalen Membranpermeationskonstante k_T, die nur von Geräte- und Versuchsparametern abhängig ist (Volumen des Donor und Akzeptors, Dialysemembran).

$$k_T = \frac{ln\left(1 - \frac{C_a(t)}{C_\infty}\right)}{t} = \left[\frac{A \cdot k_M \cdot (V_a(t) + V_d)}{\delta \cdot V_a \cdot V_d}\right] \tag{11}$$

Die Berechnung in Stella Architect® erfolgt über eine lineare Extrapolation, um ein kontinuierliches Profil über die ermittelten Wirkstoffkonzentrationen im Akzeptorkompartiment anzunähern. Dazu wird alle 3 s ein Wert für k_T für extrapolierte zwischen den gemessenen Werten berechnet. Die Membranpermeationskonstante k_M kann durch Umstellen der Gleichung 6 aus k_T wie folgt ermittelt werden (Gleichung 12):

$$k_M = \left[\frac{k_T \cdot \delta \cdot V_a \cdot V_d}{A \cdot (V_a(t) + V_d)}\right] \tag{12}$$

Jedes Dialysat hat dabei, abhängig von den Versuchsbedingungen (Umdrehungszahl, Dialysemembran, Temperatur, Freisetzungsmedium, Volumen, Anfangskonzentration), eine eigene Membranpermeationskonstante k_M. Trotzdem kommt es zu Abweichungen von der erwarteten Kinetik 1. Ordnung während des Experiments. Dies betrifft vor allem Zeitpunkte am Beginn und am Ende der Permeation. Zu Beginn der Permeation können kleine Temperaturschwankungen durch die Injektion der Probe in das Donorkompartiment und die Adsorption des Wirkstoffs an der Membran einen verlangsamenden Einfluss haben. Adsorptionsuntersuchungen des Wirkstoffs an verschiedenen Membranen sind deshalb essentieller Bestandteil von Vorversuchen, um eine optimale Dialysemembran auszuwählen. In der Plateauphase am Ende des Permeationsversuches können die mit der HPLC ermittelten Ergebnisse aufgrund der zufälligen Streuung eine höhere Variabilität aufweisen.

Um diese Phänomene bei der Berechnung von k_M auszugleichen, wurde im Modell ein durchschnittlicher Wert im Bereich von 15 % bis 85 % Wirkstofffreisetzung für k_M mit Gleichung 13 berechnet.

$$\overline{k_M} = \frac{1}{n_{15\,\%-85\,\%}} \cdot \sum_{85\,\%}^{15\,\%} k_M \tag{13}$$

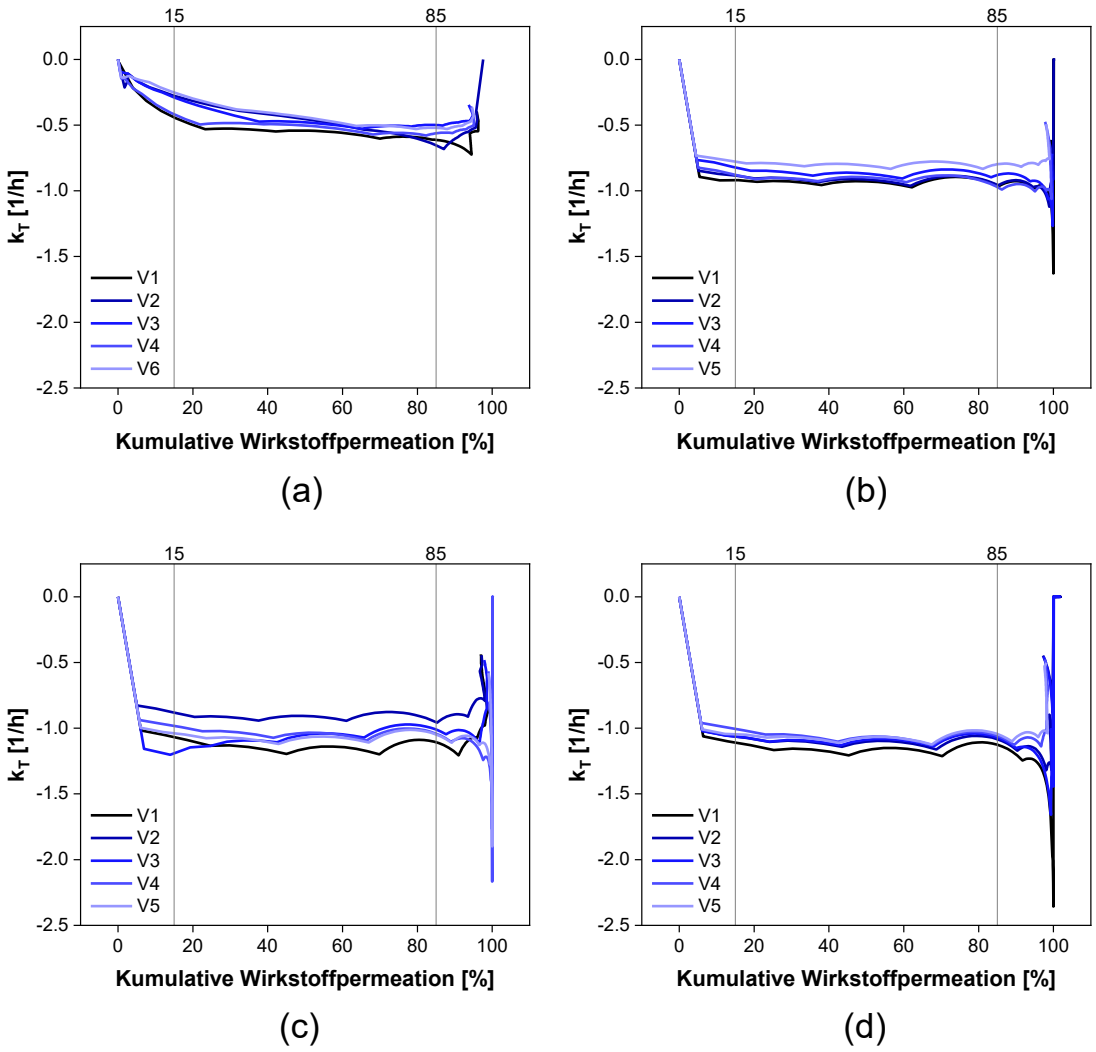

Abbildung 10: *Darstellung der berechneten k_T-Werte mit dem in silico Modell in Abhängigkeit der kumulierten Wirkstoffpermeation. Die Berechnung erfolgte für eine Diclofenac-Lösung bei 0 UPM (a), 25 UPM (b), 50 UPM (c) und 100 UPM (d). Abbildung modifiziert nach [101].*

In diesem Bereich der Freisetzung wurde ein *steady state* erreicht und die Werte für k_T waren konstant (Abbildung 10). Die Permeationsversuche mit Diclofenac in PBS 7,4 mit variierenden Umdrehungszahlen von 0 UPM bis 100 UPM wurden dazu ausgewertet. Dabei zeigte sich eine verringerte Variabilität bei 100 UPM. Wurden die beiden Kompartimente im PTDR nicht gerührt, gab es einen kleineren konstanten Bereich (40 % bis 85 %) für die im mathematischen Modell ermittelten k_T-Werte. Die ermittelten Durchschnittswerte von k_M für die durchgeführten Versuche sind in Tabelle 4 zusammengefasst. Die Membranpermationkonstante verdoppelte sich annähernd beim Wechsel von 0 UPM auf 25 UPM (von 0,99 ± 0,9 x 10^{-3} cm²/h auf 1,76 ± 0,10 x 10^{-3} cm²/h). Der Wert von k_M erhöhte sich weiter auf 2,13 ± 0,18 x 10^{-3} cm²/h bei 50 UPM und blieb bei weiterer Erhöhung der Umdrehungszahl auf 100 UPM konstant (2,17 ± 0,09 x 10^{-3} cm²/h). Dabei unterschieden sich die Werte von k_M bis auf bei den Umdrehungszahlen 50 UPM und

100 UPM signifikant (ANOVA, $p < 0,05$), was den großen Einfluss des Rührens auf die Permeation, vor allem im niedrigen Bereich, belegt.

Um die neue Methode zur Berechnung der Membranpermeationskonstante zu überprüfen, wurde eine interne Validierung durchgeführt. Dazu wurde mit Hilfe von Stella Architect® ein *in silico* Modell für den Permeationsprozess im PTDR geschrieben. Grundlage war dabei das Fick'sche Diffusionsgesetz und die an den PTDR angepasste Gleichung 5. Mit den in Tabelle 4 ermittelten Durchschnittswerten von k_M (die Werte für die Volumina des Donor- und Akzeptorkompartiment sowie die verdunstete Menge Freisetzungsmedium wurden aus den Beobachtungen der eingesetzten fünf Vessel gemittelt) wurde ein Permeationsprofil für die Wirkstoffkonzentration im Akzeptor- und Donorkompartiment simuliert. Zur Bewertung der Simulationsgüte wurde der *absolute average fold error* (AAFE) berechnet (Gleichung 14) [117].

$$AAFE = 10^{\frac{1}{n} \cdot \sum |\log \frac{Simulierter\ Wert_t}{Gemessener\ Wert_t}|} \quad (14)$$

Dazu wurden die Unterschiede von den simulierten Werten zu den quantifizierten Werten an den Probenzugzeitpunkten verglichen [71, 95, 98, 118-120]. Nimmt der AAFE einen Wert von eins an, sind die simulierten und beobachteten Daten identisch. Im Allgemeinen wird ein AAFE-Wert von bis zu zwei für eine akzeptable Simulation angenommen [118, 119].

Tabelle 4: Berechnete Membranpermeationskonstanten k_M einer Diclofenac-Lösung in PBS 7,4 bei verschiedenen Umdrehungszahlen. Jede Berechnung wurde mit fünf Vessel und 5-6 Messzeitpunkten (im Bereich 15 % bis -85 % Wirkstofffreisetzung) durchgeführt (n = 25 oder n = 30). Mit den berechneten Werten für k_M wurden Permeationen simuliert. Für alle Umdrehungszahlen wurde das simulierte Permeationsprofil im Akzeptorkompartiment mit allen ermittelten Wirkstoffkonzentrationen mit der Berechnung des AAFE bewertet. Bei 100 UPM wurde zusätzlich das simulierte Permeationsprofil mit den ermittelten Konzentrationen im Donorkompartiment verglichen (Zeitpunkte: 15 min, 30 min, 120 min). *Tabelle modifiziert nach [101].*

Drehzahl	k_M [cm²/h]	SD [cm²/h]	AAFE
0 UPM	$0,99 \times 10^{-3}$	$0,9 \times 10^{-3}$	1,27
25 UPM	$1,76 \times 10^{-3}$	$0,10 \times 10^{-3}$	1,03
50 UPM	$2,13 \times 10^{-3}$	$0,18 \times 10^{-3}$	1,03
100 UPM	$2,17 \times 10^{-3}$	$0,09 \times 10^{-3}$	1,03 (Akzeptor) 1,23 (Donor)

Die simulierten Permeationsprofile (Abbildung 11, blaue Linie) stimmten mit den quantifizierten Werten (Abbildung 11, blaue Quadrate) sehr gut überein (AAFE = 1,03). Für die Permeation unter statischen Bedingungen lag der AAFE bei 1,27. In Abbildung 11 kann man erkennen, dass die Simulation die Permeation anfänglich überschätzte, im weiteren

Verlauf aber unterschätzte. Dies liegt an der bereits diskutierten Verzögerung der Diffusion zu Versuchsbeginn. Zusätzlich wurde für 100 UPM eine Auswertung des Donorkompartiments mit den quantifizierten Zeitpunkten 15 min, 30 min und 120 min vorgenommen. Dabei ergab sich beim Vergleich der simulierten mit den gemessenen Datenpunkten ein AAFE von 1,23 (Tabelle 4). Für diese Überschätzung der simulierten Wirkstoffkonzentrationen im Donorkompartiment kann die Adsorption des Diclofenacs an der Dialysemembran verantwortlich sein (Abbildung 11d, rote Linie und rote Dreiecke). Trotzdem liegt der AAFE im akzeptablen Bereich und die Berechnung von k_M in Stella Architect® ist mit dem neuen Modell zuverlässig.

Um die die Berechnung der Membranpermeationskonstante zu erleichtern, wurde ein webbasiertes Nutzer-Interface mit Stella Architect® (*Dialysis Membrane Permeation Calculator*[1] (DiMeC)) entwickelt. Dieses ist unter *Commons Creative License* frei verfügbar und bietet die Möglichkeit, die versuchsspezfischen Parameter direkt darin einzugeben. Im Anschluss erfolgt die Berechnung automatisch.

[1] Website zur Nutzung des DiMeC: https://exchange.iseesystems.com/public/matthiaswacker/dimec/index.html#page1
(zuletzt aufgerufen am 07. März 2023)

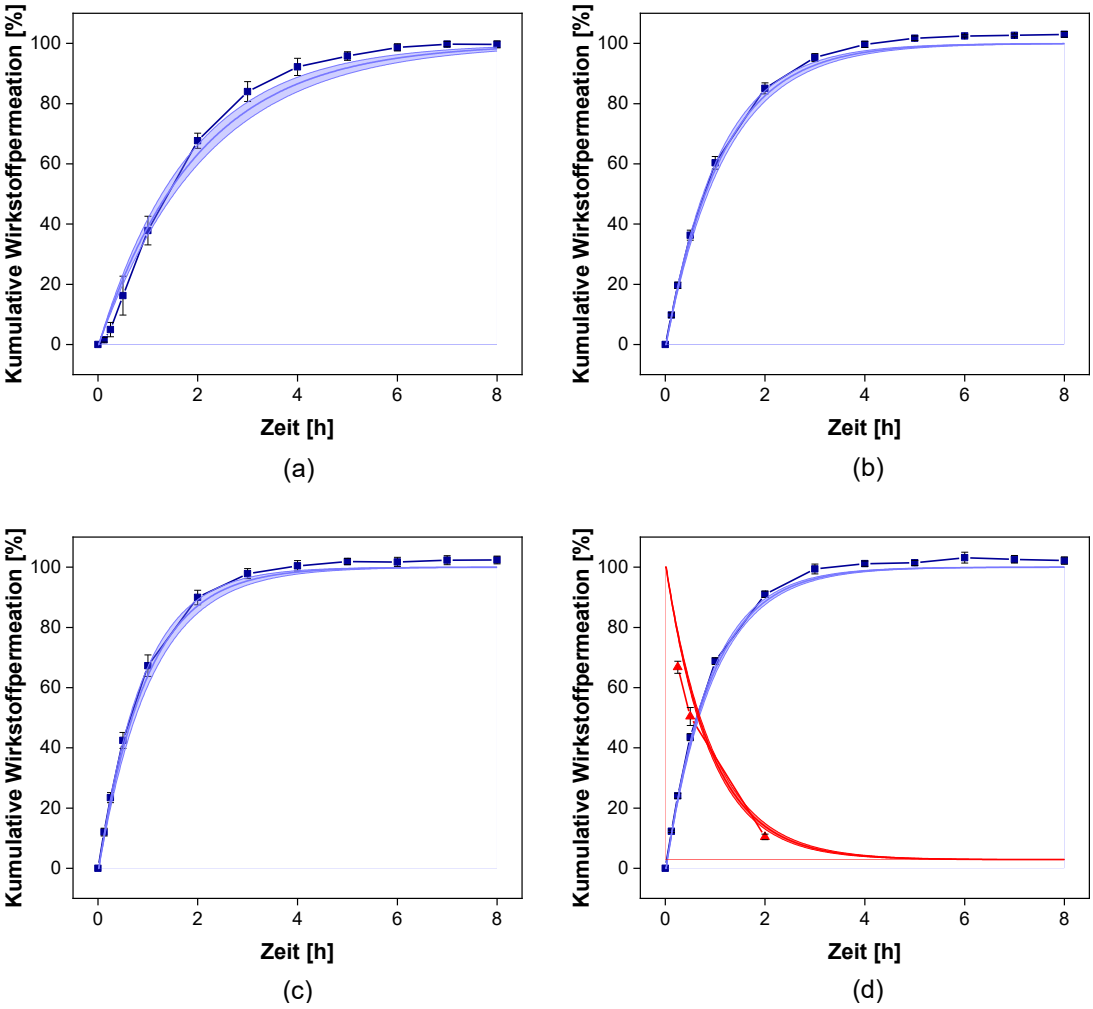

Abbildung 11: *Vergleich der ermittelten kumulativen Wirkstoffpermeationen einer Diclofenac-Lösung anhand simulierter Permeationsprofile bei (a) 0 UPM, (b) 25 UPM, (c) 50 UPM und (d) 100 UPM. Blaue Quadrate stellen die Mittelwerte ± SD der ermittelten Diclofenac-Permeation dar (n = 6). Die hellblaue Linie symbolisiert die mit dem in silico Modell berechnete Permeation. Die Konzentration des Donorkompartiments wurde in (d) zusätzlich ausgewertet. Die roten Quadrate stellen die ermittelten Konzentrationen im Donor dar (Mittelwert ± SD, n = 6). Die hellrote Linie ist die korrespondierende Berechnung mittels mathematischem Modell. Abbildung modifiziert nach [101].*

3.2.3 Leistungsqualifizierung des Dispersion Releasers

3.2.3.1 Einfluss von Hilfsstoffen auf die Permeation

Formulierungen enthalten für unterschiedliche Zwecke Hilfsstoffe. Vor allem halbfeste Zubereitung haben eine hochkomplexe Zusammensetzung mit vielen verschiedenen lipophilen und hydrophilen Komponenten. Diese können sich an die Dialysemembran adsorbieren und die Wirkstoffpermeation verändern. Dadurch wird die mit der aus einer

Wirkstofflösung ermittelten Membranpermeationskonstante k_M berechnete Wirkstofffreisetzung verfälscht. Um den Einfluss der verschiedenen Hilfsstoffe zu untersuchen, wurde Voltaren® Emulgel in die Donorkammer eingewogen und mit PBS 7,4 verdünnt. Nach 24 h war die Freisetzung abgeschlossen und dieselbe Menge Diclofenac wurde als Lösung in das Donorkompartiment hinzugegeben. Die Permeation wurde anschließend für weitere 24 h untersucht (Abbildung 12a). Die Permeation des Diclofenacs erfolgte rasch, da es im vorliegenden Puffer sehr gut löslich war. Nach Hinzufügen der Diclofenac-Lösung wurden keine signifikanten Unterschiede zwischen den beiden Permeationen festgestellt (Abbildung 12b). Damit verursachten die Hilfsstoffe weder Veränderungen an der Dialysemembran noch der Permeationsrate des Wirkstoffs. Dies war Voraussetzung für die Berechnungen unter Annahme einer konstanten Membranpermeationskonstante k_M im nächsten Schritt. Zu festgelegten Zeitpunkten wurden die Vessel mit dem PTDR über 48 h fotographisch aufgezeichnet (Abbildung 13). Visuell konnte kein Austritt der halbfesten Zubereitung aus dem Donorkompartiment festgestellt werden, wodurch die These zweier abgetrennter Kompartimente gestützt wurde.

Im Gegensatz zum PTDR zeigen andere dialysebasierte Freisetzungssysteme ein „Verstopfen“ der Membran, was die Freisetzung negativ beeinflusst. Durch das konstante Mischen des Donorkompartiments im PTDR werden Einflüsse durch Hilfsstoffe auf die Dialysemembran vermieden und die Zuverlässigkeit des PTDR bestätigt. Zusätzlich dient der hier etablierte Versuch einer nachträglichen Injektion einer Wirkstofflösung als Anleitung für die Entwicklung einer Methodenvalidierung für zukünftige Anwender.

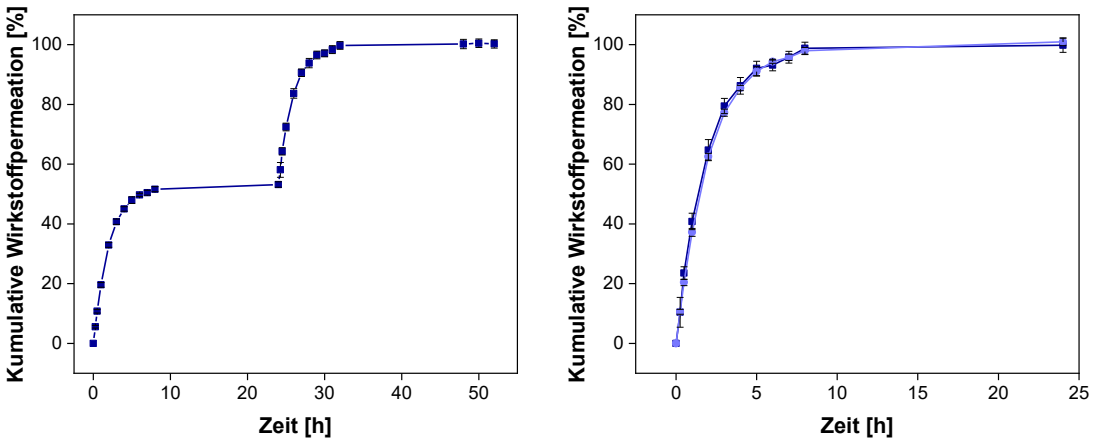

Abbildung 12: *Kumulative Freisetzung von Diclofenac-Diethylammonium aus einem Emulgel mit anschließender Injektion einer Diclofenac-Diethylammonium-Lösung nach 24 h. In (a) ist das gesamte Profil über 48 h dargestellt. In (b) wurden die beiden Permeationsprofile übereinandergelegt. Dargestellt sind Mittelwerte ± SD (n = 3). Abbildung modifiziert nach [101].*

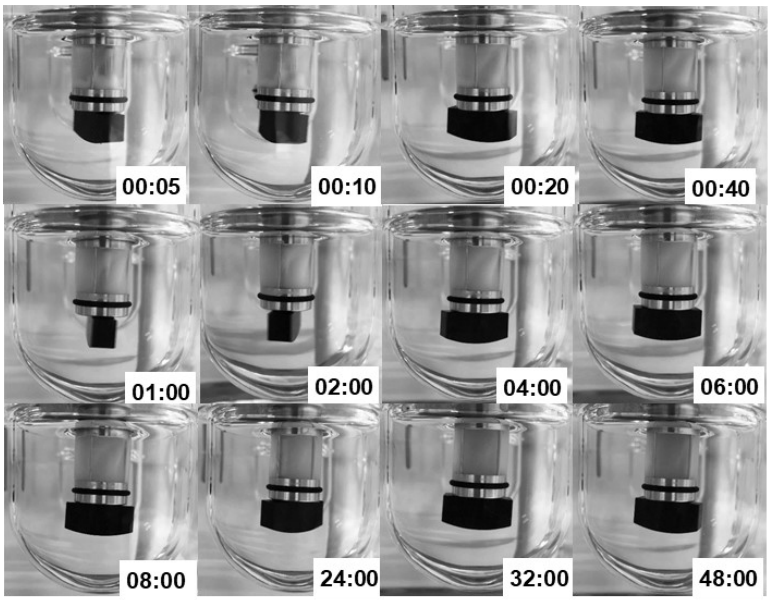

Abbildung 13: *Aufnahme des Donorkompartiments während des Permeationsexperiments mit Voltaren® Emulgel. Die Zeitangaben sind im Format Stunden:Minuten.*

3.2.3.2 Wirkstofffreisetzung aus zwei verschiedenen halbfesten Zubereitungen von Diclofenac

Die beiden halbfesten Zubereitungen unterschieden sich in ihrer Liste in den verwendeten Hilfsstoffen und dem verwendeten Salz des Diclofenacs. Im Falle des Voltaren® Emulgels wurde Diclofenac-Diethylammonium in einem Gel mit Fettanteil eingearbeitet. Im Gegensatz dazu besteht Olfen® Gel (Mepha Pharma AG, Basel, Schweiz) aus Diclofenac-Natrium und enthält keine lipophile Komponente (Tabelle 5). Die Löslichkeit des Diclofenacs spielt bei der Freisetzung eine wesentliche Rolle. Zwischen den beiden Gelen gab es bei der Wirkstofffreisetzung unter *sink*-Bedingungen keine signifikanten Unterschiede. Um die Leistung des PTDR zu untersuchen, wurde das Medium für die Freisetzung an den pH-Wert der Haut (pH 5 bis 6) angepasst [121]. Trotzdem stellen die Bedingungen des Freisetzungstests nicht die physiologischen Bedingungen für eine topische Anwendung auf der Haut, bezogen auf die Umdrehungsgeschwindigkeit des zur Verfügung stehenden Flüssigkeitsvolumens und auf die Pufferkapazität, dar. Allerdings kann die Freisetzungsuntersuchung im PTDR bei der zur Untersuchung des Einflusses der verwendeten Hilfsstoffe eine nützliche Hilfestellung sein. Dies kann ferner die Auswahl der zu verwendenden Hilfsstoffe unterstützen.

Unter *non-sink*-Bedingungen zeigten die beiden Gele Unterschiede in ihrer Wirkstofffreisetzung. Die kumulative Wirkstofffreisetzung von Voltaren® Emulgel und Olfen® Gel ist

in Abbildung 14 dargestellt. Das linearkolloidale Hydrogel des Olfen® Gels zeigte im Vergleich zum Emulgel eine verlangsamte Freisetzung und erreichte nach 48 h etwa 40 % Freisetzung. Das im Olfen® Gel enthaltene Isopropanol sorgt für die Lösung von Diclofenac-Natrium in der Formulierung. In der Freisetzungsuntersuchung fehlt allerdings eine ausreichende Menge Isopropanol, sodass Diclofenac ausfällt. Das wurde im durchgeführten Versuch beobachtet und erklärt die langsame Freisetzung. Im Gegensatz dazu zeigt Voltaren® Emulgel eine schnellere Freisetzung und erreichte nach 48 h 60 % kumulierte Wirkstofffreisetzung. Dies entsprach der reduzierten Löslichkeit im schwach saureren Medium bei 32 °C (0,0314 ± 0,0008 mg/mL für Diclofenac-Natrium und 0,0332 ± 0,0020 mg/mL für Diclofenac-Diethylammonium) [101]. Die Verbesserung der Löslichkeit durch Tenside im Emulgel sorgte für die schnellere und, unter Einbezug der verminderten Löslichkeit, vollständige Freisetzung. Es konnte kein verzögernder Effekt der Emulsion festgestellt werden. Der Effekt der Hilfsstoffe auf die Permeation bei der topischen Anwendung auf der Haut ist mit Hilfe geeigneter Methoden zu evaluieren.

Tabelle 5: *Weitere Inhaltsstoffe der verwendeten Fertigarzneimittel Voltaren® Emulgel und Olfen® Gel (Vorhandensein durch "X" markiert). Tabelle modifiziert nach [101].*

Hilfsstoff	Voltaren® Emulgel	Olfen® Gel
Milchsäure		X
Diisopropyladipat		X
Isopropanol	X	X
Natriummetabisulfit		X
Hydroxyethylcellulose		X
Hydroxypropylcellulose		X
Diethylamin	X	
Propylenglykol	X	
Mineralöl	X	
Cocoylcaprylocaprat	X	
Polyoxyl-20-cetostearylether	X	
Carbomer	X	
Parfümcreme	X	
Gereinigtes Wasser	X	X

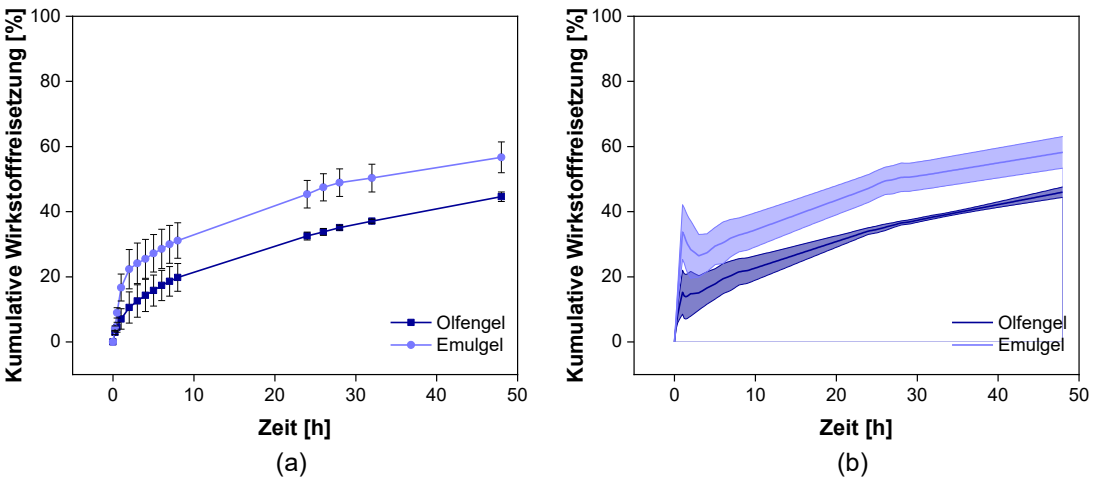

Abbildung 14: *Kumulative Freisetzungsprofile von zwei verschiedenen Diclofenac-Gelen (Olfen® Gel und Voltaren® Emulgel®) in non-sink-Bedingungen. Die gemessene Diclofenac-Konzentration im Akzeptorkompartiment (a) ist der normalisierten Freisetzung (b) gegenübergestellt. Dargestellt sind die Mittelwerte ± SD (n = 4).*

Zur finalen Auswertung der Freisetzung aus halbfesten Zubereitungen mit dem PTDR wurde eine Normalisierung durchgeführt. Dazu wurde die mit Stella Architect® berechnete Membranpermeationskonstante k_M für Diclofenac-Natrium und Diclofenac-Diethylammonium genutzt (vgl. Kapitel 3.2.2). Diese betrugen 1,54 ± 0,12 x 10^{-3} cm²/h für das Natriumsalz beziehungsweise 1,75 ± 0,19 x 10^{-3} cm²/h für das Diethylammoniumsalz [101]. Mit Hilfe des Modells in Stella Architect® konnte die Membranpermeation aus dem Permeationsprofil subtrahiert und eine Wirkstofffreisetzung mit dem Modell PTDR *Release Normalizer*[2] (PTDR ReNo) im Donorkompartiment bestimmt werden. Das normalisierte Freisetzungsprofil ist in Abbildung 14b dargestellt. Bei beiden Gelen wurde eine anfängliche, schlagartige Freisetzung des Diclofenacs festgestellt. Diese war beim Olfen® Gel mit 16 % etwa halb so groß wie beim Voltaren® Emulgel. Anschließend zeigten beide Gele ab 5 h eine konstante Zunahme des freigesetzten Diclofenacs, was einer langsamen Auflösung entsprach. Damit ist vor allem die Löslichkeit des Wirkstoffs zum Ende der Freisetzung geschwindigkeitsbestimmend, wohingegen der Hilfsstoffeinfluss zu Beginn am größten ist.

[2] Die Normalisierung des Freisetzungsprofils ist unter folgender Website für die Öffentlichkeit zugänglich:
https://exchange.iseesystems.com/public/matthiaswacker/ptdr-reno/index.html#page1
(zuletzt aufgerufen am 07. März 2023)

3.3 Dokumentation der Parameter eines Freisetzungstests

Während der Validierung des PTDRs sind viele Parameter untersucht worden, die einen Einfluss auf die Membranpermeation haben. Diese sind bei einer Methodenentwicklung ausreichend zu charakterisieren und zu dokumentieren. Bei vielen Dialyseexperimenten in der Literatur sind die Versuchsbedingungen allerdings nur unzureichend dokumentiert. Auf Grundlage der beschriebenen Versuche werden in Tabelle 6 relevante Parameter vorgeschlagen, die für eine vollständige Dokumentation von dialysebasierten Freisetzungsexperimenten notwendig sind. Dazu gehören neben Medienkomposition, Freisetzungstemperatur auch Informationen zu den Volumina des Akzeptor- und Donorkompartiments. Zusätzlich sollte neben den typischen Parametern einer Dialysemembran, wie MWCO und Material, auch die Membranoberfläche und das Protokoll zur Vorbereitung der Membran des Membranherstellers für den Versuch dokumentiert werden. Dabei kann vor allem bei trockenen Dialysemembranen, die Glycerin enthalten, das unzureichende Rehydrieren eine Rolle spielen. Bei unzureichenden Abspülen des Glycerins können Reste einen störenden Einfluss auf die Membrankinetik haben [85]. Zusätzlich sollte auch genau festgehalten werden, wie die verschiedenen Proben in die Donorkammer eingebracht werden (Injektionsprotokoll). Der Ablauf zur Bestimmung der Wirkstofffreisetzung mit den in der Arbeit etablierten Modellen *DiMeC* und *PTDR ReNo* sind in Abbildung 15 dargestellt.

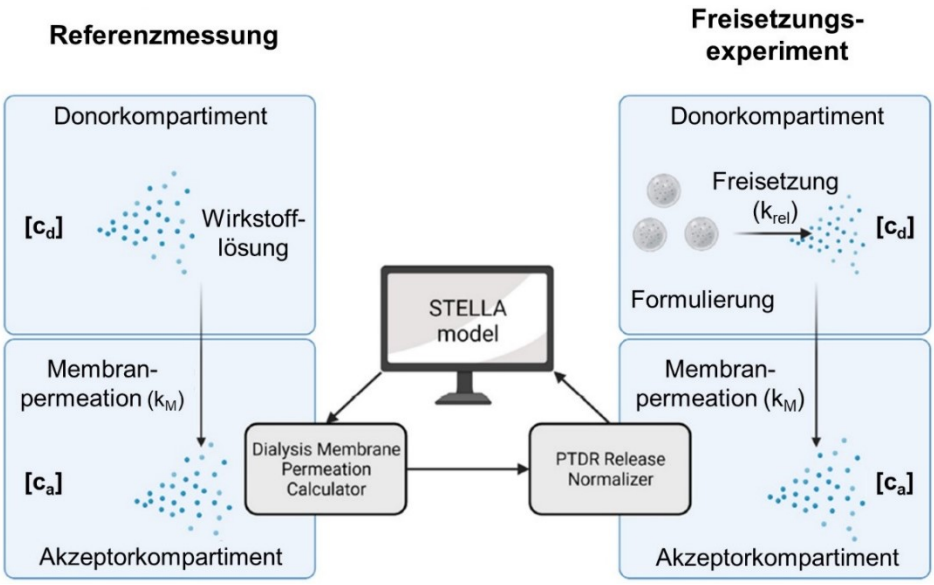

Abbildung 15: *Vorgeschlagener Arbeitsfluss zur Bestimmung der Wirkstofffreisetzung aus Arzneistoffträgern. Zuerst wird ein Referenzexperiment mit einer Wirkstofflösung durchgeführt. Daraus kann mit dem Dialysis Membrane Permeation Calculator die Membranpermeationskonstante k_M bestimmt werden. Zusammen mit k_M und der Freisetzungsuntersuchung der Formulierung kann mit dem PTDR Release Normalizer die Freisetzung des Wirkstoffs berechnet werden. Abbildung modifiziert nach [101].*

Tabelle 6: *Wichtige Versuchsparameter, die zur Dokumentation eines Dialyseexperiments benötigt werden. Tabelle modifiziert nach [101].*

Parameter	Beispiel
Membranmaterial	Regenerierte Cellulose
MWCO	50 kDa
Membrandicke	0,0065 cm
Membrandurchmesser (flach)	28 mm
Lagerbedingungen der Membran	Feucht, in 0,5 % Natriumazid bei 2-8 °C
Vorbereitung der Membran	Abspülen mit Wasser, 30 min in Wasser einweichen
Hersteller	Repligen® (USA)
Volumen des Donorkompartiments (jeweils vor und nach dem Experiment)	3,4 mL
Volumen des Akzeptorkompartiments (jeweils vor und nach dem Experiment)	120 mL
Oberfläche der Donorkammer/Membran	10,95 cm²
Zusammensetzung des Mediums	Unterschiedlich (z. B. PBS 7,4)
Temperatur	32 °C
Umdrehungszahl	50 UPM
Probenvolumen	200 µL
Probenzeitpunkte	Unterschiedlich (z. B. 15 min, 30 min, 60 min etc.)
Referenzexperiment (Wirkstofflösung)	3,4 mL einer Diclofenac-Lösung (1,47 mg/mL, PBS 7,4) wurden injiziert.
Formulierung	Das Gel (entsprechend 5 mg Diclofenac) wurde in die Donorkammer eingewogen und mit restlichem Medium auf 3,4 mL aufgefüllt.

3.4 Untersuchungen eines liposomalen Vaginalgels

Vier verschiedene proliposomale Formulierungen mit der Modellsubstanz Hydrocortison wurden hergestellt, um den Wirkstoff lokal in der vaginalen Umgebung freizusetzen. Dabei wurden die verschiedenen Formulierungen mit einer kommerziell erhältlichen Creme (Ebenol®, Strathmann GmbH & Co. KG, Hamburg, Deutschland) und dem reinen Wirkstoff verglichen. Die Wirkstofffreisetzung und die Permeabilität wurden als Einflussgrößen *in vivo* Performance festgelegt und *in vitro* untersucht. Die Freisetzungsrate des Hydrocortisons aus den verschiedenen Formulierungen wurde mit dem PTDR in simulierter Vaginalflüssigkeit ermittelt. Ein Zellmonoschichtmodell mit zwei verschiedenen Zelltypen, die in der Vagina präsent sind, wurde zur Untersuchung der Permeabilität verwendet. Die verschiedenen proliposomalen Formulierungen wurden zusätzlich noch hinsichtlich ihrer Größe, Polydispersitätsindex (PDI), Zetapotenzial und EE% charakterisiert.

3.4.1 Herstellung und physikochemische Eigenschaften der proliposomalen Formulierungen

In Vorversuchen wurden Sorbitol, sprühgetrocknete Lactose und Sucrose als inertes Trägermaterial getestet. Zusätzlich wurden die eingesetzte Menge des Trägermaterials, das Volumen und die Art des organischen Lösemittels, die Größe des Rundkolbens und die Partikelgröße des Trägermaterials (verschiedene gesiebte Fraktionen) variiert und hinsichtlich der Ausbeute eines rieselfähigen Pulvers nach dem zweiten Sieben des proliposomalen Pulvers und Partikelgröße der hydratisierten Liposomen bewertet. Für die beschriebene Untersuchung wurde Sorbitol als geeignetes Trägermaterial ausgewählt. Sucrose und Lactose waren als sprühgetrocknete Trägermaterialien mit poröser Oberfläche nicht geeignet, weil sich eine geringere Ausbeute rieselfähiger Proliposomen ergab. Im Fall der Sucrose wurde ausschließlich verklebtes Pulver erhalten. Die genauen Zusammensetzungen der vier proliposomalen Formulierungen sind in Tabelle 7 zusammengefasst. Dabei wird der Wirkstoff Hydrocortison mit dem Lipid und gegebenenfalls mit Cholesterin im organischen Lösungsmittel gelöst. Im Anschluss wird gesiebtes Sorbitol hinzugefügt und das Lösemittel im Rotationsverdampfer schrittweise entfernt. Das getrocknete proliposomale Pulver wird nach dem Überführen aus dem Rundkolben erneut gesiebt, um ein rieselfähiges Pulver zu erhalten (Abbildung 16). Zur Untersuchung der Zytotoxizität wurden Referenzformulierungen ohne die Zugabe von Hydrocortison hergestellt.

Tabelle 7: *Zusammensetzung der verschiedenen Proliposomen mit der jeweiligen Ausbeute nach dem zweiten Siebschritt. Die Lipidphase wurde zusammen mit dem Wirkstoff vor der Zugabe des Sorbitols in 8,25 mL einer organischen Lösung aus Chloroform und Methanol (8:2 (V/V)) in einem 100 mL Rundkolben gelöst. Die Ausbeute des erhaltenen, frei fließenden, proliposomalen Pulvers wurde, bezogen auf die eingesetzte Gesamtmasse von 2,75 g, berechnet. Die Referenzformulierungen (Blank) wurden ohne Einwaage von Hydrocortison hergestellt.*

Formulierung	Ei-PC (EPC) [mg]	Soja-PC (SPC) [mg]	Cholesterin (C) [mg]	Hydrocortison (HC) [mg]	Sorbitol [mg]	Ausbeute
EPC	250,0	-	-	15	2,5	69 %
EPC+C	227,3	-	22,7	15	2,5	70 %
SPC	-	250,0	-	15	2,5	66 %
SPC+C	-	227,3	22,7	15	2,5	68 %
Blank EPC	250,0	-	-	-	2,5	78 %
Blank EPC+C	227,3	-	22,7	-	2,5	78 %
Blank SPC	-	250,0	-	-	2,5	80 %
Blank SPC+C	-	227,3	22,7	-	2,5	78 %

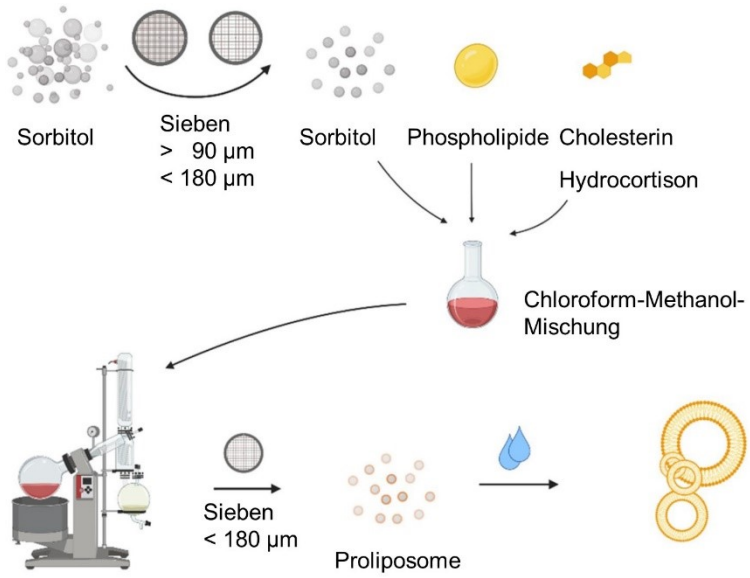

Abbildung 16: *Herstellung der Proliposomen im Rotationsverdampfer mit der Film-auf-Träger-Methode. Abbildung modifiziert nach [122].*

Die Größe und Größenverteilung, das Zetapotenzial, die Verkapselungseffizienz und die Hydrocortison-Konzentration der Proliposome wurde bestimmt (Tabelle 8). Die entstandenen Vesikel hatten bei allen vier Formulierungen eine ähnliche Größe in ihren mittleren Durchmessern. Der Zusatz von Cholesterin (C) erhöhte die Vesikelgröße nur für die Liposomen aus Ei-Phosphatidylcholin (EPC). Der PDI variierte zwischen 0,437 und 0,534 und ließ auf eine breite Verteilung schließen. Durch einen anschließenden Extrusionsschritt an die Hydratisierung können PDI kleiner 0,3 erreicht werden, das unilamellaren, monodispersen Liposomen entsprechen würde [123]. Im vorliegenden Fall sollte

jedoch eine feste Darreichungsform untersucht werden, deren Vesikel *in situ* gebildet werden und deshalb keine kontrollierte Partikelgröße hat. Dies garantiert eine verlängerte physikochemische Haltbarkeit. Trotzdem war der PDI innerhalb des Messbereichs (PDI kleiner 0,7) [123]. Je nach Ursprung des verwendeten Phospholipids (Soja oder Hühner-Ei) veränderte sich das Zetapotenzial. Liposome aus Soja-Phosphatidylcholin (SPC) wiesen schwach negativ geladene Vesikel zwischen -6 mV und -12 mV auf, wohingegen Vesikel aus EPC ein Zetapotenzial von -34 mV hatten (Tabelle 8, $p < 0,05$). Die unterschiedliche Reinheit des SPC und EPC (100 % vs. 80 %) kann ursächlich für die Unterschiede sein. Negativ geladene Partikel sind aufgrund des negativ geladenen Mucins in der Vagina weniger mucoadhäsiv [49, 124]. Andererseits bilden stark mucoadhäsive Formulierungen Agglomerate mit dem Mucin und können so schneller aus der Vagina eliminiert werden. Die vorliegenden proliposomalen Formulierungen zeigten ein stabiles Vesikelsystem.

***Tabelle 8**: Physikochemische Eigenschaften (mittlere Partikelgröße, Polydispersitätsindex (PDI), Zeta-Potential, Verkaspelungseffizienz (EE%) sowie der Hydrocortisongehalt der vier verschiedenen proliposomalen Formulierungen nach Hydratisierung. Die Ergebnisse sind als Mittelwert ± SD dargestellt (n = 3). Der Stern (*) markiert einen statistischen Unterschied im Vergleich zur Formulierung mit EPC (p < 0,05). Tabelle modifiziert nach [122].*

Formulierung	Größe [nm]	PDI	Zeta-Potential [mV]	EE% [%]	Hydrocortison - gehalt [%]
EPC	213 ± 4	0,437 ± 0,016	-34 ± 3	20,4 ± 1,9	0,33 ± 0,02
EPC+C	230 ± 9	0,426 ± 0,014	-34 ± 2	17,9 ± 2,0	0,40 ± 0,04
SPC	215 ± 2	0,448 ± 0,015	-6 ± 1*	28,4 ±0,9*	0,52 ± 0,06
SPC+C	213 ± 4	0,534 ± 0,130	-13 ± 2*	24,5 ± 2,3*	0,43 ± 0,07

Im Gegensatz zur Vesikelgröße hatte der Zusatz von Cholesterin einen Einfluss auf die EE% des Hydrocortisons. Da Cholesterin chemisch mit Hydrocortison verwandt ist, konkurrieren die beiden Moleküle um die gleichen Interaktionsstellen innerhalb der Phospholipidmembran. Bei beiden Phospholipiden EPC und SPC reduzierte sich deshalb erwartungsgemäß die verkapselte Menge an Hydrocortison. Diese fiel jedoch im Falle des EPCs, im Gegensatz zum SPC, nicht signifikant aus. Zusätzlich war die Verkapselungseffizienz bei SPC im Vergleich zu EPC höher (Tabelle 8). Der Hydrocortisongehalt in den Formulierungen variierte zwischen 0,33 % und 0,52 %.

3.4.1.1 Morphologische Charakterisierung der rekonstituierten Proliposomen

Die proliposomalen Formulierungen wurden in Wasser rekonstituiert und die entstandenen Liposomen wurden im Transmissionselektronenmiskroskop (TEM) morphologisch

charakterisiert. Es wurden Vesikel im Größenbereich von 50 nm bis 2500 nm gefunden (Abbildung 17). Da die mikroskopische Methode Vakuum voraussetzt, konnten die Liposome nur im getrockneten Zustand untersucht werden. Dabei reduzierte sich allerdings die Partikelgröße der Liposomen im Vergleich zum hydrodynamischen Durchmesser der Vesikel bei der Messung mittels DLS. Generell unterstützt die mikroskopische Untersuchung aber die Größenmessung mittels DLS.

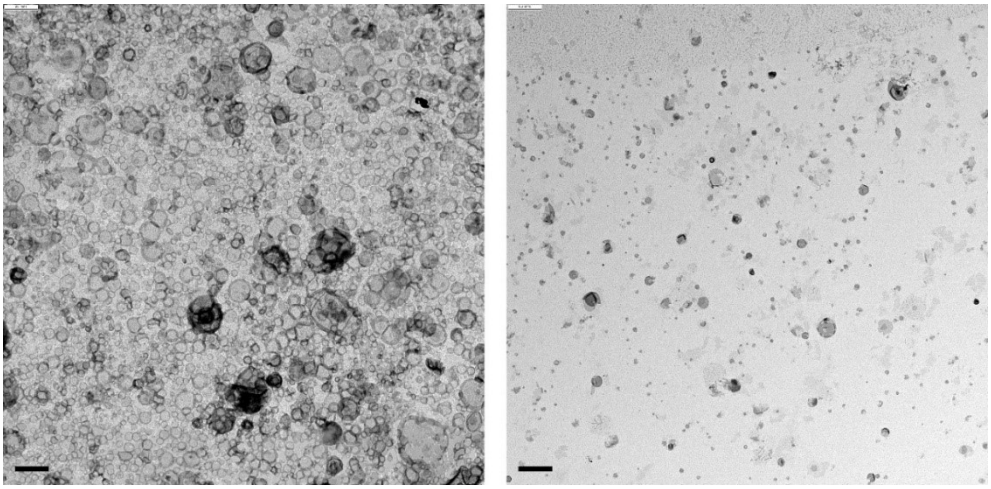

Abbildung 17: *Aufnahmen von den wirkstofffreien Referenzformulierungen SPC (linke Seite) und SPC+C (rechte Seite) mit einem Transmissionselektronenmikroskop. Der schwarze Balken entspricht 1000 nm (links unten). Abbildung modifiziert nach [122].*

3.4.1.2 Kristallinitätsuntersuchungen

Dynamische Differenzkalorimetrie (DSC) wurde genutzt, um Phasenübergänge der proliposomalen Formulierungen zu untersuchen. Jede der verwendeten Einzelsubstanzen wurde ebenfalls untersucht (Abbildung 18). Sorbitol, Cholesterin und Hydrocortison zeigten einen scharfen endothermischen Peak bei ihren korrespondierenden Schmelzpunkten. Der Schmelzpunkt von Cholesterin lag bei 151,6 °C und von Hydrocortison bei 228,1 °C (Abbildung 18A, B). Ein endothermischer Peak wurde bei 99,9 °C für Sorbitol beobachtet. Dies entspricht dem Phasenübergang des Gamma-Polymorphs [125]. Die spezifische Wärmekapazität (ΔH) des Schmelzens betrug 176,6 J/g (Abbildung 18C) und war mit Werten aus vorherigen Untersuchungen vergleichbar [125-127].

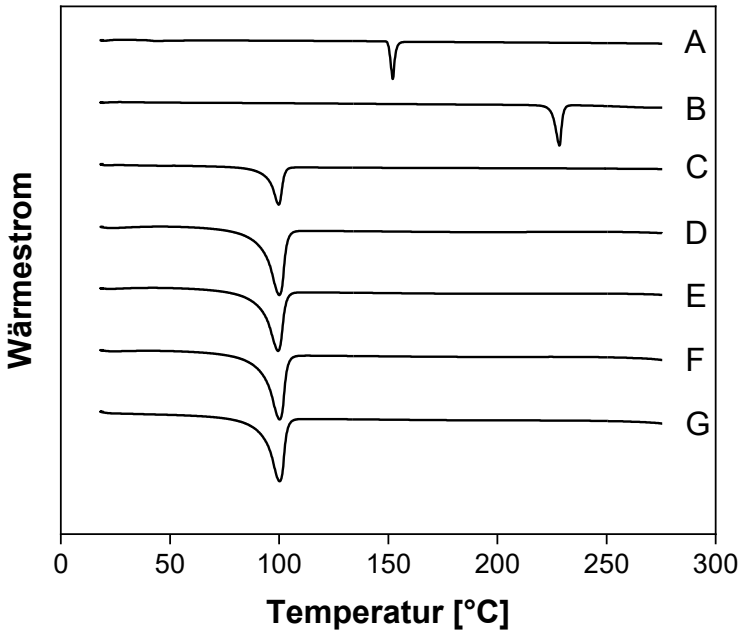

***Abbildung 18**: Überlagerte DSC-Diagramme der Ausgangssubstanzen Cholesterin (A), Hydrocortison (B) und Sorbitol (C) sowie der hergestellten Proliposomen EPC (D), EPC+C (E), SPC (F) und SPC+C (G). Abbildung modifiziert nach [122].*

Beim Vergleich der Profile der Einzelsubstanzen Cholesterin und Hydrocortison mit denen der proliposomalen Formulierungen wurden keine Phasenübergänge bei den entsprechenden Schmelzpunkten festgestellt. Dies spricht für ein vollständiges Einschließen der Substanzen in die Phospholipide. Trotzdem ist die DSC nicht sensitiv genug, um kleine kristalline Mengen Hydrocortisons zu detektieren. Eine größere Fraktion kristallinen Wirkstoffs ist unter Einbezug der großen Lipidmenge unwahrscheinlich. Zusätzlich konnte bei zwei physikalischen Mischungen ein Phasenübergang des Hydrocortisons beobachtet werden (Formulierungen EPC und EPC+C). Die Formulierungen wiesen nur den Sorbitol-Peak bei etwa 99 °C auf (Abbildung 18D-G). Bei den proliposomalen Formulierungen reduzierte sich die spezifische Wärmekapazität des Sorbitols um circa 17 % auf 144,9 J/g bis 149,8 J/g im Vergleich zur Reinsubstanz (176,6 J/g). Dies kann einerseits an den Interaktionen des Sorbitols mit den Phospholipiden oder andererseits an der Rekristallisation partiell gelösten Sorbitols in ein anderes Polymorph liegen [125]. Vergleichbare Ergebnisse wurden mit Mannitol als inertem Träger beobachtet [128].

3.4.2 *In vitro* Permeabilitätsuntersuchungen

Um die Permeabilität des Hydrocortisons in freier oder verkapselter Form zu untersuchen, wurden zwei Zellmodelle verwendet. Dabei wurden sowohl immortalisierte Zellen

der humanen Zervix (CaSki) als auch des humanen Endometriums (HEC-1-A) eingesetzt. Obwohl die beiden Zelltypen nicht aus der Vagina selbst, sondern aus benachbarten Regionen entstammen, werden sie breit eingesetzt, um die Permeabilität von Wirkstoffen durch das Vaginalepithel zu schätzen. Zusätzlich bieten die Permeabilitätsuntersuchungen eine Annäherung der Wirkstoffabsorption *in vivo* [58, 59].

Bevor die Permeabilität im Zellmodel untersucht werden kann, muss die Verträglichkeit der Formulierungen und des Hydrocortisons mit den Zellen gewährleistet sein. Hierzu wurden Zytotoxizitätsversuche in beiden Zelllinien CaSki und HEC-1-A mit Hydrocortison, hydrocortisonhaltigen und wirkstofffreien Proliposomen durchgeführt. Die Zellen wurden für 24 h mit den verschiedenen Formulierungen inkubiert und die Zellviabilität bestimmt. Dabei wurden keine zytotoxischen Effekte für Hydrocortison und die Formulierungen festgestellt. Die Viabilität lag bis auf eine Ausnahme oberhalb des minimalen Grenzwertes von 70 %, bei dem Substanzen und Formulierungen als potenziell sicher gelten (Tabelle 9) [129]. Einzig die Blanko-Formulierung SPC+C zeigte interessanterweise bei einer theoretischen Konzentration von 10 µg/mL Hydrocortison in HEC-1-A Zellen eine Viabilität unter 70 %. Trotzdem suggerieren die ermittelten Daten keine Toxizität und es gab keine Bedenken die Permeabilität bei 5 µg/mL Hydrocortison zu untersuchen.

Tabelle 9: *Ermittelte mittlere zytotoxische Konzentrationen (CC_{50}) von Hydrocortison und den vier proliposomalen Formulierungen jeweils mit und ohne (Blank) Hydrocortison. Tabelle modifiziert nach [122].*

Sample	CC_{50} [µg/mL]	
	CaSki	HEC-1-A
Hydrocortison	> 10	> 10
EPC+C	> 10	> 10
EPC	> 10	> 10
SPC	> 10	> 10
SPC+C	> 10	> 10
Blank EPC+C	> 10	> 10
Blank EPC	> 10	> 10
Blank SPC	> 10	> 10
Blank SPC+C	> 10	8,2

Das Ausbilden einer Zellmonoschicht vor der Permeabilitätsmessung wurde mittels Messung des transepithelialen elektrischen Widerstands (TEER) überprüft. Auch während der Permeabilitätsexperimente wurde der TEER gemessen, um die Unversehrtheit der Zellbarriere zu überprüfen. Das Überprüfen der intakten Zellbarriere mittels TEER-Messung gewährleistet, dass Hydrocortison durch die Zellen diffundiert, und letztlich auch das Auftreten verfälschter Messdaten verringert. Die Permeabilität von Hydrocortison war in beiden Zelllinien vergleichbar (Abbildung 19). Etwa 30 % bis 40 % Hydrocortison

permeierten nach 4 h durch die Zellmembran. Bei den verschiedenen Formulierungen variierte die permeierte Hydrocortisonmenge zwischen 30 % und70 %. Die Profile der rekonstituierten Proliposome war vergleichbar mit denen des freien Hydrocortisons in beiden Zelllinien ($p > 0,05$) und zeigten einen stetigen Anstieg der Hydrocortisonmenge, wobei in manchen Fällen eine maximale Hydrocortisonkonzentration bereits nach 2 h bis 4 h erreicht wurde. Die für die Proliposomen individuell berechneten scheinbaren Permeabilitätskonstanten P_{app} waren ebenfalls vergleichbar (Tabelle 10). Interessanterweise war die ermittelte P_{app} für freies Hydrocortison in beiden Zelllinien ähnlich, wenn auch tendenziell etwas niedriger als die mit Caco-2-Zellen ermittelte Permeabilitätskonstante ($17,5 \pm 4,1 \times 10^{-6}$ cm²/s) [130]. Angesichts der Tatsache, dass Hydrocortison extensiv über den Darm absorbiert wird und unter Berücksichtigung der von Corbo et al. publizierten Hasenstudie[3], unterstützen die ermittelten Werte die starke Permeabilität von Hydrocortison über die Vagina [110]. Setzt man die P_{app}-Werte ins Verhältnis zum freien Hydrocortison, erhält man ein Maß für die Verbesserung der Permeabilität der Formulierung. Diese lag für die untersuchten Proliposomen zwischen 1,0 und 1,8, was einer gleichbleibenden bis mäßig verbesserten Permeabilität entsprach (Tabelle 10).

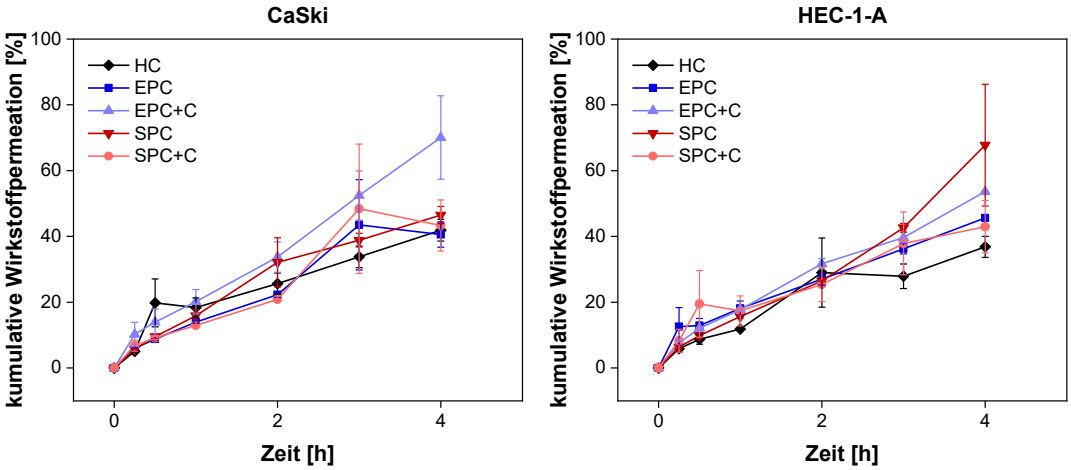

Abbildung 19: *Permeabilitätsprofile von Hydrocortison (HC) als freier Wirkstoff (schwarze Raute) oder in Proliposomen verkapselt durch Zellmonoschichten aus CaSki- (linke Seite) und HEC-1-A-Zellen (rechte Seite). Dargestellt sind die Mittelwerte ± SE (n = 3). Abbildung modifiziert nach [122].*

[3] Hydrocortison zeigte hier nach vaginaler Applikation eine hohe systemische Absorption

Tabelle 10: *Scheinbare Permeabilitätskonstante (P_{app}) von freiem und verkapseltem Hydrocortison in zwei verschiedenen vaginalen Zellmodellen. Die Werte sind als Mittelwerte ± SD angegeben (n = 3). Zusätzlich ist das mittlere Verhältnis der P_{app} zu freiem Hydrocortison als Maß für die Verbesserung der Permeabilität durch die Formulierung angegeben (Permeability Enhacement Ratio, PER). Tabelle modifiziert nach [122].*

Probe	P_{app} [cm²/s x 10^{-6}]		PER	
	CaSki	HEC-1-A	CaSki	HEC-1-A
Hydrocortison	9,9 ± 1,4	8,7 ± 1,3	-	-
EPC	9,6 ± 1,6	10,8 ± 0,2	1,0	1,2
EPC+C	16,6 ± 5,2	12,7 ± 0,1	1,7	1,5
SPC	11,0 ± 1,1	16,0 ± 7,3	1,1	1,8
SPC+C	10,3 ± 3,2	10,2 ± 3,3	1,0	1,2

Bei beiden Zelllinien CaSki und HEC-1-A hatten die Proliposome mit SPC einen höheren P_{app}-Wert als die EPC-Proliposome (Tabelle 10). Diese Beobachtung ist jedoch nicht signifikant. Die beiden Formulierungen unterscheiden sich in der Herkunft ihrer Phospholipide (Soja beziehungsweise Ei) und deshalb auch in ihrer Fettsäurezusammensetzung. Diese Unterschiede könnten prinzipiell die Interaktion mit den vaginalen Epithelzellen verändern und für den Unterschied in der Permeabilität verantwortlich sein. Neben der Zusammensetzung der Phospholipide beeinflusste Cholesterin die Zellmembranpermeabilität ebenfalls [131, 132]. EPC+C Liposomen zeigten in beiden Zelllinien höhere P_{app}-Wert, wenn auch nicht signifikant, wenn Cholesterin in den Phospholipiden integriert wurde. Der positive Effekt auf die Permeabilität konnte beim Einschluss von Cholesterin in SPC Proliposomen nicht festgestellt werden.

Um die Ergebnisse der Permeabilitätsuntersuchungen besser bewerten zu können, sollte zudem die EE% berücksichtigt werden. Es gab zwar keinen signifikanten Unterschied zwischen den Permeabilitätskonstanten, aber die Rangfolge der P_{app}-Werte der Proliposomen entsprach der Verkapselungseffizienz (höhere Verkapselung entsprach einer niedrigeren Permeabilität). Nach der Rekonstitution werden etwa 70 % bis 80 % des Hydrocortisons freigesetzt, wobei die übrige Fraktion in den Liposomen verbleibt. Dieser kleine Unterschied macht es schwierig, die Liposomen im Permeabilitätsexperiment zu unterscheiden, wenn es keinen Einfluss auf die Permeabilität gibt und die Freisetzung einen wichtigeren Stellenwert einnimmt. Trotzdem stellt die eingeschlossene Hydrocortisonmenge zwar im vorliegenden Fall eine kleine aber sehr interessante Stellschraube in der Formulierungsentwicklung dar, die in Wirkstofffreisetzungsuntersuchungen besser charakterisiert werden kann.

Hydrocortison, das mit der Zellmembran assoziiert beziehungsweise in den Zellen eingeschlossen ist, wurde zusätzlich quantifiziert. Die Proben wiesen aber Konzentrationen

unterhalb des Detektionslimits auf. Damit ergab sich eine maximale Hydrocortisonmenge, die mit der Zellmonoschicht assoziiert ist, von 0,3 % der Gesamtdosis. Neben der Depotwirkung durch die Verkapselung von Wirkstoff in den Liposomen hat die gewählte lipidbasierte Formulierung weitere Vorteile. So kann beispielsweise eine verlängerte Verweilzeit in der Vagina durch adhäsive Interaktionen mit der vaginalen Mucosa und damit eine verlängerte Kontaktzeit des Wirkstoffs am Wirkort erzielt werden [45, 133]. Zusätzlich können Liposome die Penetration unterstützen und damit tiefere Gewebeschichten erreichen, die auch von der anti-inflammatorischen Wirkungen des Hydrocortisons profitieren[134].

3.4.3 Untersuchung der Wirkstofffreisetzung im Dispersion Releaser

Im Gegensatz zur Untersuchung der Permeabilität im zellbasierten Assay, bei der Wirkstofffreisetzung und Permeation gleichzeitig stattfindet, verfügt der PTDR über ein wässriges Messumfeld, das im Wesentlichen durch die Zusammensetzung des Akzeptorkompartiments kontrolliert wird. Dadurch kann der Freisetzungsprozess des untersuchten Wirkstoffs aus verschiedenen Formulierungen mithilfe des PTDRs sensitiver charakterisiert werden. Dabei sind vor allem die Einflüsse kleiner Änderungen im Mikroumfeld der Formulierung auf die Freisetzungsrate von Interesse.

Die Wirkstofffreisetzung aller vier proliposomalen Formulierungen wurde im PTDR untersucht. Zusätzlich wurde eine Hydrocortison-Lösung dialysiert, um den Einfluss der Dialysemembran zu bewerten. Als Referenz wurde eine kommerzielle Creme mit identischer Hydrocortisonkonzentration (Ebenol®) untersucht. Als Freisetzungsmedium wurde sVSF mit Cyclodextrinen gewählt, um der schlechten Löslichkeit des Hydrocortisons (0,39 mg/mL bei 37 °C) entgegenzuwirken [122]. Unter optimalen Löslichkeitsbedingungen (1,46 mg/mL bei 37 °C, *sink*-Bedingungen [122]) zeigten alle untersuchten Proben eine vollständige Freisetzung innerhalb von 4 h bis 6 h. Es konnten keine Unterschiede zwischen den proliposomalen Formulierungen und der kommerziellen Formulierung festgestellt werden (Abbildung 20, linke Abbildung, $f1 < 15$ und $f2 > 50$). Im Vergleich zum freien Wirkstoff zeigten die Lipid-Formulierungen eine leichte Verzögerung in der Permeation, was für einen erfolgreichen Einschluss des Hydrocortisons in die Liposomenmembran sprach. Die in dem Freisetzungsmedium enthaltenen Cyclodextrine bildeten ein besseres Reservoir für das Hydrocortison und solubilisierten den Wirkstoff besser im Vergleich zum liposomalen Träger. Deshalb konnte unter *sink*-Bedingungen keine Diskriminierung der Proben erfolgen.

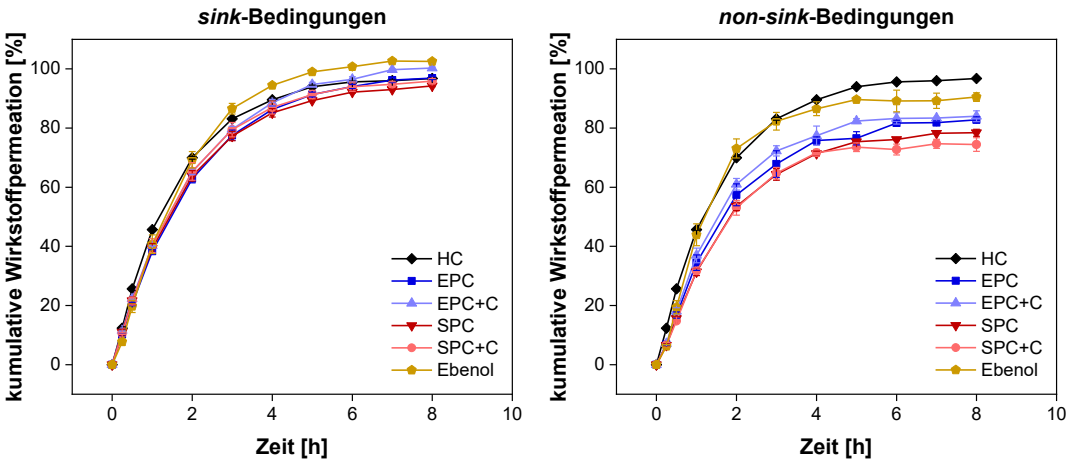

Abbildung 20: *Permeationsprofile des Hydrocortisons (HC) im PTDR, formuliert als Proliposomen (EPC, EPC+C, SPC, SPC+C) oder Creme (Ebenol®). Als Freisetzungsmedium diente jeweils sVSF, einmal unter sink-Bedingungen (linke Seite) mit Cyclodextrinen, einmal unter biorelevanten Löslichkeitsbedingungen ohne Cyclodextrin-Zusatz (non-sink-Bedingungen, rechte Seite). Das Permeationsprofil des freien Hydrocortisons (schwarze Raute) ist jeweils in Medien mit Cyclodextrin untersucht worden und dient als Referenz. Dargestellt sind die Mittelwerte ± SD (n = 3). Abbildung modifiziert nach [122].*

Die verschiedenen Formulierungen wurden zusätzlich unter *non-sink*-Bedingungen untersucht, wobei die Löslichkeit des Hydrocortisons einen größeren Stellenwert einnahm und mit der Löslichkeit *in vivo* vergleichbar war. Dabei konnte eine Rangfolge der proliposomalen Formulierungen beobachtet werden (Abbildung 20, rechte Seite). Proliposome mit EPC erreichten ein höheres Plateau von 82 % im Gegensatz zu den Proliposomen mit SPC, deren Plateau bei 75 % bis 78 % lag. Die verbleibende, nicht freigesetzte Hydrocortisonmenge entsprach der EE% mit Ausnahme der SPC-Liposomen (Tabelle 8). Der f1- und f2-Test wurde genutzt, um die sechs Freisetzungsprofile unter *non-sink*-Bedingungen statistisch zu vergleichen. Aber die Auswertung erfolgte nicht auf Basis der Richtlinie der US-FDA für schnellfreisetzende, feste, orale Darreichungsformen, die eine Freisetzung von mindestens 85 % und zwölf Testeinheiten verlangt. Einige der untersuchten Formulierungen erreichten keine Freisetzung über 85 %. Da aber der Variationskoeffizient aller Wirkstofffreisetzungen unter 5 % lag (unter dem Limit von 10 % für schnellfreisetzende Tabletten), konnte ein Vergleich der verschiedenen Hydrocortison-Zubereitungen unter der Annahme eines mittleren Unterschiedes von 10 % angenommen werden. Dabei stellte sich heraus, dass die Freisetzungsprofile der vier untersuchten Proliposomen vergleichbar waren ($f1 < 15$ und $f2 > 50$). Verglich man jedoch die Proliposomen mit der kommerziellen Creme und dem freien Wirkstoff, zeigten die langsamer freisetzenden Formulierungen SPC und SPC+C einen signifikanten Unterschied.

Zusätzlich wurden die Probenzeitpunkte nach 8 h mit einem t-Test statistisch ausgewertet. Unter *sink*-Bedingungen wurden keine Unterschiede zwischen den untersuchten Proben festgestellt. Bei den Freisetzungstests unter biorelevanten Bedingungen unterschieden sich alle Formulierungen, außer Ebenol®, von der Probe mit freiem Hydrocortison signifikant.

Die Permeabilitätsstudien (Kapitel 3.4.2) kamen zu einem ähnlichen Ergebnis wie die Untersuchungen im PTDR, wobei eine statistische Interpretation aufgrund der großen Standardabweichung nicht möglich war. Im Allgemeinen zeigten EPC-Liposome eine schnellere Permeation als Liposome mit SPC. Die kommerzielle Creme verzögerte die Freisetzung des Hydrocortisons im Vergleich zu den Liposomen nicht und das Freisetzungsprofil war mit dem des freien Hydrocortisons innerhalb der ersten 3 h vergleichbar. Danach zeigte die Freisetzung ein Plateau bei 90 %. Die Liposome zeigen vermutlich bei der vaginalen Anwendung eine schwache Adhäsion am vaginalen Mukus aufgrund ihrer negativen Ladung [49, 124]. Deshalb sollte sich ein lokales Depot aufgrund einer moderaten Penetration der Liposomen in die äußere Schicht Mukosa bilden. Unter Einbezug der Ergebnisse der Permeabilitäts- und Wirkstofffreisetzungsexperimente ist die Verkapselungseffizient EE% der wichtigste Parameter für die verzögernde Wirkung der liposomalen Formulierung. Dabei bildet die eingeschlossene Wirkstofffraktion in der Membran der Liposomen ein Depot, das für die kontrollierte Freisetzung des Wirkstoffs relevant ist. Weitere Formulierungen mit einer verbesserten EE% können zu einem verlängerten therapeutischen Effekt beitragen.

4 Zusammenfassung und Ausblick

Der Dispersion Releaser ist ein dialysebasiertes Gerät, das zur Untersuchung der Wirkstofffreisetzung von kolloidalen Arzneistoffträgern an der Goethe Universität Frankfurt am Main entwickelt wurde. In der vorliegenden Arbeit wurde der Prototyp des DRs gemeinsam mit der Firma Pharma Test Apparatebau AG (Hainburg, Deutschland) mit dem Ziel der Verbesserung der Anwenderfreundlichkeit und der Anpassung an die Anforderungen der pharmazeutischen Industrie zu einem robusten System weiterentwickelt. Im Zuge der Rekonstruktion wurden die Anzahl der einzelnen Bestandteile verringert, sodass der PTDR fortan schneller und einfacher zusammengebaut werden kann. Außerdem wurde die Schraubverbindung als Kopplung zum Freisetzungstester durch eine Bajonett-Kupplung ersetzt, was eine zusätzliche Zeitersparnis bei der Durchführung des Freisetzungstests bedeutet. Zusätzlich wurden die Maße des Donorkompartiments angepasst, sodass möglichst alle kommerziell erhältlichen Dialyseschläuche mit dem PTDR kombiniert werden können. Die verschiedenen Vesselgrößen aus den verschiedenen Arzneibüchern sind nach dem Umbau auch flexibel nutzbar. Dadurch kann das neu designte Gerät in Laboren weltweit genutzt werden. Das Ziel eine Standardmethode zu etablieren, wurde erfüllt.

Neben der Anpassung des Gerätes an internationale Anforderungen wurde eine umfangreiche Validierung des PTDRs im Zuge dieser Arbeit vorgestellt. Dabei wurde zuerst eine Methode zur Untersuchung der Dichtigkeit des Systems mit Nanopartikeln aus Gold für die neue Konstruktion etabliert. Diese nutzte zwei weit verbreitete analytische Methoden, sodass Dichtigkeitsuntersuchungen auch mit anderen Membranen in anderen Laboren weltweit durchgeführt werden können. Zum einen wird die Eigenschaft der Goldpartikel Licht zu absorbieren genutzt, um das spezifische Absorptionsspektrum mittels UV/Vis-Spektroskopie nachzuweisen. Zum anderen können DLS-Messungen eingesetzt werden. Neben der Dichtigkeitsuntersuchung wurden weitere Einflüsse auf die Membranpermeation (Umdrehungszahl, Proteingehalt im Freisetzungsmedium) untersucht. Dabei konnte ein Bereich von 25 UPM bis 100 UPM als typischer Anwendungsbereich für Freisetzungstests festgelegt werden. Durch die Zugabe von Proteinen in das Freisetzungsmedium entstanden verschiedene Größenfraktionen des Wirkstoffs Diclofenac (frei gelöst und proteingebunden) im Donorkompartiment, die zu unterschiedlichen Permeationsraten führten. Dadurch konnte gezeigt werden, dass die Auswahl der richtigen Membran nicht nur abhängig von den Wirkstoff- und Formulierungseigenschaften ist, sondern auch von der Zusammensetzung des Mediums, wenn das Medium einen Ein-

fluss auf die freie Wirkstofffraktion hat. Vergleichende Messungen mit zwei verschiedenen MWCO können das Verständnis der Wirkstofffreisetzung in verschiedenen Medien verbessern. Der Einfluss von Proteinen auf die Freisetzungsrate kann bewertet werden.

Untersuchungen von zwei unterschiedlichen halbfesten Zubereitungen mit Diclofenac wurden das erste Mal im Dispersion Releaser untersucht. Dabei konnte unter *non-sink*-Bedingungen der Einfluss der lipophilen Phase des Voltaren® Emulgels gezeigt werden. Das Emulgel zeigte eine bessere und vollständige Freisetzung unter den erschwerten Löslichkeitsbedingungen im Vergleich zum Olfen® Gel. Die Untersuchung der Wirkstoffverteilung mit verschiedenen Wirkstoffen in verschiedenen halbfesten Grundlagen ist Teil eines neuen Projektes, das auf Basis der vorliegenden Arbeit eingeworben wurde. Des Weiteren wurde vier proliposomale Gele im Dispersion Releaser untersucht verglichen. Dabei konnte der PTDR sensitiver den Einfluss der EE% im Vergleich zum Permeabilitätsexperiment im zellbasierten Assay zeigen.

Neben der Standardisierung der Apparatur wurde der Auswerteprozess mit Hilfe eines neuen Modells Stella Architect® entwickelt und für die Öffentlichkeit zugänglich gemacht. Dies ermöglicht eine einheitliche Normalisierung der Freisetzung im PTDR ohne den störenden Einfluss der Dialysemembran. Die Berechnung der Membranpermeationskonstante k_M ist als *Dialysis Membrane Permeation Calculator* (DiMeC) und die Berechnung der Normalisierung der Wirkstofffreisetzung aus Formulierungen als PTDR *Release Normalizer* (PTDR ReNo) frei im Internet zugänglich und ermöglicht eine Integration in verschiedene physiologiebasierte, pharmakokinetische Modelle. Dieses Verknüpfung konnte schon erfolgreich mit vier verschiedene Doxorubicin-Formulierungen durchgeführt werden und eine Korrelation zwischen der *in vivo*-Plasmakonzentration und der *in vitro*-Freisetzung etabliert werden [96]. Die Normalisierung der Freisetzung eines liposomalen Gels mit Rifampicin zur Behandlung von Wunden wurde auch mit dem hier erfolgten Auswerteprozess durchgeführt [135, 136].

Mittlerweile sind weitere Konstruktionsverbesserungen durchgeführt worden, die das Montieren des Donorkompartiments in den Käfighalter erleichtern: Statt dem Einstecken des Käfigs wird dieser auf den Halter aufgeschraubt. Dies gewährleistet, dass der Käfig immer korrekt positioniert ist und nicht versehentlich vom Anwender bewegt werden kann. Andernfalls könnte ein verschobener Käfig zu Abrieb führen, wenn der Innenrüher den Boden des Käfigs berührt.

Das Interesse an neuen, robusten Methoden zur Untersuchung der Wirkstofffreisetzung ist groß und mittlerweile wird der Dispersion Releaser in verschiedenen Laboren der pharmazeutischen Industrie für den routinemäßigen Einsatz getestet.

5 Literaturverzeichnis

[1] Barenholz Y. Doxil® — The first FDA-approved nano-drug: Lessons learned. J Control Rel. 2012;160:117-34.

[2] Naseri N, Valizadeh H, Zakeri-Milani P. Solid Lipid Nanoparticles and Nanostructured Lipid Carriers: Structure, Preparation and Application. Adv Pharm Bull. 2015;5:305-13.

[3] Villa Nova M, Janas C, Schmidt M, Ulshoefer T, Grafe S, Schiffmann S, et al. Nanocarriers for photodynamic therapy-rational formulation design and medium-scale manufacture. Int J Pharm Sci. 2015;491:250-60.

[4] Merisko-Liversidge E, Liversidge GG. Nanosizing for oral and parenteral drug delivery: A perspective on formulating poorly-water soluble compounds using wet media milling technology. Adv Drug Deliv Rev. 2011;63:427-40.

[5] Janas C, Mostaphaoui Z, Schmiederer L, Bauer J, Wacker MG. Novel polymeric micelles for drug delivery: Material characterization and formulation screening. Int J Pharm Sci. 2016;509:197-207.

[6] Torchilin VP. Passive and Active Drug Targeting: Drug Delivery to Tumors as an Example. In: Schäfer-Korting M, editor. Drug Deliv. Berlin, Heidelberg: Springer Berlin Heidelberg; 2010. p. 3-53.

[7] D'Mello SR, Cruz CN, Chen ML, Kapoor M, Lee SL, Tyner KM. The evolving landscape of drug products containing nanomaterials in the United States. Nat Nanotechnol. 2017;12:523-9.

[8] Mast MP, Modh H, Champanhac C, Wang JW, Storm G, Kramer J, et al. Nanomedicine at the crossroads - A quick guide for IVIVC. Adv Drug Deliv Rev. 2021:113829.

[9] US-FDA. Doxorubicin hydrochloride liposome injection (Doxil®) approval letter (NDA 50-718/S-50). 2015.

[10] Eric AF. The design and development of DaunoXome(R) for solid tumor targeting in vivo. Adv Drug Deliv Rev. 1997;24:133-50.

[11] Adler-moore JP, Proffitt RT. Development, Characterization, Efficacy and Mode of Action of Ambisome, A Unilamellar Liposomal Formulation of Amphotericin B. J Liposome Res. 1993;3:429-50.

[12] Swenson CE, Perkins WR, Roberts P, Janoff AS. Liposome technology and the development of Myocet™ (liposomal doxorubicin citrate). The Breast. 2001;10:1-7.

[13] Chowdhary RK, Shariff I, Dolphin D. Drug release characteristics of lipid based benzoporphyrin derivative. J Pharm Pharm Sci. 2003;6:13-9.

[14] Bedikian AY, Vardeleon A, Smith T, Campbell S, Namdari R. Pharmacokinetics and urinary excretion of vincristine sulfate liposomes injection in metastatic melanoma patients. J Clin Pharmacol. 2006;46:727-37.

[15] Drummond DC, Noble CO, Guo Z, Hong K, Park JW, Kirpotin DB. Development of a highly active nanoliposomal irinotecan using a novel intraliposomal stabilization strategy. Cancer Research. 2006;66:3271-7.

[16] Krauss AC, Gao X, Li L, Manning ML, Patel P, Fu W, et al. FDA Approval Summary: (Daunorubicin and Cytarabine) Liposome for Injection for the Treatment of Adults with High-Risk Acute Myeloid Leukemia. Clinical Cancer Research. 2019;25:2685-90.

[17] US-FDA. Abraxane approval letter (NDA 21-660). Clinical Pharmacology and Biopharmaceutics Review(s)2005.

[18] US-FDA. Ferumoxytol approval letter (NDA 22-180). Clinical Pharmacology and Biopharmaceutics Review(s)2009.

[19] Garber K. Alnylam launches era of RNAi drugs. Nat Biotechnol. 2018;36:777-8.

[20] US-FDA. Onpattro 2 mg/mL injection for intravenous use approval letter (NDA 210922). 2018.

[21] Patravale VB, Mandawgade SD. Novel cosmetic delivery systems: an application update. Int J Cosmetic Sci. 2008;30:19-33.

[22] Zhang H. Thin-Film Hydration Followed by Extrusion Method for Liposome Preparation. In: D'Souza GGM, editor. Liposomes: Methods and Protocols. New York, NY: Springer New York; 2017. p. 17-22.

[23] Ait-Oudhia S, Mager DE, Straubinger RM. Application of Pharmacokinetic and Pharmacodynamic Analysis to the Development of Liposomal Formulations for Oncology. Pharmaceutics. 2014;6:137-74.

[24] Sharma A, Sharma US. Liposomes in drug delivery: Progress and limitations. Int J Pharm Sci. 1997;154:123-40.

[25] Rao MR, Babrekar LS. Liposomal drug delivery for solubility and bioavailability enhancement of efavirenz. Indian J Pharm Sci. 2018;80:1115-24.

[26] Bozzuto G, Molinari A. Liposomes as nanomedical devices. Int J Nanomedicine. 2015;10:975 - 99.

[27] Han JY, La Fiandra JN, DeVoe DL. Microfluidic vortex focusing for high throughput synthesis of size-tunable liposomes. Nat Commun. 2022;13:6997.

[28] Grit M, Crommelin DJA. Chemical stability of liposomes: implications for their physical stability. Chem Phys Lipids. 1993;64:3-18.

[29] Hunt CA, Tsang S. α-Tocopherol retards autoxidation and prolongs the shelf-life of liposomes. Int J Pharm Sci. 1981;8:101-10.

[30] Wong M, Thompson TE. Aggregation of dipalmitoylphosphatidylcholine vesicles. Biochemistry. 1982;21:4133-9.

[31] Kuntsche J, Freisleben I, Steiniger F, Fahr A. Temoporfin-loaded liposomes: Physicochemical characterization. Eur J Pharm Sci. 2010;40:305-15.

[32] Payne NI, Ambrose CV, Timmins P, Ward MD, Ridgway F. Proliposomes: A Novel Solution to an Old Problem. J Pharm Sci. 1986;75:325-9.

[33] Payne NI, Browning I, Hynes CA. Characterization of Proliposomes. J Pharm Sci. 1986;75:330-3.

[34] Alves GP, Santana MHA. Phospholipid dry powders produced by spray drying processing: structural, thermodynamic and physical properties. Powder Technol. 2004;145:139-48.

[35] Parhizkar E, Sadeghinia D, Hamishehkar H, Yaqoubi S, Nokhodchi A, Alipour S. Carrier Effect in Development of Rifampin Loaded Proliposome for Pulmonary Delivery: A Quality by Design Study. Adv Pharm Bull. 2022;12:336-45.

[36] Xia F, Hu D, Jin H, Zhao Y, Liang J. Preparation of lutein proliposomes by supercritical anti-solvent technique. Food Hydrocoll. 2012;26:456-63.

[37] Xia F, Jin H, Zhao Y, Guo X. Supercritical Antisolvent-based Technology for Preparation of Vitamin D3 Proliposome and Its Characteristics. Chin J Chem Eng. 2011;19:1039-46.

[38] Chen C-M, Alli D. Use of Fluidized Bed in Proliposome Manufacturing. J Pharm Sci. 1987;76:419.

[39] Gala RP, Khan I, Elhissi AMA, Alhnan MA. A comprehensive production method of self-cryoprotected nano-liposome powders. Int J Pharm Sci. 2015;486:153-8.

[40] Kumar R, Gupta RB, Betegeri G. Formulation, Characterization, and In Vitro Release of Glyburide from Proliposomal Beads. Drug Deliv. 2001;8:25-7.

[41] Singh N, Kushwaha P, Ahmad U, Abdullah M. Proliposomas: Una aproximación para el desarrollo de liposoma estables. Ars Pharm. 2019;60:231-40.

[42] Chu C, Tong S-s, Xu Y, Wang L, Fu M, Ge Y-r, et al. Proliposomes for oral delivery of dehydrosilymarin: preparation and evaluation in vitro and in vivo. Acta Pharmacol Sin. 2011;32:973-80.

[43] Kurakula M, Srinivas C, Kasturi N, Diwan PD. Formulation and Evaluation of Prednisolone Proliposomal Gel for Effective Topical Pharmacotherapy. Int J Pharm Sci Drug Res. 2012;4:35-43.

[44] Rojanarat W, Nakpheng T, Thawithong E, Yanyium N, Srichana T. Levofloxacin-Proliposomes: Opportunities for Use in Lung Tuberculosis. Pharmaceutics. 2012;4:385-412.

[45] Ning M-Y, Guo Y-Z, Pan H-Z, Yu H-M, Gu Z-W. Preparation and Evaluation of Proliposomes Containing Clotrimazole. Chem Pharm Bull. 2005;53:620-4.

[46] Tietz K, Klein S. Simulated genital tract fluids and their applicability in drug release/dissolution testing of vaginal dosage forms. Dissolut Technol. 2018;25:40-51.

[47] das Neves J, Notario-Pérez F, Sarmento B. Women-specific routes of administration for drugs: A critical overview. Adv Drug Deliv Rev. 2021;176:113865.

[48] Pavelić Ž, Škalko-Basnet N, Schubert R. Liposomal gels for vaginal drug delivery. Int J Pharm Sci. 2001;219:139-49.

[49] das Neves J, Amiji M, Sarmento B. Mucoadhesive nanosystems for vaginal microbicide development: friend or foe? WIREs Nanomed Nanobiotechnol. 2011;3:389-99.

[50] Vanić Ž, Škalko-Basnet N. Nanopharmaceuticals for improved topical vaginal therapy: Can they deliver? Eur J Pharm Sci. 2013;50:29-41.

[51] Richardson JL, Whetstone J, Fisher AN, Watts P, Farraj NF, Hinchcliffe M, et al. Gamma-scintigraphy as a novel method to study the distribution and retention of a bioadhesive vaginal delivery system in sheep. J Control Rel. 1996;42:133-42.

[52] Vermani K, Garg S. The scope and potential of vaginal drug delivery. Pharm Sci Technol Today. 2000;3:359-64.

[53] Owen DH, Katz DF. A vaginal fluid simulant. Contraception. 1999;59:91-5.

[54] Rastogi R, Su J, Mahalingam A, Clark J, Sung S, Hope T, et al. Engineering and characterization of simplified vaginal and seminal fluid simulants. Contraception. 2016;93:337-46.

[55] Sugano K, Kansy M, Artursson P, Avdeef A, Bendels S, Di L, et al. Coexistence of passive and carrier-mediated processes in drug transport. Nat Rev Drug Discov. 2010;9:597-614.

[56] Sassi AB, McCullough KD, Cost MR, Hillier SL, Rohan LC. Permeability of tritiated water through human cervical and vaginal tissue. J Pharm Sci. 2004;93:2009-16.

[57] Brannon-Peppas L. Novel vaginal drug release applications. Adv Drug Deliv Rev. 1993;11:169-77.

[58] Machado RM, Palmeira-de-Oliveira A, Gaspar C, Martinez-de-Oliveira J, Palmeira-de-Oliveira R. Studies and methodologies on vaginal drug permeation. Adv Drug Deliv Rev. 2015;92:14-26.

[59] Gorodeski GI. Estrogen increases the permeability of the cultured human cervical epithelium by modulating cell deformability. Am J Physiol Cell Physiol. 1998;275:C888-C99.

[60] Grammen C, Augustijns P, Brouwers J. In vitro profiling of the vaginal permeation potential of anti-HIV microbicides and the influence of formulation excipients. Antivir Res. 2012;96:226-33.

[61] das Neves J, Araújo F, Andrade F, Michiels J, Ariën KK, Vanham G, et al. In Vitro and Ex Vivo Evaluation of Polymeric Nanoparticles for Vaginal and Rectal Delivery of the Anti-HIV Drug Dapivirine. Mol Pharm. 2013;10:2793-807.

[62] das Neves J, Sarmento B. Precise engineering of dapivirine-loaded nanoparticles for the development of anti-HIV vaginal microbicides. Acta Biomater. 2015;18:77-87.

[63] US-FDA. Guidance for Industry: Liposome Drug Products Chemistry, Manufacturing, and Controls; Human Pharmacokinetics and Bioavailability; and Labeling Documentation. 2018.

[64] EMA. Reflection paper on the data requirements for intravenous liposomal products developed with reference to an innovator liposomal product, Committee for Human Medicinal Products. London (UK)2013.

[65] Shen J, Burgess DJ. In vitro dissolution testing strategies for nanoparticulate drug delivery systems: recent developments and challenges. Drug Del Trans Res. 2013;3:409-15.

[66] D'Souza SS, DeLuca PP. Methods to Assess in Vitro Drug Release from Injectable Polymeric Particulate Systems. Pharm Res. 2006;23:460-74.

[67] Nothnagel L, Wacker MG. How to measure release from nanosized carriers? Eur J Pharm Sci. 2018;120:199-211.

[68] Wacker MG, Lu X, Burke M, Nir I, Fahmy R, Zaidi K. Testing the in-vitro product performance of nanomaterial-related drug products: View of the USP Expert Panel. Pharmacop Forum. 2022.

[69] Heng D, Cutler DJ, Chan H-K, Yun J, Raper JA. What is a Suitable Dissolution Method for Drug Nanoparticles? Pharm Res. 2008;25:1696-701.

[70] Jung F, Nothnagel L, Gao F, Thurn M, Vogel V, Wacker MG. A comparison of two biorelevant in vitro drug release methods for nanotherapeutics based on advanced physiologically-based pharmacokinetic modelling. Eur J Pharm Sci. 2018;127:462-70.

[71] Jung F, Thurn M, Krollik K, Gao GF, Hering I, Eilebrecht E, et al. Predicting the environmental emissions arising from conventional and nanotechnology-related pharmaceutical drug products. Environ Res. 2021;192:110219.

[72] Cipolla D, Wu H, Eastman S, Redelmeier T, Gonda I, Chan HK. Development and Characterization of an In Vitro Release Assay for Liposomal Ciprofloxacin for Inhalation. J Pharm Sci. 2014;103:314-27.

[73] Weng J, Tong HHY, Chow SF. In Vitro Release Study of the Polymeric Drug Nanoparticles: Development and Validation of a Novel Method. Pharmaceutics. 2020;12:732.

[74] Juenemann D, Jantratid E, Wagner C, Reppas C, Vertzoni M, Dressman JB. Biorelevant in vitro dissolution testing of products containing micronized or nanosized fenofibrate with a view to predicting plasma profiles. Eur J Pharm Biopharm. 2011;77:257-64.

[75] Wallace SJ, Li J, Nation RL, Boyd BJ. Drug release from nanomedicines: selection of appropriate encapsulation and release methodology. Drug Del Trans Res. 2012;2:284-92.

[76] Poole CF. New trends in solid-phase extraction. TrAC Trends in Analytical Chemistry. 2003;22:362-73.

[77] Song W, Tweed JA, Visswanathan R, Saunders JP, Gu Z, Holliman CL. Bioanalysis of Targeted Nanoparticles in Monkey Plasma via LC-MS/MS. Anal Chem. 2019;91:13874-82.

[78] Su C, Yang H, Sun H, Fawcett JP, Sun D, Gu J. Bioanalysis of free and liposomal Amphotericin B in rat plasma using solid phase extraction and protein precipitation followed by LC-MS/MS. J Pharm Biomed Anal. 2018;158:288-93.

[79] Varache M, Ciancone M, Couffin A-C. Optimization of a Solid-Phase Extraction Procedure for the Analysis of Drug-Loaded Lipid Nanoparticles and its Application to the Determination of Leakage and Release Profiles. J Pharm Sci. 2020;109:2527-35.

[80] Ohnishi N, Yamamoto E, Tomida H, Hyodo K, Ishihara H, Kikuchi H, et al. Rapid determination of the encapsulation efficiency of a liposome formulation using column-switching HPLC. Int J Pharm Sci. 2013;441:67-74.

[81] Guillot A, Couffin A-C, Sejean X, Navarro F, Limberger M, Lehr C-M. Solid Phase Extraction as an Innovative Separation Method for Measuring Free and Entrapped Drug in Lipid Nanoparticles. Pharm Res. 2015;32:3999-4009.

[82] Janas C, Mast MP, Kirsamer L, Angioni C, Gao F, Mantele W, et al. The dispersion releaser technology is an effective method for testing drug release from nanosized drug carriers. Eur J Pharm Sci. 2017;115:73-83.

[83] Xie L, Beyer S, Vogel V, Wacker MG, Mantele W. Assessing the drug release from nanoparticles: Overcoming the shortcomings of dialysis by using novel optical techniques and a mathematical model. Int J Pharm Sci. 2015;488:108-19.

[84] Janas C. Entwicklung einer Apparatur zur *in vitro* Testnung der Wirkstoffreisetzung aus kolloidalen Arzneistoffträgern. Frankfurt am Main: Goethe Universität; 2019.

[85] Xu X, Khan MA, Burgess DJ. A two-stage reverse dialysis in vitro dissolution testing method for passive targeted liposomes. Int J Pharm Sci. 2012;426:211-8.

[86] Manna S, Wu Y, Wang Y, Koo B, Chen L, Petrochenko P, et al. Probing the mechanism of bupivacaine drug release from multivesicular liposomes. J Control Rel. 2019;294:279-87.

[87] Kumar S, Xu X, Gokhale R, Burgess DJ. Formulation parameters of crystalline nanosuspensions on spray drying processing: A DoE approach. Int J Pharm Sci. 2014;464:34-45.

[88] Bhardwaj U, Burgess DJ. A novel USP apparatus 4 based release testing method for dispersed systems. Int J Pharm Sci. 2010;388:287-94.

[89] Yuan W, Kuai R, Dai Z, Yuan Y, Zheng N, Jiang W, et al. Development of a Flow-Through USP-4 Apparatus Drug Release Assay to Evaluate Doxorubicin Liposomes. AAPS J. 2017;19:150-60.

[90] Diaz de Leon-Ortega R, D'Arcy DM, Lamprou DA, Fotaki N. In vitro - in vivo relations for the parenteral liposomal formulation of Amphotericin B: A clinically relevant approach with PBPK modeling. Eur J Pharm Biopharm. 2020.

[91] Díaz de León–Ortega R, D'Arcy DM, Lamprou DA, Fotaki N. In vitro - in vivo relations for the parenteral liposomal formulation of Amphotericin B: A clinically relevant approach with PBPK modeling. Eur J Pharm Biopharm. 2021;159:177-87.

[92] Tang J, Srinivasan S, Yuan W, Ming R, Liu Y, Dai Z, et al. Development of a flow-through USP 4 apparatus drug release assay for the evaluation of amphotericin B liposome. Eur J Pharm Biopharm. 2019;134:107-16.

[93] Díaz de León-Ortega R, D'Arcy DM, Bolhuis A, Fotaki N. Investigation and simulation of dissolution with concurrent degradation under healthy and hypoalbuminaemic simulated parenteral conditions- case example Amphotericin B. Eur J Pharm Biopharm. 2018;127:423-31.

[94] Wacker MG, Janas C. DIALYSIS CELL FOR AN IN-VITRO RELEASE TEST APPARATUS, USE OF THE DIALYSIS CELL AND IN-VITRO RELEASE TEST APPARATUS. In: Office EP, editor.2014.

[95] Jablonka L, Ashtikar M, Gao GF, Thurn M, Modh H, Wang JW, et al. Predicting human pharmacokinetics of liposomal temoporfin using a hybrid in silico model. Eur J Pharm Sci. 2020;149:121-34.

[96] Modh H, Fang DJ, Ou YH, Yau JNN, Kovshova T, Nagpal S, et al. Injectable drug delivery systems of doxorubicin revisited: In vitro-in vivo relationships using human clinical data. Int J Pharm Sci. 2021;608:121073.

[97] Wallenwein CM, Nova MV, Janas C, Jablonka L, Gao GF, Thurn M, et al. A dialysis-based in vitro drug release assay to study dynamics of the drug-protein transfer of temoporfin liposomes. Eur J Pharm Sci. 2019;143:44-50.

[98] Jablonka L, Ashtikar M, Gao G, Jung F, Thurn M, Preuss A, et al. Advanced in silico modeling explains pharmacokinetics and biodistribution of temoporfin nanocrystals in humans. J Control Rel. 2019;308:57-70.

[99] Gao GF, Ashtikar M, Kojima R, Yoshida T, Kaihara M, Tajiri T, et al. Predicting drug release and degradation kinetics of long-acting microsphere formulations of tacrolimus for subcutaneous injection. J Control Rel. 2021;329:372-84.

[100] Gao GF, Thurn M, Wendt B, Parnham MJ, Wacker MG. A sensitive in vitro performance assay reveals the in vivo drug release mechanisms of long-acting medroxyprogesterone acetate microparticles. Int J Pharm Sci. 2020;586:119540.

[101] Mast M-P, Modh H, Knoll J, Fecioru E, Wacker MG. An Update to Dialysis-Based Drug Release Testing - Data Analysis and Validation Using the Pharma Test Dispersion Releaser. Pharmaceutics. 2021;13:12.

[102] Barzegar-Jalali M. Kinetic analysis of drug release from nanoparticles. J Pharm Pharm Sci. 2008;11:167-77.

[103] B.Chuasuwan, Binjesoh V, Polli JE, Zhang H, Amidon GL, Junginger HE, et al. Biowaiver Monographs for Immediate Release Solid Oral Dosage Forms: Diclofenac Sodium and Diclofenac Potassium. J Pharm Sci. 2009;98:1206-19.

[104] Auler J, Espada E, Crivelli E, Quintavalle TBG, Kurata A, Stolf N, et al. Diclofenac plasma protein binding: PK-PD modelling in cardiac patients submitted to cardiopulmonary bypass. Braz J Med Biol Res. 1997;30:369-74.

[105] Bou-Abdallah F, Sprague SE, Smith BM, Giffune TR. Binding thermodynamics of Diclofenac and Naproxen with human and bovine serum albumins: A calorimetric and spectroscopic study. J Chem Thermodyn. 2016;103:299-309.

[106] Willis JV, Kendall MJ, Flinn RM, Thornhill DP, Welling PG. The pharmacokinetics of diclofenac sodium following intravenous and oral administration. Eur J Clin Pharmacol. 1979;16:405-10.

[107] Anderson M, Kutzner S, Kaufman RH. Treatment of vulvovaginal lichen planus with vaginal hydrocortisone suppositories. Obstet Gynecol. 2002;100:359-62.

[108] Manfre M, Adams D, Callahan G, Gould P, Lang S, McCubbins H, et al. Hydrocortisone Cream to Reduce Perineal Pain after Vaginal Birth: A Randomized Controlled Trial. MCN Am J Matern Child Nurs. 2015;40.

[109] Lennernäs H, Skrtic S, Johannsson G. Replacement therapy of oral hydrocortisone in adrenal insufficiency: the influence of gastrointestinal factors. Expert Opin Drug Metab Toxicol. 2008;4:749 - 58.

[110] Corbo DC, Liu J-C, Chien YW. Drug Absorption Through Mucosal Membranes: Effect of Mucosal Route and Penetrant Hydrophilicity. Pharm Res. 1989;6:848-52.

[111] Wikipedia. Diclofenac. https://de.wikipedia.org/wiki/Diclofenac. (aufgerufen am 06. März 2023)

[112] Wikipedia. Cortisol. https://de.wikipedia.org/wiki/Cortisol. (aufgerufen am 06. März 2023)

[113] Smeraldi J, Ganesh R, Safarik J, Rosso D. Statistical evaluation of photon count rate data for nanoscale particle measurement in wastewaters. J Environ Monit. 2012;14:79-84.

[114] Vysotskii VV, Uryupina OY, Gusel'nikova AV, Roldugin VI. On the feasibility of determining nanoparticle concentration by the dynamic light scattering method. Colloid J. 2009;71:739.

[115] Wang D, Zhang Y, Liu Y-N, Wang J. Estimation of Binding Constants for Diclofenac Sodium and Bovine Serum Albumin by Affinity Capillary Electrophoresis and Fluorescence Spectroscopy. J Liq Chromatogr Relat Technol. 2008;31:2077-88.

[116] Nagpal S, Braner S, Modh H, Tan AXX, Mast MP, Chichakly K, et al. A physiologically-based nanocarrier biopharmaceutics model to reverse-engineer the in vivo drug release. Eur J Pharm Biopharm. 2020;153:257-72.

[117] Chow S-C. Bioavailability and Bioequivalence in Drug Development. Wiley Interdiscip Rev Comput Stat. 2014;6:304-12.

[118] Hansmann S, Darwich A, Margolskee A, Aarons L, Dressman J. Forecasting oral absorption across biopharmaceutics classification system classes with physiologically based pharmacokinetic models. J Pharm Pharmacol. 2016;68:1501-15.

[119] Hansmann S, Miyaji Y, Dressman J. An in silico approach to determine challenges in the bioavailability of ciprofloxacin, a poorly soluble weak base with borderline solubility and permeability characteristics. Eur J Pharm Sci. 2018;122:186-96.

[120] Jung F, Thurn M, Krollik K, Li D, Dressman J, Alig E, et al. Sustained-release hot melt extrudates of the weak acid TMP-001: A case study using PBB modelling. Eur J Pharm Sci. 2021;160:23-34.

[121] Olejnik A, Goscianska J, Nowak I. Active Compounds Release from Semisolid Dosage Forms. J Pharm Sci. 2012;101:4032-45.

[122] Mast M-P, Mesquita L, Gan K, Gelperina S, das Neves J, Wacker MG. Encapsulation and release of hydrocortisone from proliposomes govern vaginal delivery. Drug Del Trans Res. 2023;13:1022-34. (Veröffentlicht 2022 im Verlag Springer Nature)

[123] Danaei M, Dehghankhold M, Ataei S, Hasanzadeh Davarani F, Javanmard R, Dokhani A, et al. Impact of Particle Size and Polydispersity Index on the Clinical Applications of Lipidic Nanocarrier Systems. Pharmaceutics. 2018;10:2.

[124] Pavelić Ž, Škalko-Basnet N, Filipović-Grčić J, Martinac A, Jalšenjak I. Development and in vitro evaluation of a liposomal vaginal delivery system for acyclovir. J Control Rel. 2005;106:34-43.

[125] Nezzal A, Aerts L, Verspaille M, Henderickx G, Redl A. Polymorphism of sorbitol. J Cryst Growth. 2009;311:3863-70.

[126] Khan I, Yousaf S, Subramanian S, Korale O, Alhnan MA, Ahmed W, et al. Proliposome powders prepared using a slurry method for the generation of beclometasone dipropionate liposomes. Int J Pharm Sci. 2015;496:342-50.

[127] Suitchmezian V, Jeß I, Näther C. Structural, Thermodynamic, and Kinetic Aspectsof the Trimorphism of Hydrocortisone. J Pharm Sci. 2008;97:4516-27.

[128] Byeon JC, Lee S-E, Kim T-H, Ahn JB, Kim D-H, Choi J-S, et al. Design of novel proliposome formulation for antioxidant peptide, glutathione with enhanced oral bioavailability and stability. Drug Deliv. 2019;26:216-25.

[129] Standardization IOf. ISO 10993-5:2009 Biological Evaluation of Medical Devices - Part 5: Tests for In Vitro Cytotoxicity. Geneva, Switzerland2009.

[130] Heimbach T, Oh D-M, Li LY, Forsberg M, Savolainen J, Leppänen J, et al. Absorption Rate Limit Considerations for Oral Phosphate Prodrugs. Pharm Res. 2003;20:848-56.

[131] Cao Z, Zhang X, Wang C, Liu L, Zhao L, Wang J, et al. Different effects of cholesterol on membrane permeation of arginine and tryptophan revealed by bias-exchange metadynamics simulations. J Chem Phys. 2019;150:084106.

[132] Zhang L, Bennett WFD, Zheng T, Ouyang P-K, Ouyang X, Qiu X, et al. Effect of Cholesterol on Cellular Uptake of Cancer Drugs Pirarubicin and Ellipticine. J Phys Chem B. 2016;120:3148-56.

[133] Ramanathan R, Jiang Y, Read B, Golan-Paz S, Woodrow KA. Biophysical characterization of small molecule antiviral-loaded nanolipogels for HIV-1 chemoprophylaxis and topical mucosal application. Acta Biomater. 2016;36:122-31.

[134] Jøraholmen MW, Basnet P, Acharya G, Škalko-Basnet N. PEGylated liposomes for topical vaginal therapy improve delivery of interferon alpha. Eur J Pharm Biopharm. 2017;113:132-9.

[135] Wallenwein CM, Ashtikar M, Hofhaus G, Haferland I, Thurn M, König A, et al. How wound environments trigger the release from Rifampicin-loaded liposomes. Int J Pharm Sci. 2023;633:122606.

[136] Wallenwein CM, Weigel V, Hofhaus G, Dhakal N, Schatton W, Gelperina S, et al. Pharmaceutical Development of Nanostructured Vesicular Hydrogel Formulations of Rifampicin for Wound Healing. Int J Mol Sci. 2022;23:16207.

6 Anhang

6.1 Publikationen

6.1.1 Publikationsliste

Peer-review **Publikationen im Rahmen der Promotion (Erstautorenschaft),** Originalpublikationen sind Bestandteil dieser Dissertation und Artikel übernommen von

1. Mast MP, Modh H, Champanhac C, et al. Nanomedicine at the crossroads - A quick guide for IVIVC. Adv Drug Deliv Rev. 2021:113829. doi:10.1016/j.addr.2021.113829
2. Mast MP, Modh H, Knoll J, Fecioru E, Wacker MG. An Update to Dialysis-Based Drug Release Testing-Data Analysis and Validation Using the Pharma Test Dispersion Releaser. Pharmaceutics. 2021;13:12. doi:10.3390/pharmaceutics13122007
3. Mast MP, Mesquita L, Gan K, Gelperina S, das Neves J, Wacker MG. Encapsulation and release of hydrocortisone from proliposomes govern vaginal delivery. Drug Deliv Transl Res. 2023;13:1022-34. doi:10.1007/s13346-022-01263-x (Veröffentlicht 2022 im Verlag Springer Nature)

Peer-review **Publikationen außerhalb der Promotion (Mitautorenschaft)**

Nagpal S, Braner S, Modh H, Tan AXX, Mast MP, Chichakly K, et al. A physiologically-based nanocarrier biopharmaceutics model to reverse-engineer the in vivo drug release. Eur J Pharm Biopharm. 2020;153:257-72. doi:10.1016/j.ejpb.2020.06.004

Posterbeiträge

Ashtikar M, Gao F, Mast MP, Beilke D, Meyer H, Wacker MG. How to assess drug release from nanosized carriers?. ECA, Nano and Micro Formulations, Berlin, Deutschland, 2018.

6.1.2 Anteile des Autors und der Co-Autoren an den Publikationen

1. Mast MP, Modh H, Champanhac C, Wang JW, Storm G, Kramer J, et al. Nanomedicine at the crossroads - A quick guide for IVIVC. Adv Drug Deliv Rev. 2021:113829.. (Übersichtsartikel) . doi:10.1016/j.addr.2021.113829 (Übersichtsartikel)

Anteile des Autors (Marc-Phillip Mast)

Literaturrecherche, Be- und Auswertung der recherchierten klinischen Studien, Verfassen und Korrektur des Manuskripts, Erstellen von Graphiken

Anteile der Co-Autoren:

- Harshvardhan Modh: Korrektur des Manuskripts, fachliche Unterstützung zum Abschnitt Wirkstofffreisetzung
- Carole Champanhac: Literaturrecherche, Verfassen und Korrektur des Manuskriptes insbesondere der Abschnitt zur Immuntherapie
- Jiong-Wei Wang: Korrektur des Manuskripts, fachliche Unterstützung zu Exosomen
- Gerrit Storm: Verfassen und Korrektur des Manuskripts
- Johannes Krämer: Korrektur des Manuskripts, fachliche Unterstützung zu *in vivo-in vitro* Korrelation
- Volker Mailänder: Verfassen und Korrektur des Manuskripts insbesondere der Abschnitt zur Immuntherapie
- Giorgia Pastorin: Verfassen und Korrektur des Manuskripts insbesondere zum Abschnitt über Exosomen
- Matthias G. Wacker: Supervision, Verfassen und Korrektur des Manuskripts, Erstellen von Graphiken

2. Mast MP, Modh H, Knoll J, Fecioru E, Wacker MG. An Update to Dialysis-Based Drug Release Testing - Data Analysis and Validation Using the Pharma Test Dispersion Releaser. Pharmaceutics. 2021;13:12. doi:10.3390/pharmaceutics13122007

Anteile des Autors (Marc-Phillip Mast)

Versuchsplanung und -durchführung, statistische Auswertung und Darstellung der Versuchsergebnisse, Verfassen und Korrektur des Manuskripts, Erstellen der graphischen Darstellungen

Anteile der Co-Autoren:

- Harshvardhan Modh: Unterstützung in der Erstellung des mathematischen Modells in Stella Architect®, Korrektur des Manuskripts
- Julian Knoll: Erstellung des mathematischen Modells in Stella Architect®, Verfassen des Manuskripts insbesondere der Abschnitt zum mathematischen Modell
- Elena Fecioru: Unterstützung in der Erstellung des mathematischen Modells in Stella Architect®
- Matthias Wacker: Supervision, Einholen von Fördermitteln, Korrektur des Manuskripts

3. Mast MP, Mesquita L, Gan K, Gelperina S, das Neves J, Wacker MG. Encapsulation and release of hydrocortisone from proliposomes govern vaginal delivery. Drug Deliv Transl Res. 2023;13:1022-34

Anteile des Autors (Marc-Phillip Mast)

Konzept, Planung und Durchführung der Experimente (Herstellung und Charakterisierung der Proliposomen, Untersuchung der Wirkstofffreisetzung, HPLC-Messung der Permeabilitätsuntersuchung), statistische Auswertung, Graphische Darstellung der Ergebnisse, Verfassen und Korrektur des Manuskripts

Anteile der Co-Autoren:

- Letícia Mesquita: Planung und Durchführung der Untersuchung der Zytotoxizität und Permeabilität der Proliposomen, Auswertung der Permeabilitätsdaten
- Kennard Gan: Korrektur des Manuskripts, statistische Auswertung der Ergebnisse der Wirkstofffreisetzung
- Svetlana Gelperina: Korrektur des Manuskripts
- José das Neves: Auswertung der Permeabilitätsdaten, Korrektur des Manuskripts, Einholen finanzieller Fördermittel
- Matthias G. Wacker: Supervision, Korrektur des Manuskripts, Einholen finanzieller Fördermittel

6.2 Publikationsmanuskripte

Advanced Drug Delivery Reviews 179 (2021) 113829

Contents lists available at ScienceDirect

Advanced Drug Delivery Reviews

journal homepage: www.elsevier.com/locate/adr

Nanomedicine at the crossroads – A quick guide for IVIVC

Marc-Phillip Mast [a,b], Harshvardhan Modh [c], Carole Champanhac [d], Jiong-Wei Wang [e,f,g,h], Gerrit Storm [e,h,i], Johannes Krämer [j], Volker Mailänder [d,k], Giorgia Pastorin [c], Matthias G. Wacker [c,*]

[a] Fraunhofer Institute for Translational Medicine and Pharmacology ITMP, Theodor-Stern-Kai 7, 60596 Frankfurt am Main, Germany
[b] Institute of Pharmaceutical Technology, Goethe University, Max-von-Laue-Str. 9, 60438 Frankfurt am Main, Germany
[c] National University of Singapore, Department of Pharmacy, 5 Science Drive 2, 117545 Singapore
[d] Max Planck Institute for Polymer Research, Mainz, Germany
[e] Department of Surgery, Yong Loo Lin School of Medicine, National University of Singapore, 119228 Singapore
[f] Cardiovascular Research Institute, National University Heart Centre Singapore, 117599 Singapore, Singapore
[g] Department of Physiology, Yong Loo Lin School of Medicine, National University of Singapore, 117593 Singapore. Singapore
[h] Nanomedicine Translational Research Programme, Centre for NanoMedicine, Yong Loo Lin School of Medicine, National University of Singapore, 117609 Singapore, Singapore
[i] Utrecht University, Department of Pharmaceutics, the Netherlands
[j] DISSO GmbH, Homburg (Saar), Germany
[k] Department of Dermatology, University Medical Center of the Johannes Gutenberg-University Mainz, Mainz, Germany

ARTICLE INFO

Article history:
Received 18 March 2021
Revised 17 May 2021
Accepted 10 June 2021
Available online 24 June 2021

Keywords:
Nanomedicine / nanoparticles / nanomaterials
Clinical
Liposomes
In vitro-in vivo correlation / relationship (IVIVC / IVIVR)
Translational

ABSTRACT

For many years, nanomedicine is pushing the boundaries of drug delivery. When applying these novel therapeutics, safety considerations are not only a key concern when entering clinical trials but also an important decision point in product development. Standing at the crossroads, nanomedicine may be able to escape the niche markets and achieve wider acceptance by the pharmaceutical industry. While there is a new generation of drug delivery systems, the extracellular vesicles, standing on the starting line, unresolved issues and new challenges emerge from their translation from bench to bedside. Some key features of injectable nanomedicines contribute to the predictability of the pharmacological and toxicological effects. So far, only a few of the physicochemical attributes of nanomedicines can be justified by a direct mathematical relationship between the *in vitro* and the *in vivo* responses. To further develop extracellular vesicles as drug carriers, we have to learn from more than 40 years of clinical experience in liposomal delivery and pass on this knowledge to the next generation. Our quick guide discusses relationships between physicochemical characteristics and the *in vivo* response, commonly referred to as *in vitro-in vivo* correlation. Further, we highlight the key role of computational methods, lay open current

Abbreviations: AAFE, Absolute Average Fold Error; ADME, Absorption, Distribution, Metabolism, Elimination; AF4, Asymmetric flow field-flow fractionation; ALIX, ALG-2 interacting protein X; ALL, Acute lymphoblastic leukemia; AML, Acute myeloid leukemia; Anti-HER2 scFv (F5)-PEG-DSPE, Polyethylene glycol-distearoyl phosphatidylethanolamine conjugated with an antibody fragment binding HER2; APC, Antigen-presenting cells; API, Active pharmaceutical ingredient; AUC, Area under the curve; BA, Bioavailability; BE, Bioequivalence; BSA, Bovine serum albumin; c_{max}, Peak plasma drug concentration; CQA, Critical quality attribute; DLin-MC3-DMA, (6Z,9Z,28Z,31Z)-heptatriacont-6,9,28,31-tetraene-19-yl 4-(dimethylamino)butanoate; DMPC, Dimyristoyl phosphatidylcholine; DMPG, Dimyristoyl phosphatidylglycerol; DNA, Desoxyribonucleic acid; DOPS, Dioleoyl phosphatidylserine; DPPC, Dipalmitoyl phosphatidylcholine; DSC, Differential scanning calorimetry; DSPC, Distearoly phosphatidylcholine; DSPE, Distearyl phosphatidylethanolamine; DSPG, Distearoyl phosphatidylglycerol; EMA, European Medicines Agency; EPC, Egg phosphatidylcholine; EPG, Egg phosphatidylglycerol; ESCRT, Endosomal Sorting Complex Required for Transport; EV, Extracellular vesicle; f_{accum}, Drug efflux from the carrier accumulated in the periphery; $f_{release}$, Drug release from the carrier; FRET, Förster Fluorescence Resonance Energy Transfer; F_{target}, Targeting capability; FTIR, Fourier-transform infrared spectroscopy; HER2, Human epidermal growth factor receptor 2; GMP, Good Manufacturing Practice; HSP, Heat Shock Protein; HSPC, Hydrogenated soy phosphatidylcholine; ILV, Intraluminal vesicle; IVIVC, *In vitro-in vivo* correlation; IVIVR, *In vitro-in vivo* relationship; m_{accum}, Amount of the encapsulated drug being accumulated in the periphery; $m_{carrier}$, Amount of the drug in the carrier compartment; miRNA, microRNA; $mPEG_{2000}$-DSPE, Methoxy-polyethylene glycol-distearoyl phosphatidylethanolamine; MRI, Magnetic resonance imaging; MSPC, Myristoylstearoyl phosphatidylcholinemean; MSPC, Myristoylstearoyl phosphatidylcholine; MVB, Multivesicular Bodies; NBCD, Non-biological complex drug; NSCLC, Non-small-cell lung carcinoma; NV, Nanovaccine; PBB model, Physiologically based biopharmaceutics model; PBNB, Physiologically based nanocarrier biopharmaceutics model; PBPK model, Physiologically based pharmacokinetic model; PEG, Polyethylene glycol; PEG_{2000}-DMG, 1,2-dimyristoyl-*rac*-glycero-3-methoxypolyethylene glycol-2000; pKa, Negative log of the acid dissociation constant; PLA, Polylactic acid; PLGA, Poly(lactide-co-glycolide); POPC, Palmitoyloleoyl phophatidylcholine; PSMA, Prostate-specific membrane antigen; RNA, Ribonucleic acid; scFv, Single chain variable fragment; sEV, Small extracellular vesicle; SM, Sphingomyelin; siRNA, Short interfering RNA; $t_{1/2}$, Elimination Half-life; $t_{50\%}$, Time for 50% drug to dissolve or release; $t_{90\%}$, Time for 90% drug to dissolve or release; t_{last}, Time to last measured plasma; t_{max}, Time to peak plasma drug concentration; TSG101, Tumour susceptibility gene 101; UK, The United Kingdom of Great Britain and Northern Ireland; USA, The United States of America; USD, United States Dollar; US-FDA, Food and Drug Administration of the United States; USP, United States Pharmacopeia; V_D, Volume of distribution; V_{DC}, Volume of distribution of the nanocarrier; V_{DF}, Volume of distribution of the free drug.

* Corresponding author at: Department of Pharmacy | Faculty of Science, National University of Singapore, Building S9 Level 15, 5 Science Drive 2, Singapore 117545, Singapore.
E-mail address: matthias.g.wacker@nus.edu.sg (M.G. Wacker).

https://doi.org/10.1016/j.addr.2021.113829
0169-409X/

Extracellular vesicles (EVs)
Prediction

knowledge gaps, and question the established design strategies. Has the recent progress improved the predictability of targeted delivery or do we need another change in perspective?

Contents

1. Introduction

For decades, nanomedicines have evolved under the umbrella of disruptive innovation and entered the global healthcare market. Among other therapies, with approximately 33% of nanomaterial-related dossier submissions to the Food and Drug Administration of the United States of America (US-FDA) [1], liposomes are the largest fraction, expecting sustainable growth as indicated by a revenue market volume of 3.6 billion USD (2019) and a predicted compound annual growth rate of 10.27% in 2023 [2]. These vesicles are manufactured from phospholipids with the active pharmaceutical ingredient (API) incorporated into the hydrophilic core or the lipophilic membrane. They have been used for a wide variety of applications including injectable drug products [3]. Industrial manufacture is achieved by extrusion or high-pressure homogenization of the phospholipids dissolved in the organic phase [4]. Intravenous nanomedicines were most successfully applied in cancer therapy. They are sometimes referred to as non-biological complex drugs (NBCDs) [5,6]. Owing to their composition, the physicochemical characteristics of liposomes rather than the chemical identity or the properties of the API are responsible for the *in vivo* performance [5,6]. Today, a wide variety of clinical trials provide evidence for the processes involved in liposomal drug delivery [3]. However, the resolution of clinical data is broadly driven by the bioanalytical methods employed. For example, during the early days of nanomedicine, the total drug amount in the blood plasma rather than the encapsulated and the non-encapsulated fraction was reported (see Section 4.4). As a consequence, recent guidelines published by the US-FDA demand more sophisticated measures of bioavailability (BA) [7]. The missing link between the physicochemical features of vesicle-based delivery systems and their clinical response represents one of the major challenges in clinical translation [8,9]. Table 1 summarizes the common terminology and definitions related to nanomedicine.

Currently, the nanomedicine industry gains new momentum by developing the next generation of vesicle-based therapeutics. Extracellular vesicles (EVs) such as exosomes and microvesicles are spherical vesicles released by a wide variety of cells. They play a key role in the exchange of messenger molecules and intercellular communication [10,11]. Equipped with a unique combination of (surface) proteins, genetic material, and recognized by the target tissues, they provide many advantages as compared to their liposomal counterparts [12–14]. Some of them even exhibit inherent pharmacological effects including immunomodulation, regenerative therapies as well as anti-tumor therapy, and vaccination [15].

The smallest type of EVs, the exosomes, with a size of 30–150 nm, are formed naturally through endosomal invagination and subsequent extracellular secretion (see Section 2). Being part of the intercellular communication system, they deliver cytoplasmic contents, mainly messengerRNAs (mRNAs), microRNAs (miRNAs), and proteins, in the extracellular space [16]. They retain the natural targeting properties of their parent cells [17,18]. Moreover, EVs utilize innate mechanisms of internalization and trafficking [18], which enhance permeability into target cells and can be further explored for selective drug delivery. Due to their biogenesis and isolation, EVs are a very heterogeneous family of nanomedicines. Therefore, the cell source, culture conditions as well as separation and concentration protocols have to be standardized, ensuring their clinical safety. To allow a direct comparison with liposomal vesicles, we will focus on drug delivery applications of EVs. When applying them as a facilitator of drug therapy rather than a treatment, criteria for *in vitro-in vivo* correlation (IVIVC)

Table 1
Common terms and definitions used to describe nanomedicines.

Term	Definition
Nanomedicine	Highly specific medical intervention at the molecular scale that uses nanotechnology to cure or diagnose diseases or repair damaged tissues.
Nanotechnology	Manipulation of materials with at least one dimension at the nanoscale (~1–100 nm) or the intended engineering of materials with physicochemical properties or biological effects related to its dimensions in the range of 1–1000 nm.
Nanocarrier	A drug delivery system in the nanoscale (1–1000 nm) capable of altering the biodistribution or penetration behavior of drugs, acting as an exogenous carrier.
Liposome	Spherical vesicles composed of phospholipids with at least one lipid bilayer.
Nanoparticle	Particle in a size range between 1 and 1000 nm. These particles can be composed of inorganic materials (e.g. gold, silver), organic polymers (e.g. PLGA, PLA), or proteins.
Non-biological complex drugs	Assemblies of drug and excipient molecules in the nanoscale manufactured in complex production processes, which enable the physicochemical attributes to be controlled at the molecular scale. They are defined by the physical form and nanotechnology-related surface characteristics rather than the chemical identity.
Drug delivery system	A formulation or a device that controls the rate, time, and place of release of an APIin the body.
Extracellular vesicle	Natural spherical vesicles, released by cells without the ability to replicate but with a very unique composition depending on cell type and biogenesis.

can be defined. Also, many lessons can be learned from decades of nanotechnology research. For more information on the application of EVs as active ingredients, the reader is kindly referred to recent publications of the International Society of Extracellular Vesicles [15,19–21].

For many years, the scientific community has explored the preclinical and clinical applications of first-generation nanomedicines including nanoparticles and liposomes. Still, their *in vivo* performance is unpredictable. The US-FDA defines IVIVC as a mathematical relationship between the *in vitro* characteristics of a drug product and therapeutically relevant *in vivo* responses [22]. After successful validation, the IVIVC can be used to provide clinically relevant *in vitro* methods, justify the specifications ranges applied in quality control, or even support process development [22]. Also, it can be used as a surrogate for bioequivalence studies [22].

Emphasizing injectable nanomedicines, we will elucidate the current state-of-the-art in the development of these mechanistic *in vitro-in vivo* relationships (IVIVRs) with an outlook to engineered EVs. Also, we will illustrate the key role of modeling and computational methods and highlight important knowledge gaps.

2. Biogenesis and composition of extracellular vesicles

Although there are certain similarities between liposomes and EVs, the latter are heterogeneous in nature and require a more detailed characterization. While liposomes exhibit a bilayer membrane that comprises a selection of commercially available phospholipids, the composition of EVs is defined by the biological identity and cell type involved in their biogenesis.

EVs are released by many different eukaryotic and prokaryotic cells and can be classified by their size, size distribution, and origin [23]. The components of each type of vesicle can further be analyzed by using a proteomic, lipidomic, and transcriptomic approach. These methods may provide additional information on the identity, molecular mechanisms of biogenesis, (patho-) physiological functions, and cargo sorting of EVs. Several databases systematically collect this information, for example, EVpedia [24], Vesiclepedia [25], and ExoCarta [26]. A common classification based on their cellular origin includes microvesicles, apoptotic bodies, and exosomes. Microvesicles (also referred to as ectosomes) are formed through outward budding and pinched off from the plasma membrane into the extracellular space. They have a size of 100–1000 nm. The role in intercellular communication is still uncertain, however, they can deliver large molecules such as different types of RNA, and proteins. For comparison, apoptotic bodies are generated from apoptotic cells only. They package components of each cellular sub-compartment into vesicles broadly distributed in size, ranging from 50 to 5000 nm [27,28]. During apoptosis, they provide an orderly process for the disposal of cellular components. Smaller EVs, the exosomes, originate from the multivesicular bodies (MVB). The size of exosomes is discussed in recent literature with the broadest size distribution ranging within 30–150 nm [15,29–34]. Asymmetric flow field-flow fractionation (AF4) has been used to investigate two exosome subpopulations ranging from 60 to 80 nm and 90–120 nm, respectively. Both are most likely involved in intercellular signaling. The size distribution of EVs can be heterogeneous and there is a certain overlap between all three groups. Therefore, the International Society for Extracellular Vesicles (ISEV) recommends purified particle populations to be termed EV preparations or small extracellular vesicle (sEV) preparations. Particles with a size of less than 30 nm were isolated using asymmetrical flow field-flow fractionation (AF4) and is often referred to as exomers. They are lacking the common exosome markers and are therefore not considered EVs [35]. So far, the biogenesis and biological roles of these smaller structures are widely unknown [36].

Exosomes are most comparable to liposomes but they may contain a broad array of surface proteins and phospholipids [13,37]. They originate from the early endosomes and start forming from the plasma membrane through inward budding or endocytosis [38]. Early endosomes mature into intraluminal vesicles (ILVs) inside the late endosomes, also known as multivesicular bodies (MVB) [33,39]. In most cases, MVB fuse with the plasma membrane and release the ILVs into the extracellular space. These vesicles are known as exosomes.

An illustration of the biogenesis of exosomes is presented in Fig. 1a. ILVs are formed in MVB through Endosomal Sorting Complex Required for Transport (ESCRT)-dependent and -independent mechanisms. The ESCRT machinery comprises five protein complexes including ESCRT-0, I, II, III, and Vps4. Other components are ALG-2 interacting protein X (ALIX) and tumor susceptibility gene 101 (TSG101). ESCRT-0 uses ubiquitinated protein receptors at the site of the endosomal membrane while ESCRT-I and -II are suggested to catalyze budding of the endosomal membrane and transport of the necessary cargoes into the lumen of MVB. ESCRT-III completes the budding, segmenting the EVs from the donor cell [29,40,41]. Interestingly, even when cells are depleted of ESCRT components, they are still able to form intraluminal vesicles (ILVs) using an ESCRT-independent mechanism. This involves tetraspanins, heat shock proteins (HSP), and lipids [13,41]. Although there exists an ExoCarta database that classifies 9,769 proteins, 3,408 mRNAs, 2,838 miRNAs, and 1,116 lipids as key components in exosomes, the exosomal content is highly variable and strongly influenced by the condition and the type of cells exosomes are derived from [33]. Nonetheless, a few key molecules can be used as markers for EV detection and isolation. Some of them include ALIX, TSG101, HSP 70 and 90 as well as tetraspanins (e.g. CD9, CD63, CD81) [29,42]. A combination of these markers can be used for exosome identification. Other common contents of exosomes are illustrated in Fig. 1b.

EVs have been investigated for several biomedical applications [12,44,45]. The isolation processes are even more complex than

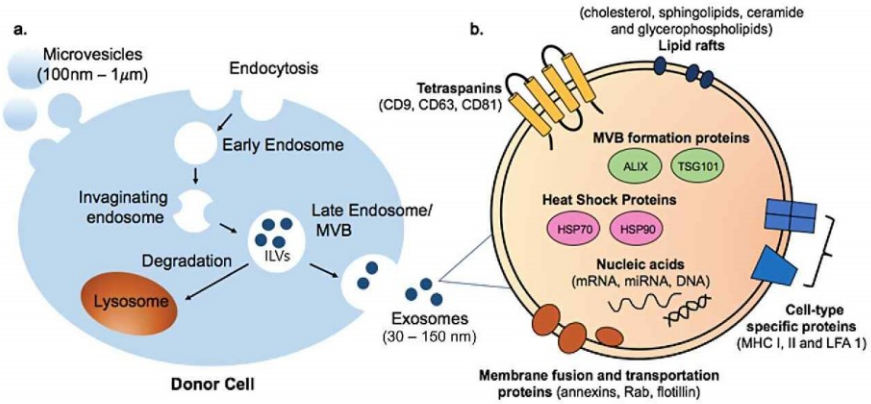

Fig. 1. Biogenesis of exosomes (a) begins by endocytosis of the plasma membrane. Before early endosomes mature into late endosomes, intraluminal vesicles (ILVs) form through the invagination of endosomal membranes. After fusion of multivesicular bodies (MVB) with the plasma membrane, ILVs are released into extracellular space as exosomes, with a size of approximately 30–150 nm. The composition of exosomes (b) can include proteins, lipids, and genetic materials. Some of the components (e.g. ALIX, TSG101, CD63 proteins) are seen as hallmarks for exosomes, while others (e.g. MHC 1, II, LFA 1) vary according to the parent cells from which EVs are secreted. Some of the exosomal markers include MVB formation proteins, ALIX and TSG101 mentioned already, and heat shock proteins (e.g. HSP70 and HSP90), which are involved in sorting proteins into ILVs. Other components include CD9, CD63, and CD81 in the tetraspanin family, lipid rafts (cholesterol, sphingolipids, ceramide, and glycerophospholipids), proteins involved in membrane fusion and transportation (annexins, Rab, flotillin), and nucleic acids (mRNAs, non-coding RNAs such as miRNAs, and DNAs). Modified from [13,27,34,42,43].

the ones used in the production of liposomes and often result in vesicle populations broadly distributed in size combined with a poor process yield [46]. The parameters applied in their separation and concentration have a strong impact on the physicochemical characteristics of the EVs. To identify a preferred concentration method a wide variety of considerations have to be made. These include the intended therapeutic application, the route of administration, the cellular material, and the desired product characteristics e.g. with regards to the size, lipid, and protein composition. Additionally, the method must be robust and reproducible to be used in an industrial environment under good manufacturing practice (GMP) conditions. In drug delivery, EVs would be used as an excipient material facilitating the delivery of the active substance. However, as outlined by the US-FDA guidance on liposomal drug products, excipients with a strong impact on quality and performance should be characterized at a level of detail comparable to that for a drug substance [47]. Commonly, differential or density gradient ultracentrifugation methods are used to concentrate the vesicles. These methods are hardly scalable. Therefore, size exclusion methods or tangential flow filtration could be considered [20,48–50]. Because the isolation process may not lead to vesicles generated by one of the abovementioned biosynthesis pathways alone, EVs in size range from 50 to 200 nm should be described as small extracellular vesicle preparation rather than exosomes [19]. To understand the role of EVs in comparison to liposomal drug products, a summary of the last 30 years of clinical research on nanomedicines is provided.

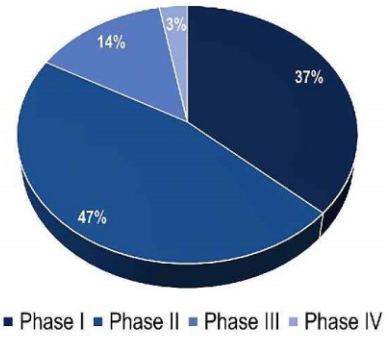

Fig. 2. Distribution (percentage) of 172 nanomedicine-related clinical trials by clinical stage (phase I-IV).

3. Nanomedicines in clinical research

Over the years, a wide variety of clinical trials have been conducted using NBCDs. Fueled by first successes in the 1990s [51,52], anticancer agents were encapsulated into liposomal carriers, to reduce their toxicity and to deliver drugs to a specific site of action. During the 2000s, the nanoparticle albumin-bound (nab) technology, originally designed by Abraxis BioScience but nowadays brought to market by Bristol-Myers Squibb, was applied to load hydrophobic compounds into albumin nanoparticles [53]. These and other discoveries shaped the era of nanomedicine. In the following, some of the most promising approaches utilizing nanocarrier technology will be presented.

So far liposomal drug delivery systems account for most of the clinical trials involving nanocarrier-technology. To elucidate the clinical development of these NBCDs, a total of 385 completed clinical trials, reported by the US National Library of Medicine website (www.clinicaltrials.gov) under the keywords "liposome" and "IV" have been reviewed. After an initial selection, only 172 studies using intravenously applied liposomes remained and they were classified by clinical stage (Fig. 2) and drug molecule (Fig. 3). More than 80% of the studies are in the early phases I (36%) or II (46%). Only 25 phase III clinical trials and 5 phase IV clinical trials were found (Fig. 2). While the total number of clinical trials is encourag-

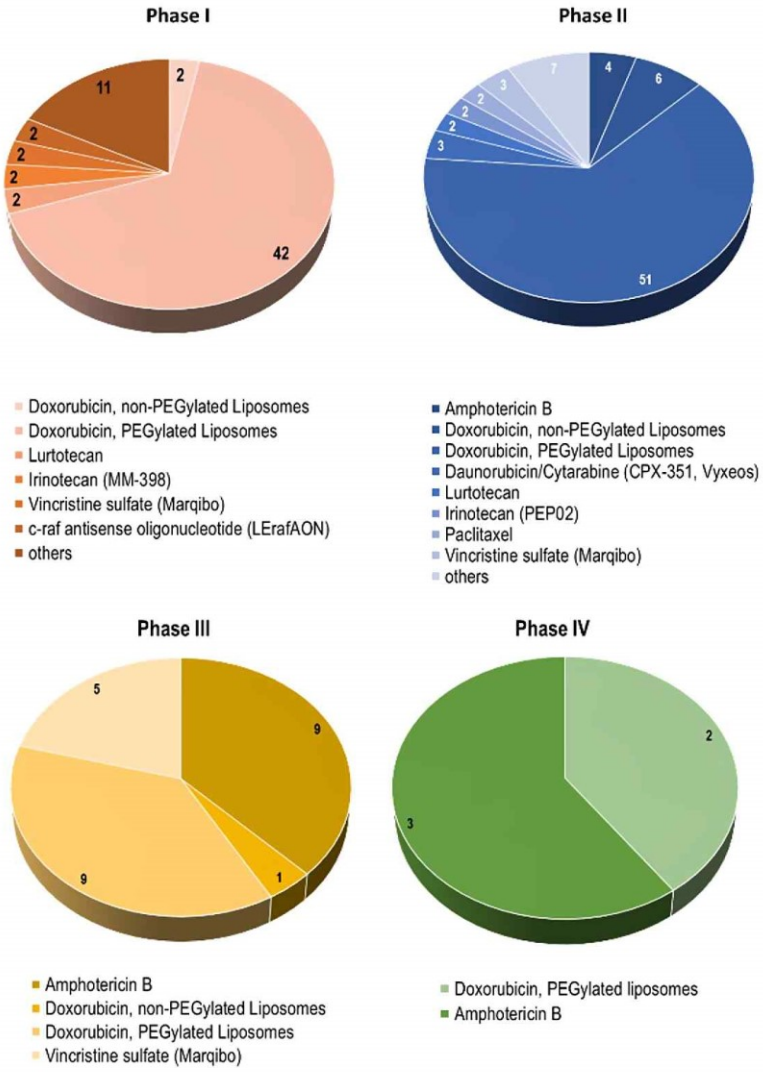

Fig. 3. Number of studies identified from 172 nanomedicine-related clinical trials (clinicaltrials.gov) sorted by the drug molecule. For phase I clinical trials *'others'* include mono-therapeutics of amphotericin B, topotecan, daunorubicin, mitoxantron, mitomycin, annamycin, docetaxel, eribulin-LF, oxaliplatin, Fus-1 gene (DOTAP:Chol-fus 1), and antitoxin agent (CAL-02). For phase II clinical trials *'others'* include mono-therapeutics of daunorubicin, annamycin, SN-38, docetaxel, cisplatin, tretinoin, and alendronate.

ing, the poor "developability" of liposomes into market-ready drug products gives reason for concern. To achieve wider acceptance, a more predictable therapeutic and economic success will be a key priority for the next generation of NBCDs. To allow more manufacturers to participate in the niche market of nanocarrier-based delivery, the influence of process parameters on the clinical responses must be understood in more detail. This will not only define the future of liposomes but also pave the way for more advanced biotechnological drug products such as EV preparations.

3.1. Liposomal drug formulations

Most of the phase I clinical trials were conducted using liposomal doxorubicin (Fig. 3) modified on the surface with polyethylene

Table 2
Selected intravenously administered nanocarrier drug products. Molar ratios are expressed as a function of the average molecular mass of the excipients.

Liposomal systems	Description	Drug	Market approval	Reference
Doxil® (Johnson & Johnson, USA)	**Composition** • HSPC • Cholesterol • $mPEG_{2000}$-DSPE **Molar ratio** 56:39:5 **Indications** • Ovarian cancer • AIDS-related Kaposi's sarkoma • Multiple Myeloma	Doxorubicin	1995 (US-FDA)	[92]
DaunoXome® (Gilead Sciences, USA)	**Composition** • DSPC • Cholesterol **Molar ratio** 2:1 **Indications** • AIDS-related Kaposi's sarkoma	Daunorubicin	1996 (US-FDA)	[93]
AmBisome® (Astellas Pharma, USA)	**Composition** • HSPC • Cholesterol • DSPG **Molar ratio** 26:13:10 **Indications** • Systemic fungal infections (e.g *Aspergillus*, *Candida*, *Cryptococcus* species) • Visceral leishmaniasis	Amphotericin B	1997 (US-FDA)	[94]
Myocet® (Teva B.V., Netherlands)	**Composition** • EPC • Cholesterol **Molar ratio** 55:45 **Indications** • Metastatic breast cancer	Doxorubicin	2000 (EMA)	[95]
Visudyne® (Novartis Pharmaceuticals, USA)	**Composition** • DMPC • EPG **Molar ratio** unknown **Indications** • Subfoveal choroidal neovascularization	Verteporfin	2000 (US-FDA)	[96]
Mepact® (Takeda France SAS, France)	**Composition** • DOPS • POPC **Molar ratio** 3:7 **Indications** • Non-metastatic osteosarcoma	Mifamurtide	2004 (EMA)	[97]
Marqibo™ (Talon Therapeutics, USA)	**Composition** • SM • Cholesterol **Molar ratio** 58:42 **Indications** • Philadelphia chromosome-negative acute lymphoblastic leukemia	Vincristine	2012 (US-FDA)	[98]
Lipodox™ (Sun Pharma, India)	Generic Doxil®	Doxorubicin	2013 (US-FDA)	[99]
Onivyde™ (Merrimack Pharmaceuticals, USA)	**Composition** • DSPC • Cholesterol • $mPEG_{2000}$-DSPE **Molar ratio** 3:2:0.015 **Indications** • Metastatic adenocarcinoma of the pancreas	Irinotecane	2015 (US-FDA)	[100]
DOXOrubicin HCl Liposome Injection (Dr. Reddy's Laboratories, India)	Generic Doxil®	Doxorubicin	2017 (US-FDA)	[101]
Vyxeos® (Jazz Pharmaceuticals, USA)	**Composition** • DSPC • DSPG • Cholesterol **Molar ratio** 7:2:1 **Indications** • Therapy-related acute myeloid leukemia • Acute myeloid leukemia with myelodysplasia-related changes	Cytarabine Daunorubicin (1:5 molar ratio)	2017 (US-FDA)	[57]

Table 2 (*continued*)

Non-liposomal systems	Description	Drug	Market approval	Reference
Abraxane™ (Bristol-Myers Squibb, USA)	**Composition** • Human albumin **Molar drug:protein ratio** 9:1 **Indications** • Metastatic breast cancer	Paclitaxel	2005 (US-FDA)	[102]
Feraheme™ (AMAG Pharmaceuticals, USA)	**Composition** • Polyglucose sorbitol carboxymethyl ether **Iron oxide:Carbohydrate ratio** 6:4 **Indications** • Iron deficiency anemia	Iron oxide	2009 (US-FDA)	[103]
Onpattro™ (Alnylam Pharmaceuticals, USA)	**Composition** • DLin-MC3-DMA • PEG_{2000}-DMG • DSPC • Cholesterol **Molar ratio** 49:2:10:39 **Indications** • hereditary transthyretin-mediated amyloidosis	siRNA	2018 (US-FDA)	[104,105]
Abelcet® (Sigma-Tau Pharmaceuticals, USA)	**Composition** • DMPC • DMPG **Molar ratio** 7:3 **Indications** • Invasive fungal infections	Amphotericin B	1995 (US-FDA)	[106]

Abbreviations: DSPC, Distearoly phosphatidylcholine; DSPG, Distearoyl phosphatidylglycerol; HSPC, Hydrogenated soy phosphatidylcholine; PEG, Polyethylene glycol; DSPE, Distearyl phosphatidylethanolamine; EPC, Egg phosphytidylcholine; DOPS, Dioleoyl phosphatidylserine; POPC, Palmitoyloleoyl phophatidylcholine; $mPEG_{2000}$-DSPE, methoxy-polyethylene glycol-distearoyl phosphatidylethanolamine; DMPC, Dimyristoyl phosphatidylcholine; DMPG, Dimyristoyl phosphatidylglycerol; EPG, egg phosphatidylglycerol; DLin-MC3-DMA, (6Z,9Z,28Z,31Z)-heptatriacont-6,9,28,31-tetraene-19-yl 4-(dimethylamino)butanoate; PEG_{2000}-DMG, α-(3′-{[1,2-di(myristyloxy)propanoxy] carbonylamino}propyl)-ω-methoxy polyoxyethylene

glycol (PEG) in monotherapy or combination with trastuzumab, carboplatin, carfilzomib, and bortezomib to evaluate safety and efficacy in cancer treatment. This highlights the clinical and economic success of this liposomal drug product. Several bioequivalence (BE) studies gave rise to a new family of generics including Lipodox® (Sun Pharma, India) and DOXOrubicin HCl Liposome Injection (Dr. Reddy's Laboratories, India). Other anthracyclines such as daunorubicin, mitoxantrone, mitomycin, and annamycin were encapsulated into liposomes as well, but the success was limited as compared to doxorubicin (Fig. 3). AmBisome® provides another example of the niche markets that were successfully conquered by liposome technology (Fig. 3). It comprises the antifungal agent amphotericin B encapsulated into single-bilayer liposomes. A generic version was developed by Taiwan Liposomal Company (Taiwan) and evaluated in a BE study. Interestingly, AmBisome® exhibits a prolonged circulation time even without the presence of pegylated lipids [54]. In current literature, surface pegylation is one of the most important strategies employed to extend the circulation time of nanocarriers. More than 10 years after AmBisome® entered the market, Onivyde™, Vyxeos™, and Marqibo™ were approved by the US-FDA (Table 2). Marqibo®, a formulation of vincristine sulfate, is indicated for the treatment of adults with acute lymphoblastic leukemia (ALL) [55]. Onivyde™ is a pegylated liposomal formulation of irinotecan, a topoisomerase inhibitor, indicated for the treatment of patients with metastatic adenocarcinoma of the pancreas in combination with fluorouracil and leucovorin after disease progression following gemcitabine-based therapy. Vyxeos® is the first dual-drug liposomal carrier comprising the anthracycline daunorubicin in combination with the nucleoside analog cytarabine in a molar ratio of one to five [56]. It is indicated for the treatment of therapy-related or myelodysplasia-related high-risk acute myeloid leukemia (AML) [57]. Cytarabine is encapsulated by diffusion during the extrusion process whereas daunorubicin is actively loaded into the liposomes using an intra-liposomal copper complex [58]. A synergistic antineoplastic effect was found *in vitro*, reflecting the exact molar ratio encapsulated into the liposome [59,60]. The therapeutic value of this novel treatment stems from improved efficacy in the treatment of poor-risk AML subgroups. Compared to the standard treatment with overall survival of 5.95 months, Vyxeos® was able to improve this outcome to 9.56 months [56]. Consequently, patient stratification plays a key role in clinical success.

Emphasizing the formulation process, several drug products including Doxil®, Onivyde™, Vyxeos™, and Marqibo™, were loaded with drug molecules using an ion gradient technique commonly referred to as *'remote loading'*. Even in the absence of pegylated lipids (Marqibo™, Vyxeos™), the sustained drug release resulting from this procedure [61] led to a significantly prolonged apparent elimination half-life [62–65]. This sustains a key role of drug release in the prolonged circulation time of the encapsulated drug. Also, comparing major influences on plasma pharmacokinetics, the strong impact of surface pegylation must be questioned. Pegylation enables the accumulation of particles in the malignant tissue by virtue of a prolonged circulation time of the carrier. Although this may be true to a certain extent, the quantitative influence of drug release has proven much stronger and, from a formulation perspective, deserves considerable attention. While the sustained release together with favorable stability features of nanocarriers often correlate to a prolonged circulation half-life [54,66–69], surface pegylation alone delivers only a moderate decrease in drug clearance. Noteworthy, we cannot conclude that the pegylation does not play a central role in clinical success, however, the influence on kinetics in the blood plasma is lower as compared to other parameters.

Lipoplatin™ (Regulon Inc., USA) and SPI-077 (Sequus Pharmaceuticals Inc., USA) are two more examples highlighting the importance of drug release in the clinical response. SPI-077 was evaluated in two clinical trials treating either patients with advanced non-small-cell lung carcinoma (NSCLC) or inoperable head and neck cancer. In both cases, the clinical response rates were negligible [70,71]. On the contrary, Lipoplatin™ was tested in two phase III clinical trials, achieving acceptable response rates and reduced side effects [72–74]. The superiority over non-liposomal cisplatin was further revealed by meta-analysis [75]. Exploring the reasons behind the clinical failure of SPI-077, Zamboni and co-workers investigated localized BA of the drug in the tumor by means of a microdialysis study in mice [76]. The liposomes accumulated in the tumor and led to effective tumor growth inhibition in the mouse model, but no free platinum was detected in the tumor extracellular fluid suggesting a very poor release of the drug [76]. Further studies were carried out, to understand the interplay between carrier composition and the drug release rate [77,78]. The difference between these two formulations indicates that there is a fine balance responsible for clinical success. The drug release in the blood plasma and the intracellular release of a drug fraction accumulated at the target site both contribute to the performance. Even for those formulations with controlled-release behavior and longer circulation times, the availability of this accumulated fraction in the tumor can be of major importance.

Essentially, the intracellular or extravascular release of the compound from the dosage form will not be covered by an IVIVC based on plasma pharmacokinetics. Consequently, a combination of drug release and relevant cell-based *in vitro* assays will be necessary to elucidate clinical success. However, as a novel clinical parameter specific for nanomedicines, the targeting capability can provide evidence of the probability of localized accumulation.

Another recent strategy to control the drug release behavior from liposomes has been applied in the drug formulation ThermoDox®. The clinical candidate (Celsion Inc., USA) is indicated for the treatment of liver cancer and comprises dipalmitoyl phosphatidylcholine (DPPC), the lysolipid myristoylstearoyl phosphatidylcholine (MSPC), and $mPEG_{2000}$-DSPE. Only at an elevated temperature of approximately 39–42 °C, the formulation releases doxorubicin. In the clinical setting, this release is triggered by high-intensity focused ultrasound [79,80]. Currently, a phase III OPTIMA study is evaluating ThermoDox® for the treatment of hepatocellular carcinoma using standardized radiofrequency ablation treatment (NCT02112656) after subgroup evaluation in the phase III HEAT study indicating a beneficial survival in a subgroup only [81]. Such stimuli-responsive nanomedicines are of high interest due to the enhanced selectivity of the treatment. Improved efficacy and reduced side effects are expected by taking advantage of these exogenous (e.g. heat, ultrasound) or endogenous (e.g. pH shift or enzyme activity at the site of action) triggers. A very recent article provides a comprehensive summary of the most recent developments. However, these nanomedicines must be further evaluated clinically [82].

So far, injectable nanomedicines have been most successful in the re-formulation of well-known compounds. Only five out of 172 clinical trials involve new drug applications. They include a delivery system for nucleic acids (LErafAON, Fus-1 gene) and an antitoxin binding agent (CAL-02). In addition to their dominance in the phase I studies, doxorubicin-loaded liposomes account for 70% of phase II clinical trials (Fig. 3). New indications such as recurrent endometrial cancer, metastatic breast cancer, or prostate cancer were explored. In 2003, Caelyx®, the European brand name of Doxil®, was approved for monotherapy of metastatic breast cancer in patients with high cardiovascular risk.

An active targeting strategy was followed by BBB Therapeutics. They decorated the surface of *'stealth liposomes'* with glutathione, to actively target receptors at the surface of the blood-brain barrier. Unfortunately, the development was stopped in the early clinical stages [83]. From all clinical studies evaluated, drug formulations of doxorubicin, amphotericin B, and vincristine sulfate are found in phase III clinical trials. Only AmBisome® and Doxil® underwent phase IV clinical trials (Fig. 3).

In summary, the current nanomedicine market is strongly driven by a small number of liposomal drug products. All formulations control the drug release either by using *'remote loading'* (Doxil®, Marqibo®, Onivyde®, Vyxeos®) or by taking advantage of unspecific interactions between the drug molecule and the lipid bilayer (AmBisome®). Among the approved liposomal formulations, Doxil® and Onivyde® are the only ones utilizing pegylated lipids to prolong the circulation time of the carrier particles. Accordingly, with regards to their quantitative contributions to plasma pharmacokinetics, the release is the strongest influence and will certainly play a key role in the success of EV preparations as well. Also, active targeting strategies have not been translated into a major clinical breakthrough, indicating a medical need for enhanced selectivity.

3.2. Non-Liposomal nanocarrier systems

Over the past decades, a wide variety of polymeric and inorganic nanoparticle delivery systems have been developed, but only a small number entered the market [4]. The differences between those non-liposomal carriers and EV preparations are more significant with regards to composition and chemistry. However, some lessons may be learned from these synthetic nanocarriers as well. The surface chemistry has a strong impact on the overall circulation time and, as such, seems to be the biggest advantage of liposomes due to their lowered recognition and elimination as compared to polymeric or inorganic nanoparticle systems. Therefore, EV preparations may be well-suited for drug delivery applications although the presence of proteins on the surface may endow them with a biological identity that leads to elimination effects very similar to non-liposomal drug delivery systems. In the following, the most important examples of non-liposomal nanocarriers will be discussed in more detail.

The most prominent example of a non-liposomal nanocarrier delivery system is ABI-007. It utilizes the nab-technology™ and was registered under the trade name of Abraxane® in 2007. The drug product comprises paclitaxel nanocrystals stabilized by the presence of human serum albumin. Emphasizing the clinical disadvantages of the conventional Taxol®, the clinical development of Abraxane® provided evidence for a significant reduction of side effects. A pharmacokinetic crossover study comparing nab-paclitaxel and the solvent-based paclitaxel-formulation Taxol® revealed comparable systemic exposure of total paclitaxel despite higher nab-paclitaxel dose. However, the free paclitaxel fraction was significantly higher with nab-paclitaxel as compared to the solvent-based formulation. This may have contributed to the improved response rates of Abraxane®. Due to the higher tolerated dose and the absence of hypersensitivity caused by the solvent Cremophor EL (polyoxyethylated castor oil) in conventional Taxol®, nab-paclitaxel was therapeutically more effective [84,85]. Other prototypes using the same technology include nab-docetaxel (ABI-008), nab-rapamycin (ABI-009), nab-17AAG (ABI-010), and nab-CY196 (ABI-013). They are still under investigation.

AZD2811 and BIND-014 are two polymeric nanomedicines developed by BIND Therapeutics (UK) together with AstraZeneca (UK). AZD2811 targets aurora kinase B and was investigated in a phase I clinical dose-escalation study. The treatment was found safe with approximately 30% of patients' solid tumors showing stabilization in tumor growth. The drug is undergoing further investigation in NSCLC [86]. AZD2811 was formulated in an *in situ* ion-

pairing emulsification process using hydrophobic acids to manufacture optimized ultra-slow-release nanoparticles. A block copolymer composed of polylactic acid and polyethylene glycol (PLA-PEG) was used [87]. BIND-014 is a docetaxel-loaded prostate-specific membrane antigen (PSMA) targeted nanoparticle formulation of a very similar composition [88]. A phase II study was carried out in patients with metastatic castration-resistant prostate cancer [89]. Moderate antitumor activity was found in the study population (30% response rate, 9.9 months progression-free survival) whereas patients with evaluable PSMA-positive circulating tumor cells showed a decrease of these cells in the blood. This correlated with improved overall survival [90]. Therefore, further studies may require a careful selection of the target population to better evaluate the improved safety and efficacy of PSMA-targeted therapy [91]. Additionally, individual biological profiling of the disease with reliable diagnostic markers may further improve efficacy.

3.3. Nanomaterials in immunotherapy

Many review articles focus on the application of nanomedicines in immunotherapy. Therefore, we will provide a brief summary of the most recent developments only. For interested readers, more information is offered by Dacoba et al. [107] and, with a focus on cancer treatment, by Irvine et al. [108].

Nanovaccines (NVs) are administered subcutaneously at a very low dose and exhibit a different pharmacokinetic behavior as compared to nanocarriers for intravenous administration. Still, some of the cascades and pathways should be considered in the development of EV preparations. Commonly, the immune system is stimulated by the antigens presented during viral infection, cancer, or allergies [109]. NVs may carry the antigen and act as an adjuvant. However, nanomaterials may exhibit a stabilizing effect on the antigen as well.

Because of their size, sEV preparations allow enhanced recognition by the immune system and improve its activation as compared to the soluble antigen-adjuvant mixture [110,111]. Lipid-based [112], polymeric [113], and inorganic [114,115] NVs are most commonly used because of their biodegradability, high loading capacity, and a variety of established procedures for surface functionalization. The main attributes responsible for the elevated immune response of NVs over traditional vaccines are the size and surface properties that lead to a faster recognition by the immune system [116,117].

Particles with a size of approximately 30–100 nm [117–120] can easily accumulate in the lymph nodes whereas larger particles with a size of more than 500 nm are transported by the dendritic cells located at the injection site [121]. Hirosue et al. highlighted that a disulfide bond between the nanocarrier and the antigen led to stronger activation of CD8+ T cells [113,116,122]. Consequently, surface functionalization plays a prominent role in their success. Zheng et al. developed polymeric micelles comprising cationic polyethyleneimine-stearic acid conjugates loaded with CpG and anionic $mPEG_{2000}$-DSPE loaded with Trp2 antigen. These micelles had a stronger cytotoxic T-cell response and improved anti-tumor efficacy as compared to the soluble Trp2 antigen and CpG adjuvant mixture [112].

As compared to synthetic nanocarriers, EV preparations have intrinsic immunomodulatory properties. Antigen-presenting cell (APC)-derived EVs are enriched with major histocompatibility complex (MHC) I, MHC II, and immunomodulatory proteins [123]. Additionally, they contain CD86 and integrins that play a critical role in antigen presentation [124]. Thus, even though EVs are not viable APCs, they are capable of inducing T-cell stimulation and recognition of APC-derived EVs by naïve CD8+ T-cells [125]. Also, EVs can stimulate the primary adaptive immune response by exchanging peptide-MCH complexes with dendritic cells (a type of APCs) [126]. Furthermore, EVs secreted from dendritic cells (also known as dexosomes) have shown supportive effects on CD4 + T-cell survival *in vitro* by activating a transcription factor, NF-κB [125]. Taken together, EVs are often considered as potential candidates in vaccine development due to their innate immunostimulatory actions that widely depend on the type of cells they were isolated from. To apply EVs as cancer vaccines, antigens presented by the tumor must be identified. In many cases, the patient's immune system exhibits a high tolerance against tumor antigens, and overcoming the immunosuppression is one of the major challenges [127,128]. Also, cancer cells originate from the patient's tissue and few surface structures provide sufficient selectivity to qualify as a target [127,128].

With regards to infectious diseases, the identification of pathogen-specific antigens can be much easier. The EVs isolated from bacteria, fungi, or parasitic protozoa can be used for vaccination. EVs originating from bacteria are sometimes referred to as outer membrane vesicles. Novartis uses this strategy in the manufacture of their vaccine Bexsero® against serogroup B meningococcal disease in children. EVs from *Neisseria meningitides* are used [129,130]. Also, EVs derived from pathogen-infected cells have been used in preclinical mouse models [131–133]. The application of EVs as vaccines has been summarized in more detail by Fuhrmann and colleagues as part of the same special issue and will therefore not be further discussed [134]. In addition to the immunostimulant effects, unmodified EV preparations can be applied for immunomodulatory and regenerative therapies [15].

In recent years, reports indicated that the therapeutic performance of mesenchymal stem cells largely depends on paracrine-secreted soluble factors and EVs. Since most stem cell-based therapeutics did not receive further attention due to the high costs of manufacture and considerable safety concerns, more emphasis was given to EVs. In this context, EVs obtained from mesenchymal stem cells were successfully tested in a steroid-refractory graft-versus-host disease patient proving their effect on the immune system. The infusion was well-tolerated and no severe side effects occurred. Immunosuppression of natural killer cells and other peripheral blood leukocytes were held responsible for the therapeutic effect [135]. Also, the cardioprotective, renoprotective, hepatoprotective, and neuroprotective effects of mesenchymal stem cell-derived EVs are examined in several preclinical models including animal models of stroke, multiple sclerosis, and Alzheimer's disease. Previous articles summarize the therapeutic applications [15,136] and biologically active molecules [137] present in the vesicle preparations. Also, new standards for the preparation of drug products based on EVs are being developed [21].

In response to the current pandemic, nanotechnology-based vaccines against Sars-Cov-2 gained approval by EMA or US-FDA. The vaccines of BioNTech (Mainz, Germany) and Moderna (Cambridge, USA) deliver mRNA, encoding for the spike protein of the Corona virus. The nucleic acid has been encapsulated into solid lipid nanoparticles to protect the biomolecule from enzymatic degradation. Cationic lipids were used for the complexation of the negatively charged RNA. In addition to a protective effect, the nanoparticles enable RNA to cross the cell membrane to facilitate protein translation. Compared to other vaccination techniques using viral vectors, mRNA-based vaccines can be rapidly developed and the RNA can be modified in response to virus mutations more easily. In comparison, the manufacturers AstraZeneca (UK) and Johnson & Johnson (USA) were using non-replicating viral vectors for the delivery. The different technologies involved in the development of COVID vaccines are discussed in more detail by Batty et al. [138]. EVs could be used as an alternative to lipid nanoparticles presenting the spike protein at their surface or by delivering mRNA into the cell [139]. Tsai and co-workers used mRNA encap-

Table 3
Challenges and potential solutions in the development of EVs for drug delivery applications.

Challenge	Challenge	Solution
Complexity	Complex structures produced by living cells involving multiple biochemical pathways. The composition widely depends on the physiological function, leading to high diversity in the composition. Also, isolation processes are widely based on their physical characteristics while their function is defined by the chemical and physical attributes.	Detailed physical and chemical characterization using lipidomic, proteomic, and transcriptomic profiling together with physical characterization methods to define particle size, size distribution, and other critical quality attributes with impact on biodistribution.
Production process	Manufacture in 2D cell systems with limited scalability followed by physicochemical isolation methods with poor process yield.	Scale-up and standardization and of the culture conditions and extraction method. Development of novel processes leading to improved process yield.
Safety	Safety profile is determined by the composition and purity of the product with a higher risk of immunogenic impurities. This is combined with the common challenges of nanomedicines including the characterization of critical quality attributes (Section 4).	Development of improved *in vitro* and *in vivo* models to monitor the immunogenicity and complement activation observed for nanomedicines.
Selectivity and circulation time	Limited influence on circulation and biodistribution because of a limited understanding of the underlying pathways. EVs are known to act as a cellular messenger system but the exact role of the surface proteins is often unknown.	Investigation of the influence of the exact composition of EVs on circulation time and selectivity *in vitro* and *in vivo*.
Predictability	Limited predictability of the therapeutic performance due to a poor resolution of conventional pharmacokinetic analysis in the evaluation of bioavailability and biodistribution of nanomedicines.	Application of computational methods to estimate specific effects of the formulation on the distribution of the compound.
Regulatory pathway	Characterization and safety evaluation requires a combination of expertises with a regulatory pathway that depends on the functionality and therapeutic purpose of the formulation.	Combining expertise in the characterization and evaluation of biotechnological, colloidal, and small-molecular drug products (similar to drug conjugates).

sulated into EVs to successfully vaccinate mice against Sars-Cov-2 without observing any adverse reactions [140]. In another study, two different EV preparations were used to vaccinate the animals resulting in neutralizing and cellular immune responses [141].

Evidently, with regards to EVs, a change in the protein decoration could affect circulating carriers as well. This would increase the safety risks and may even affect pharmacokinetics. However, modulating the protein and phospholipid decoration could also lead to a shift in the selectivity of nanocarrier-based delivery and, without even altering the plasma concentration-time profile, lead to improved clinical responses. Exploring the role of surface proteins and their effect on biodistribution is one of the current aims of EVs research.

3.4. Implications for the development of EVs

Currently, the development of commercially attractive drug products based on EV preparations is still at the infant stage and several hurdles must be addressed before they can be successfully translated from bench to bedside. One limitation lies in the complexity of the production process because many of the established methods are characterized by a poor process yield. Also, standardized techniques for isolation, purification, and characterization are required to provide evidence for the reproducibility of manufacture. For example, the established gold standard for isolation of EVs, differential ultrafiltration, has significant limitations in terms of the morphological changes in the vesicular structure. These changes depend on the centrifugation rate and the runtime [46]. Because of the high content of cellular proteins, characterization should include a combination of lipidomic, proteomic, and transcriptomic profiling [3]. This is necessary to minimize safety concerns, particularly for EVs obtained from virus-infected cells [142]. Furthermore, since each parent cell has a limited secretion capacity, scale-up depends on the exact parent cell type. More often, the yield of EVs is lower than one microgram per milliliter of cell culture medium [143]. Higher yields can be achieved by using stimulants, for example, the detachment of adherent parent cells, hypoxic conditions, and Ca^{2+} ionophores, or by using small molecular modulators such as *N*-methyl dopamine and norepinephrine. They were shown to increase the secretion of exosomes from mesenchymal stem cells by a factor of three [144]. Indeed, selecting the most suitable parent cell together with the optimization of the biotechnological incubation and concentration process may play a dominant role in the development of EVs with desirable properties. Mesenchymal stem cells are known to produce large amounts of EVs [145]. Furthermore, cells can be harvested from patients and cultured as the parent cell to provide an avenue for *'personalized medicines'* with reduced immunogenicity.

Another challenge lies in the definition of a relevant regulatory pathway for EVs. Depending on the manufacturing process and composition, many EVs for drug delivery would qualify as biological drug products. Most of them are composed of non-living and non-replicating structures [15,20]. However, depending on the drug-loaded into the carrier, chemical, and biological attributes would be included in the quality and safety assessment as well. In the European Union, EVs that contain biologically active transgene material would fall under the legislation of Advanced Therapy Medicinal Products [146]. Each of these regulatory pathways comes with specific requirements. Comparing liposomal drug products and EVs, liposomes have always been a challenge due to a complex physical identity that cannot be fully characterized. EVs combine this complex physical identity with an even more complex chemical and biochemical diversity and, therefore, may not be easily addressed in the standard processes applicable to other nanomedicines.

Understanding the function and properties of EVs may lead to drug products with higher selectivity for the target site as compared to liposomal carriers [12]. However, the most successful nanomedicines were characterized by a simple formulation design together with a solid business strategy. While most liposomal vesicles followed the example of Doxil® or Ambisome®, the nab-technology™ was utilized to reduce formulation-related adverse reactions. A strong medical need came together with an improved safety profile. With further customization of the surface decoration of the vesicles, the immunogenic effects will become more important. Recent findings suggest that the life-threatening complement activation-related pseudoallergy observed with the commercial drug product Doxil® was attributed to the pegylated phospholipid [147–149]. Similar effects could certainly occur more often when using vesicles decorated with multiple surface proteins. Table 3 summarizes the challenges in the development of EVs as drug delivery systems and provides several potential solutions.

Additionally, with regards to clinical performance attributes such as the BA, high stability of the vesicles in presence of physiological fluids, and a sustained release of the drug from the carrier

are of paramount importance. In this context, the US-FDA defines BA as the rate and extent to which the active ingredient is absorbed from a drug product and becomes available at the target site. This definition assumes that the total plasma concentration corresponds to the drug concentration in the malignant tissues. Learning from the experiences with liposomal drug products, this assumption cannot be applied to nanomedicines. While the encapsulated fraction is regarded as an inactive form of the API, the free fraction becomes available at the target site and contributes to the pharmacological effect. Against this background, *in vitro* performance assays measuring the drug release, can be used to quantify the free fraction and establish the IVIVC/IVIVR. However, even though the released fraction is contributing to the clinical performance of nanomedicines, the encapsulated fraction and, more importantly, the fraction of the encapsulated drug accumulated in the periphery contribute to efficacy and safety as well. These aspects will be discussed in more detail in the later sections.

4. Key attributes of nanomedicines

During the development of new drug products, a thorough investigation of the pharmaceutical quality, safety, and efficacy is required. In the following section, some key characteristics of nanomedicines, the critical quality attributes (CQA), will be discussed in more detail. In the regulatory context, the critical material attributes and critical process parameters involve all characteristics of the raw material or the manufacturing process that influence the quality of medicines. While the IVIVCs discussed in the later sections are widely based on human data, the mechanistic investigations leading to the identification of CQAs often rely on preclinical data. Preclinical biodistribution data are in good correlation with human semi-quantitative imaging studies with nuclear tracers (see Table 5) CQAs are quality attributes that are linked to the clinical performance of the drug product. Commonly, the IVIVC/IVIVR provides a scientific justification for the definition of CQAs.

4.1. Particle size and size distribution

The particle size and size distribution play a key role in the uptake and biodistribution of nanomedicines. In the regulatory context, a combination of different techniques may be required to measure these important characteristics [3,150]. A selection of methods is presented in Table 4.

In the *in vivo* setting, the adsorption of biomolecules to the surface of the carrier can have an impact on particle diameter and, in consequence, on distribution, degradation, erosion, agglomeration, and drug release. Taking this influence of the physiological envi-

Table 4
Methods frequently used for particle size measurement in submissions to the US-FDA [1] and novel methodologies suggested for the characterization of EVs. The table was adopted from [150].

Method	Principle	Outcomes	Comments
Dynamic light scattering	Measures fluctuations of the scattered light caused by the particles during Brownian motion (Stokes-Einstein equation). Recent systems include a fluorescence filter wheel to select specific particle populations.	Hydrodynamic particle diameter and polydispersity index.	Only for suspensions, the resolution is bad for polydisperse samples or high background scattering, sensitive to viscosity and refractive index, rapid measurement
Nanoparticle tracking analysis	A laser beam illuminates the sample which is placed on a dark background. A very sensitive camera tracks the scattered light and the movement of the particles under Brownian motion through an optical microscope. NTA is equipped with a fluorescence filter wheel to select specific particle populations.	Particle size, size distribution including agglomeration and aggregation effects.	Only for suspensions, small particle distances cause loss of sensitivity, sensitive to background scattering, can track fluorescent particles
(cryogenic) transmission electron microscopy	During the interaction of an electron beam passing the sample, electrons get scattered. These are focused and create an image.	Particle size, size distribution, shape, lamellarity, agglomeration, aggregation, crystal structure.	Operates in a high vacuum, Samples must be solid or frozen. For conventional TEM, the drying process leads to a shrinkage of vesicles. The method is cost-intensive and requires time in the sample preparation. Cryo-TEM is the method of choice because the vesicles are measured in the hydrated state.
Scanning electron microscopy	A focused electron beam scans the surface of the sample. During the interaction, secondary electrons get ejected from the surface creating an image.	Particle size, size distribution, shape, agglomeration, aggregation, crystal structure.	Operates in high vacuum leading to "shrinkage" of vesicles during the drying process. The method is cost-intensive and requires time in the sample preparation.
Atomic force microscopy	A probe tip scans the surface of the sample. Interactions between both surfaces lead to measurable forces which create an image of the surface topography.	Particle size, size distribution, Shape, agglomeration, Aggregation, Surface properties (e.g. hardness and texture)	Difficult sample preparation, Time consuming.
ExoView	Vesicles are labeled and immobilized using an antibody labeling chip. The size is measured by interferometric imaging.	Particle size, the size distribution for a selected particle population with multiple surface markers (recognized by the antibody).	Higher selectivity for vesicles is achieved by using a fluorescence label for specific exosome markers.
Asymmetrical flow field-flow fractionation	Flow-separation of particle populations in the carrier liquid followed by a multi-detector analysis.	Particle size, size distribution, and multiple additional analytical parameters including UV and fluorescence detection systems.	A strong and widely uncontrolled dilution of the sample in the carrier liquid and incomplete particle re-collection depending on the crossflow.
NanoFCM	Combination of flow cytometry together with light scattering detection and fluorescence detection.	Hydrodynamic particle diameter, size distribution, using marker-based vesicle selection.	Detection of the hydrodynamic diameter and poor resolution for polydisperse particle systems.

Table 5
Pharmacokinetic studies carried out with nanomedicines in humans using nuclear tracers.

Nanomedicine	Formulation characteristics	Reference
188-Rhenium-liposomes	**Composition** • Hydrogen soybean phosphatidylcholine • Cholesterol • $mPEG_{2000}$-DSPE **Molar ratio** 3:2:0.3 **Particle size** 72.3 – 95.1 nm	[156]
99m-Technecium-liposomes	**Composition** • Dimyristoyl phosphatidylcholine • Dimyristoyl phosphatidylglycerol **Molar ratio** 7:3 **Particle size** 0.2 - 5 μm	[157]
111-In-liposomes	**Composition** • Distearyl phosphatidylcholine • Cholesterol • Ionophore A23187 **Molar ratio** 2:1:0.004 **Particle size** 40 – 70 nm	[158,159]
111-In-liposomes	**Composition** • Egg phosphatidylcholine • Phosphatidylglycerol • Cholesterol • D-alpha tocopherol succinate **Molar ratio** 7:3:4:0.2 **Particle size** 0.3-0.5 μm	[160]
64-Cu-liposomes	**Composition** • Hydrogenated Soy Phosphatidylcholine • Cholesterol • $mPEG_{2000}$-DSPE • Anti-HER2 scFv (F5)-PEG-DSPE **Molar ratio** 3:2:0.3 **Average particle size** 100 nm	[161]

ronment into consideration, recent guidelines suggest the evaluation of carrier stability in physiological medium (e.g. 10–90% of human serum or plasma [47]). The *in vitro* stability has been quantified for a wide variety of formulations including polymer nanoparticles [151], liposomes [67], nanocrystals [66], and micelles [152]. Due to their relatively low scattering intensity, liposomes, vesicles, and micelles often do not allow the measurement of particle size in presence of physiological fluids. To monitor some of the physical changes, Göpferich and co-workers utilized a Förster Fluorescence Resonance Energy Transfer (FRET) assay to measure the stability of micelles in serum [152,153]. This technique could be applied to EVs as well. The application of nanoparticle tracking analysis (NTA) after labeling the vesicles with a fluorescent dye is another valid option.

Also, recent characterization methods for measuring the particle size of exosomes include the ExoView (ExoView Biosciences, USA). In a publication, higher sensitivity as compared to conventional methods is claimed. Although detection of the size by interference measurement after immobilization of the particles offers certain advantages with regards to the exact dimensions, the current data is not completely comparable. In a publication comparing the ExoView and the NTA method standard procedure for the ExoView includes labeling of the vesicles with a Tetraspanin labeling kit. NTA offers similar functionalities but no labeling of the vesicles was performed before the measurement to select the particle population of interest [154]. Other studies suggest combinations of flow cytometry, light scattering, and fluorescence detection such as the NanoFCM (Nanofcm Co., Ltd, UK). The NanoFCM selects specific particle populations by using fluorescence markers together with a light scattering detection system. Other than the ExoView, it measures the hydrodynamic diameter. The common weaknesses of light scattering methods apply to the NanoFCM as well [155]. A more advanced method for the separation of particle populations is AF4. It separates particle populations in a flow channel using a time-resolved measurement of the eluted fraction and allows multiple detectors to be used. Although the method has received significant attention, the impact of dilution of the particles in the carrier liquid should be carefully considered. While stable particles can be measured at high resolution, the elution of loose complexes is widely driven by the dilution and shear forces applied during sample separation. Noteworthy, the high resolution of methods selecting specific particle populations by fluorescence comes at a high cost with regards to the detection of unexpected impurities and other particle populations. Therefore, background corrections have a high value to investigate the mechanistic relationships between vesicle composition and the interactions observed in an *in vitro* environment. In parallel, being used in the characterization of drug products, this "background correction" reduces the safety level and must be considered very carefully.

Several clinical studies have investigated the biodistribution of nanomedicines in humans using nuclear imaging. For most of them, particle size has been reported. However, some of the investigations date back to the 1980s and 1990s. These formulations were characterized by a very broad size range as indicated in Table 5. Still, there seems to be a strong relationship between the particle size and the clearance of the carrier from blood circulation.

In this context, the quality of the clinical data and, in specific, the dissociation and release of labeled phospholipids from the carrier have to be considered. In presence of plasma or serum, this effect is even more pronounced [162,163]. Man et al. reviewed different radiolabelling methods in humans, concluding that label stability and release play a central role in the outcome of the investigations [162]. Therefore, biodistribution studies with EVs should be carried out in conjunction with an investigation of label stability and release. Other studies suggest genetic labeling techniques to avoid artifacts during the measurement. Cells can be genetically modified to express fluorescent proteins fused with an exosome marker protein such as CD63 to trace their biodistribution in real-time [19]. Gupta and co-workers applied this method, investi-

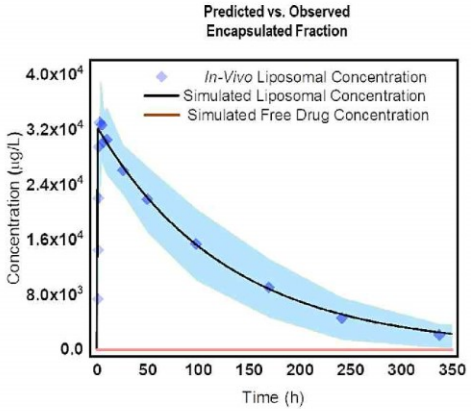

Fig. 4. Identification of the liposomal fraction using the PBNB model for Doxil®. The algorithm identifies the encapsulated fraction from the total drug concentration-time profile. The blue area denotes the standard deviation range observed in the clinical data (24 patients), blue squares highlight the mean of the encapsulated fraction found by the bioanalytical assay [54].

gating the biodistribution of EV subpopulations. EVs were found in several organs only minutes after the injection, mainly in the liver and spleen. Similar effects have been observed for liposomes as well. The interaction with cells of the reticuloendothelial system (RES) has been held responsible for this effect [32].

With regards to the development of an IVIVR, older studies focus on a correlation between the particle size determined after synthesis and the plasma concentration-time profile of the drug molecule. This total drug concentration is a convoluted signal, defined by the complex interplay between drug release, particle accumulation, distribution, and elimination [54,66,67]. Therefore, recent regulatory guidelines include a quantification of the encapsulated and non-encapsulated fraction of the drug from the blood plasma, for example by using centrifugation or solid-phase extraction [164–166]. In a more recent investigation, we utilized a customized *in silico* model, to extract the half-life of the carrier-bound fraction of the drug [54].

This physiologically based nanocarrier biopharmaceutics (PBNB) model identified carrier half-life and drug release rates in humans [54] and rodents [167]. After training the model, a deconvolution of the total plasma concentration-time profile into the encapsulated and non-encapsulated fraction profiles was achieved. In addition to Doxil® (Fig. 4), the investigation included nanomedicines ranging in size between 90 nm and 190 nm. The half-life of the liposomal carrier was the shortest for Myocet® (14.34 h) with a hydrodynamic diameter of approximately 190 nm. However, even between liposomes comparable in diameter, there was a significant difference in the half-lives observed. For example, the drug formulation Foslip® with a size of 92 nm exhibits a half-life of 23.93 h while for AmBisome® with a diameter of 100 nm, a carrier half-life of 98.26 h was calculated [54]. Consequently, multiple parameters can be involved in the elimination of liposomes from blood circulation and the elimination half-life cannot be extrapolated based on this quality attribute alone. With regards to EV, this would indicate a significant impact of phospholipid or protein composition on the circulation time.

A variety of animal studies reported the accumulation of very similar vesicles in the ranking order of their size. For example, an investigation on stealth liposomes in female C57BL/6 mice revealed faster clearance of nanomedicines with diameters of more than 300 nm as compared to smaller vesicles [168]. In another study, intravital imaging of the nanoparticle distribution was performed in mice. The authors found that nanoparticles with a size of 12 nm effectively extravasated, while nanoparticles with a size of 60 nm particles remained within a 10 μm radius of the vessel walls [169]. Particles with a size of 125 nm particles did not extravasate to a considerable extent [169]. Perrault et al. investigated the accumulation of intravenously administered gold nanoparticles after injection [170]. The elimination rate and BA were altered significantly for particles in a size range of 25.2–75.7 nm (Fig. 5).

Noteworthy, most mechanistic studies involving biodistribution were carried out in rodents and may provide limited information on the situation in humans. In a recent investigation, we used allometric scaling to predict liposomal clearance in humans. An extrapolation of the particle clearance found in male Wistar rats provided a good estimate of the elimination rate of the investigational medicinal product Foslip® [67]. Other animal studies in mice did not lead to an acceptable correlation [67]. The correlation between particle size and circulation time has been studied for several nanoparticle and vesicle-based formulations. To apply EV preparations in drug delivery, similar investigations must be made. So far, most successful nanomedicines were ranging in size between 60 and 150 nm. This size range can be used as a starting point for the identification of vesicle populations suitable for similar drug delivery applications.

4.2. Surface charge and hydrophilicity

The surface characteristics of nanocarriers are responsible for a wide variety of interactions including the formation of a protein corona [171,172] or the drug-protein transfer [173]. Among other features, the net charge is a CQA suggested by the US-FDA and European Medicines Agency (EMA) [3,174]. The zeta potential is the potential difference between the dispersion medium and the stationary fluid layer on the surface of the particles and can be quantified from particle mobility in an electric field [175]. It is the effective electric charge of the particle and depends on a wide variety of environmental parameters such as the ion concentration and the pH value. To provide a more comprehensive characterization, a pH profile or salt concentration profile of the zeta potential can be determined [4,176]. In a preclinical or clinical setting, the zeta potential can have a strong influence on the uptake and cytotoxicity of particles. Cationic liposomal formulations are often used as *in vitro* transfection agents (e.g. Lipofectamine™). The interaction of positively charged colloids with cellular surfaces limits the *in vivo* circulation time considerably [177] and may lead to undesired immune responses. Therefore, most drug products rely on a more conventional formulation design with a slightly negative

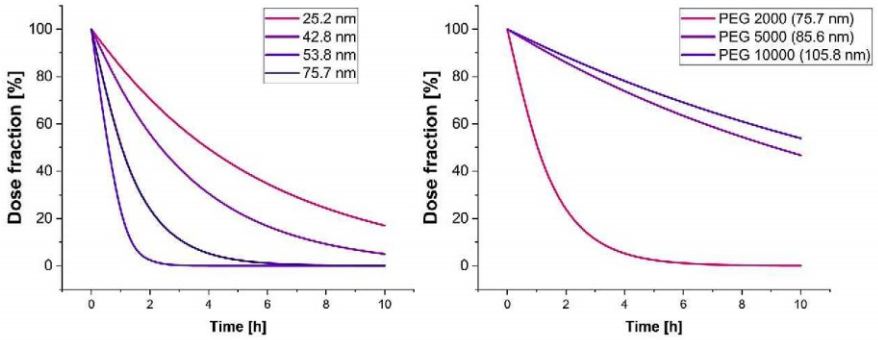

Fig. 5. Simulation of the dose fraction of pegylated gold nanoparticles (with a molecular weight of the PEG chain of 2000 Da) eliminated from the blood circulation after intravenous injection into CD1 mice. The simulations are based on the half-lives reported by Perrault et al. [170] assuming a one-compartment model and first-order elimination (left). A second simulation was carried out to illustrate the impact of surface PEGylation (2000–10000 Da) reported by the same study (right).

surface charge and defined surface chemistry. In the past, the modification of the particle surface with PEG affected the overall circulation time (Fig. 5). Among others, the drug products Onivyde™ and Doxil® [149], the preclinical formulation candidate Fospeg® [178], and an investigational medicinal product for the delivery of prednisolone phosphate [179,180] are using this advanced strategy. This was confirmed in several preclinical studies as well [181]. However, looking at the clinical reports, the quantitative effect of surface pegylation on drug clearance was much lower as compared to the impact of drug release.

With regards to EV preparations, the effect of the surface proteins on pharmacokinetics has been investigated [182]. To provide a reference without protein decoration, the surface proteins were digested using proteinase K resulting in exosomes with comparable size and surface charge. Also, with approximately 100 nm, the diameter of the vesicles was comparable to many of the established liposomal formulations [182]. Only a slight change in the area under the curve (AUC) was reported [182]. However, the small number of animals together with the fact that animal studies are often characterized by high variability mandate further exploration of this effect.

Another study elucidated the pharmacokinetics of EV preparations obtained from different cell lines in mice [183]. The study was aiming at the delivery of the nanocarriers to the brain [183] and compared EV preparations from humans and mice. Unfortunately, the species of origin had no significant effect on brain permeation, indicating that there were no specific transport processes involved [183]. The half-life was very short ranging between 1.51 and 7.29 min [183]. In another study, an elimination half-life of 1.2–1.3 min of the EV preparation was observed [32]. The presence of surface proteins did not prolong the circulation time [183]. For comparison, the long-circulating liposomal formulations AmBisome® [94] and Doxil® [184] exhibit half-lives of approximately 4 and 15 h in mice, respectively.

So far, the strongest effect on the therapeutic performance of nanomedicines has been achieved by modifying drug release (Section 4.4) and the circulation time of the carrier. The latter is widely driven by the recognition of vesicles by the immune system and therefore, by parameters such as the surface charge and hydrophilicity. Considering that even drug delivery systems using an active targeting strategy must circulate over a certain time to reach their target site, the charge and surface properties of EV preparation as well as their ability to escape the RES must be further elucidated.

4.3. Crystallinity

The crystallinity of drugs and phospholipids can have a strong impact on the stability and release characteristics of vesicles [53,185]. For example, the transition of the lipid bilayer of liposomes from a gel structure into the liquid crystalline state may affect the retention of drug molecules [186,187]. Consequently, the lipid composition and glass transition temperature must be monitored as indicated by the US-FDA guidelines [47]. Although similar quality standards may be more difficult to achieve for EV preparations, a general influence of the protein and phospholipid composition on the permeability of the bilayer can be assumed as well.

Also, the crystallinity of the drug molecule can be used to sustain the release of the drug from the carrier. Doxil® comprises intraliposomal crystals of doxorubicin sulfate [188], stabilized by an ammonium gradient [189,190]. About 15 years later, this strategy has been applied in the development of Marqibo® as well [61]. The liposomal vesicle provides a perfect microenvironment, stabilizing the crystal structure over a prolonged period. Therefore, drug crystallinity is an important quality feature. Pastorin and co-workers applied the '*remote loading*' strategy to encapsulate doxorubicin into a new class of cell-derived vesicles. They are obtained by extrusion of cells followed by several purification steps and exhibit characteristics very similar to EV preparations [191].

To measure the crystallinity Raman spectroscopy [192], X-ray scattering [193], Fourier-transform infrared spectroscopy (FTIR) [194], and differential scanning calorimetry (DSC) [195] can be applied. Bakonyi et al. utilized DSC to measure the encapsulation of lidocaine in large multilamellar vesicles [196]. Gelperina and co-workers utilized a release assay to detect differences in the performances of two polymeric nanoparticle formulations. The crystallinity of doxorubicin was held responsible for the sustained release [167,197,198]. The two formulation prototypes are currently considered for further clinical development [199,200]. Iron oxide nanoparticles provide another example of the impact of crystallinity. They have been used as contrast agents for magnetic resonance imaging (MRI) in humans. Differences in the crystallinity between the generic and the innovator product potentially lead to an initial release of iron from the carrier causing severe side effects after the infusion [201]. Iron oxide particles are often coated by carbohydrates which, in combination with the small crystal size and low crystallinity of the sample, make the detection more challenging [201,202]. The carbohydrate layer can also mask the Raman signals [203]. Since the crystallinity of the drug substance provides a certain control over the release behavior of the formulation, this parameter essentially contributes to the *in vivo* performance and qualifies as a CQA. When applying EV preparations for the delivery of compounds, characterization of both, the drug and the vesicle for changes in crystallinity would be mandated. Although EV preparations contain a wider range of phospholipids, the release of the drug substance over the time of storage or after administration would be influenced by their glass transition temperature as well. Also, a change in the polymorphic form of the drug substance loaded into the vesicles could lead to a different release behavior.

4.4. Drug release and in vitro performance testing

The drug release plays an important role in the *in vivo* performance of peroral dosage forms. Following this tradition, the scientific term "*in vitro* performance testing" signifies a broadly inclusive approach, covering a wide variety of biorelevant mechanisms that contribute to the pharmacological and toxicological effect. In the area of nanomedicines, the drug available in the blood plasma depends on drug release and physical stability of the carrier. The encapsulated fraction undergoes an accumulation process, redirecting the drug to cells, organs or tissues [3,200]. Kinetic measurements of the drug release provide more detailed information on the inherent attraction forces of the API and the excipient molecules [204]. The release behavior of formulations strongly depends on the microenvironment and should be investigated under conditions reflecting the *in vivo* situation [204–206]. The release rate can be used as a surrogate parameter for BA and was correlated to the *in vivo* absorption rate of peroral dosage forms [206]. With regards to nanomedicines and when following recent US-FDA guidelines [47], the interplay between drug release and tissue uptake mandates a time-resolved quantification of the encapsulated and non-encapsulated fraction of the API from the blood plasma [47]. Accordingly, there is a strong overlap between the bioanalytical methods used for the quantification of these fractions in both, pharmacokinetic studies and performance testing.

Performance testing of nanomedicines requires a sensitive assay, providing a certain selectivity to isolate nanocarriers from the release medium. A wide variety of techniques have been applied to separate nanoparticles and liposomes from physiological media [204]. They include centrifugation [167,207,208], filtra-

tion [209], solid-phase extraction [210,211], and dialysis techniques [152,173,212]. When stimuli-responsive liposomes are used, the assay should be able to measure drug release in response to the trigger such as a rise in temperature or a shift in pH. So far, enhancing the selectivity of nanomedicine by using external or endogenous triggers has been successfully tested in animals. The human clinical trials involving the drug formulation Thermodox® were not conclusive and did not outperform conventional therapies. However, there are several methods under investigation.

To prevent disruption of the carrier structure, biopredictive assays should not involve much stronger shear forces than observed in the *in vivo* setting. With a rising number of separation methods being utilized for drug release testing, the kinetic component becomes more critical in the validation. While the established release methods such as syringe filtration [213–215], or centrifugation [210,211] often guarantee extraction of the released drug within a few seconds, other techniques may require several minutes or even hours for a complete separation of the particle population from the medium and the free drug. To address this issue, dialysis methods often involve a permeation experiment carried out with the dissolved API. The membrane permeation rate is an important reference, providing evidence for the response of the assay to fluctuations in the release profile [212]. One recent example of a method associated with a time-consuming separation step is asymmetric flow field-flow fractionation (AF4). While this technique provides excellent resolution in the separation of complex mixtures of particle populations at lowered shear forces, run times of 20–60 min [216,217] and the strong dilution in the flow channel limit its value for *in vitro* performance testing [204]. Therefore, the applications suggested by current literature must be substantiated with hard evidence before AF4 can be recommended for drug release testing. Most recent investigations are based on drug conjugates or formulations with negligible release rates and do not deliver a market-ready solution [216]. Therefore, the critical reflections provided by other authors are a starting point for further validation [218].

In the future, more challenges can be expected for EV preparations. The biotechnological manufacturing process leads to the presence of multiple particle fractions in combination with residues of proteins and other organic impurities. Therefore, only methods balancing the sensitivity, selectivity, and application of shear forces during the separation can be considered. The available methods applied in drug release testing of nanomedicines have been discussed in more detail in a previous article [204]. Therefore, the present work will focus on implications for the *in vivo* response. There are several mechanisms involved in the release and absorption of drugs from nanocarriers (Fig. 6). The BA widely depends on the presence of the three major fractions of the drug including the amount bound to the carrier, the amount bound to plasma proteins, and the free fraction of the drug. More often, NBCDs undergo an initial burst effect due to the strong dilution of the formulation in blood circulation, followed by rapid diffusion of compounds into the surrounding liquid [212].

Generally speaking, the release behavior of most nanomedicines is well-described by the three release mechanisms of dispersion, dissolution, and dissociation [212,219] (Fig. 6). Additionally, the transfer of small-molecular drugs from the carrier to proteins [173] and membranes [220] has been reported. In the *in vivo* situation, the interplay between these overlapping processes may lead to a more complex release pattern. Each of these fractions is characterized by a different volume of distribution. Consequently, both processes, the transition from the encapsulated into the free fraction of the drug as well as the kinetics of the drug-protein transfer [173] have a strong impact on BA. Díaz de León-Ortega et al. compared clinical data of hypoalbuminaemic and healthy patients to illustrate the influence of serum proteins on the *in vivo* release from AmBisome® [221,222]. Plasma pharmacokinetics of nanomedicines is widely driven by the conversion of the encapsulated into the non-encapsulated fraction, and the tissue accumulation of the carrier. The latter summarizes all processes leading to a reduction of the particle concentration in the blood plasma. This includes a significant fraction of particles adhering to blood cells [167] as well as the extravasation, or disruption of the carrier. There have been a variety of investigations of blood partitioning confirming that the distribution of nanoparticles and liposomes into the cellular body of the blood reaches a rapid equilibrium without the release of colloids or intracellular release being responsible for significant recirculation into the blood plasma. Therefore, this accumulation is sufficiently described by an unidirectional transport and does not interfere with a detection of the drug release from the blood plasma. Commonly, nanomedicines have reduced mobility in blood circulation compared to the small-molecular compounds and even serum proteins. A more detailed description of the interplay between those influences will

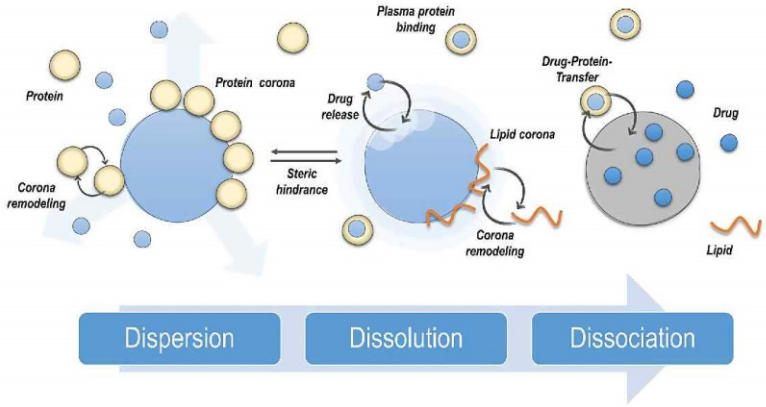

Fig. 6. Illustration of proposed mechanisms of drug release involved in the delivery of drugs using nanomedicines.

be provided in Section 5.1. So far, because of the limited amounts of EVs being available, there have been almost no systematic investigations of the release behavior of drug-loaded engineered EVs. However, in a recent investigation, our group tested the release of doxorubicin from nano-cell vesicle technology systems. The vesicles exhibited a biphasic release pattern because of the differences in particle size and composition. This is a first indication that the manufacturing process applied to EVs may lead to a hard-to-control drug release. The release of drugs from EV preparations would certainly have a major impact on pharmacokinetics and, thus, IVIVC development. The complexity of these next-generation vesicle drug products mandates a thorough investigation of the release mechanism as well. For example, the formation of a protein corona sometimes allows the release of poorly soluble drug molecules in a direct transfer from the vesicle to the protein [173]. Also, a continuous exchange of phospholipids with other membranes has been discovered. Therefore, the impact of lipid exchange and protein content must be considered. Although many studies describe the superior properties of EV preparations in the interaction with cells, clinical evaluation is widely based on pharmacokinetic criteria. In this context, drug release is one of the most important parameters and even an advanced cell interaction would not lead to significant outcomes without controlling this property. Therefore, this key attribute applies to both, liposomes and EV preparations.

5. Quick guide for IVIVC

The quality of the IVIVR developed for a specific drug product vastly depends on the quality of the *in vitro* and, even more important, the *in vivo* data. In many cases, the collection of relevant *in vivo* data, for example on the biodistribution of nanomedicines, is carried out in animals. Human trials are limited to a small number of patients. Consequently, a meaningful evaluation of the existing data is mandated. Model-informed deconvolution techniques can support this process by providing the theoretical framework. The US-FDA describes the different quality levels of the IVIVC in their guidance on extended-release oral dosage forms. Also, a chapter of the United States Pharmacopeia (USP) is dealing with this topic (Table 6).

Table 6
Explanation of the different correlation levels of *in vitro-in vivo* correlations as defined by the US-FDA [22] and USP [7].

Level A
This is the highest category of a correlation and represents a point-to-point relationship between the *in vitro* and the *in vivo* input rate. Based on the experiences made with extended release oral dosage forms, relevant guidelines often refer to a correlation between the fraction absorbed and the fraction dissolved. The fraction absorbed is obtained by deconvolution of the pharmacokinetic profile. Deconvolution can be accomplished using mass balance model-dependent methods, such as the Wagner-Nelson or Loo-Riegelman methods, or by model-independent, mathematical deconvolution. Level A correlations are predictive.
Level B
The mean *in vitro* dissolution time is either compared to a mean *in vivo* residence or an *in vivo* dissolution time. A level B uses all available data points but does not correlate the actual *in vivo* data but rather a parameter that results from statistical moment analysis of a plasma profile component such as the mean residence time.
Level C
A level C correlation establishes a relationship between one *in vitro* time point (e.g. *in vitro* dissolution $t_{50\%}$, $t_{90\%}$) and one or more pharmacokinetic parameters (c_{max}, t_{max}, AUC). Following the US-FDA guideline for extended release formulations, at least three time points should be used. A level C correlation has very limited capability to predict the product's performance or to justify a specification range for quality control.

Noteworthy, these guidelines are widely based on the experiences made with extended-release oral dosage forms and, as such, may not always apply to nanomedicines. With regards to the development of the IVIVC, they use the BA of the drug product as a surrogate parameter for the expected *in vivo* response. BA is defined as the rate and extent to which the API is absorbed from the drug product (absorbed fraction) and becomes available at the site of action. The absorbed fraction is calculated by deconvolution from the plasma concentration-time profile of the formulation using model-dependent techniques such as the Wagner-Nelson method, Loo-Riegelmann method, model-independent numerical techniques, or algebraical techniques (e.g. linear system analysis). The plasma concentration is assumed to be in equilibrium with the concentration at the target site. The quantified amount of the drug represents the pharmacologically active form of the drug [22,223].

With regards to nanomedicines, some changes to the existing methodology are required. Because there is no absorption step involved (as they are administered directly into the circulation) even for fast-releasing formulations the release rate determines the fraction of the drug that becomes available at the target site [54,167]. However, this fraction is not solely responsible for the pharmacological effect. The second drug fraction is still bound to the carrier when it extravasates from blood circulation. This accumulated fraction is similarly important and is responsible for differences between the pharmacological or toxicological effects of nanomedicines as compared to a solution of the free drug. Having both pharmacokinetic data sets, the one of the encapsulated and the non-encapsulated drug, this accumulated fraction can be estimated based on the assumption that the carrier cannot be directly excreted from the body. It must undergo an accumulation and degradation process. While in the area of peroral dosage forms some formulations enabled the development of the IVIVC without using computational methods [224], most nanomedicines will lead to less predictable pharmacokinetics because of the overlapping processes of infusion, release, and distribution effects. This behavior is associated with the concept of nanomedicines and, therefore, applies to novel dosage forms such as EVs as well. In the following, a quick guide provides the workflow for establishing an IVIVC in this area.

5.1. Mapping the processes involved in the in vivo performance

Commonly, IVIVR involves the correlation of clinical pharmacokinetic data to *in vitro* kinetic measurements. The plasma or blood concentration-time profile provides a quantitative measure of the BA and, to a certain extent, the biodistribution of the drug. With regards to nanomedicines, it can be used as a surrogate parameter for the pharmacological effects of the free fraction. Because of the accumulation of the drug-loaded carrier in the periphery, imaging and biodistribution studies are required. The extent of this accumulation can be estimated based on the carrier half-life. The targeting capability is a nanomaterial-specific parameter, indicating the extent of this accumulation. Our current understanding of the elimination and distribution involved in the pharmacokinetics of intravenously applied nanomedicines is presented in Fig. 7. After the infusion of nanomedicines into blood circulation, some formulations exhibit a significant delay between the

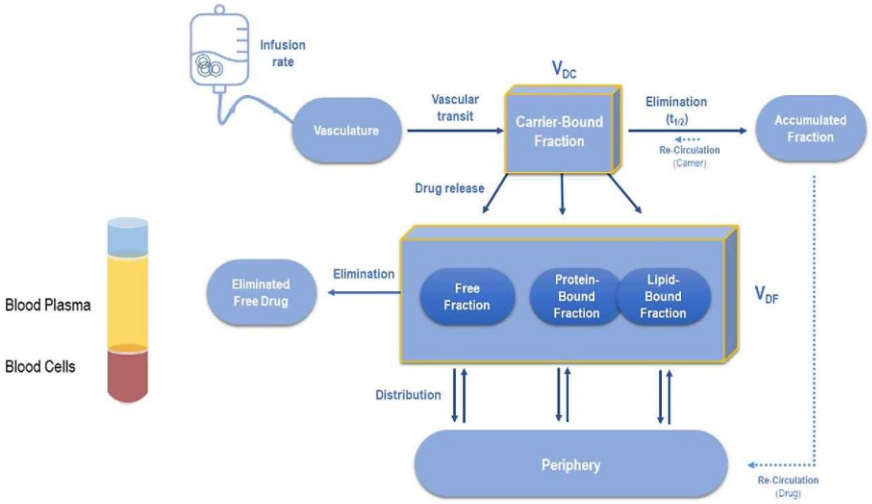

Fig. 7. Schematic of the kinetic processes involved in the elimination and distribution of liposomal carriers following the physiologically based biopharmaceutics model verified by Jablonka et al. [67] and by Nagpal et al. [54] using human pharmacokinetic data. The differences in the volumes of distribution are indicated by the two cuboids comprising the carrier-bound (V_{DC}) and the released fraction (V_{DF}) of the drug. The arrows represent kinetic processes with the dotted lines indicating potentially insignificant contributions to the blood plasma concentration. The compartments detected in the blood plasma have been highlighted in yellow. The drug responsible for the pharmacological and toxicological effect includes the accumulated fraction, the drug in the periphery, as well as the free drug.

end of the infusion and t_{max}. This initial distribution phase, the vascular transit, has been observed for the liposomal drug products Doxil® [54] and AmBisome® as well as for macromolecular therapeutics such as IgG antibodies [225]. The delay is even more significant for AmBisome®, however, there is currently no convincing explanation for this phenomenon. So far, surface interactions with the vascular endothelium are held responsible for the effect [225]. Once the formulation reaches the blood circulation, the liposomal carrier fraction remains in the vascular system [54,167]. A model-based deconvolution of the pharmacokinetic profiles of Doxil®, Myocet®, AmBisome®, and two investigational drug products concluded that the volume of distribution of the carrier fraction (V_{DC}) corresponds to the plasma volume of the patient population [54]. Similar findings have been made in rodents as well [167]. They were supported by real-time imaging studies in mice highlighting that particles with a size of 125 nm do not extravasate to a considerable extent [169]. However, extravasation is responsible for a part of the accumulated fraction which encompasses the overall amount of the carrier that cannot be found in the blood plasma anymore.

From blood circulation, a certain amount of the carrier is accumulated in the periphery (m_{accum}). This amount, expressed as a dose fraction and termed the targeting capability (F_{target}), is mainly responsible for the altered biodistribution of nanomedicine. It corresponds to the theoretical amount of the drug that is available to passively or actively target specific organs or tissues [54]. For the drug product Doxil® and over a period of 350 h approximately 93.2% of the drug were available for drug targeting. There was no significant drug release in blood plasma observed [54]. For comparison, the non-pegylated liposomal doxorubicin formulation Myocet® (on average) released 100% of its payload into the blood plasma [54] with a targeting capability (F_{target}) of 0%. While the outcome observed for Doxil® mandates a biodistribution study, Myocet® has only a moderate risk for formulation-related side effects. Some studies hypothesized a re-circulation of the accumulated fraction from the RES into blood circulation before or after the intracellular release of the drug from the carrier. In this context, two considerations should be made. Firstly, the partitioning between the carrier and blood cells has been investigated. A rapid equilibrium without a strong influence on the kinetics was confirmed. In the human setting this distribution process overlaps with the infusion time and would therefore not change the plasma concentration considerably. Secondly, the released fraction is characterized by a larger volume of distribution and can therefore contribute to the plasma concentration to a very limited extent. The apparent volume of distribution of the drug formulation (V_D) is a combination of both, the volume of distribution of the encapsulated and the non-encapsulated fraction of the drug (V_{DF}). The drug release provides an alternative route to the accumulation pathway. This fraction appears in the blood plasma and is distributed by the circulatory system. The free fraction leads to pharmacological and toxicological responses. Most liposomal carriers are known to reduce this fraction as compared to a solution of the drug. The free fraction is often characterized by a high volume of distribution due to the pronounced lipophilicity of compounds loaded into nanomedicines (Fig. 7). It is reduced by the drug molecules bound to serum proteins or lipids. Common deconvolution techniques do not distinguish between these three fractions, however, a calculation based on the plasma protein binding or a physiologically relevant *in vitro* experiment can be approached [67]. The shift from the low-volume to the high-volume compartment is responsible for the strong effect of drug release on the pharmacokinetic profile of nanomedicines [54,67]. A workflow for the identification of relevant processes *in vivo* during the development of the IVIVC is suggested in Fig. 8.

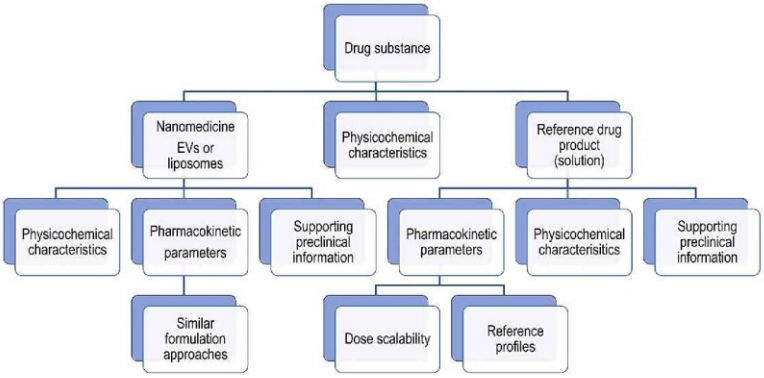

Fig. 8. Workflow suggested for the identification of relevant *in vivo* processes to accurately describe the *in vivo* performance of nanomedicines.

When mapping the processes involved in drug delivery, a broadly inclusive approach is advised. This includes the characterization of physicochemical properties of the drug substance and the nanocarrier formulation. The volume of distribution of the carrier (V_{DC}) can be estimated based on the plasma volume of the species. Clearance and distribution of the free drug are obtained from pharmacokinetic data of a reference formulation. This is a good starting point for the deconvolution of the pharmacokinetic profile to obtain the *in vivo* release.

One challenge lies in the selection of suitable reference formulations. For example, the only reference to the nanoparticle-based drug product Abraxane® is Taxol®, a formulation that comprises a considerable amount of the emulsifying agent Cremophor EL [4]. Consequently, the impact of the excipients on the pharmacokinetics of paclitaxel would be reflected by the deconvoluted *in vivo* release rate. A similar experience has been reported for the nanocrystal formulation Foscan® [66]. A custom-made pharmacokinetic model was required to account for the *in situ* precipitation of the drug [66]. The pharmacokinetic parameters obtained for the free drug were used in deconvolution of the pharmacokinetic profile of the liposomal investigational drug product Foslip® [67].

5.2. Quantitative analysis of simulation parameters

Commonly, a quantitative analysis of the *in vivo* parameters begins with the qualitative mechanistic observations that have been made during process mapping. Under ideal conditions, the IVIVC is based on a single, isolated, or release rate-limiting process that can be monitored *in vivo* and measured or simulated *in vitro*. However, with regards to nanomedicines, the convoluted signal provided by the plasma concentration-time profile rarely supports such an ideal scenario. As a consequence, the bioanalytical methods for new drug applications commonly include quantification of the encapsulated and non-encapsulated fraction of the drug [47]. Additionally, due to the implications for targeted delivery and in addition to the absorption rate, the accumulation rate of the carrier plays an eminent role. By definition, an IVIVC is either based on a point-to-point mathematical relationship between the rates observed *in vitro* and *in vivo* (level A), a correlation between two statistical parameters calculated from the complete *in vivo* and *in vitro* data set (level B), or a single-point correlation of selected *in vitro* and *in vivo* parameters (level C).

BIND therapeutics recently published the strategy applied for the development of their nanoparticle-based Accurin™ technology [69]. The IVIVC was based on the rank order of the drug release observed *in vitro* and the total plasma concentration-time profile of the particle formulations [69]. In the same study, no such relationship was observed between the zeta potential and the particle clearance [69]. Recent progress has been made by using physiologically based pharmacokinetic (PBPK) modeling and physiologically based biopharmaceutics (PBB) modeling techniques to explain the *in vivo* behavior of nanocarriers [54,226]. Traditionally, PBPK models are based on complex differential equations using known physiological variables to obtain a quantitative mechanistic framework describing absorption, distribution, metabolism, and excretion (ADME) of compounds and their formulations [227]. PBB modeling refers to all approaches combining absorption modeling, biopredictive release testing, and PBPK modeling for the purpose of IVIVC [201,228,229].

The requirements of a quantitative parameter analysis, involving a simulation of the intended scenario (e.g. the pharmacokinetics for a particular patient population) as well as comprehensive model evaluation, have been described by both, US-FDA [228] and EMA guidelines [230]. Followed by a description of all parameters used for the *in silico* model [228,230], simulations are carried out within the error range found for each parameter to provide an estimate of the expected simulation error. Additionally, as part of the parameter sensitivity analysis, all model parameters are systematically altered exceeding those error ranges (e.g. ± 20%) to explore the sensitivity of the model. Parameters leading to a strong response in the simulation are often reported as the normalized sensitivity coefficient [231]. They are critical to the model simulations and require more attention during data collection.

5.3. Scalability and parameter extrapolation

So far, only a few studies have systematically investigated the influence of the *in vivo* degradation of nanocarriers or repeated dose phenomena on the predictability of the *in vivo* effects. Most simulations carried out to establish the IVIVC are either based on preclinical data or single-dose administration during the first-in-men clinical trials. However, several studies indicate that a

repeated administration of pegylated lipids may lead to undesired side effects as well as high variability in the dose-response. For example, repeated administration of doxorubicin-loaded '*stealth liposomes*' led to significant changes in the carrier elimination rate [232,233]. Another investigation was carried out in rhesus monkeys and rats using radioactively labeled lipids. The influence of repeated administration was considerably lower [233]. In human subjects, no significant change in the pharmacokinetic parameters occurred [234]. After an extreme dose-escalation only, increasing retention and a reduced clearance were reported [235]. An investigation using repeated treatments with Doxil® suggests the inhibition of clearance mediated by the RES [236]. In comparison, repeated administrations of colloidal amphotericin B in rats [237] and beagle dogs did not lead to any significant changes in the plasma half-life of the drug [238]. As mentioned previously, these effects may not be involved in the development of the IVIVC but could reduce the predictive power in formulation development. Also, dose scalability has to be taken into consideration. Nanomedicines reduce BA of the free drug in blood circulation. Consequently, depending on the drug release, changes in the elimination rate at lower doses of the free drug could affect the IVIVC as well.

5.4. Development of the in vitro performance assay

A broad array of methods has been evaluated to test the drug release from nanomedicines. They include solid-phase extraction, centrifugation, and dialysis methods. A comprehensive summary of the existing methodology has been published by Nothnagel and Wacker [204], and Fecioru et al. [239]. Also, some of the more recent approaches such as asymmetric flow field flow fractionation were critically reviewed in a stimuli article published by the respective USP expert panel [240]. In this section, we will focus on major differences between *in vitro* release and the *in vivo* release rate relevant in the development of the IVIVC.

5.5. Modeling transfer processes in vitro and in silico

As compared to the *in vitro* setting, the influx and the outflux of nanomedicines from the vascular compartment have a strong impact on the *in vivo* release kinetics. In this context, animal studies in rodents and larger animals are facilitated by intravenous injection of small volumes of the formulation followed by the accumulation, distribution, and elimination of the drug and the carrier [167]. In humans, common administration protocols include an infusion following zero-order kinetics [54]. For some drug products such as AmBisome® [164] and Doxil® [165], this is followed by a prolonged vascular transit period before the major fraction of the drug becomes available in the blood plasma (see Section 5.1). Therefore, infusion and transit are overlapping with the absorption of the drug in humans but not in the animal [167]. Also, the accumulation of the carrier from the bloodstream [54,167] sets the time frame for the release and absorption of the drug.

In the *in vitro* setting, the total dose of the formulation is exposed to the release medium over the whole duration of the experiment and there is no ongoing elimination process reducing the concentration of the carrier. Therefore, more recent modeling approaches take infusion and vascular transit into consideration when calculating the *in vivo* release rate [54].

5.6. Selection of performance attributes

The performance of a drug product depends on the ability to deliver compounds to the pharmacological target site. Traditionally, plasma concentration-time profiles are an accessible marker for drug absorption and, as such, can be used as a surrogate for therapeutic efficacy. The major localization of the nanomedicines in the vascular system (see Section 5.1) as compared to the free drug provides the theoretical background for using the encapsulated and unencapsulated fractions to estimate BA by deconvolution [3,7,47]. However, the performance of NBCDs may be affected by other parameters as well. Consequently, a wide variety of quality attributes have been evaluated, each of which is assumed to contribute to the *in vivo* performance. As presented in Section 4 of this article, the drug release and the time-resolved stability profile in the presence of physiological fluids (*in vitro* stability) are well-accepted by both, the regulatory authorities and the scientific community [3,7,47]. Another parameter of influence is the surface decoration with polymers or ligands. While surface modifications with polyethylene glycol have been studied in much detail [181], at present, there is no convincing evidence for a quantitative relationship between ligand density and target accumulation. Even though a number of studies have reported positive effects of a lowered ligand density on target recognition [241], the mechanisms underlying this relationship are barely understood. With regards to EVs, the surface decoration holds great promise in enhancing the selectivity of nanomedicines. However, these effects must be studied more thoroughly before conclusions can be drawn. Relying on the knowledge gained with liposomal carriers, evidently, the drug release behavior of EVs must be optimized to take advantage of enhanced selectivity. It is one of the strongest parameters of influence with regards to plasma pharmacokinetics. When establishing the IVIVC *in silico* modeling can be applied. It enables a description of each individual process and can be customized based on the expected drug-related or formulation-related changes in pharmacokinetics.

5.7. Verification of the IVIVC and in silico models

After developing the IVIVC, a validation of the mathematical relationship must be performed to provide evidence for its predictive power. A recommendation suggests internal or external verification and the evaluation of the average absolute percent prediction error. Based on the experiences with peroral drug products a threshold of 10% was suggested. In the case of internal validation, the initial data set is used to evaluate the predictability of the relationship. The *in vitro* input parameter is used to estimate the impact on the *in vivo* parameter using the IVIVC. The difference between the predicted and observed data sets in percent is the prediction error. For external verification, an additional independent data set is required [223].

For evaluating the PBPK models the predicted *in vivo* data are examined graphically and key PK parameters c_{max}, t_{max} and AUC are compared to their observed counterparts [242]. The predicted *in silico* values (e.g. fraction of free drug) can differ by maximum two-fold referred to the observed which is a generally accepted criterion. The difference between the simulated and observed plasma concentration-time profile can be calculated with the absolute average fold error (AAFE). It describes how well the *in silico* profile fits the observed data where an AAFE of 1 denotes a perfect fit. An AAFE < 2 is a well-accepted but relatively insensitive measure [243,244]. Additionally, the PK parameters c_{max}, $t_{max,}$ and AUC can be evaluated using the BE criteria. BE is achieved if the geometric means ratio lies within a 90% confidence interval between the test and reference drug product, *in silico* and observed values respectively, is within the limits of 80–125% [244].

6. Conclusion

Over the years, a wide variety of nanomedicines have entered the global healthcare market. Vesicle-based delivery systems

improve the selectivity in drug therapy and hold great potential in personalized medicine. However, with the next generation of vesicle-based drug products (EVs) under development, open questions from more than 30 years of nanotechnology-related research need to be addressed. The reliability of the therapeutic performance of EVs will widely depend on the CQAs investigated during formulation development. A direct mathematical relationship between these attributes, for example the drug release or the *in vitro* stability of the cell-based nanocarriers, and the pharmacological and toxicological effects in humans will play a key role in their 'developability'. Evidently, the complex interplay between the physicochemical features of nanomedicines and the *in vivo* performance requires a new theoretical framework to explain pharmacokinetics and biodistribution as well. Imaging methods may provide more information on the expected biodistribution pattern in humans and bridge the gap between different species. Recent approaches have highlighted the advantages of smart computational models and revealed the mechanistic relationships leading to the development of IVIVCs. Against this background, the next generation of nanomedicines can be developed using biopredictive *in vitro* assays to estimate the *in vivo* performance.

Declaration of Competing Interest

The authors declare that they have no known competing financial interests or personal relationships that could have appeared to influence the work reported in this paper.

Acknowledgments

Marc-Phillip Mast acknowledges the State of Hessen for financial contributions to the LOEWE research center for Translational Medicine and Pharmacology (Frankfurt, Germany). Matthias G. Wacker and Harshvardhan Modh acknowledge the National University of Singapore (WBS R-148-000-282-133, WBS-148-0000-297-114, WBS R-148-000-282-750) for financial support. Giorgia Pastorin, Gerrit Storm, Jiong-Wei Wang, and Matthias G. Wacker acknowledge the financial support by the NUS NanoNASH Program (NUHSRO/2020/002/NanoNash/LOA). Giorgia Pastorin, Gerrit Storm, and Jiong-Wei Wang acknowledge the financial support by the Singapore Ministry of Health's National Medical Research Council (NMRC/OFYIRG/0081/2018) and NUHS (NUHSRO/2018/095/RO5 + 5/Seed-Nov/05). Gerrit Storm acknowledges the financial support by the National University of Singapore, Office of the Deputy President for Research & Technology (NUHSRO/2019/077/STARTUP/03-ODPRT), and Yong Loo Lin School of Medicine (NUHSRO/2019/077/STARTUP/03-NUSMed).

References

[1] S.R. D'Mello, C.N. Cruz, M.-L. Chen, M. Kapoor, S.L. Lee, K.M. Tyner, The evolving landscape of drug products containing nanomaterials in the United States, Nat. Nanotechnol. 12 (2017) 523–529.
[2] Global Liposome Drug Delivery (Liposomes Drug Delivery) Market 2018 by Manufacturers, Regions, Type and Application, Forecast to 2023 (WGR3423000), 2018, www.wiseguyreports.com.
[3] M.R.C. Marques, Q. Choo, M. Ashtikar, T.C. Rocha, S. Bremer-Hoffmann, M.G. Wacker, Nanomedicines - Tiny particles and big challenges, Adv. Drug Deliv. Rev. 151–152 (2019) 23–43.
[4] M. Wacker, Nanocarriers for intravenous injection–the long hard road to the market, Int. J. Pharm. 457 (2013) 50–62.
[5] L. Hussaarts, S. Muhlebach, V.P. Shah, S. McNeil, G. Borchard, B. Fluhmann, V. Weinstein, S. Neervannan, E. Griffiths, W. Jiang, E. Wolff-Holz, D.J.A. Crommelin, J.S.B. de Vlieger, Equivalence of complex drug products: advances in and challenges for current regulatory frameworks, Ann. N. Y. Acad. Sci. 1407 (2017) 39–49.
[6] C. Holloway, J. Mueller-Berghaus, B.S. Lima, S.L. Lee, J.S. Wyatt, J.M. Nicholas, D.J. Crommelin, Scientific considerations for complex drugs in light of established and emerging regulatory guidance, Ann. N. Y. Acad. Sci. 1276 (2012) 26–36.
[7] US-FDA, Draft Guidance for Industry: Drug Products, Including Biological Products, that Contain Nanomaterials, 2017.
[8] K. Park, The drug delivery field at the inflection point: Time to fight its way out of the egg, J. Control. Release 267 (2017) 2–14.
[9] K. Park, The beginning of the end of the nanomedicine hype, J. Control. Release 305 (2019) 221–222.
[10] C. Tricarico, J. Clancy, C. D'Souza-Schorey, Biology and biogenesis of shed microvesicles, Small GTPases 8 (2017) 220–232.
[11] E.R. Abels, X.O. Breakefield, Introduction to extracellular vesicles: biogenesis, RNA cargo selection, content, release, and uptake, Cell. Mol. Life Sci. 36 (2016) 301–312.
[12] Y.-H. Ou, S. Zou, W.J. Goh, J.-W. Wang, M. Wacker, B. Czarny, G. Pastorin, Cell-Derived Nanovesicles as Exosome-Mimetics for Drug Delivery: Uses and Recommendations, in: K. Narayanan (Ed.), Bio-Carrier Vectors: Methods and Protocols, Springer, US, New York, NY, 2021, pp. 147–170.
[13] G. van Niel, G. D'Angelo, G. Raposo, Shedding light on the cell biology of extracellular vesicles, Nat. Rev. Mol. Cell Biol. 19 (2018) 213–228.
[14] P. Akuma, O.D. Okagu, C.C. Udenigwe, Naturally Occurring Exosome Vesicles as Potential Delivery Vehicle for Bioactive Compounds, Front. Sustain. Food Syst. 3 (2019).
[15] T. Lener, M. Gimona, L. Aigner, V. Börger, E. Buzas, G. Camussi, N. Chaput, D. Chatterjee, F.A. Court, H.A.d. Portillo, L. O'Driscoll, S. Fais, J.M. Falcon-Perez, U. Felderhoff-Mueser, L. Fraile, Y.S. Gho, A. Görgens, R.C. Gupta, A. Hendrix, D.M. Hermann, A.F. Hill, F. Hochberg, P.A. Horn, D.D. Kleijn, L. Kordelas, B.W. Kramer, E.-M. Krämer-Albers, S. Laner-Plamberger, S. Laitinen, T. Leonardi, M. J. Lorenowicz, S.K. Lim, J. Lötvall, C.A. Maguire, A. Marcilla, I. Nazarenko, T. Ochiya, T. Patel, S. Pedersen, G. Pocsfalvi, S. Pluchino, P. Quesenberry, I.G. Reischl, F.J. Rivera, R. Sanzenbacher, K. Schallmoser, I. Slaper-Cortenbach, D. Strunk, T. Tonn, P. Vader, B.W.M.v. Balkom, M. Wauben, S.E. Andaloussi, C. Théry, E. Rohde, B. Giebel, Applying extracellular vesicles based therapeutics in clinical trials – an ISEV position paper, J. Extracell. Vesicles 4 (2015) 30087.
[16] H.C. Christianson, K.J. Svensson, M. Belting, Exosome and microvesicle mediated phene transfer in mammalian cells, Semin. Cancer Biol. 28 (2014) 31–38.
[17] S.A. Kooijmans, P. Vader, S.M. van Dommelen, W.W. van Solinge, R.M. Schiffelers, Exosome mimetics: a novel class of drug delivery systems, Int. J. Nanomed. 7 (2012) 1525–1541.
[18] S.C. Jang, Y.S. Gho, Could bioengineered exosome-mimetic nanovesicles be an efficient strategy for the delivery of chemotherapeutics?, Nanomedicine (Lond) 9 (2014) 177–180.
[19] M. Gimona, M.F. Brizzi, A.B.H. Choo, M. Dominici, S.M. Davidson, J. Grillari, D. M. Hermann, A.F. Hill, D. de Kleijn, R.C. Lai, C.P. Lai, R. Lim, M. Monguió-Tortajada, M. Muraca, T. Ochiya, L.A. Ortiz, W.S. Toh, Y.W. Yi, K.W. Witwer, B. Giebel, S.K. Lim, Critical considerations for the development of potency tests for therapeutic applications of mesenchymal stromal cell-derived small extracellular vesicles, Cytotherapy 23 (2021) 373–380.
[20] A.T. Reiner, K.W. Witwer, B.W.M. van Balkom, J. de Beer, C. Brodie, R.L. Corteling, S. Gabrielsson, M. Gimona, A.G. Ibrahim, D. de Kleijn, C.P. Lai, J. Lötvall, H.A. del Portillo, I.G. Reischl, M. Riazifar, C. Salomon, H. Tahara, W.S. Toh, M.H.M. Wauben, V.K. Yang, Y. Yang, R.W.Y. Yeo, H. Yin, B. Giebel, E. Rohde, S.K. Lim, Concise Review: Developing Best-Practice Models for the Therapeutic Use of Extracellular Vesicles, Stem Cells Transl. Med. 6 (2017) 1730–1739.
[21] K.W. Witwer, B.W.M. Van Balkom, S. Bruno, A. Choo, M. Dominici, M. Gimona, A.F. Hill, D. De Kleijn, M. Koh, R.C. Lai, S.A. Mitsialis, L.A. Ortiz, E. Rohde, T. Asada, W.S. Toh, D.J. Weiss, L. Zheng, B. Giebel, S.K. Lim, Defining mesenchymal stromal cell (MSC)-derived small extracellular vesicles for therapeutic applications, J. Extracell. Vesicles 8 (2019) 1609206.
[22] US-FDA, Guidance for Industry: Extended Release Oral Dosage Forms: Development, Evaluation, and Application of In Vitro/In Vivo Correlations, 1997.
[23] N.P. Hessvik, A. Llorente, Current knowledge on exosome biogenesis and release, Cell. Mol. Life Sci. 75 (2018) 193–208.
[24] D.-K. Kim, J. Lee, S.R. Kim, D.-S. Choi, Y.J. Yoon, J.H. Kim, G. Go, D. Nhung, K. Hong, S.C. Jang, S.-H. Kim, K.-S. Park, O.Y. Kim, H.T. Park, J.H. Seo, E. Aikawa, M. Baj-Krzyworzeka, B.W.M. van Balkom, M. Belting, L. Blanc, V. Bond, A. Bongiovanni, F.E. Borràs, L. Buée, E.I. Buzás, L. Cheng, A. Clayton, E. Cocucci, C. S. Dela Cruz, D.M. Desiderio, D. Di Vizio, K. Ekström, J.M. Falcon-Perez, C. Gardiner, B. Giebel, D.W. Greening, J.C. Gross, D. Gupta, A. Hendrix, A.F. Hill, M.M. Hill, E. Nolte-'t Hoen, D.W. Hwang, J. Inal, M.V. Jagannadham, M. Jayachandran, Y.-K. Jee, M. Jørgensen, K.P. Kim, Y.-K. Kim, T. Kislinger, C. Lässer, D.S. Lee, H. Lee, J. van Leeuwen, T. Lener, M.-L. Liu, J. Lötvall, A. Marcilla, S. Mathivanan, A. Möller, J. Morhayim, F. Mullier, I. Nazarenko, R. Nieuwland, D.N. Nunes, K. Pang, J. Park, T. Patel, G. Pocsfalvi, H. del Portillo, U. Putz, M.I. Ramirez, M.L. Rodrigues, T.-Y. Roh, F. Royo, S. Sahoo, R. Schiffelers, S. Sharma, P. Siljander, R.J. Simpson, C. Soekmadji, P. Stahl, A. Stensballe, E. Stępień, H. Tahara, A. Trummer, H. Valadi, L.J. Vella, S.N. Wai, K. Witwer, M. Yáñez-Mó, H. Youn, R. Zeidler, Y.S. Gho, EVpedia: a community web portal for extracellular vesicles research, Bioinformatics 31 (2015) 933–939.
[25] H. Kalra, R.J. Simpson, H. Ji, E. Aikawa, P. Altevogt, P. Askenase, V.C. Bond, F.E. Borràs, X. Breakefield, V. Budnik, E. Buzas, G. Camussi, A. Clayton, E. Cocucci, J. M. Falcon-Perez, S. Gabrielsson, Y.S. Gho, D. Gupta, H.C. Harsha, A. Hendrix, A. F. Hill, J.M. Inal, G. Jenster, E.-M. Krämer-Albers, S.K. Lim, A. Llorente, J. Lötvall, A. Marcilla, L. Mincheva-Nilsson, I. Nazarenko, R. Nieuwland, E.N.M. Nolte-'t Hoen, A. Pandey, T. Patel, M.G. Piper, S. Pluchino, T.S.K. Prasad, L. Rajendran, G. Raposo, M. Record, G.E. Reid, F. Sánchez-Madrid, R.M. Schiffelers, P.

Siljander, A. Stensballe, W. Stoorvogel, D. Taylor, C. Thery, H. Valadi, B.W.M. van Balkom, J. Vázquez, M. Vidal, M.H.M. Wauben, M. Yáñez-Mó, M. Zoeller, S. Mathivanan, Vesiclepedia: A Compendium for Extracellular Vesicles with Continuous Community Annotation, PLoS Biol. 10 (2012) e1001450.
[26] R.J. Simpson, H. Kalra, S. Mathivanan, ExoCarta as a resource for exosomal research, J. Extracell. Vesicles 1 (2012) 18374.
[27] M. Colombo, G. Raposo, C. Théry, Biogenesis, Secretion, and Intercellular Interactions of Exosomes and Other Extracellular Vesicles, Annu. Rev. Cell Dev. Biol. 30 (2014) 255–289.
[28] M. Battistelli, E. Falcieri, Apoptotic Bodies: Particular Extracellular Vesicles Involved in Intercellular Communication, Biology 9 (2020) 21.
[29] J.C. Akers, D. Gonda, R. Kim, B.S. Carter, C.C. Chen, Biogenesis of extracellular vesicles (EV): Exosomes, microvesicles, retrovirus-like vesicles, and apoptotic bodies, J. Neuro-Oncol. 113 (2013) 1–11.
[30] M.F. Baietti, Z. Zhang, E. Mortier, A. Melchior, G. Degeest, A. Geeraerts, Y. Ivarsson, F. Depoortere, C. Coomans, E. Vermeiren, P. Zimmermann, G. David, Syndecan–syntenin–ALIX regulates the biogenesis of exosomes, Nat. Cell Biol. 14 (2012) 677–685.
[31] M. Colombo, C. Moita, G. van Niel, J. Kowal, J. Vigneron, P. Benaroch, N. Manel, L.F. Moita, C. Théry, G. Raposo, Analysis of ESCRT functions in exosome biogenesis, composition and secretion highlights the heterogeneity of extracellular vesicles, J. Cell Sci. 126 (2013) 5553–5565.
[32] D. Gupta, X. Liang, S. Pavlova, O.P.B. Wiklander, G. Corso, Y. Zhao, O. Saher, J. Bost, A.M. Zickler, A. Piffko, C.L. Maire, F.L. Ricklefs, O. Gustafsson, V.C. Llorente, M.O. Gustafsson, R.B. Bostancioglu, D.R. Mamand, D.W. Hagey, A. Görgens, J.Z. Nordin, S. El Andaloussi, Quantification of extracellular vesicles in vitro and in vivo using sensitive bioluminescence imaging, J. Extracell. Vesicles 9 (2020) 1800222.
[33] C. Théry, L. Zitvogel, S. Amigorena, Exosomes: composition, biogenesis and function, Nat. Rev. Immunol. 2 (2002) 569–579.
[34] P. Vader, E.A. Mol, G. Pasterkamp, R.M. Schiffelers, Extracellular vesicles for drug delivery, Adv. Drug Deliv. Rev. 106 (2016) 148–156.
[35] H. Zhang, D. Freitas, H.S. Kim, K. Fabijanic, Z. Li, H. Chen, M.T. Mark, H. Molina, A.B. Martin, L. Bojmar, J. Fang, S. Rampersaud, A. Hoshino, I. Matei, C.M. Kenific, M. Nakajima, A.P. Mutvei, P. Sansone, W. Buehring, H. Wang, J.P. Jimenez, L. Cohen-Gould, N. Paknejad, M. Brendel, K. Manova-Todorova, A. Magalhães, J.A. Ferreira, H. Osório, A.M. Silva, A. Massey, J.R. Cubillos-Ruiz, G. Galletti, P. Giannakakou, A.M. Cuervo, J. Blenis, R. Schwartz, M.S. Brady, H. Peinado, J. Bromberg, H. Matsui, C.A. Reis, D. Lyden, Identification of distinct nanoparticles and subsets of extracellular vesicles by asymmetric flow field-flow fractionation, Nat. Cell Biol. 20 (2018) 332–343.
[36] A. Latifkar, R.A. Cerione, M.A. Antonyak, Probing the mechanisms of extracellular vesicle biogenesis and function in cancer, Biochem. Soc. Trans. 46 (2018) 1137–1146.
[37] T. Skotland, N.P. Hessvik, K. Sandvig, A. Llorente, Exosomal lipid composition and the role of ether lipids and phosphoinositides in exosome biology, J. Lipid Res. 60 (2019) 9–18.
[38] H. Gu, A.-M.C. Overstreet, Y. Yang, Exosomes Biogenesis and Potentials in Disease Diagnosis and Drug Delivery, Nano Life 04 (2014) 1441017.
[39] R.J. Simpson, J.W.E. Lim, R.L. Moritz, S. Mathivanan, Exosomes: proteomic insights and diagnostic potential, Expert Rev. Proteomics 6 (2009) 267–283.
[40] P. Duan, J. Tan, Y. Miao, Q. Zhang, Potential role of exosomes in the pathophysiology, diagnosis, and treatment of hypoxic diseases, Am. J. Transl. Res. 11 (2019) 1184–1201.
[41] J. Kowal, M. Tkach, C. Théry, Biogenesis and secretion of exosomes, Curr. Opin. Cell Biol. 29 (2014) 116–125.
[42] R.A. Badierah, V.N. Uversky, E.M. Redwan, Dancing with Trojan horses: an interplay between the extracellular vesicles and viruses, J. Biomol. Struc. Dyn. (2020) 1–27.
[43] R. Kalluri, V.S. LeBleu, The biology, function, and biomedical applications of exosomes, Science 367 (2020) eaau6977.
[44] S.Y. Chong, C.K. Lee, C. Huang, Y.H. Ou, C.J. Charles, A.M. Richards, Y.R. Neupane, M.V. Pavon, O. Zharkova, G. Pastorin, J.W. Wang, Extracellular Vesicles in Cardiovascular Diseases: Alternative Biomarker Sources, Therapeutic Agents, and Drug Delivery Carriers, Int. J. Mol. Sci. 20 (2019).
[45] I.-M. Chung, G. Rajakumar, B. Venkidasamy, U. Subramanian, M. Thiruvengadam, Exosomes: Current use and future applications, Clin. Chim. Acta 500 (2020) 226–232.
[46] W. Meng, C. He, Y. Hao, L. Wang, L. Li, G. Zhu, Prospects and challenges of extracellular vesicle-based drug delivery system: considering cell source, Drug Deliv. 27 (2020) 585–598.
[47] US-FDA, Guidance for Industry: Liposome Drug Products Chemistry, Manufacturing, and Controls; Human Pharmacokinetics and Bioavailability; and Labeling Documentation, 2018
[48] C. Gardiner, D.D. Vizio, S. Sahoo, C. Théry, K.W. Witwer, M. Wauben, A.F. Hill, Techniques used for the isolation and characterization of extracellular vesicles: results of a worldwide survey, J. Extracell. Vesicles 5 (2016) 32945.
[49] C. Théry, K.W. Witwer, E. Aikawa, M.J. Alcaraz, J.D. Anderson, R. Andriantsitohaina, A. Antoniou, T. Arab, F. Archer, G.K. Atkin-Smith, D.C. Ayre, J.-M. Bach, D. Bachurski, H. Baharvand, L. Balaj, S. Baldacchino, N.N. Bauer, A.A. Baxter, M. Bebawy, C. Beckham, A. Bedina Zavec, A. Benmoussa, A. C. Berardi, P. Bergese, E. Bielska, C. Blenkiron, S. Bobis-Wozowicz, E. Boilard, W. Boireau, A. Bongiovanni, F.E. Borràs, S. Bosch, C.M. Boulanger, X. Breakefield, A.M. Breglio, M.Á. Brennan, D.R. Brigstock, A. Brisson, M.L.D. Broekman, J.F. Bromberg, P. Bryl-Górecka, S. Buch, A.H. Buck, D. Burger, S. Busatto, D. Buschmann, B. Bussolati, E.I. Buzás, J.B. Byrd, G. Camussi, D.R.F. Carter, S. Caruso, L.W. Chamley, Y.-T. Chang, C. Chen, S. Chen, L. Cheng, A.R. Chin, A. Clayton, S.P. Clerici, A. Cocks, E. Cocucci, R.J. Coffey, A. Cordeiro-da-Silva, Y. Couch, F.A.W. Coumans, B. Coyle, R. Crescitelli, M.F. Criado, C. D'Souza-Schorey, S. Das, A. Datta Chaudhuri, P. de Candia, E.F. De Santana Junior, O. De Wever, H.A. del Portillo, T. Demaret, S. Deville, A. Devitt, B. Dhondt, D. Di Vizio, L.C. Dieterich, V. Dolo, A.P. Dominguez Rubio, M. Dominici, M.R. Dourado, T.A.P. Driedonks, F.V. Duarte, H.M. Duncan, R.M. Eichenberger, K. Ekström, S. El Andaloussi, C. Elie-Caille, U. Erdbrügger, J.M. Falcón-Pérez, F. Fatima, J.E. Fish, M. Flores-Bellver, A. Försönits, A. Frelet-Barrand, F. Fricke, G. Fuhrmann, S. Gabrielsson, A. Gámez-Valero, C. Gardiner, K. Gärtner, R. Gaudin, Y.S. Gho, B. Giebel, C. Gilbert, M. Gimona, I. Giusti, D.C.I. Goberdhan, A. Görgens, S.M. Gorski, D.W. Greening, J.C. Gross, A. Gualerzi, G. N. Gupta, D. Gustafson, A. Handberg, R.A. Haraszti, P. Harrison, H. Hegyesi, A. Hendrix, A.F. Hill, F.H. Hochberg, K.F. Hoffmann, B. Holder, H. Holthofer, B. Hosseinkhani, G. Hu, Y. Huang, V. Huber, S. Hunt, A.G.-E. Ibrahim, T. Ikezu, J. M. Inal, M. Isin, A. Ivanova, H.K. Jackson, S. Jacobsen, S.M. Jay, M. Jayachandran, G. Jenster, L. Jiang, S.M. Johnson, J.C. Jones, A. Jong, T. Jovanovic-Talisman, S. Jung, R. Kalluri, S.-I. Kano, S. Kaur, Y. Kawamura, E.T. Keller, D. Khamari, E. Khomyakova, A. Khvorova, P. Kierulf, K.P. Kim, T. Kislinger, M. Klingeborn, D.J. Klinke Ii, M. Kornek, M.M. Kosanović, Á.F. Kovács, E.-M. Krämer-Albers, S. Krasemann, M. Krause, I.V. Kurochkin, G.D. Kusuma, S. Kuypers, S. Laitinen, S.M. Langevin, L.R. Languino, J. Lannigan, C. Lässer, L.C. Laurent, G. Lavieu, E. Lázaro-Ibáñez, S. Le Lay, M.-S. Lee, Y.X.F. Lee, D.S. Lemos, M. Lenassi, A. Leszczynska, I.T.S. Li, K. Liao, S.F. Libregts, E. Ligeti, R. Lim, S.K. Lim, A. Linē, K. Linnemannstöns, A. Llorente, C.A. Lombard, M.J. Lorenowicz, Á.M. Lörincz, J. Lötvall, J. Lovett, M.C. Lowry, X. Loyer, Q. Lu, B. Lukomska, T.R. Lunavat, S.L.N. Maas, H. Malhi, A. Marcilla, J. Mariani, J. Mariscal, E.S. Martens-Uzunova, L. Martin-Jaular, M.C. Martinez, V.R. Martins, M. Mathieu, S. Mathivanan, M. Maugeri, L.K. McGinnis, M.J. McVey, D.G. Meckes Jr, K.L. Meehan, I. Mertens, V.R. Minciacchi, A. Möller, M. Møller Jørgensen, A. Morales-Kastresana, J. Morhayim, F. Mullier, M. Muraca, L. Musante, V. Mussack, D.C. Muth, K.H. Myburgh, T. Najrana, M. Nawaz, I. Nazarenko, P. Nejsum, C. Neri, T. Neri, R. Nieuwland, L. Nimrichter, J.P. Nolan, E.N.M. Nolte-'t Hoen, N. Noren Hooten, L. O'Driscoll, T. O'Grady, A. O'Loghlen, T. Ochiya, M. Olivier, A. Ortiz, L.A. Ortiz, X. Osteikoetxea, O. Østergaard, M. Ostrowski, J. Park, D.M. Pegtel, H. Peinado, F. Perut, M.W. Pfaffl, D.G. Phinney, B.C.H. Pieters, R.C. Pink, D.S. Pisetsky, E. Pogge von Strandmann, I. Polakovicova, I.K.H. Poon, B.H. Powell, I. Prada, L. Pulliam, P. Quesenberry, A. Radeghieri, R.L. Raffai, S. Raimondo, J. Rak, M.I. Ramirez, G. Raposo, M.S. Rayyan, N. Regev-Rudzki, F.L. Ricklefs, P.D. Robbins, D.D. Roberts, S.C. Rodrigues, E. Rohde, S. Rome, K.M.A. Rouschop, A. Rughetti, A.E. Russell, P. Saá, S. Sahoo, E. Salas-Huenuleo, C. Sánchez, J.A. Saugstad, M.J. Saul, R.M. Schiffelers, R. Schneider, T.H. Schøyen, A. Scott, E. Shahaj, S. Sharma, O. Shatnyeva, F. Shekari, G.V. Shelke, A.K. Shetty, K. Shiba, P.R.M. Siljander, A.M. Silva, A. Skowronek, O.L. Snyder Ii, R.P. Soares, B.W. Sódar, C. Soekmadji, J. Sotillo, P.D. Stahl, W. Stoorvogel, S.L. Stott, E.F. Strasser, S. Swift, H. Tahara, M. Tewari, K. Timms, S. Tiwari, R. Tixeira, M. Tkach, W.S. Toh, R. Tomasini, A.C. Torrecilhas, J.P. Tosar, V. Toxavidis, L. Urbanelli, P. Vader, B.W.M. van Balkom, S.G. van der Grein, J. Van Deun, M.J.C. van Herwijnen, K. Van Keuren-Jensen, G. van Niel, M.E. van Royen, A.J. van Wijnen, M.H. Vasconcelos, I.J. Vechetti Jr, T.D. Veit, L.J. Vella, É. Velot, F.J. Verweij, B. Vestad, J.L. Viñas, T. Visnovitz, K.V. Vukman, J. Wahlgren, D.C. Watson, M.H.M. Wauben, A. Weaver, J.P. Webber, V. Weber, A.M. Wehman, D.J. Weiss, J.A. Welsh, S. Wendt, A.M. Wheelock, Z. Wiener, L. Witte, J. Wolfram, A. Xagorari, P. Xander, J. Xu, X. Yan, M. Yáñez-Mó, H. Yin, Y. Yuana, V. Zappulli, J. Zarubova, V. Žėkas, J.-y. Zhang, Z. Zhao, L. Zheng, A.R. Zheutlin, A.M. Zickler, P. Zimmermann, A.M. Zivkovic, D. Zocco, E. K. Zuba-Surma, Minimal information for studies of extracellular vesicles 2018 (MISEV2018): a position statement of the International Society for Extracellular Vesicles and update of the MISEV2014 guidelines, J. Extracell. Vesicles 7 (2018) (2018) 1535750.
[50] K.W. Witwer, E.I. Buzás, L.T. Bemis, A. Bora, C. Lässer, J. Lötvall, E.N. Nolte-'t Hoen, M.G. Piper, S. Sivaraman, J. Skog, C. Théry, M.H. Wauben, F. Hochberg, Standardization of sample collection, isolation and analysis methods in extracellular vesicle research, J. Extracell. Vesicles 2 (2013) 20360.
[51] J.R. Eckardt, E. Campbell, H.A. Burris, G.R. Weiss, G.I. Rodriguez, S.M. Fields, A. M. Thurman, N.W. Peacock, P. Cobb, M.L. Rothenberg, et al., A phase II trial of DaunoXome, liposome-encapsulated daunorubicin, in patients with metastatic adenocarcinoma of the colon, Am. J. Clin. Oncol. 17 (1994) 498–501.
[52] B. Uziely, S. Jeffers, R. Isacson, K. Kutsch, D. Wei-Tsao, Z. Yehoshua, E. Libson, F.M. Muggia, A. Gabizon, Liposomal doxorubicin: antitumor activity and unique toxicities during two complementary phase I studies, J. Clin. Oncol. 13 (1995) 1777–1785.
[53] N. Desai, T. De, S. Ci, L. Louie, V. Trieu, Characterization and in vitro/in vivo dissolution of nab-paclitaxel nanoparticles, Cancer Res. 68 (2008), 5624 5624.
[54] S. Nagpal, S. Braner, H. Modh, A.X.X. Tan, M.P. Mast, K. Chichakly, V. Albrecht, M.G. Wacker, A physiologically-based nanocarrier biopharmaceutics model to reverse-engineer the in vivo drug release, Eur. J. Pharm. Biopharm. 153 (2020) 257–272.
[55] S. O'Brien, G. Schiller, J. Lister, L. Damon, S. Goldberg, W. Aulitzky, D. Ben-Yehuda, W. Stock, S. Coutre, D. Douer, L.T. Heffner, M. Larson, K. Seiter, S. Smith, S. Assouline, P. Kuriakose, L. Maness, A. Nagler, J. Rowe, M. Schaich, O. Shpilberg, K. Yee, G. Schmieder, J.A. Silverman, D. Thomas, S.R. Deitcher, H. Kantarjian, High-Dose Vincristine Sulfate Liposome Injection for Advanced, Relapsed, and Refractory Adult Philadelphia Chromosome-Negative Acute Lymphoblastic Leukemia, J. Clin. Oncol. 31 (2013) 676–683.

[56] E.L. Jeffrey, L.U. Geoffrey, E.C. Jorge, F.N. Laura, L.L. Tara, K.R. Ellen, K.S. Robert, A.S. Stephen, H. Donna, R.S. Scott, M.S. Richard, L.B. Dale, E.K. Jonathan, J.S. Gary, J.W. Matthew, H.R. Daniel, H. Antje, B. Kamalika, C. Michael, C.L. Arthur, C.M. Bruno, CPX-351 (cytarabine and daunorubicin) Liposome for Injection Versus Conventional Cytarabine Plus Daunorubicin in Older Patients With Newly Diagnosed Secondary Acute Myeloid Leukemia, J. Clin. Oncol. 36 (2018) 2684–2692.

[57] A.C. Krauss, X. Gao, L. Li, M.L. Manning, P. Patel, W. Fu, K.G. Janoria, G. Gieser, D.A. Bateman, D. Przepiorka, Y.L. Shen, S.S. Shord, C.M. Sheth, A. Banerjee, J. Liu, K.B. Goldberg, A.T. Farrell, G.M. Blumenthal, R. Pazdur, FDA Approval Summary: (Daunorubicin and Cytarabine) Liposome for Injection for the Treatment of Adults with High-Risk Acute Myeloid Leukemia, Clin. Cancer Res. 25 (2019) 2685–2690.

[58] L.D. Mayer, P. Tardi, A.C. Louie, CPX-351: a nanoscale liposomal co-formulation of daunorubicin and cytarabine with unique biodistribution and tumor cell uptake properties, Int. J. Nanomed. 14 (2019) 3819–3830.

[59] W.-S. Lim, P.G. Tardi, N. Dos Santos, X. Xie, M. Fan, B.D. Liboiron, X. Huang, T. O. Harasym, D. Bermudes, L.D. Mayer, Leukemia-selective uptake and cytotoxicity of CPX-351, a synergistic fixed-ratio cytarabine:daunorubicin formulation, in bone marrow xenografts, Leuk. Res. 34 (2010) 1214–1223.

[60] P. Tardi, S. Johnstone, N. Harasym, S. Xie, T. Harasym, N. Zisman, P. Harvie, D. Bermudes, L. Mayer, In vivo maintenance of synergistic cytarabine:daunorubicin ratios greatly enhances therapeutic efficacy, Leuk. Res. 33 (2009) 129–139.

[61] J.A. Silverman, S.R. Deitcher, Marqibo® (vincristine sulfate liposome injection) improves the pharmacokinetics and pharmacodynamics of vincristine, Cancer Chemother. Pharmacol. 71 (2013) 555–564.

[62] N.L. Boman, P.R. Cullis, L.D. Mayer, M.B. Bally, M.S. Webb, Liposomal Vincristine: The Central Role of Drug Retention in Defining Therapeutically Optimized Anticancer Formulations, in: M.C. Woodle, G. Storm (Eds.), Long Circulating Liposomes: Old Drugs, New Therapeutics, Springer, Berlin Heidelberg, Berlin, Heidelberg, 1998, pp. 29–49.

[63] M.J.W. Johnston, S.C. Semple, S.K. Klimuk, K. Edwards, M.L. Eisenhardt, E.C. Leng, G. Karlsson, D. Yanko, P.R. Cullis, Therapeutically optimized rates of drug release can be achieved by varying the drug-to-lipid ratio in liposomal vincristine formulations, Biochim. Biophys. Acta 1758 (2006) 55–64.

[64] D.N. Waterhouse, T.D. Madden, P.R. Cullis, M.B. Bally, L.D. Mayer, M.S. Webb, Preparation, Characterization, and Biological Analysis of Liposomal Formulations of Vincristine, in: N. Düzgüneş (Ed.), Liposomes, Acad. Press, Amsterdam, 2005, pp. 40–57.

[65] M.S. Webb, T.O. Harasym, D. Masin, M.B. Bally, L.D. Mayer, Sphingomyelin-cholesterol liposomes significantly enhance the pharmacokinetic and therapeutic properties of vincristine in murine and human tumour models, Br. J. Cancer 72 (1995) 896–904.

[66] L. Jablonka, M. Ashtikar, G. Gao, F. Jung, M. Thurn, A. Preuss, D. Scheglmann, V. Albrecht, B. Roder, M.G. Wacker, Advanced in silico modeling explains pharmacokinetics and biodistribution of temoporfin nanocrystals in humans, J. Control. Release 308 (2019) 57–70.

[67] L. Jablonka, M. Ashtikar, G.F. Gao, M. Thurn, H. Modh, J.W. Wang, A. Preuss, D. Scheglmann, V. Albrecht, B. Roder, M.G. Wacker, Predicting human pharmacokinetics of liposomal temoporfin using a hybrid in silico model, Eur. J. Pharm. Biopharm. 149 (2020) 121–134.

[68] Y. Liu, M.H.A.M. Fens, R.B. Capomaccio, D. Mehn, L. Scrivano, R.J. Kok, S. Oliveira, W.E. Hennink, C.F. van Nostrum, Correlation between in vitro stability and pharmacokinetics of poly(ε-caprolactone)-based micelles loaded with a photosensitizer, J. Control Release (2020).

[69] G. Troiano, J. Nolan, D. Parsons, C. Van Geen Hoven, S. Zale, A Quality by Design Approach to Developing and Manufacturing Polymeric Nanoparticle Drug Products, AAPS J. 18 (2016) 1354–1365.

[70] K.J. Harrington, C.R. Lewanski, A.D. Northcote, J. Whittaker, H. Wellbank, R.G. Vile, A.M. Peters, J.S. Stewart, Phase I-II study of pegylated liposomal cisplatin (SPI-077) in patients with inoperable head and neck cancer, Ann. Oncol. 12 (2001) 493–496.

[71] S.C. White, P. Lorigan, G.P. Margison, J.M. Margison, F. Martin, N. Thatcher, H. Anderson, M. Ranson, Phase II study of SPI-77 (sterically stabilised liposomal cisplatin) in advanced non-small-cell lung cancer, Br. J. Cancer 95 (2006) 822–828.

[72] G.P. Stathopoulos, D. Antoniou, J. Dimitroulis, P. Michalopoulou, A. Bastas, K. Marosis, J. Stathopoulos, A. Provata, P. Yiamboudakis, D. Veldekis, N. Lolis, N. Georgatou, M. Toubis, C. Pappas, G. Tsoukalas, Liposomal cisplatin combined with paclitaxel versus cisplatin and paclitaxel in non-small-cell lung cancer: a randomized phase III multicenter trial, Ann. Oncol. 21 (2010) 2227–2232.

[73] G.P. Stathopoulos, D. Antoniou, J. Dimitroulis, J. Stathopoulos, K. Marosis, P. Michalopoulou, Comparison of liposomal cisplatin versus cisplatin in non-squamous cell non-small-cell lung cancer, Cancer Chemother. Pharmacol. 68 (2011) 945–950.

[74] G.P. Stathopoulos, T. Boulikas, Lipoplatin formulation review article, J. Drug. Deliv. 2012 (2012) 581363.

[75] B. Xu, M. Zeng, J. Zeng, J. Feng, L. Yu, Meta-analysis of clinical trials comparing the efficacy and safety of liposomal cisplatin versus conventional nonliposomal cisplatin in nonsmall cell lung cancer (NSCLC) and squamous cell carcinoma of the head and neck (SCCHN), Medicine (Baltimore) 97 (2018) e13169.

[76] C.Z. William, C.G. Anne, J.E. Merrill, H.M.S. Jan, G.Z. Elleanor, P. Dick, J. Erin, R. H. Deborah, K.W. Peter, C. Gail, E.T. Margaret, M.P. Douglas, L.E. Julie, Systemic and tumor disposition of platinum after administration of cisplatin or STEALTH liposomal-cisplatin formulations (SPI-077 and SPI-077 B103) in a preclinical tumor model of melanoma, Cancer Chemother. Pharmacol. 53 (2004) 329–336.

[77] J. Gerard, H. Ning, C. Su-Ming, F. Richard, H. Van, S. Michele, F. Iduna, N. Ch, E. Crispin, New liposomal formulations of cisplatin with improved therapeutic index, Cancer Res. 64 (2004) 1065.

[78] H.M. Kieler-Ferguson, D. Chan, J. Sockolosky, L. Finney, E. Maxey, S. Vogt, F.C. Szoka, Encapsulation, controlled release, and antitumor efficacy of cisplatin delivered in liposomes composed of sterol-modified phospholipids, Eur. J. Pharm. Sci. 103 (2017) 85–93.

[79] J. Chen, C.-Q. He, A.-H. Lin, W. Gu, Z.-P. Chen, W. Li, B.-C. Cai, Thermosensitive liposomes with higher phase transition temperature for targeted drug delivery to tumor, Int. J. Pharm. 475 (2014) 408–415.

[80] R.T.P. Poon, N. Borys, Lyso-thermosensitive liposomal doxorubicin: a novel approach to enhance efficacy of thermal ablation of liver cancer, Expert Opin. Pharmacother. 10 (2009) 333–343.

[81] W.Y. Tak, S.-M. Lin, Y. Wang, J. Zheng, A. Vecchione, S.Y. Park, M.H. Chen, S. Wong, R. Xu, C.-Y. Peng, Y.-Y. Chiou, G.-T. Huang, J. Cai, B.J.J. Abdullah, J.S. Lee, J.Y. Lee, J.-Y. Choi, J. Gopez-Cervantes, M. Sherman, R.S. Finn, M. Omata, M. O'Neal, L. Makris, N. Borys, R. Poon, R. Lencioni, Phase III HEAT Study Adding Lyso-Thermosensitive Liposomal Doxorubicin to Radiofrequency Ablation in Patients with Unresectable Hepatocellular Carcinoma Lesions, Clin. Cancer Res. 24 (2018) 73–83.

[82] L. Wei, J. Chen, J. Ding, Sequentially stimuli-responsive anticancer nanomedicines, Nanomedicine (Lond.) 16 (2021) 261–264.

[83] B.M. Kerklaan, A. Jager, P. Aftimos, V. Dieras, S. Altintas, C. Anders, M. Arnedos, H. Gelderblom, P. Soetekouw, W. Gladdines, P. Gaillard, C. Sousa, A. Awada, J. Schellens, M. van Linde, D. Brandsma, NT-23 * Phase 1/2A study of glutathione pegylated liposomal doxorubicin (2B3-101) in breast cancer patients with brain metastases (BCBM) or recurrent high grade gliomas (HGG), Neuro-Oncol. 16 (2014), v163.

[84] E.R. Gardner, W.L. Dahut, C.D. Scripture, J. Jones, J.B. Aragon-Ching, N. Desai, M.J. Hawkins, A. Sparreboom, W.D. Figg, Randomized crossover pharmacokinetic study of solvent-based paclitaxel and nab-paclitaxel, Clin. Cancer Res. 14 (2008) 4200–4205.

[85] W.J. Gradishar, Albumin-bound paclitaxel: a next-generation taxane, Expert Opin. Pharmacother. 7 (2006) 1041–1053.

[86] M.L. Johnson, J.G.C.E. Cosaert, G.S. Falchook, S.F. Jones, D. Strickland, C. Greenlees, J. Charlton, A. MacDonald, P. Overend, C. Adelman, H.A. Burris, E.J. Pease, G.S. Patel, J.S.-Z. Wang, A phase I, open label, multicenter dose escalation study of AZD2811 nanoparticle in patients with advanced solid tumors, J. Clin. Oncol. 37 (2019) 3098.

[87] Y.H. Song, E. Shin, H. Wang, J. Nolan, S. Low, D. Parsons, S. Zale, S. Ashton, M. Ashford, M. Ali, D. Thrasher, N. Boylan, G. Troiano, A novel in situ hydrophobic ion pairing (HIP) formulation strategy for clinical product selection of a nanoparticle drug delivery system, J. Control. Release 229 (2016) 106–119.

[88] J. Hrkach, D. Hoff, M.M. Ali, E. Andrianova, J. Auer, T. Campbell, D. Witt, M. Figa, M. Figueiredo, A. Horhota, S. Low, K. McDonnell, E. Peeke, B. Retnarajan, A. Sabnis, E. Schnipper, J.J. Song, Y.H. Song, J. Summa, D. Tompsett, G. Troiano, T. van Geen Hoven, J. Wright, P. LoRusso, P.W. Kantoff, N.H. Bander, C. Sweeney, O.C. Farokhzad, R. Langer, S. Zale, Preclinical Development and Clinical Translation of a PSMA-Targeted Docetaxel Nanoparticle with a Differentiated Pharmacological Profile, Sci. Transl. Med. 4 (2012) 128ra139.

[89] D.D. Hoff, M.M. Mita, R.K. Ramanathan, G.J. Weiss, A.C. Mita, P.M. LoRusso, H. A. Burris, L.L. Hart, S.C. Low, D.M. Parsons, S.E. Zale, J.M. Summa, H. Youssoufian, J.C. Sachdev, Phase I Study of PSMA-Targeted Docetaxel-Containing Nanoparticle BIND-014 in Patients with Advanced Solid Tumors, Clin. Cancer Res. 22 (2016) 3157.

[90] O. Čapoun, V. Mikulová, M. Jančíková, H. Honová, K. Kološtová, R. Sobotka, P. Michael, T. Zima, T. Hanuš, V. Soukup, Prognosis of Castration-resistant Prostate Cancer Patients - Use of the AdnaTest® System for Detection of Circulating Tumor Cells, Anticancer Res. 36 (2016) 2019–2026.

[91] K.A. Autio, R. Dreicer, J. Anderson, J.A. Garcia, A. Alva, L.L. Hart, M.I. Milowsky, E.M. Posadas, C.J. Ryan, R.P. Graf, R. Dittamore, N.A. Schreiber, J.M. Summa, H. Youssoufian, M.J. Morris, H.I. Scher, Safety and Efficacy of BIND-014, a Docetaxel Nanoparticle Targeting Prostate-Specific Membrane Antigen for Patients With Metastatic Castration-Resistant Prostate Cancer: A Phase 2 Clinical Trial, JAMA Oncol. 4 (2018) 1344–1351.

[92] US-FDA, Doxorubicin hydrochloride liposome injection (Doxil®) approval letter (NDA 50-718/S-50), 2015.

[93] A.F. Eric, The design and development of DaunoXome(R) for solid tumor targeting in vivo, Adv. Drug Deliv. Rev. 24 (1997) 133–150.

[94] J.P. Adler-moore, R.T. Proffitt, Development, Characterization, Efficacy and Mode of Action of Ambisome, A Unilamellar Liposomal Formulation of Amphotericin B, J. Liposome Res. 3 (1993) 429–450.

[95] C.E. Swenson, W.R. Perkins, P. Roberts, A.S. Janoff, Liposome technology and the development of Myocet™ (liposomal doxorubicin citrate), Breast 10 (2001) 1–7.

[96] R.K. Chowdhary, I. Shariff, D. Dolphin, Drug release characteristics of lipid based benzoporphyrin derivative, J. Pharm. Pharm. Sci. 6 (2003) 13–19.

[97] D.M. Vail, E.G. MacEwen, I.D. Kurzman, R.R. Dubielzig, S.C. Helfand, W.C. Kisseberth, C.A. London, J.E. Obradovich, B.R. Madewell, C.O. Rodriguez, Liposome-encapsulated muramyl tripeptide phosphatidylethanolamine adjuvant immunotherapy for splenic hemangiosarcoma in the dog: a randomized multi-institutional clinical trial, Clin. Cancer Res. 1 (1995) 1165–1170.

[98] A.Y. Bedikian, A. Vardeleon, T. Smith, S. Campbell, R. Namdari, Pharmacokinetics and urinary excretion of vincristine sulfate liposomes injection in metastatic melanoma patients, J. Clin. Pharmacol. 46 (2006) 727–737.

[99] V. Burade, S. Bhowmick, K. Maiti, R. Zalawadia, H. Ruan, R. Thennati, Lipodox® (generic doxorubicin hydrochloride liposome injection): in vivo efficacy and bioequivalence versus Caelyx® (doxorubicin hydrochloride liposome injection) in human mammary carcinoma (MX-1) xenograft and syngeneic fibrosarcoma (WEHI 164) mouse models, BMC Cancer 17 (2017) 405.

[100] D.C. Drummond, C.O. Noble, Z. Guo, K. Hong, J.W. Park, D.B. Kirpotin, Development of a highly active nanoliposomal irinotecan using a novel intraliposomal stabilization strategy, Cancer Res. 66 (2006) 3271–3277.

[101] US-FDA, DOXOrubicin Hydrochloride Liposome Injection approval letter (ANDA 208657), 2017.

[102] US-FDA, Abraxane approval letter (NDA 21-660), Clinical Pharmacology and Biopharmaceutics Review(s), 2005.

[103] US-FDA, Ferumoxytol approval letter (NDA 22-180), Clinical Pharmacology and Biopharmaceutics Review(s), 2009.

[104] K. Garber, Alnylam launches era of RNAi drugs, Nat. Biotechnol. 36 (2018) 777–778.

[105] US-FDA, Onpattro 2 mg/mL injection for intravenous use approval letter (NDA 210922), 2018.

[106] J. Lister, Amphotericin B Lipid Complex (Abelcet) in the treatment of invasive mycoses: the North American experience, Eur. J. Haematol. Suppl. 57 (1996) 18–23.

[107] T.G. Dacoba, A. Olivera, D. Torres, J. Crecente-Campo, M.J. Alonso, Modulating the immune system through nanotechnology, Semin. Immunol. 34 (2017) 78–102.

[108] D.J. Irvine, E.L. Dane, Enhancing cancer immunotherapy with nanomedicine, Nat. Rev. Immunol. 20 (2020) 321–334.

[109] X. Feng, W. Xu, Z. Li, W. Song, J. Ding, X. Chen, Immunomodulatory Nanosystems, Adv. Sci. 6 (2019) 1900101.

[110] O.P. Joffre, E. Segura, A. Savina, S. Amigorena, Cross-presentation by dendritic cells, Nat. Rev. Immunol. 12 (2012) 557–569.

[111] G. Zhu, F. Zhang, Q. Ni, G. Niu, X. Chen, Efficient Nanovaccine Delivery in Cancer Immunotherapy, ACS nano 11 (2017) 2387–2392.

[112] J. Gao, L.J. Ochyl, E. Yang, J.J. Moon, Cationic liposomes promote antigen cross-presentation in dendritic cells by alkalizing the lysosomal pH and limiting the degradation of antigens, Int. J. Nanomed. 12 (2017) 1251–1264.

[113] S. Hirosue, I.C. Kourtis, A.J. van der Vlies, J.A. Hubbell, M.A. Swartz, Antigen delivery to dendritic cells by poly(propylene sulfide) nanoparticles with disulfide conjugated peptides: Cross-presentation and T cell activation, Vaccine 28 (2010) 7897–7906.

[114] D. Mahony, A.S. Cavallaro, F. Stahr, T.J. Mahony, S.Z. Qiao, N. Mitter, Mesoporous silica nanoparticles act as a self-adjuvant for ovalbumin model antigen in mice, Small 9 (2013) 3138–3146.

[115] H. Jiang, Q. Wang, L. Li, Q. Zeng, H. Li, T. Gong, Z. Zhang, X. Sun, Turning the Old Adjuvant from Gel to Nanoparticles to Amplify CD8(+) T Cell Responses, Adv. Sci. 5 (2018) 1700426.

[116] Y. Fan, J.J. Moon, Nanoparticle Drug Delivery Systems Designed to Improve Cancer Vaccines and Immunotherapy, Vaccines (Basel) 3 (2015) 662–685.

[117] L. Jeanbart, M. Ballester, A. de Titta, P. Corthesy, P. Romero, J.A. Hubbell, M.A. Swartz, Enhancing efficacy of anticancer vaccines by targeted delivery to tumor-draining lymph nodes, Cancer Immunol. Res. 2 (2014) 436–447.

[118] H. Liu, K.D. Moynihan, Y. Zheng, G.L. Szeto, A.V. Li, B. Huang, D.S. Van Egeren, C. Park, D.J. Irvine, Structure-based programming of lymph-node targeting in molecular vaccines, Nature 507 (2014) 519–522.

[119] S. De Koker, J. Cui, N. Vanparijs, L. Albertazzi, J. Grooten, F. Caruso, B.G. De Geest, Engineering Polymer Hydrogel Nanoparticles for Lymph Node-Targeted Delivery, Angew. Chem. Int. Ed. 55 (2016) 1334–1339.

[120] M. Luo, L.Z. Samandi, Z. Wang, Z.J. Chen, J. Gao, Synthetic nanovaccines for immunotherapy, J. Control. Release 263 (2017) 200–210.

[121] V. Manolova, A. Flace, M. Bauer, K. Schwarz, P. Saudan, M.F. Bachmann, Nanoparticles target distinct dendritic cell populations according to their size, Eur. J. Immunol 38 (2008) 1404–1413.

[122] J.J. Moon, H. Suh, A. Bershteyn, M.T. Stephan, H. Liu, B. Huang, M. Sohail, S. Luo, S. Ho Um, H. Khant, J.T. Goodwin, J. Ramos, W. Chiu, D.J. Irvine, Interbilayer-crosslinked multilamellar vesicles as synthetic vaccines for potent humoral and cellular immune responses, Nat. Mater. 10 (2011) 243–251.

[123] N. Raab-Traub, D.P. Dittmer, Viral effects on the content and function of extracellular vesicles, Nat. Rev. Microbiol. 15 (2017) 559–572.

[124] S. Pant, H. Hilton, M.E. Burczynski, The multifaceted exosome: Biogenesis, role in normal and aberrant cellular function, and frontiers for pharmacological and biomarker opportunities, Biochem. Pharmacol. 83 (2012) 1484–1494.

[125] K. Matsumoto, T. Morisaki, H. Kuroki, M. Kubo, H. Onishi, K. Nakamura, C. Nakahara, H. Kuga, E. Baba, M. Nakamura, K. Hirata, M. Tanaka, M. Katano, Exosomes secreted from monocyte-derived dendritic cells support in vitro naive CD4+ T cell survival through NF-κB activation, Cell. Immunol. 231 (2004) 20–29.

[126] I. Hwang, X. Shen, J. Sprent, Direct stimulation of naïve T cells by membrane vesicles from antigen-presenting cells: Distinct roles for CD54 and B7 molecules, Proc. Natl. Acad. Sci. USA 100 (2003) 6670.

[127] R.E. Hollingsworth, K. Jansen, Turning the corner on therapeutic cancer vaccines, Vaccines 4 (2019) 7.

[128] J. Jou, K.J. Harrington, M.-B. Zocca, E. Ehrnrooth, E.E.W. Cohen, The Changing Landscape of Therapeutic Cancer Vaccines—Novel Platforms and Neoantigen Identification, Clin. Cancer Res. 27 (2021) 689.

[129] N.J. Carter, Multicomponent Meningococcal Serogroup B Vaccine (4CMenB; Bexsero®): A Review of its Use in Primary and Booster Vaccination, BioDrugs 27 (2013) 263–274.

[130] J. Holst, D. Martin, R. Arnold, C.C. Huergo, P. Oster, J. O'Hallahan, E. Rosenqvist, Properties and clinical performance of vaccines containing outer membrane vesicles from Neisseria meningitidis, Vaccine 27 (2009) B3–B12.

[131] S. Bhatnagar, K. Shinagawa, F.J. Castellino, J.S. Schorey, Exosomes released from macrophages infected with intracellular pathogens stimulate a proinflammatory response in vitro and in vivo, Blood 110 (2007) 3234–3244.

[132] L. Martin-Jaular, E.S. Nakayasu, M. Ferrer, I.C. Almeida, H.A. del Portillo, Exosomes from Plasmodium yoelii-Infected Reticulocytes Protect Mice from Lethal Infections, PLOS ONE 6 (2011) e26588.

[133] P.P. Singh, V.L. Smith, P.C. Karakousis, J.S. Schorey, Exosomes Isolated from Mycobacteria-Infected Mice or Cultured Macrophages Can Recruit and Activate Immune Cells In Vitro and In Vivo, J. Immunol. 189 (2012) 777.

[134] M. Mehanny, C.-M. Lehr, G. Fuhrmann, Extracellular vesicles as antigen carriers for novel vaccination avenues, Adv. Drug Deliv. Rev. 173 (2021) 164–180.

[135] L. Kordelas, V. Rebmann, A.K. Ludwig, S. Radtke, J. Ruesing, T.R. Doeppner, M. Epple, P.A. Horn, D.W. Beelen, B. Giebel, MSC-derived exosomes: a novel tool to treat therapy-refractory graft-versus-host disease, Leukemia 28 (2014) 970–973.

[136] S. Keshtkar, N. Azarpira, M.H. Ghahremani, Mesenchymal stem cell-derived extracellular vesicles: novel frontiers in regenerative medicine, Stem Cell Res. Ther. 9 (2018) 63.

[137] K.-S. Park, E. Bandeira, G.V. Shelke, C. Lässer, J. Lötvall, Enhancement of therapeutic potential of mesenchymal stem cell-derived extracellular vesicles, Stem Cell Res. Ther. 10 (2019) 288.

[138] C.J. Batty, M.T. Heise, E.M. Bachelder, K.M. Ainslie, Vaccine formulations in clinical development for the prevention of severe acute respiratory syndrome coronavirus 2 infection, Adv. Drug Deliv. Rev. 169 (2021) 168–189.

[139] B. Sabanovic, F. Piva, M. Cecati, M. Giulietti, Promising Extracellular Vesicle-Based Vaccines against Viruses, Including SARS-CoV-2, Biology 10 (2021) 94.

[140] S.-J. Tsai, C. Guo, N.A. Atai, S.J. Gould, Exosome-Mediated mRNA Delivery For SARS-CoV-2 Vaccination, bioRxiv, 2020, 2020.2011.2006.371419.

[141] K. Polak, N. Greze, M. Lachat, D. Merle, S. Chiumento, C. Bertrand-Gaday, B. Trentin, R.Z. Mamoun, Extracellular vesicle-based vaccine platform displaying native viral envelope proteins elicits a robust anti-SARS-CoV-2 response in mice, bioRxiv, 2020, 2020.2010.2028.357137.

[142] S. Gurunathan, M.-H. Kang, M. Jeyaraj, M. Qasim, J.-H. Kim, Review of the Isolation, Characterization, Biological Function, and Multifarious Therapeutic Approaches of Exosomes, Cells 8 (2019).

[143] T. Yamashita, Y. Takahashi, Y. Takakura, Possibility of Exosome-Based Therapeutics and Challenges in Production of Exosomes Eligible for Therapeutic Application, Biol. Pharm. Bull. 41 (2018) 835–842.

[144] J. Wang, E.E. Bonacquisti, A.D. Brown, J. Nguyen, Boosting the Biogenesis and Secretion of Mesenchymal Stem Cell-Derived Exosomes, Cells 9 (2020).

[145] E.V. Batrakova, M.S. Kim, Development and regulation of exosome-based therapy products, Wiley Interdiscip. Rev. Nanomed. Nanobiotechnol. 8 (2016) 744–757.

[146] E. Hanna, C. Rémuzat, P. Auquier, M. Toumi, Advanced therapy medicinal products: current and future perspectives, J. Mark. Access Health Policy 4 (2016) 31036.

[147] T. Fulop, G.T. Kozma, I. Vashegyi, T. Meszaros, L. Rosivall, R. Urbanics, G. Storm, J.M. Metselaar, J. Szebeni, Liposome-induced hypersensitivity reactions: Risk reduction by design of safe infusion protocols in pigs, J. Control. Release 309 (2019) 333–338.

[148] J. Szebeni, P. Bedocs, D. Csukas, L. Rosivall, R. Bunger, R. Urbanics, A porcine model of complement-mediated infusion reactions to drug carrier nanosystems and other medicines, Adv. Drug Deliv. Rev. 64 (2012) 1706–1716.

[149] J. Szebeni, P. Bedocs, Z. Rozsnyay, Z. Weiszhar, R. Urbanics, L. Rosivall, R. Cohen, O. Garbuzenko, G. Bathori, M. Toth, R. Bunger, Y. Barenholz, Liposome-induced complement activation and related cardiopulmonary distress in pigs: factors promoting reactogenicity of Doxil and Am Bisome, Nanomedicine 8 (2012) 176–184.

[150] S. Soares, J. Sousa, A. Pais, C. Vitorino, Nanomedicine: Principles, Properties, and Regulatory Issues, Front. Chem. 6 (2018) 360.

[151] M. Villa Nova, C. Janas, M. Schmidt, T. Ulshoefer, S. Grafe, S. Schiffmann, N. de Bruin, A. Wiehe, V. Albrecht, M.J. Parnham, M. Luciano Bruschi, M.G. Wacker, Nanocarriers for photodynamic therapy-rational formulation design and medium-scale manufacture, Int. J. Pharm. 491 (2015) 250–260.

[152] C. Janas, Z. Mostaphaoui, L. Schmiederer, J. Bauer, M.G. Wacker, Novel polymeric micelles for drug delivery: Material characterization and formulation screening, Int. J. Pharm. 509 (2016) 197–207.

[153] T. Miller, R. Rachel, A. Besheer, S. Uezguen, M. Weigandt, A. Goepferich, Comparative investigations on in vitro serum stability of polymeric micelle formulations, Pharm. Res. 29 (2012) 448–459.

[154] D. Bachurski, M. Schuldner, P.-H. Nguyen, A. Malz, K.S. Reiners, P.C. Grenzi, F. Babatz, A.C. Schauss, H.P. Hansen, M. Hallek, E. Pogge von Strandmann, Extracellular vesicle measurements with nanoparticle tracking analysis – An accuracy and repeatability comparison between NanoSight NS300 and ZetaView, J. Extracell. Vesicles 8 (2019) 1596016.

[155] R.C. Zieren, L. Dong, P.M. Pierorazio, K.J. Pienta, T.M. de Reijke, S.R. Amend, Extracellular vesicle isolation from human renal cancer tissue, Med. Oncol. 37 (2020) 28.
[156] S.-J. Wang, W.-S. Huang, C.-M. Chuang, C.-H. Chang, T.-W. Lee, G. Ting, M.-H. Chen, P.M.-H. Chang, T.-C. Chao, H.-W. Teng, Y. Chao, Y.-M. Chen, T.-P. Lin, Y.-J. Chang, S.-J. Chen, Y.-R. Huang, K.-L. Lan, A phase 0 study of the pharmacokinetics, biodistribution, and dosimetry of 188Re-liposome in patients with metastatic tumors, EJNMMI Res. 9 (2019) 46.
[157] G. Lopez-Berestein, L. Kasi, M.G. Rosenblum, T. Haynie, M. Jahns, H. Glenn, R. Mehta, G.M. Mavligit, E.M. Hersh, Clinical pharmacology of 99mTc-labeled liposomes in patients with cancer, Cancer Res. 44 (1984) 375–378.
[158] K. Atsushi, N. Kayoko, S. Toshikazu, K. Michiaki, H. Teisuke, H. Shozo, K. Hiroshi, T. Tatsuo, Indium-111-labelled liposomes: dosimetry and tumour detection in patients with cancer, Eur. J. Nucl. Med. 20 (1993) 107–113.
[159] G.M. Jensen, T.H. Bunch, Conventional liposome performance and evaluation: lessons from the development of Vescan, J. Liposome Res. 17 (2007) 121–137.
[160] A. Gabizon, R. Chisin, S. Amselem, S. Druckmann, R. Cohen, D. Goren, I. Fromer, T. Peretz, A. Sulkes, Y. Barenholz, Pharmacokinetic and imaging studies in patients receiving a formulation of liposome-associated adriamycin, Br. J. Cancer 64 (1991) 1125–1132.
[161] H. Lee, A.F. Shields, B.A. Siegel, K.D. Miller, I. Krop, C.X. Ma, P.M. LoRusso, P.N. Munster, K. Campbell, D.F. Gaddy, S.C. Leonard, E. Geretti, S.J. Blocker, D.B. Kirpotin, V. Moyo, T.J. Wickham, B.S. Hendriks, 64Cu-MM-302 Positron Emission Tomography Quantifies Variability of Enhanced Permeability and Retention of Nanoparticles in Relation to Treatment Response in Patients with Metastatic Breast Cancer, Clin. Cancer Res. 23 (2017) 4190–4202.
[162] F. Man, P.J. Gawne, R.T.M. de Rosales, Nuclear imaging of liposomal drug delivery systems: A critical review of radiolabelling methods and applications in nanomedicine, Adv. Drug Deliv. Rev. 143 (2019) 134–160.
[163] R. Münter, K. Kristensen, D. Pedersbæk, J.B. Larsen, J.B. Simonsen, T.L. Andresen, Dissociation of fluorescently labeled lipids from liposomes in biological environments challenges the interpretation of uptake studies, Nanoscale 10 (2018) 22720–22724.
[164] I. Bekersky, R.M. Fielding, D.E. Dressler, J.W. Lee, D.N. Buell, T.J. Walsh, Pharmacokinetics, excretion, and mass balance of liposomal amphotericin B (AmBisome) and amphotericin B deoxycholate in humans, Antimicrob. Agents Chemother. 46 (2002) 828–833.
[165] S. Bhowmik, S. Bhowmick, K. Maiti, A. Chakra, P. Shahi, D. Jain, T. Rajamannar, Two multicenter Phase I randomized trials to compare the bioequivalence and safety of a generic doxorubicin hydrochloride liposome injection with Doxil(®) or Caelyx(®) in advanced ovarian cancer, Cancer Chemother. Pharmacol. 82 (2018) 521–532.
[166] K. Mross, B. Niemann, U. Massing, J. Drevs, C. Unger, R. Bhamra, C.E. Swenson, Pharmacokinetics of liposomal doxorubicin (TLC-D99; Myocet) in patients with solid tumors: an open-label, single-dose study, Cancer Chemother. Pharmacol. 54 (2004) 514–524.
[167] T. Kovshova, N. Osipova, A. Alekseeva, J. Malinovskaya, A. Belov, A. Budko, G. Pavlova, O. Maksimenko, S. Nagpal, S. Braner, H. Modh, V. Balabanyan, M.G. Wacker, S. Gelperina, Exploring the Interplay between Drug Release and Targeting of Lipid-Like Polymer Nanoparticles Loaded with Doxorubicin, Molecules 26 (2021).
[168] D.C. Litzinger, A.M.J. Buiting, N. van Rooijen, L. Huang, Effect of liposome size on the circulation time and intraorgan distribution of amphipathic poly (ethylene glycol)-containing liposomes, Biochim. Biophys. Acta 1190 (1994) 99–107.
[169] Z. Popović, W. Liu, V.P. Chauhan, J. Lee, C. Wong, A.B. Greytak, N. Insin, D. G. Nocera, D. Fukumura, R.K. Jain, M.G. Bawendi, A nanoparticle size series for in vivo fluorescence imaging, Angew. Chem. Int. Ed. 49 (2010) 8649–8652.
[170] S.D. Perrault, C. Walkey, T. Jennings, H.C. Fischer, W.C. Chan, Mediating tumor targeting efficiency of nanoparticles through design, Nano Lett. 9 (2009) 1909–1915.
[171] D. Docter, C. Bantz, D. Westmeier, H.J. Galla, Q. Wang, J.C. Kirkpatrick, P. Nielsen, M. Maskos, R.H. Stauber, The protein corona protects against size- and dose-dependent toxicity of amorphous silica nanoparticles, Beilstein J. Nanotechnol. 5 (2014) 1380–1392.
[172] K. Partikel, R. Korte, D. Mulac, H.-U. Humpf, K. Langer, Serum type and concentration both affect the protein-corona composition of PLGA nanoparticles, Beilstein J. Nanotechnol. 10 (2019) 1002–1015.
[173] C.M. Wallenwein, M.V. Nova, C. Janas, L. Jablonka, G.F. Gao, M. Thurn, V. Albrecht, A. Wiehe, M.G. Wacker, A dialysis-based in vitro drug release assay to study dynamics of the drug-protein transfer of temoporfin liposomes, Eur. J. Pharm. Biopharm. 143 (2019) 44–50.
[174] M.G. Wacker, A. Proykova, G.M.L. Santos, Dealing with nanosafety around the globe-Regulation vs. innovation, Int. J. Pharm. 509 (2016) 95–106.
[175] J. Austin, D. Fernandes, M.J.A. Ruszala, N. Hill, J. Corbett, Routine, ensemble characterisation of electrophoretic mobility in high and saturated ionic dispersions, Sci. Rep. 10 (2020) 4628.
[176] M. Wacker, A. Zensi, J. Kufleitner, A. Ruff, J. Schutz, T. Stockburger, T. Marstaller, V. Vogel, A toolbox for the upscaling of ethanolic human serum albumin (HSA) desolvation, Int. J. Pharm. 414 (2011) 225–232.
[177] W. Zhao, S. Zhuang, X.-R. Qi, Comparative study of the in vitro and in vivo characteristics of cationic and neutral liposomes, Int. J. Nanomed. 6 (2011) 3087–3098.
[178] H. Xie, P. Svenmarker, J. Axelsson, S. Gräfe, M. Kyriazi, N. Bendsoe, S. Andersson-Engels, K. Svanberg, Pharmacokinetic and biodistribution study following systemic administration of Fospeg®–a Pegylated liposomal mTHPC formulation in a murine model, J. Biophotonics 8 (2015) 142–152.
[179] F.M. van der Valk, D.F. van Wijk, M.E. Lobatto, H.J. Verberne, G. Storm, M.C.M. Willems, D.A. Legemate, A.J. Nederveen, C. Calcagno, V. Mani, S. Ramachandran, M.P.M. Paridaans, M.J. Otten, G.M. Dallinga-Thie, Z.A. Fayad, M. Nieuwdorp, D.M. Schulte, J.M. Metselaar, W.J.M. Mulder, E.S. Stroes, Prednisolone-containing liposomes accumulate in human atherosclerotic macrophages upon intravenous administration, Nanomedicine 11 (2015) 1039–1046.
[180] M.E. Lobatto, C. Calcagno, M.J. Otten, A. Millon, S. Ramachandran, M.P.M. Paridaans, F.M. van der Valk, G. Storm, E.S.G. Stroes, Z.A. Fayad, W.J.M. Mulder, J.M. Metselaar, Pharmaceutical development and preclinical evaluation of a GMP-grade anti-inflammatory nanotherapy, Nanomedicine 11 (2015) 1133–1140.
[181] J. Wang, R. Bai, R. Yang, J. Liu, J. Tang, Y. Liu, J. Li, Z. Chai, C. Chen, Size- and surface chemistry-dependent pharmacokinetics and tumor accumulation of engineered gold nanoparticles after intravenous administration, Metallomics 7 (2015) 516–524.
[182] C. Charoenviriyakul, Y. Takahashi, M. Morishita, M. Nishikawa, Y. Takakura, Role of Extracellular Vesicle Surface Proteins in the Pharmacokinetics of Extracellular Vesicles, Mol. Pharm. 15 (2018) 1073–1080.
[183] W.A. Banks, P. Sharma, K.M. Bullock, K.M. Hansen, N. Ludwig, T.L. Whiteside, Transport of Extracellular Vesicles across the Blood-Brain Barrier: Brain Pharmacokinetics and Effects of Inflammation, Int. J. Mol. Sci. 21 (2020) 4407.
[184] A. Gabizon, D. Tzemach, L. Mak, M. Bronstein, A.T. Horowitz, Dose Dependency of Pharmacokinetics and Therapeutic Efficacy of Pegylated Liposomal Doxorubicin (DOXIL) in Murine Models, J. Drug Target. 10 (2002) 539–548.
[185] K.D. Fugit, T.X. Xiang, H. Choi du, S. Kangarlou, E. Csuhai, P.M. Bummer, B.D. Anderson, Mechanistic model and analysis of doxorubicin release from liposomal formulations, J. Control. Release 217 (2015) 82–91.
[186] M. Anderson, A. Omri, The Effect of Different Lipid Components on the In Vitro Stability and Release Kinetics of Liposome Formulations, Drug Deliv. 11 (2004) 33–39.
[187] S. Leekumjorn, A.K. Sum, Molecular studies of the gel to liquid-crystalline phase transition for fully hydrated DPPC and DPPE bilayers, Biochim. Biophys. Acta Biomembr. 1768 (2007) 354–365.
[188] X. Wei, D. Shamrakov, S. Nudelman, S. Peretz-Damari, E. Nativ-Roth, O. Regev, Y. Barenholz, Cardinal Role of Intraliposome Doxorubicin-Sulfate Nanorod Crystal in Doxil Properties and Performance, ACS Omega 3 (2018) 2508–2517.
[189] Y. Barenholz, Doxil(R)–the first FDA-approved nano-drug: lessons learned, J. Control. Release 160 (2012) 117–134.
[190] D.D. Lasic, P.M. Frederik, M.C. Stuart, Y. Barenholz, T.J. McIntosh, Gelation of liposome interior. A novel method for drug encapsulation, FEBS Lett. 312 (1992) 255–258.
[191] W.J. Goh, C.K. Lee, S. Zou, E.C. Woon, B. Czarny, G. Pastorin, Doxorubicin-loaded cell-derived nanovesicles: an alternative targeted approach for anti-tumor therapy, Int. J. Nanomed. 12 (2017) 2759–2767.
[192] P.D. Schmitt, N.S. Trasi, L.S. Taylor, G.J. Simpson, Finding the Needle in the Haystack: Characterization of Trace Crystallinity in a Commercial Formulation of Paclitaxel Protein-Bound Particles by Raman Spectroscopy Enabled by Second Harmonic Generation Microscopy, Mol. Pharm. 12 (2015) 2378–2383.
[193] Y. Schilt, T. Berman, X. Wei, Y. Barenholz, U. Raviv, Using solution X-ray scattering to determine the high-resolution structure and morphology of PEGylated liposomal doxorubicin nanodrugs, Biochim. Biophys. Acta 2016 (1860) 108–119.
[194] X. Shuai, H. Ai, N. Nasongkla, S. Kim, J. Gao, Micellar carriers based on block copolymers of poly(epsilon-caprolactone) and poly(ethylene glycol) for doxorubicin delivery, J. Control. Release 98 (2004) 415–426.
[195] X. Wei, R. Cohen, Y. Barenholz, Insights into composition/structure/function relationships of Doxil® gained from "high-sensitivity" differential scanning calorimetry, Eur. J. Pharm. Biopharm. 104 (2016) 260–270.
[196] M. Bakonyi, S. Berkó, M. Budai-Szűcs, A. Kovács, E. Csányi, DSC for evaluating the encapsulation efficiency of lidocaine-loaded liposomes compared to the ultracentrifugation method, J. Therm. Anal. Calorim. 130 (2017) 1619–1625.
[197] O. Maksimenko, J. Malinovskaya, E. Shipulo, N. Osipova, V. Razzhivina, D. Arantseva, O. Yarovaya, U. Mostovaya, A. Khalansky, V. Fedoseeva, A. Alekseeva, L. Vanchugova, M. Gorshkova, E. Kovalenko, V. Balabanyan, P. Melnikov, V. Baklaushev, V. Chekhonin, J. Kreuter, S. Gelperina, Doxorubicin-loaded PLGA nanoparticles for the chemotherapy of glioblastoma: Towards the pharmaceutical development, Int. J. Pharm. 572 (2019) 118733.
[198] E. Pereverzeva, I. Treschalin, M. Treschalin, D. Arantseva, Y. Ermolenko, N. Kumskova, O. Maksimenko, V. Balabanyan, J. Kreuter, S. Gelperina, Toxicological study of doxorubicin-loaded PLGA nanoparticles for the treatment of glioblastoma, Int. J. Pharm. 554 (2019) 161–178.
[199] O. Filon, P. Krivorotko, G. Kobyakov, V. Razjivina, O. Maximenko, S. Gelperina, J. Kreuter, A phase I study of safety and pharmacokinetics of NanoBB-1-Dox in patients with advanced solid tumors, J. Clin. Oncol. 35 (2017), e13537.
[200] M.G. Wacker, Frontiers in pharmaceutical nanotechnology, Beilstein J. Nanotechnol. 10 (2019) 2538–2540.
[201] P. Zou, K. Tyner, A. Raw, S. Lee, Physicochemical Characterization of Iron Carbohydrate Colloid Drug Products, AAPS J. 19 (2017) 1359–1376.
[202] S. Futterer, I. Andrusenko, U. Kolb, W. Hofmeister, P. Langguth, Structural characterization of iron oxide/hydroxide nanoparticles in nine different

parenteral drugs for the treatment of iron deficiency anaemia by electron diffraction (ED) and X-ray powder diffraction (XRPD), J. Pharm. Biomed. Anal. 86 (2013) 151–160.
[203] M. Szybowicz, M. Koralewski, J. Karoń, L. Melnikova, Micro-Raman Spectroscopy of Natural and Synthetic Ferritins and Their Mimetics, Acta Phys. Pol. A 127 (2015) 534–536.
[204] L. Nothnagel, M.G. Wacker, How to measure release from nanosized carriers?, Eur J. Pharm. Sci. 120 (2018) 199–211.
[205] C.A. Bergstrom, R. Holm, S.A. Jorgensen, S.B. Andersson, P. Artursson, S. Beato, A. Borde, K. Box, M. Brewster, J. Dressman, K.I. Feng, G. Halbert, E. Kostewicz, M. McAllister, U. Muenster, J. Thinnes, R. Taylor, A. Mullertz, Early pharmaceutical profiling to predict oral drug absorption: current status and unmet needs, Eur. J. Pharm. Sci. 57 (2014) 173–199.
[206] E.S. Kostewicz, B. Abrahamsson, M. Brewster, J. Brouwers, J. Butler, S. Carlert, P.A. Dickinson, J. Dressman, R. Holm, S. Klein, J. Mann, M. McAllister, M. Minekus, U. Muenster, A. Mullertz, M. Verwei, M. Vertzoni, W. Weitschies, P. Augustijns, In vitro models for the prediction of in vivo performance of oral dosage forms, Eur. J. Pharm. Sci. 57 (2014) 342–366.
[207] C. Li, X. Li, S. Li, Y. Weng, K. Wang, T. Zhang, S. Chen, X. Lu, Y. Jiang, J. Xu, X. Liang, Development and Validation of a Method for Determination of Encapsulation Efficiency of CPT-11/DSPE-mPEG2000 Nanoparticles, Med. Chem. (Los Angeles) 6 (5) (2016) 345–348.
[208] S. Daneshmand, S. Golmohammadzadeh, M.R. Jaafari, J. Movaffagh, M. Rezaee, A. Sahebkar, B. Malaekeh-Nikouei, Encapsulation challenges, the substantial issue in solid lipid nanoparticles characterization, J. Cell. Biochem. 119 (2018) 4251–4264.
[209] K.D. Fugit, A. Jyoti, M. Upreti, B.D. Anderson, Insights into accelerated liposomal release of topotecan in plasma monitored by a non-invasive fluorescence spectroscopic method, J. Control. Release 197 (2015) 10–19.
[210] A. Guillot, A.-C. Couffin, X. Sejean, F. Navarro, M. Limberger, C.-M. Lehr, Solid Phase Extraction as an Innovative Separation Method for Measuring Free and Entrapped Drug in Lipid Nanoparticles, Pharm. Res. 32 (2015) 3999–4009.
[211] K. Maiti, S. Bhowmick, P. Jain, M. Zope, K. Doshi, T. Rajamannar, Comparison of Physicochemical Properties of Generic Doxorubicin HCl Liposome Injection with the Reference Listed Drug, Anti-Cancer Agents Med. Chem. 18 (2018) 597–609.
[212] C. Janas, M.P. Mast, L. Kirsamer, C. Angioni, F. Gao, W. Mantele, J. Dressman, M.G. Wacker, The dispersion releaser technology is an effective method for testing drug release from nanosized drug carriers, Eur. J. Pharm. Biopharm. 115 (2017) 73–83.
[213] F. Jung, L. Nothnagel, F. Gao, M. Thurn, V. Vogel, M.G. Wacker, A comparison of two biorelevant in vitro drug release methods for nanotherapeutics based on advanced physiologically-based pharmacokinetic modelling, Eur. J. Pharm. Biopharm. 127 (2018) 462–470.
[214] F. Jung, M. Thurn, K. Krollik, G.F. Gao, I. Hering, E. Eilebrecht, Y. Emara, M. Weiler, N. Gunday-Tureli, E. Tureli, M.J. Parnham, M.G. Wacker, Predicting the environmental emissions arising from conventional and nanotechnology-related pharmaceutical drug products, Environ. Res. 192 (2020) 110219.
[215] L. Nothnagel, F. Jung, T. Rossmanith, M. Thurn, M. Ashtikar, G. Geisslinger, M. J. Parnham, M.G. Wacker, Predictive PBPK modeling as a tool in the formulation of the drug candidate TMP-001, Eur. J. Pharm. Biopharm. 134 (2019) 144–152.
[216] F. Caputo, D. Mehn, J.D. Clogston, M. Rosslein, A. Prina-Mello, S.E. Borgos, S. Gioria, L. Calzolai, Asymmetric-flow field-flow fractionation for measuring particle size, drug loading and (in)stability of nanopharmaceuticals. The joint view of European Union Nanomedicine Characterization Laboratory and National Cancer Institute - Nanotechnology Characterization Laboratory, J. Chromatogr. A 1635 (2021) 461767.
[217] S. Holzschuh, K. Kaess, A. Fahr, C. Decker, Quantitative In Vitro Assessment of Liposome Stability and Drug Transfer Employing Asymmetrical Flow Field-Flow Fractionation (AF4), Pharm. Res. 33 (2016) 842–855.
[218] F. Quattrini, G. Berrecoso, J. Crecente-Campo, M.J. Alonso, Asymmetric flow field-flow fractionation as a multifunctional technique for the characterization of polymeric nanocarriers, Drug Deliv. Transl. Res. (2021) 373–395.
[219] L. Zeng, L. An, X. Wu, Modeling drug-carrier interaction in the drug release from nanocarriers, J. Drug. Deliv. 2011 (2011), 370308.
[220] J.A. Shabbits, G.N. Chiu, L.D. Mayer, Development of an in vitro drug release assay that accurately predicts in vivo drug retention for liposome-based delivery systems, J. Control. Release 84 (2002) 161–170.
[221] R. Diaz de Leon-Ortega, D.M. D'Arcy, D.A. Lamprou, N. Fotaki, In vitro - in vivo relations for the parenteral liposomal formulation of Amphotericin B: A clinically relevant approach with PBPK modeling, Eur. J. Pharm. Biopharm. (2020).
[222] M.E. Malone, O.I. Corrigan, P.V. Kavanagh, C. Gowing, M. Donnelly, D.M. D'Arcy, Pharmacokinetics of amphotericin B lipid complex in critically ill patients undergoing continuous venovenous haemodiafiltration, Int. J. Antimicrob. Agents 42 (2013) 335–342.
[223] J. Emami, In vitro - in vivo correlation: from theory to applications, J. Pharm. Pharm. Sci. 9 (2006) 169–189.
[224] C. Stillhart, X. Pepin, C. Tistaert, D. Good, B. van den, N. Parrott, F. Kesisoglou, PBPK Absorption Modeling: Establishing the In Vitro-In Vivo Link-Industry Perspective, AAPS J. 21 (2019) 19.
[225] J.A.A. Reijers, M.J.C. Dane, A.J. van Zonneveld, J. Burggraaf, M. Moerland, Potential Influence of Endothelial Adsorption on the Delayed Time to Maximum Concentration of Biopharmaceuticals, Eur. J. Drug Metab. Pharmacokinet. 43 (2018) 103–113.
[226] M. Li, P. Zou, K. Tyner, S. Lee, Physiologically Based Pharmacokinetic (PBPK) Modeling of Pharmaceutical Nanoparticles, AAPS J. 19 (2017) 26–42.
[227] H. Jones, K. Rowland-Yeo, Basic concepts in physiologically based pharmacokinetic modeling in drug discovery and development, CPT Pharmacometr. Syst. Pharmacol. 2 (8) (2013) 1–12, https://doi.org/10.1038/psp.2013.41.
[228] US-FDA, Draft Guidance for Industry: The Use of Physiologically Based Pharmacokinetic Analyses — Biopharmaceutics Applications for Oral Drug Product Development, Manufacturing Changes, and Controls, 2020.
[229] T. Heimbach, S. Suarez-Sharp, M. Kakhi, N. Holmstock, A. Olivares-Morales, X. Pepin, E. Sjögren, E. Tsakalozou, P. Seo, M. Li, X. Zhang, H.P. Lin, T. Montague, A. Mitra, D. Morris, N. Patel, F. Kesisoglou, Dissolution and Translational Modeling Strategies Toward Establishing an In Vitro-In Vivo Link-a Workshop Summary Report, AAPS J. 21 (2019) 29.
[230] EMA, Guideline on the reporting of physiologically based pharmacokinetic (PBPK) modelling and simulation, 2018.
[231] K. McNally, R. Cotton, G.D. Loizou, A Workflow for Global Sensitivity Analysis of PBPK Models, Front. Pharmacol. 2 (2011), 31–31.
[232] R.D. Arnold, D.E. Mager, J.E. Slack, R.M. Straubinger, Effect of repetitive administration of Doxorubicin-containing liposomes on plasma pharmacokinetics and drug biodistribution in a rat brain tumor model, Clin. Cancer Res. 11 (2005) 8856–8865.
[233] E.T. Dams, P. Laverman, W.J. Oyen, G. Storm, G.L. Scherphof, J.W. van Der Meer, F.H. Corstens, O.C. Boerman, Accelerated blood clearance and altered biodistribution of repeated injections of sterically stabilized liposomes, J. Pharmacol. Exp. Ther. 292 (2000) 1071–1079.
[234] O. Lyass, B. Uziely, R. Ben-Yosef, D. Tzemach, N.I. Heshing, M. Lotem, G. Brufman, A. Gabizon, Correlation of toxicity with pharmacokinetics of pegylated liposomal doxorubicin (Doxil) in metastatic breast carcinoma, Cancer 89 (2000) 1037–1047.
[235] A. Gabizon, H. Shmeeda, Y. Barenholz, Pharmacokinetics of pegylated liposomal Doxorubicin: review of animal and human studies, Clin. Pharmacokinet. 42 (2003) 419–436.
[236] A. Gabizon, R. Isacson, O. Rosengarten, D. Tzemach, H. Shmeeda, R. Sapir, An open-label study to evaluate dose and cycle dependence of the pharmacokinetics of pegylated liposomal doxorubicin, Cancer Chemother. Pharmacol. 61 (2008) 695–702.
[237] L.H. Wang, R.M. Fielding, P.C. Smith, L.S.S. Guo, Comparative Tissue Distribution and Elimination of Amphotericin B Colloidal Dispersion (Amphocil®) and Fungizone® After Repeated Dosing in Rats, Pharm. Res. 12 (1995) 275–283.
[238] R.M. Fielding, A.W. Singer, L.H. Wang, S. Babbar, L.S. Guo, Relationship of pharmacokinetics and drug distribution in tissue to increased safety of amphotericin B colloidal dispersion in dogs, Antimicrob. Agents Chemother. 36 (1992) 299–307.
[239] E. Fecioru, M. Klein, J. Kramer, M.G. Wacker, In Vitro Performance Testing of Nanoparticulate Drug Products for Parenteral Administration, Dissolut. Technol. 26 (2019) 28–37.
[240] Wacker M.G., Lu X., Burke M., Nir I., Fahmy R., Zaidi K., Testing the In-Vitro Product Performance of Nanomaterial-Based Drug Products: View of the USP Expert Panel, Pharmacop. Forum 47(6), (Accepted for public consultation).
[241] M. Dunne, J. Zheng, J. Rosenblat, D.A. Jaffray, C. Allen, APN/CD13-targeting as a strategy to alter the tumor accumulation of liposomes, J. Control. Release 154 (2011) 298–305.
[242] M. Shebley, P. Sandhu, A. Emami Riedmaier, M. Jamei, R. Narayanan, A. Patel, S.A. Peters, V.P. Reddy, M. Zheng, L. Zwart, M. Beneton, F. Bouzom, J. Chen, Y. Chen, Y. Cleary, C. Collins, G.L. Dickinson, N. Djebli, H.J. Einolf, I. Gardner, F. Huth, F. Kazmi, F. Khalil, J. Lin, A. Odinecs, C. Patel, H. Rong, E. Schuck, P. Sharma, S.-P. Wu, Y. Xu, S. Yamazaki, K. Yoshida, M. Rowland, Physiologically Based Pharmacokinetic Model Qualification and Reporting Procedures for Regulatory Submissions: A Consortium Perspective, Clin. Pharm. Ther. 104 (2018) 88–110.
[243] S.-C. Chow, Bioavailability and Bioequivalence in Drug Development, Wiley Interdiscip. Rev. Comput. Stat. 6 (2014) 304–312.
[244] P. Poulin, F.-P. Theil, Development of a novel method for predicting human volume of distribution at steady-state of basic drugs and comparative assessment with existing methods, J. Pharm. Sci. 98 (2009) 4941–4961.

pharmaceutics

MDPI

Article

An Update to Dialysis-Based Drug Release Testing—Data Analysis and Validation Using the Pharma Test Dispersion Releaser

Marc-Phillip Mast [1,2], Harshvardhan Modh [3], Julian Knoll [2], Elena Fecioru [4] and Matthias G. Wacker [3,*]

[1] Fraunhofer Institute for Translational Medicine and Pharmacology ITMP, Theodor-Stern-Kai 7, 60596 Frankfurt am Main, Germany; mast@em.uni-frankfurt.de
[2] Goethe University, Max-von-Laue-Straße 9, 60438 Frankfurt am Main, Germany; J-Knoll@outlook.com
[3] Department of Pharmacy, Faculty of Science, National University of Singapore, 4 Science Drive 2, Singapore 117544, Singapore; phahbm@nus.edu.sg
[4] Eurofins PHAST Development GmbH & Co. KG, Byk-Gulden-Straße 2, 78467 Konstanz, Germany; elena.fecioru@phast.com
* Correspondence: matthias.g.wacker@nus.edu.sg; Tel.: +65-65161133

Abstract: Currently, a wide variety of complex non-oral dosage forms are entering the global healthcare market. Although many assays have been described in recent research, harmonized procedures and standards for testing their in vitro performance remain widely unexplored. Among others, dialysis-based techniques such as the Pharma Test Dispersion Releaser are developed for testing the release of drugs from nanoparticles, liposomes, or extracellular vesicle preparations. Here, we provide advanced strategies and practical advice for the development and validation of dialysis-based techniques, including documentation, analysis, and interpretation of the raw data. For this purpose, key parameters of the release assay, including the hydrodynamics in the device at different stirring rates, the selectivity for particles and molecules, as well as the effect of excipients on drug permeation were investigated. At the highest stirring rate, a more than twofold increase in the membrane permeation rate (from 0.99×10^{-3} to 2.17×10^{-3} cm^2/h) was observed. Additionally, we designed a novel computer model to identify important quality parameters of the dialysis experiment and to calculate error-corrected release profiles. Two hydrophilic creams of diclofenac, Voltaren® Emulgel, and Olfen® gel, were tested and provide first-hand evidence of the robustness of the assay in the presence of semisolid dosage forms.

Keywords: nanomedicine; release testing; dialysis; semisolids; validation; liposomes; semisolids; creams; topical formulations; dissolution; drug release

Citation: Mast, M.-P.; Modh, H.; Knoll, J.; Fecioru, E.; Wacker, M.G. An Update to Dialysis-Based Drug Release Testing—Data Analysis and Validation Using the Pharma Test Dispersion Releaser. *Pharmaceutics* **2021**, *13*, 2007. https://doi.org/10.3390/pharmaceutics13122007

Academic Editors: Lenuța Maria Șuta and Claudia Geanina Watz

Received: 10 November 2021
Accepted: 22 November 2021
Published: 25 November 2021

1. Introduction

For the past decades, drug products comprising fine dispersions of particles have gained a significant market share globally [1–3]. Microparticle and nanoparticle drug products are being used by the pharmaceutical industry and changed the requirements in performance testing. Among others, nanomaterial-based formulations are applied in per-oral [4,5], parenteral [3], and topical drug delivery [6–8]. Recent examples include delivery systems of proteins or peptides, the Sars-Cov-2 mRNA vaccines, as well as extracellular vesicle (EV) preparations [3]. Additionally, a considerable number of conventional dosage forms such as ointments, creams, or gels challenge the compendial drug release assays. These preparations are tested using the Vertical Diffusion Cell, the Immersion Cell, or the Flow-Through Cell described by the United States Pharmacopeia (USP). All these methods are characterized by the formation of a static layer of the dosage form perfused by a limited amount of release medium. Although some of these methods reflect the physiology of the administration route to a certain extent, the instruments provide the operator with

very limited control over the release process. This makes it more difficult to apply these compendial release assays in quality control or drug development.

To date, there are several dialysis-based quality control methods established that enable a highly selective separation of fine particles from the release medium [9]. Among others, the Float-A-Lyzer® (Repligen, Waltham, MA, USA) in combination with USP dissolution apparatus I/II, the USP apparatus IV Dialysis Adapter (Sotax AG, Aesch, Switzerland), and the Pharma Test Dispersion Releaser (PTDR) (Pharma Test Apparatebau AG, Hainburg, Germany) have been described. Initially developed by Wacker and Janas at Goethe University [10], the commercial PTDR (Figure 1) is manufactured by Pharma Test Apparatebau AG (Hainburg, Germany). It is used in combination with a USP dissolution apparatus I/II. While the donor compartment is formed by a small cage holding the dialysis membrane (Figure 1), the dissolution vessel represents the acceptor compartment. The donor and acceptor compartments are constantly agitated at a similar rate.

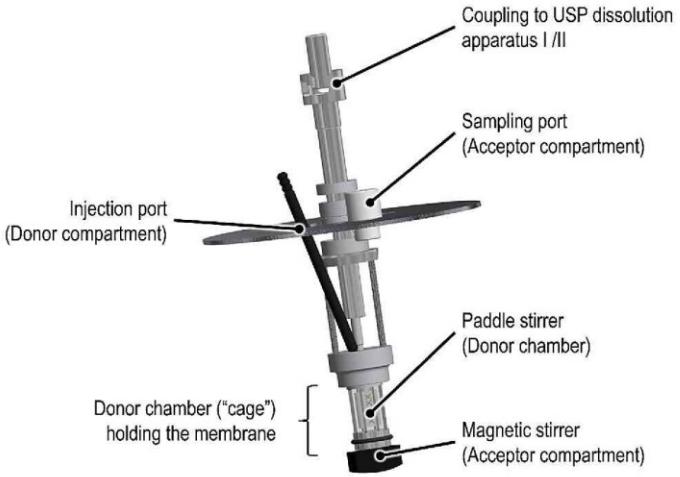

Figure 1. Schematic of the commercial Pharma Test Dispersion Releaser (PTDR).

The instrument was successfully used to investigate the drug release from liposomes [11–13], nanoparticles [5,14,15], microcrystals [16], microspheres [17], and extracellular vesicle (EV) preparations. For many applications, the capability of the assay to predict the in vivo performance was confirmed by correlation of the in vitro and in vivo release rate [3,5,11,12,14,16,17]. In the present work, we emphasize differences in the workflow with regards to parameter selection (e.g., stirring rate, membrane material), reference experiments, data evaluation, and data interpretation, when dialysis-based in vitro release tests are developed [9,18,19].

Dialysis involves two kinetic processes with an impact on the release profile, the release kinetics of the drug substance from the carrier (described by the release rate constant k_{rel}), and the permeation rate through the dialysis membrane (described by the membrane permeation rate constant k_m). Both processes, together with an illustration of their quantification, are presented in Figure 2. In the following, we lay out a recommended practice and provide an overview of the technical operations that confirm the functionality of the PTDR under various conditions. In addition, we outline reference experiments that minimize the expected analytical errors.

To harmonize the treatment of dialysis-based release data, we used the visual programming language Systems Thinking, Experimental Learning Laboratory with Animation

(STELLA) to provide a user-friendly interface for the calculation of the membrane permeation rate constant (k_m) and normalization of the release profiles. The dialysis membrane permeation calculator (DIMEC) and the PTDR Release Normalizer (ReNo) are available under the Creative Commons License.

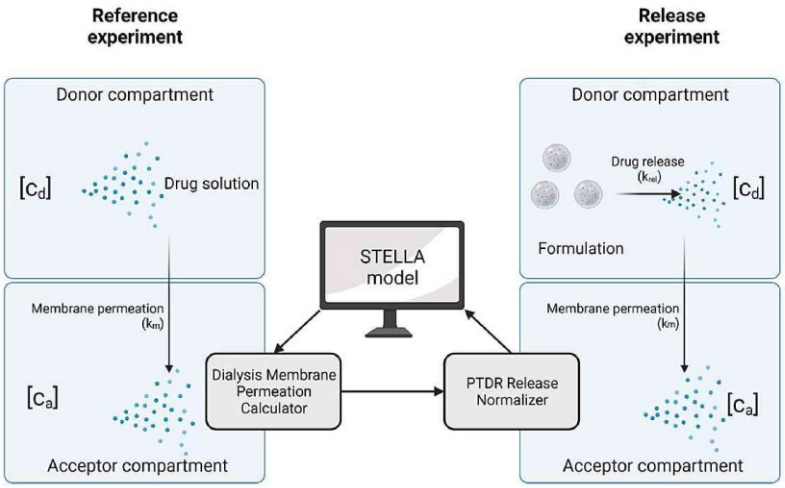

Figure 2. Kinetic processes involved in dialysis. The membrane permeation rate (k_m) is determined in a reference experiment using a drug solution. This membrane permeation rate is later applied in the normalization of the release profile. In this illustration [c_d] represents the drug concentration in the donor compartment and [c_a] the drug concentration in the acceptor compartment. Created with BioRender.com.

2. Materials and Methods

2.1. Chemicals and Materials

Spectra/Por® 6 regenerated cellulose (RC) dialysis membranes with a molecular weight cut-off (MWCO) of 50 kDa and a flat diameter of 28 mm were purchased from VWR International GmbH (Darmstadt, Germany). A stabilized suspension of reactant-free gold nanoparticles with a diameter of 50 nm (Sigma-Aldrich Chemie GmbH, Munich, Germany) in 0.1 mM phosphate-buffered saline (PBS) was used for the membrane leakage test. Diclofenac diethylamine (DEA) salt (Cayman Chemical, Ann Arbor, MI, USA) was purchased from Biomol GmbH (Hamburg, Germany) and diclofenac sodium salt was obtained from Sigma-Aldrich Chemie GmbH (Munich, Germany). Olfen® gel (10 mg/g diclofenac sodium, Mepha Pharma AG, Basel, Switzerland), and Voltaren® Emulgel (11.6 mg/g diclofenac-DEA, GlaxoSmithKline Consumer Healthcare GmbH & Co. KG, Munich, Germany) were obtained from a retail pharmacy. Idebenone was purchased from Rxn Chemicals (Hadapsar, India). All the other chemicals were of analytical grade or equivalent and used as received. An Ultra Clear® system (Evoqua water technologies, Günzburg, Germany) was used for water purification in all the experiments.

2.2. High-Performance Liquid Chromatography

The diclofenac concentrations were quantified using a Chromaster high-performance liquid chromatography (HPLC) system (VWR Hitachi, Tokyo, Japan). An HPLC pump (5160), a column oven (5310), an autosampler (5260), and a UV-Vis detector (5420) were used. The mobile phase consisted of 62% (v/v) of acetonitrile and 38% (v/v) of 0.1% (v/v) of trifluoroacetic acid in ultrapure water. Separation was carried out in a reversed-phase column (Gemini NX-C18, 5 µm, 250 × 4.60 mm, 110 A, Phenomenex Ltd., Aschaffenburg,

Germany). The flow rate was set to 1 mL/min and a temperature of 30 °C was maintained over the run time of 12 min. The detection wavelength was 276 nm [20].

The samples containing bovine serum albumin (BSA) were diluted with the sample solvent comprising 62% (*v*/*v*) of acetonitrile and 38% (*v*/*v*) of 0.01% (*v*/*v*) of trifluoroacetic acid in ultrapure water. They were incubated for 30 min (750 rpm, 16 °C) using a Thermal Shake lite (VWR International GmbH, Darmstadt, Germany). The reduced amount of acid was used to prevent the degradation of the diclofenac. Next, the precipitated protein was removed by centrifugation (14,000× *g* rpm, 15 min, 16 °C) using a Centrifuge 5430× *g* R with an FA-45-30-11 rotor (Eppendorf AG, Hamburg, Germany). The supernatant was transferred into HPLC vials and a volume of 40 µL was injected into the HPLC system. The samples without proteins were diluted similarly and a volume of 40 µL was injected without further treatment. The linearity was demonstrated in a concentration range from 0.12–30 µg/mL for both the diclofenac salts. The limit of detection (LOD) and limit of quantitation (LOQ) were determined to be 24 and 80 ng/mL, respectively.

2.3. Size Exclusion Chromatography

The BSA was quantified using a Chromaster HPLC system (VWR Hitachi, Tokyo, Japan) equipped with a pump (5160), an autosampler (5260), a column oven (5310), and a UV-Vis detector module (5420). The flow rate was set to 0.9 mL/min and a detection wavelength of 280 nm was used. The column temperature was adjusted to 25 °C. A PBS solution (pH 6.8, 0.25% sodium azide) was used as the mobile phase. A volume of 50 µL was injected into the HPLC system. For this separation, a Yarra SEC-3000 column (3 µm, 300 × 7.8 mm, 200 A, Phenomenex Ltd., Aschaffenburg, Germany) was used. Linearity was demonstrated in a range from 20–500 µg/mL.

2.4. Drug Solubility

The solubilities of diclofenac-DEA and diclofenac sodium were determined in different media with a modified shake-flask method. A volume of 4 mL of each medium was filled into glass vials with an excess of the drug substance. The vials were incubated at 37 °C (INCU-Line® Standard IL 68 R, VWR International GmbH, Darmstadt, Germany) for 24 h under constant stirring with a multi-position magnetic stirrer (Cimarec™ Poly 15, Fisher Scientific GmbH, Schwerte, Germany) at 550 rpm. After 24 h, the solid excess was separated with a polytetrafluoroethylene (PTFE) syringe filter (13 mm diameter, 0.45 µm pore size, VWR International GmbH, Darmstadt, Germany). The filtrates were diluted and analyzed by HPLC (see Section 2.2). The PTFE filters were saturated with 1 mL of drug suspension before the samples were collected. These solubility experiments were carried out at 32 °C and all the experiments were performed in triplicates.

2.5. Technical Operations

All the experiments were carried out with a commercial PTDR system (Pharma Test Apparatebau AG, Hainburg, Germany) in a PTWS 120 S dissolution apparatus II (Pharma Test Apparatebau AG, Hainburg, Germany) following the specifications of the USP. A mini-vessel (250 mL) following the specifications of the Chinese Pharmacopeia [21] was used as the acceptor compartment. The vessels were filled with 120 mL of filtered and degassed (40 °C, 300 mbar, 30 min) medium. The membrane was pre-treated according to the instructions of the manufacturer, mounted around the donor chamber, and sealed with two O-rings. The volume added to the donor compartment was 3.4 mL, leading to a total volume of 123.4 mL in the final setup. The sampling volume, time points, temperature, and stirring rates are described in the later sections of this article. The donor chamber featured a surface area of 10.95 cm^2. The thickness of the RC membrane was 0.0065 cm.

2.5.1. Membrane Leakage Test Using Gold Nanoparticles

The PTDR setup is commonly used for testing the drug release from fine particles or vesicles. The membrane leakage test evaluates the retention of the particle population

of interest by the membrane. Gold nanoparticles with a diameter of 50 nm were used as a standard. A volume of 3.4 mL of the liquid dispersion was injected into the donor chamber which was sealed by an RC membrane (50 kDa). PBS (0.1 mM) was filled into each mini-vessel and samples with a volume of 1 mL were collected after 1, 2, 4, 8, and 24 h. After 24 h, the RC membrane was punctured with a scalpel blade and, after 30 min, a 1 mL sample was collected. Additionally, one negative control (a setup without the addition of gold nanoparticles into the donor chamber) and one positive control (a setup with the membrane being punctured at the beginning of the experiment) were tested. The samples were analyzed using a Zetasizer Nano ZS (Malvern Instruments GmbH, Herrenberg, Germany). Additionally, the particle concentration was measured at a wavelength of 535 nm in a UV-Vis spectrophotometer (U-3000 Spectrophotometer, Hitachi, Tokyo, Japan). The dissolution apparatus operated at 37 ± 0.5 °C and 100 rpm.

Before quantification by UV-Vis spectroscopy, a wavelength scan was performed in a range from 300–700 nm at a rate of 300 nm/min, and linearity was confirmed for the expected concentration range. To use the Zetasizer Nano ZS to determine gold nanoparticles quantitatively, the derived photon count rate was used. For monodispersed nanoparticles smaller than the laser wavelength (633 nm), the intensity of the scattered light I is proportional to the concentration of the nanoparticles in the sample [22,23]. This mathematical relationship is described by the Rayleigh equation (Equation (1)):

$$I = I_0 \cdot \alpha \cdot \frac{m^2 - 1}{m^2 + 2} \cdot d^6 \cdot c \quad (1)$$

where I_0 is the incident light intensity, α is an instrument coefficient, m is the refractive index, d is the particle diameter, and c is the particle concentration. The instrument measures the derived photon count rates, which are a surrogate for the scattered light intensity. It can be used to estimate the particle concentration. The measurements were conducted in triplicate at a fixed position in the center of the cuvette using the parameter summarized in Table 1. Before each measurement, the temperature was equilibrated for 120 s to 25.0 °C. Linearity was confirmed in the expected range of dilution.

Table 1. Parameters used for the DLS measurement.

Parameter	Description	Value
Refractive index	Gold nanoparticles	0.200
Absorbance	Gold nanoparticles	3.320
Dispersant temperature	Water	25.0 °C
Refractive index of the dispersant	Water	1.330
Viscosity of the dispersant	Water	0.8872
Measurement angle	Backscatter	173°
Positioning method	Fixed position	4.65
Repeated measurements	-	3

These parameters are commonly used by the dynamic light scattering (DLS) system for a concentration-independent calculation of the particle size. However, in the present approach, we used the derived photon count rate to determine particle concentrations. Because of the specifics of these measurements, any reproduction of our findings requires this exact configuration.

2.5.2. Retention of Macromolecules

Dialysis membranes are commonly characterized by their MWCO. This parameter describes the molecular size of a marker molecule retained by the membrane over a defined period. For the RC membrane with an MWCO of 50 kDa, at least 90% of BSA with a molecular weight of 66 kDa is retained over 17 h. Protein retention was therefore used to determine the leakage from the PTDR as well. An amount of 100 mg bovine serum albumin (BSA) in 3.4 mL PBS 7.4 was injected into the donor chamber. The acceptor

compartment was filled with 120 mL PBS 7.4. The dissolution tester was operated at 37 °C and 50 rpm. Samples (0.2 mL) were collected after 1, 2, 3, 4, 6, 17, 20, and 24 h followed by replenishing the volume with fresh medium. The albumin was quantified using size exclusion chromatography (SEC, Section 2.3).

Additionally, a real-time permeation profile was recorded under similar conditions. The albumin was quantified using an online dip probe UV-Vis spectroscopic measurement system (TIDAS L 520 UV-NIR, Pharmatest Apparatebau AG, Hainburg, Germany). The absorption was measured in a range from 200–400 nm every 5000 ms (iteration time) and an average absorption was calculated every 25 s for 24 h. Reference measurements were conducted, and a linear range was observed ranging from 25–500 µg/mL at 277 nm.

2.5.3. Hydrodynamics in the Acceptor Compartment

In the PTDR, the donor and acceptor compartments are stirred at similar rates. The acceptor compartment has a larger volume and efficient mixing is required to accurately detect the release. Therefore, the mixing efficiency in the acceptor compartment was evaluated by adding the dye idebenone to the acceptor compartment and measuring the concentration with the online dip probe UV-Vis spectroscopic measurement system (TIDAS L 520 UV-NIR, Pharmatest Apparatebau AG, Hainburg, Germany). For this experiment, a 2% (*m*/*v*) sodium dodecyl sulfate (SDS) solution was used as the medium. A volume of 120 mL was filled into the acceptor chamber while 3 mL were added to the donor compartment. The online dip probe was aligned parallel to the center of the donor chamber and the measurement was started as soon as 37 ± 0.5 °C was maintained. One measurement was performed every 1000 ms (iteration time), averaging every 5 s in one value. A wavelength range of 200–650 nm was used. The total run time was 15 min. After 30 s, 0.6 mL of a 5 mg/mL idebenone solution in 2% sodium dodecyl sulfate was added to the acceptor compartment. The mixing efficiency was evaluated at stirring rates of 0, 25, 50, and 100 rpm. Linearity for the quantification of idebenone at 283 nm was demonstrated between 0.9–25 µg/mL.

2.5.4. Drug Permeation Studies at Different Stirring Rates

In dialysis, drug permeation studies are important reference experiments when testing drug formulations for their release properties. The permeation experiments were carried out with diclofenac sodium in PBS at 37 °C and stirring rates of 0, 25, 50, and 100 rpm. The acceptor compartment was filled with 120 mL of PBS. An amount of 5 mg of the drug dissolved in a volume of 3.4 mL of PBS was used and injected into the donor compartment. The chamber was sealed by an RC membrane (50 kDa MWCO) and two O-rings. The PTDR was mounted into the USP dissolution apparatus II (Pharma Test Apparatebau AG, Hainburg, Germany). The experiments were conducted at 37 ± 0.5 °C. Samples (0.2 mL) were collected after 0.125, 0.25, 0.5, 1, 2, 3, 4, 5, 6, 7, and 8 h and the volume was replenished with fresh medium. At the end of each experiment, the samples were collected from the donor compartment to ensure that the equilibrium between the donor and acceptor compartments had been reached. The experiments were repeated with 10 mM phosphate buffer pH 7.4 at 32 °C and 50 rpm for normalization (see Section 3.3.5).

Later steps involved modeling the drug distribution between the donor and the acceptor compartment. To validate our model, we determined the drug concentration after 0.25, 0.5, and 2 h at 100 rpm. The samples were analyzed as described in Section 2.2.

2.5.5. Selectivity of the Assay for Specific Size Fractions

The selectivity of the PTDR setup for different molecular sizes enables the retention of molecules bound to proteins in the donor chamber. In a previous investigation, we highlighted the application of dialysis-based separation to distinguish between drug release and the direct transfer of drug molecules from colloids to proteins [13]. To evaluate the separation on a molecular level, the fraction of diclofenac retained by two different concentrations of BSA was tested. The acceptor compartment was filled with 120 mL of PBS comprising 1 and 10 g/L of BSA, respectively.

An amount of 5 mg of the drug dissolved in a volume of 3.4 mL of PBS was injected into the donor compartment. The chamber was sealed by an RC membrane (50 kDa MWCO) and two O-rings. The experiments were conducted at 37 ± 0.5 °C and 100 rpm. Samples (0.2 mL) were collected after 0.125, 0.25, 0.5, 1, 2, 3, 4, 5, 6, 7, and 8 h and the volume was replenished with fresh medium. The samples were analyzed as described in Section 2.2.

2.6. Performance Testing

2.6.1. Evaluation of the Influence of Excipients on the Drug Permeation

Semisolid dosage forms are well known for their interactions with surfaces and membranes. Therefore, we evaluated the PTDR method with regards to potential changes in the detected release due to membrane-excipient interactions. For this purpose, we carried out a release experiment using an emulsion gel, followed by the injection of a drug solution into the acceptor compartment.

An amount of 430 mg of Voltaren® Gel, which corresponds to 5 mg diclofenac-DEA, was weighed into the donor chamber and the release medium was added to a total volume of 3.4 mL. The acceptor compartment was filled with 120 mL phosphate buffer pH 7.4 as the release medium. An RC membrane (MWCO 50 kDa) was used and the dissolution apparatus was operated at 32 ± 0.5 °C and 50 rpm. Samples (0.2 mL) were collected after 0.25, 0.5, 1, 2, 3, 4, 5, 6, 7, 8, and 24 h, and the volume was replenished with fresh medium. Afterward, an amount of 5 mg diclofenac-DEA dissolved in 0.5 mL of release medium was added to the donor chamber, and samples were collected as described above. The samples were analyzed as described in Section 2.2.

2.6.2. Comparative Release Studies of Two Semisolid Dosage Forms

Each vessel (acceptor compartment) was filled with a volume of 120 mL medium of a 40 mM acetate buffer pH 5.3. Olfen® and Voltaren® gels were weighed accurately into the donor chamber corresponding to 5 mg of diclofenac salt. Release medium was added to prefill the donor chamber to a total volume of 3.4 mL to avoid diffusion into the donor chamber. The dissolution tester operated at 32 ± 0.5 °C and 50 rpm. Samples (0.2 mL) were taken at 0.25, 0.5, 1, 2, 3, 4, 5, 6, 7, 8, 24, 26, 28, 32, and 48 h and the volume was replenished with fresh medium. The samples were analyzed as described in Section 2.2.

2.7. Data Analysis and Computer Model

The evaluation of release data obtained by dialysis experiments often requires a correction of the expected analytical error due to the influences of membrane permeation on the release rate. In the following section, we describe data treatment and evaluation using the four-step model [19]. Two different calculations are made using STELLA. The first calculation identifies the membrane permeation rate constant (k_m) for a given experimental design and drug permeation profile. The operator uses the reference experiment with the dissolved drug substance being added to the donor compartment. A second calculation uses this permeation rate to normalize the release profile. Both STELLA models were published under Creative Commons License.

2.7.1. Modelling Drug Permeation and Normalization

To calculate k_m, the dissolved drug is added to the donor compartment, followed by quantification from the acceptor compartment. The four-step model assumes the diffusion of the drug substance through the membrane to follow Fick's law of diffusion [15]. It depends on the concentration gradient between the donor and the acceptor compartment (ΔC), the volume of the acceptor compartment (V_a), the thickness of the dialysis membrane (δ), and the surface area of the dialysis membrane separating both compartments (A).

$$\frac{dC_a}{dt} = \left[\frac{k_m \cdot A}{\delta \cdot V_a}\right] \times [\Delta C] \quad (2)$$

For the calculation of the surface area of the dialysis membrane (A), the specifications of the PTDR donor cell (radius r_d and height h_d of the cage cylinder) can be used (Equation (3)).

$$A = 2\pi \cdot r_d \cdot h_d \tag{3}$$

The thickness of the membrane (δ) depends on the membrane material and is a common specification reported by the manufacturer. The volume in the acceptor compartment V_a depends on the size of the vessel, used for the drug release test. In the present investigation, a 250 mL mini-vessel configuration following the specifications of the Chinese Pharmacopeia [21] was used, resulting in a total volume of 120 mL in the acceptor compartment. Furthermore, the evaporation of liquid from the dissolution vessel was taken into consideration. Here, we assumed a linear evaporation process over time and corrected V_a for each of the calculated time points. The STELLA model interface uses the initial and the final vessel weight [g] for this calculation. Hence, an identical initial and final vessel weight leads to uncorrected permeation profiles. During the permeation experiment, the concentration of the drug is quantified from the acceptor compartment (C_a). Together with the drug amount injected into the PTDR (Q_0), the concentration in the donor compartment (C_d) can be calculated:

$$C_d(t) = \frac{[Q_0 - C_a(t) \cdot V_a(t)]}{V_d} \tag{4}$$

Replacing the term $C_d(t)$ with Equation (4) in Equation (2) leads to:

$$\frac{dC_a}{dt} = \left[\frac{k_m \cdot A}{\delta \cdot V_a}\right] \cdot \left[\frac{Q_0 - C_a(t) \cdot V_a(t)}{V_d} - C_a(t)\right] \tag{5}$$

Equation (5) can then be solved analytically as follows:

$$C_a(t) = \left[\frac{Q_0}{V_a(t) + V_d}\right] \cdot \left\{1 - \exp\left[\frac{A \cdot k_m \cdot (V_a(t) + V_d) \cdot t}{\delta \cdot V_a(t) \cdot V_d}\right]\right\} \tag{6}$$

For further calculations, Equation (6) was simplified:

$$C_a(t) = C_\infty \cdot [1 - \exp(k_T \cdot t)] \tag{7}$$

with C_∞ being the equilibrium concentration, the equation can now be solved resulting in the newly introduced total diffusion coefficient k_T (Equation (8)).

$$k_T = \frac{ln\left(1 - \frac{C_a(t)}{C_\infty}\right)}{t} = \left[\frac{A \cdot k_m \cdot (V_a(t) + V_d)}{\delta \cdot V_a \cdot V_d}\right] \tag{8}$$

Stella Architect® uses linear extrapolation to create a continuous profile from the data points provided by the operator. The computer model calculates one k_T value every 3 s, including measured and extrapolated time points. The values k_m and k_T remain constant for the same dialysate, and experimental conditions (membrane, stirring rate, temperature, medium) [19]. For each k_T, k_m can be calculated (Equation (9)) as follows:

$$k_m = \left[\frac{k_T \cdot \delta \cdot V_a \cdot V_d}{A \cdot (V_a(t) + V_d)}\right] \tag{9}$$

However, deviations from the assumed first-order permeation are more likely to occur during the early time points and in the plateau phase. Therefore, an average membrane permeation rate constant was calculated in a permeation range from 15–85%:

$$k_{m-Average} = \frac{1}{n_{15\%-85\%}} \cdot \sum_{85\%}^{15\%} k_m \tag{10}$$

The second calculation uses the average k_m to calculate the concentration profile in the donor chamber. To calculate the concentration in the donor compartment, the slope is continuously calculated from every two data points [19]:

$$\frac{dC_a}{dt} \approx \frac{\Delta C_a}{\Delta t} = \left[\frac{k_m \cdot A}{\delta \cdot V_a}\right] \cdot [C_d(t) - C_a(t)] \quad (11)$$

The concentration in the donor compartment is calculated for the acquired data points [19]:

$$C_d(t) = \left(\frac{\Delta C_a}{\Delta dt}\right) \cdot \left[\frac{\delta \cdot V_a}{k_m \cdot A}\right] + C_a(t) \quad (12)$$

Finally, the total quantity of released drug from the formulation (Q_r) is determined:

$$Q_r(t) = C_d(t) \cdot V_d + C_a(t) \cdot V_a \quad (13)$$

2.7.2. Validation of Drug Permeation Model

The membrane permeation rate constant k_m is applied to estimate drug concentrations in the donor and the acceptor compartment over time. To validate our in silico model of the dialysis process, we calculated k_m for the permeation of diclofenac from the drug permeation profile at three different stirring rates (25, 50, and 100 rpm) and compared the predicted with the observed concentration. The absolute average fold error (*AAFE*) was calculated using Equation (14) [11,14,24–27] with n time points. Additionally, a comparison between the predicted and the observed drug concentration in the donor compartment was made after 0.25, 0.5, and 2 h at a stirring rate of 100 rpm.

$$AAFE = 10^{\frac{1}{n} \cdot \Sigma \left| \log \frac{predicted\ value_t}{observed\ value_t} \right|} \quad (14)$$

3. Results and Discussion

Currently, a rising number of complex non-oral dosage forms enter the global healthcare market. As a consequence, there is a need for novel in vitro methodologies to evaluate their quality and safety. Dialysis-based release assays often require significant expertise. Changes in the membrane quality, as well as the influence of the dialysis rate on the release profile, are the most common challenges reported in recent literature.

However, these "urban legends" often ignore other influences on reproducibility, such as the poor standardization of the instrument and release conditions. The PTDR enables in vitro release testing of liquid and semisolid dispersions in a well-defined setup. After normalization of the release profile using the membrane permeation rate constant k_m, these release profiles are widely unaffected by the dialysis rate and enable an improved comparison between different formulations and formulation qualities. Our present investigation provides an overview of the technical operations that confirm the functionality of the PTDR and serves as a guide for experimental design, validation, data evaluation, and documentation of dialysis-based release experiments.

3.1. Solubility of Diclofenac Salts in Different Release Media

The equilibrium solubility of diclofenac in various media has an impact on permeation and release experiments. When determining the membrane permeation rate constant k_m, the permeation of a drug solution is measured. Hence, the drug substance must be dissolved completely, and sink conditions must be maintained in the donor chamber as well as in the total volume used for the release assay. Table 2 summarizes the solubilities determined in various release media.

To achieve high aqueous solubility, most of the permeation experiments were carried out in PBS at a pH of 7.4 in the presence or absence of BSA. After the addition of 1 g/L of BSA, there was no significant increase in the solubility of diclofenac sodium observed (ANOVA) as compared to PBS alone. This seems unsurprising considering the low BSA

concentration leading to the complexation of approximately 0.7% of the drug. Only at the higher BSA concentration, a significant increase was observed (ANOVA, $p < 0.05$). The release of diclofenac from the two semisolid dosage forms was carried out at lowered temperature (32 °C). Solubilities of diclofenac sodium and diclofenac-DEA in 10 mM phosphate buffer differed significantly (ANOVA, $p < 0.05$), while the difference in 40 mM acetate buffer was negligible. However, the lowered solubility at acidic pH made the detection of differences more challenging. In summary, the expected influences of pH, temperature, and salt form on drug solubility were found.

Table 2. Equilibrium solubility after 24 h of two diclofenac salts in different release media. Experiments were conducted in triplicate ($n = 3$). The values are expressed as mean ± SD.

Release Medium	pH	Temperature	Diclclofenac Sodium Salt [mg/mL]	Diclofenac-DEA Salt [mg/mL]
PBS	7.4	37.0 °C	14.2 ± 0.3	-
PBS + 1 g/L BSA	7.4	37.0 °C	15.2 ± 0.3	-
PBS + 10 g/L BSA	7.4	37.0 °C	18.5 ± 0.2	-
40 mM Acetate buffer	5.3	32.0 °C	0.0314 ± 0.0008	0.0332 ± 0.0020
10 mM Phosphate buffer	7.4	32.0 °C	13.5 ± 0.8	10.2 ± 0.2

3.2. Technical Performance of the PTDR

Before the release of drug formulations was tested, we carried out a number of technical operations with the PTDR. These included a membrane integrity test, the retention of macromolecules, an evaluation of the hydrodynamics in the acceptor compartment as well as a measurement of the selectivity of the method for the size fraction of interest.

3.2.1. Membrane Leakage Test Using Gold Nanoparticles

The membrane integrity test requires a stable particle standard that can be reliably quantified from the acceptor compartment. Serving as an indicator for the particle populations retained by the dialysis membrane, a monodisperse size distribution was one key criterium for the selection. Among other potential standards, gold nanoparticles led to the most reliable outcome. When developing this protocol, a number of commercial nanobeads and polymer nanoparticles were tested (Supplementary Table S1). The limited stability of these preparations was one of the most common weaknesses and included agglomeration or release of the dye.

The gold nanoparticles exhibited a particle diameter of 50 nm, representing a suitable lower size limit for many drug delivery systems. The particles were detected photometrically and by using the derived photon count rate in a DLS setup. The negative control was measured in the absence of gold nanoparticles (Figure 3a), while for the positive control, a small incision in the dialysis membrane allowed the particles to leak into the acceptor chamber (Figure 3e).

For all three vessels (Figure 3b–d), the absorbance of gold nanoparticles was detected after the incision only (24 h sample). This indicates that there was no leakage from the donor into the acceptor compartment over the whole duration of the experiment. The nanoparticles were successfully retained by the dialysis membrane. This was also confirmed by the mean derived photon count rate, detected by the DLS setup (Figure 3f). For the given particle size and laser wavelength, the derived count rate served as a surrogate parameter for the particle concentration. It was below 1000 kcps for all vessels before the incision and increased to values of more than 2000 kcps after the incision, except for the positive control. This provides strong evidence that particles with a size of 50 nm are retained by the membrane and do not leak into the acceptor compartment.

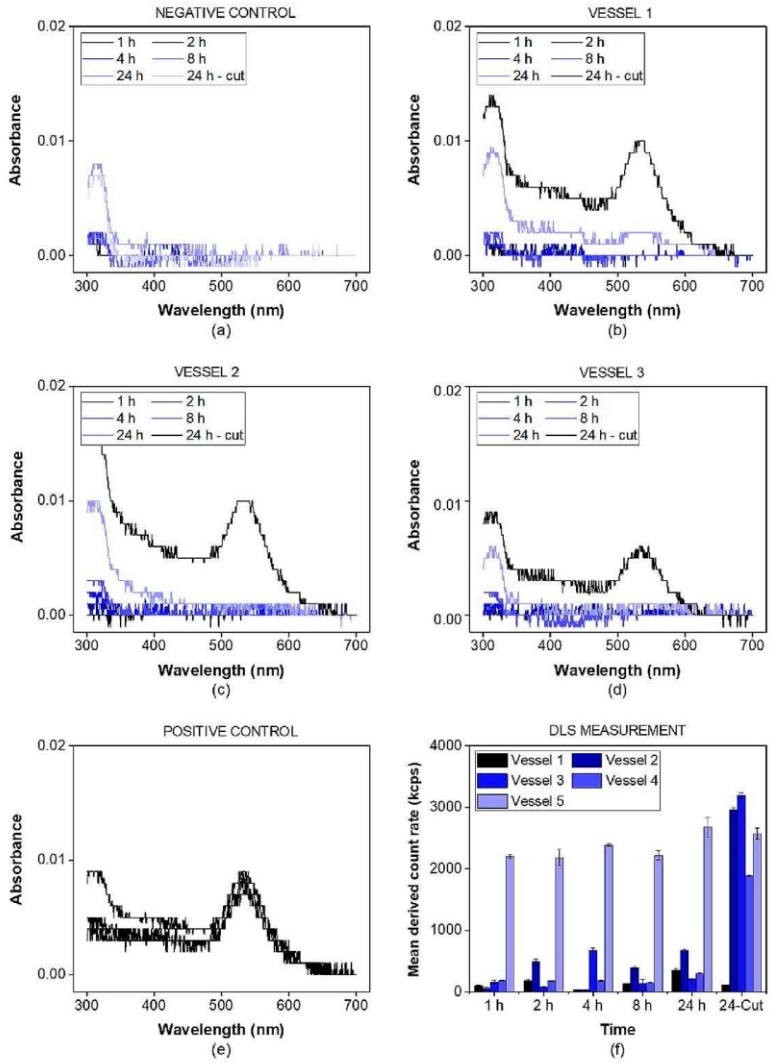

Figure 3. Membrane integrity test using a dispersion of gold nanoparticles (λ_{max} = 535 nm). The samples were analyzed by UV-VIS spectrophotometry at a wavelength of 300–700 nm. The negative control was measured without adding gold nanoparticles (**a**) while the positive control involved an incision through the membrane before starting the experiment (**e**). For all other vessels (**b**–**d**), the gold nanoparticles were added to the vessel and the spectrum was recorded at the indicated time points. After 24 h, a small incision through the membrane was performed. The spectra indicating the presence of gold nanoparticles in the acceptor compartment were highlighted in black for all vessels. Additionally, the mean derived count rate in the acceptor compartment was measured indicating the presence of gold nanoparticles in all vessels after the incision but not before this time point, except for the positive control (**f**).

3.2.2. Retention of Macromolecules

While the pore size reported for syringe filters indicates the average diameter of the filter pores, dialysis membranes are most commonly standardized by their MWCO. This parameter defines a molecular weight where 90% of a marker molecule was still retained by the membrane after 17 h [15]. For a 50 kDa dialysis membrane, we used BSA with a molecular weight of 66.5 kDa to measure the retention and quantified the protein by SEC-HPLC (see Section 2.3) and spectrophotometrically using a UV-Vis dip probe (Figure 4).

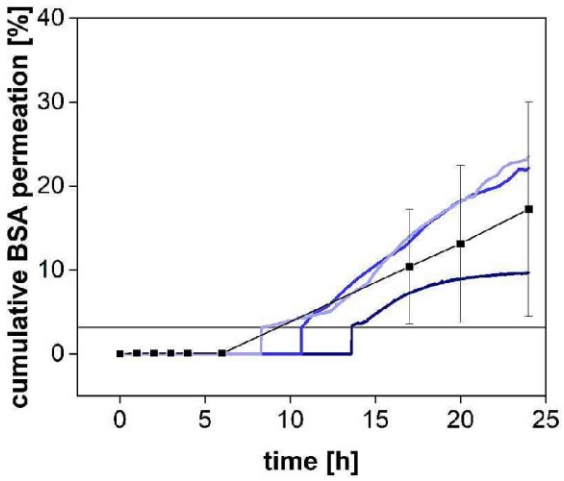

Figure 4. Cumulative permeation of bovine serum albumin (BSA) using SEC-HPLC method (black squares, Mean ± SD, $n = 3$) or an online UV-VIS dip probe (blue colored lines) at 37 °C and 50 rpm using a 50 kDa RC dialysis membrane. The horizontal grey line denotes the LOQ of the UV-VIS measurement.

BSA was retained by the membrane for the first 8 h but steadily increased in concentration afterward (Figure 4). Commonly, the MWCO is determined at room temperature under mild agitation of the acceptor compartment only. Consequently, the stirring in the donor compartment, as well as the elevated temperature (37 °C), potentially accelerated the dialysis process. Our findings indicate that leakage from the donor compartment must be considered for the separation of molecules with a molecular volume close to the MWCO of the membrane. In a previous investigation, we reported the quantification of the drug-protein transfer as one potential application of the PTDR [13]. Importantly, these measurements can still be performed. Depending on the ratio between albumin and drug molecules, even a considerable leakage of BSA from the donor chamber does not lead to a corresponding error in the release profile. However, after 15 h and using a membrane with an MWCO of 50 kDa, the leakage would potentially affect the release. Therefore, such investigations should be carried out over a shorter period or using a smaller MWCO (e.g., 30 kDa) [13].

3.2.3. Hydrodynamics in the Acceptor Compartment

The hydrodynamics in the acceptor compartment of the PTDR has a strong impact on the variability of the measured drug concentration. The common stirring rates of USP apparatus I/II are ranging from 25–100 rpm. To determine the impact of the stirring rate on drug distribution in the acceptor compartment, we utilized a dip probe and measured

the absorbance of the release medium in a fixed position after the addition of a colored dye to the acceptor compartment. The dip probe enables measurement in real-time. Different stirring rates of 0, 25, 50, and 100 rpm were tested (Figure 5). Even at a stirring rate of 25 rpm, the absorbance remained constant after 1 min. Small fluctuations were observed during this first minute only. At 50 and 100 rpm, no fluctuations were observed. Without agitation, no steady absorbance was measured. After 15 min, the absorbance was close to the plateau observed for the other vessels.

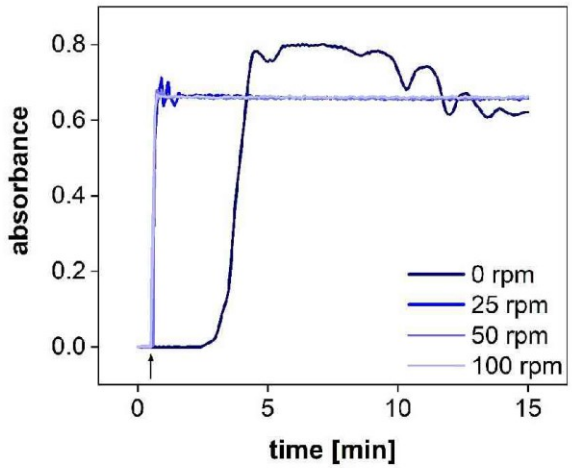

Figure 5. UV-Vis measurements of the acceptor compartment with an online dip probe at 283 nm at different stirring rates. The arrow denotes that the idebenone solution was spiked into the acceptor compartment.

Consequently, agitation of the acceptor compartment is required for the performance test. However, considering a common sampling time of 2.5–5 min, all stirring rates (25–100 rpm) enable accurate detection of the drug release.

3.2.4. Permeation Rate at Various Stirring Rates

The PTDR has the unique feature of accelerating dialysis processes by stirring the acceptor and the donor compartment. Floating, sedimentation, and agglomeration as well as the formation of layer structures in the donor chamber are common challenges of conventional dialysis experiments [9,16,17]. Although constant agitation does not always reflect the physiological environment of the administration site, it significantly reduces these effects and leads to improved reproducibility of the measurement [15,28]. Furthermore, the stirring accelerates the membrane transport and leads to a higher sensitivity when measuring kinetic processes. In dialysis, a sensitive measurement can only be achieved for dialysis rates exceeding the release rate. To measure this effect for various stirring rates, we dialyzed a solution of diclofenac sodium at 0, 25, 50, 100 rpm (Figure 6). This time-resolved permeation experiment is known as the release response test (RRT) and provides information on the separation time required by this method [29].

Without stirring, diclofenac permeated through the dialysis membrane very slowly and there was a lag time of several minutes before steady-state permeation was reached (Figure 6). Furthermore, the permeated amount was approximately 20% lower during the release phase and reached a plateau after 6 h. On the contrary, under constant stirring, the plateau was reached after 4 h only. This separation time represents the time until 100% of the total dose has been dialyzed. To estimate the sensitivity of the assay, the

dialyzed fraction per time must be taken into consideration. For all stirring rates, a fraction corresponding to approximately 10% of the total dose was dialyzed within 7.5 min. The stirring rate of 25 rpm led to a slightly lower permeation rate as compared to 50 rpm. This was also reflected by a lowered membrane permeation rate constant. A further increase to 100 rpm did not affect the permeation rate significantly. However, these parameters are strongly affected by other parameters, such as the drug substance, the MWCO, and the membrane material (50 kDa, RC). Therefore, general recommendations are difficult to make. The stirring rate must be selected considering the membrane permeation and stability of each formulation and compound. Still, the present investigation indicates that stirring rates of more than 50 rpm may not generally improve the outcome for every membrane type. Furthermore, higher stirring rates are likely to increase the shear stress in the donor chamber and may lead to a change in the release mechanism. Therefore, depending on the sensitivity of the formulation to shear stress, common stirring rates between 25 and 50 rpm are preferred.

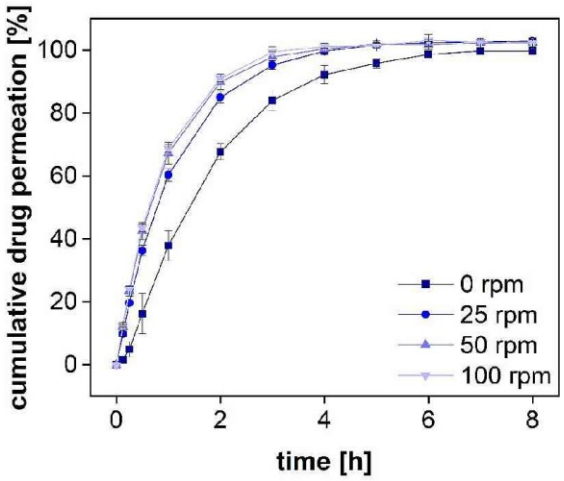

Figure 6. Mean permeation profiles of a diclofenac sodium solution at 37 °C using an RC dialysis membrane (MWCO 50 kDa). Stirring rates were changed accordingly ($n = 6$). Mean ± SD is presented.

3.2.5. Selectivity of the Assay for Specific Size Fractions

The BSA molecule binds diclofenac with high affinity through ionic and hydrophobic interactions using two unspecific binding sites [30]. A direct comparison between BSA and human serum albumin (HSA) resulted in minor differences between these two proteins, and the plasma protein binding in humans was reported to be 99% [31]. Therefore, in equilibrium, diclofenac is expected to be bound to proteins at a stoichiometric ratio of 2:1 [30,32]. We used different BSA concentrations to bind a certain fraction of the drug and investigated the specificity of the separation method for this protein-bound fraction. With a molecular weight of 66.5 kDa, BSA is reliably retained in the donor chamber during the first 8 h (see Section 3.2.2).

Following the standards of the European Pharmacopeia [33], two compendial buffer systems comprising 1 and 10 g/L of BSA were used, respectively. These concentrations are below the physiological albumin concentration of approximately 40 g/L. Diclofenac sodium was dissolved in PBS 7.4 comprising different amounts of protein. The permeation profiles were measured in the PTDR. The outcome of the investigation is presented in Figure 7. To quantitatively evaluate the difference in permeation, the area under the curve

(AUC) was calculated for each permeation profile as well. As expected, at the lower BSA concentration, no significant difference between the profiles of protein-bound and free diclofenac was identified. At a concentration of 1 g/L, approximately 0.7% of diclofenac are bound to BSA whereas at a concentration of 10 g/L BSA approximately 7% are in a protein complex. Considering the analytical error indicated by the standard deviation, the difference in the AUCs between both permeation experiments (in the presence and absence of BSA) reflected the theoretical ratio of 0.93. In the experiment, a ratio of 0.91 ± 0.02 was found (Table 3). Hence, the drug was reliably retained by the membrane enabling sensitive detection of the protein-bound and the unbound fraction.

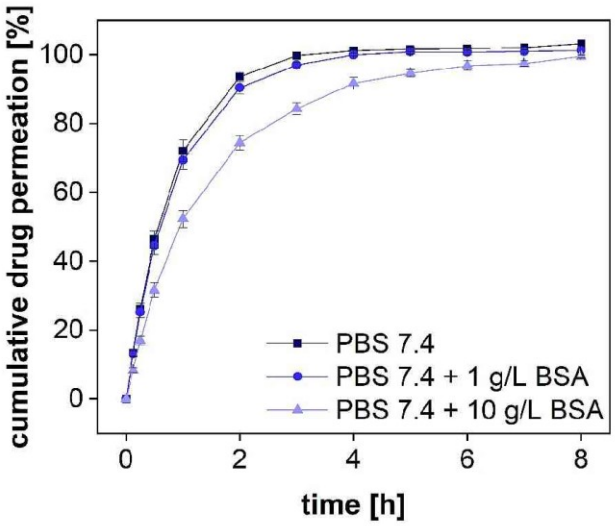

Figure 7. Cumulative permeation of diclofenac sodium with different amounts of BSA in PBS 7.4. A regenerated cellulose membrane (MWCO 50 kDa) was used to separate the two compartments. The experiment was conducted at 37 °C at 100 rpm (n = 6). Mean values ± SD are shown.

Table 3. Calculated AUC of diclofenac sodium permeation in PBS 7.4 with different BSA amounts (n = 6).

Buffer	AUC (0–8 h) [µg × h/mL]	SD [µg × h/mL]	Ratio
PBS 7.4	292	2	-
PBS 7.4 + 1 g/L BSA	292	2	1.00 ± 0.01
PBS 7.4 + 10 g/L BSA	265	4	0.91 ± 0.02

Considering the increase in BSA permeability over time, the duration of such experiments should not exceed 15 h. Afterward, an increasing analytical error is to be expected. Alternatively, smaller membrane pore sizes should be selected. For small molecules such as diclofenac, an MWCO of 20–30 kDa would still allow efficient separation of the two size fractions and may not be affected by the change in permeability to a similar extent.

3.3. In Vitro Performance Testing Using the PTDR

While the first set of experiments (Section 3.2) included procedures to assess the technical performance of the instrument, more studies were conducted to challenge the device

using a common separation problem. Semisolid dosage forms often contain highly adhesive gelation agents and lipids likely to impact the dialysis process. Therefore, we selected two semisolid drug products, Voltaren® Emulgel and Olfen® gel, for this investigation and studied the influence of the excipients on membrane permeation. The data analysis was carried out using a model-dependent normalization procedure described previously (see Section 2.4) [5,12–15].

3.3.1. Evaluation of the Influence of Excipients on Drug Permeation

To study the influence of excipients on drug permeation, the formulation Voltaren® Emulgel was added to the donor chamber of the PTDR and a release experiment was performed (Figure 8a). Of the two semisolid formulations, the emulsion system was more likely to interact with the membrane. After 24 h, a solution of diclofenac was added to the donor chamber and dialyzed under similar conditions (Figure 8a). At neutral pH, the complete dissociation of the weak acid diclofenac increases the aqueous solubility of the drug substance dramatically. Therefore, during the initial 24 h, a rapid dissolution-driven release from the commercial formulation was observed.

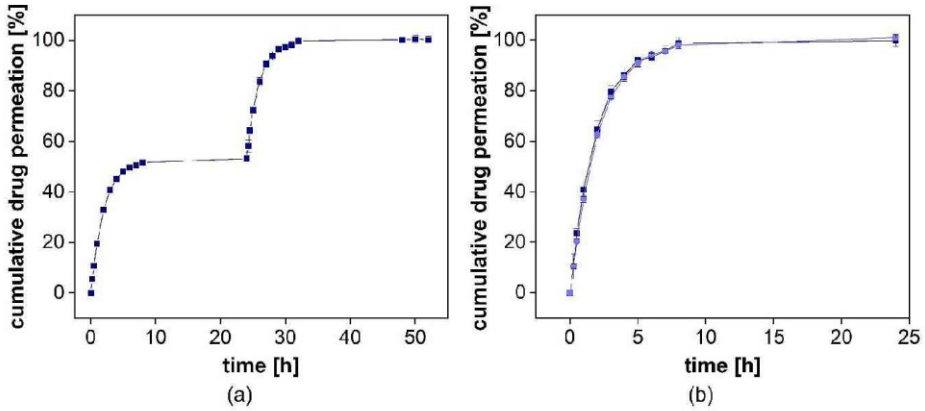

Figure 8. Cumulative release of diclofenac-DEA from Voltaren Emulgel® with diclofenac-DEA solution spiked into the donor compartment after 24 h. Mean ± SD is presented ($n = 3$). On the left, the release profile over 48 h is presented (**a**). On the right, the overlay of the initial release and the permeation profile are provided (**b**).

When adding diclofenac in solution, there was no significant difference between the release and the permeation profiles observed (Figure 8b). This indicates that the formulation had no impact on the dialysis rate. While for most dialysis processes, a strong influence of semisolids on drug separation can be assumed, the PTDR effectively inhibits these membrane interactions and leads to a more reliable release test.

3.3.2. Documentation of the Experimental Parameters

Many dialysis experiments reported in the literature do not provide accurate documentation of the exact experimental procedures. In the present investigation, we lay out a recommended methodology. Technical parameters to be reported are summarized in Table 4. They include common information such as the MWCO, or the membrane material, but also an exact description of the donor and the acceptor volume, as well as the preconditioning protocol used for this type of membrane.

Table 4. Important experimental parameters to be reported.

Parameter		Value
Membrane characteristics	Membrane material	Regenerated cellulose
	MWCO	50 kDa
	Membrane thickness	0.0065 cm
	Membrane tube flat width	28 mm
	Storage conditions	Prewetted in 0.5% sodium azide at 2–8 °C
	Preconditioning protocol of the manufacturer	Rinse with water and soak for 30 min in water Repligen (USA)
Dispersion Releaser	Volume of donor compartment	3.4 mL
	Volume of acceptor fluid (Before and after the experiment)	120 mL (mini-vessel configuration)
	Surface area of the donor cell	10.95 cm^2
Test conditions	Composition of the release medium	Various media tested (Materials and Methods)
	Temperature	32 °C or 37 °C (Materials and Methods)
	Stirring rate	0–100 rpm (Materials and Methods)
	Sampling volume	200 µL
	sampling time points	Various (Materials and Methods)
Sampling injection protocol	Reference experiment	A volume of 3.4 mL of an aqueous diclofenac solution
	Semisolid	Amount of each semisolid corresponding to 5 mg of diclofenac was weighed into the DR and the donor chamber was filled with release medium to a total volume of 3.4 mL.

3.3.3. Data Analysis Using Model-Dependent Profile Correction

The membrane permeation rate constant (k_m) is a performance indicator for the dialysis process and the separation of released drugs from the formulation. It represents an important analytical error and is therefore determined in a permeation experiment (Table 5). The four-step model uses this parameter to normalize the drug release profiles; however, for the application of dialysis-based release experiments in quality control, a specification range for k_m would allow the preselection of dialysis membranes to improve reproducibility. Also, normalized release profiles can be directly compared even when measured with membranes from various vendors.

Table 5. Permeation rates calculated for diclofenac sodium at different stirring rates. Each calculation is based on 5 vessels and included 5–6 time points (n = 25 or n = 30).

Stirring Rate	Permeation Rate Constant [cm^2/h]	SD [cm^2/h]	AAFE
0 rpm	0.99×10^{-3}	0.9×10^{-3}	1.27
25 rpm	1.76×10^{-3}	0.10×10^{-3}	1.03
50 rpm	2.13×10^{-3}	0.18×10^{-3}	1.03
100 rpm	2.17×10^{-3}	0.09×10^{-3}	1.03 [1] 1.23 [2]

[1] Evaluation of the acceptor compartment over the entire permeation profile. [2] Evaluation of the donor compartment at three time points (0.25, 0.5, 2 h).

For the calculation of k_m, the total permeation rate constant k_T is calculated for each time point of the permeation profile. Fluctuations in k_T are more likely at the beginning and the end of the permeation experiment due to the initial distribution of the drug as well as the inaccuracies associated with the small concentration differences in the plateau phase. The k_T values obtained from the permeation profiles of diclofenac at different stirring rates are presented in Figure 9. For the permeation range from 15 to 85% of the total dose, there were almost no fluctuations observed. Therefore, we decided to use this range for the

calculation of k_m. Evidently, the fluctuations are more pronounced for higher stirring rates, indicating a certain influence of the hydrodynamics on the diffusion rate.

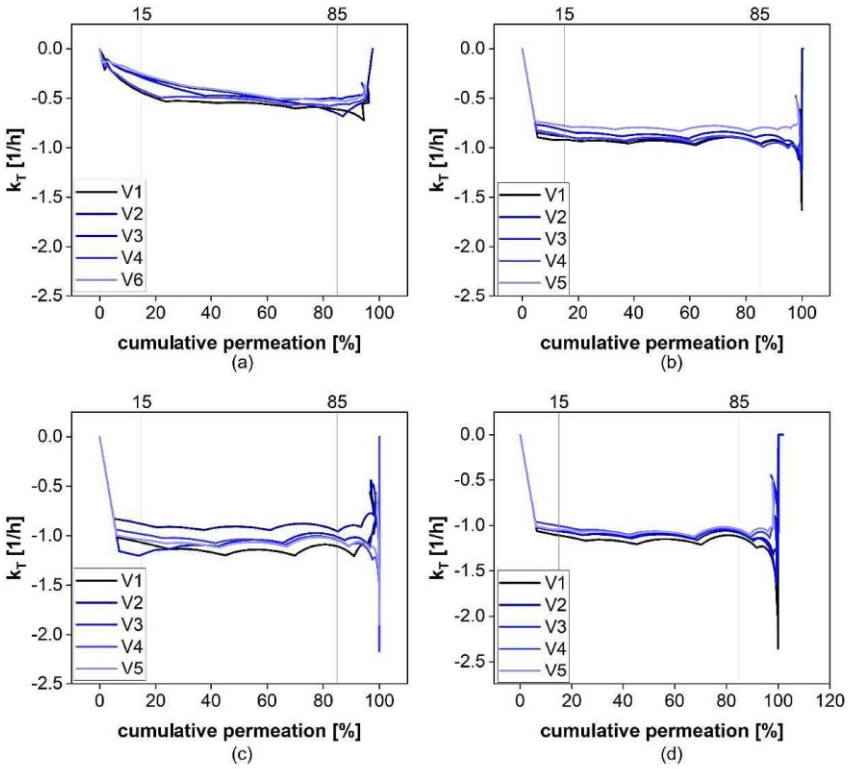

Figure 9. The calculated k_T values at 0 (**a**), 25 (**b**), 50 (**c**), and 100 rpm (**d**).

To provide a convenient solution, we automated the process of k_m calculation and published a user-friendly calculator (DIMEC) under the Creative Commons License. The operator provides the permeation profile, followed by an automated calculation of k_m. The default settings include the technical parameters of the PTDR, however, other methodologies can be used. The user interface enables the customization of all the input parameters, including the surface area and the volume of the release cell.

3.3.4. Validation of the Mathematical Model

To provide evidence for the accuracy of the STELLA model, we compared the permeation profile with the simulated permeation profile represented by the k_m value. It indicates the quality of the curve fit. The absolute average fold error (AAFE) is a simple measure of the difference between the simulated and the observed values in a simulation [11,14,24–27]. An AAFE of 1 indicates two identical profiles and values below 2 indicate a successful simulation [26,27]. For the permeation experiments carried out at stirring rates of 25–50 rpm, an AAFE of 1.03 was achieved (Table 5). At a stirring rate of 0 rpm, the lag time between injection of the solution and the constant drug flux through the membrane led to an increase in the AAFE to 1.27. At the highest stirring rate, the most considerable influence of the

stirring rate on permeation was as expected. This still resulted in an accurate reflection of the permeation profile with an AAFE of 1.03. To validate our simulation, we collected samples from the donor compartment at the highest stirring rate after 0.25, 0.5, and 2 h and compared the observed and simulated drug concentrations. This is presented in Figure 10 (d, red line/red triangles). It provides further evidence for the reliability of the mathematical model.

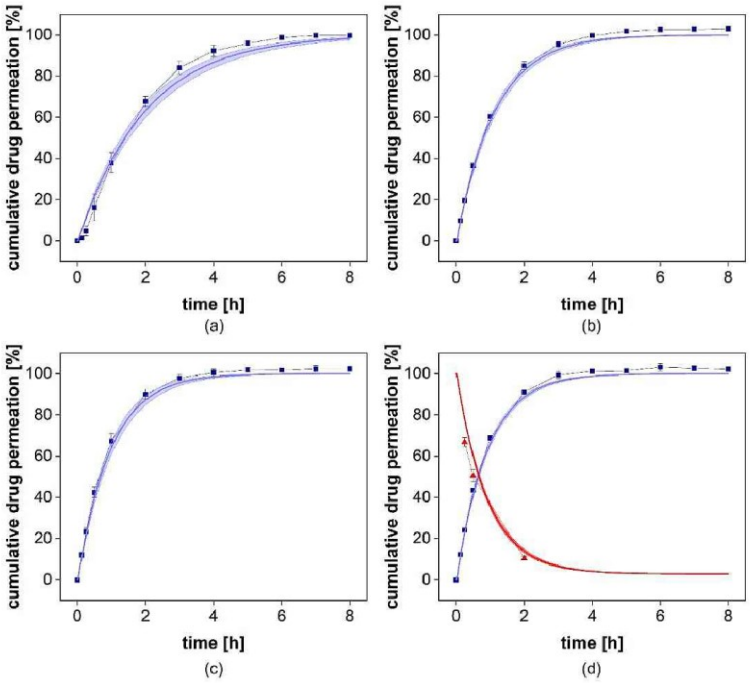

Figure 10. Comparison of observed and simulated permeation profiles at 0 (**a**), 25 (**b**), 50 (**c**), and 100 rpm (**d**). The blue squares indicate the mean ± SD (n = 6) observed cumulative drug permeation and the blue line presents the simulated cumulative drug permeation using the mean k_m ± SD. In (**d**) the donor compartment was evaluated. The red triangles indicate the observed mean ± SD (n = 6) with the corresponding simulated relative donor concentration as the red line.

The k_m values at 0 and 25 rpm were 0.99 × 10^{-3} cm^2/h and 1.76 × 10^{-3} cm^2/h, respectively (Table 6). At 50 and 100 rpm, the permeation rates increased to 2.13 × 10^{-3} cm^2/h and 2.17 × 10^{-3} cm^2/h, respectively (Table 5). This confirms the contribution of the stirring rate to membrane transport that is responsible for the higher sensitivity of this release assay. However, at higher stirring rates, the influence was negligible. Therefore, stirring rates of more than 50 rpm should not be selected without confirming the benefit for a specific formulation or membrane pore size.

The average permeation rate constants for each stirring rate (Table 5) were calculated from 5 vessels and included 5–6 measured time points, depending on the number of sampling time points falling into the range of 15–85% permeation. For the statistical evalua-tion, we considered only time points sustained by quantification and not the extrapolated time points (>100). A significant difference in the membrane permeation rate constant was observed between all k_m values except for the difference between 50 and 100 rpm (ANOVA, $p > 0.05$).

Table 6. List of excipients of Voltaren® Emulgel and Olfen® gel.

Excipient	Voltaren® Emulgel	Olfen® Gel
Lactic acid		X
Diisopropyladipate		X
Isopropylalcohol	X	X
Sodium metabisulfite		X
Hydroxyethylcellulose		X
Hydroxypropylcellulose		X
Diethylamine	X	
Propylene glycol	X	
Mineral oil	X	
Cocoyl caprylocaprate	X	
Polyoxyl-20-cetostearylether	X	
Carbomer	X	
Perfume creme	X	
Purified water	X	X

3.3.5. Performance Testing Using Two Semisolid Diclofenac Formulations

The release of diclofenac is controlled by the aqueous solubility of each salt in the medium. Under sink conditions, there was no significant difference between the two formulations expected. For the performance assay, we selected a slightly acidic pH value corresponding to the pH of the human skin (5–6) [34]. Noteworthy, the conditions of the assay, including hydrodynamics, liquid volume, and buffer capacity, do not reflect the topical route of administration. Still, the release profiles provide information on the differences between these two dosage forms and could be used for excipient selection. The composition of the two gels is summarized in Table 6. Olfen® gel comprises a conventional linear colloidal hydrogel structure with a certain amount of isopropyl alcohol embedded into the gel structure, whereas Voltaren Emulgel® is a gelled oil-in-water emulsion. The drug was dissolved in the aqueous phase.

The cumulative drug release from both formulations is presented in Figure 8a. Voltaren® Emulgel released diclofenac more rapidly compared to the Olfen® gel and, within 48 h, reached a plateau at almost 60%, corresponding to the aqueous solubility determined for this release medium at 32 °C (0.0314 ± 0.0008 mg/mL for diclofenac sodium and 0.0332 ± 0.0020 mg/mL for diclofenac-DEA). Olfen® gel released the drug much slower and reached a plateau at approximately 40%. The emulsifying agents present in Voltaren® Emulgel as well as the improved solubility of diclofenac-DEA are the most likely explanation. A delaying effect of the emulsion system on dialysis could not be detected. Furthermore, it is unlikely that, when using the highly soluble salt of diclofenac, the emulsion system had a strong impact on the drug release.

Subsequently, we calculated the k_m values using the DIMEC programmed in STELLA [19]. The permeation rate constants of the diclofenac sodium and diclofenac-DEA were 1.54 ± 0.12 × 10^{-3} cm^2/h and 1.75 ± 0.19 × 10^{-3} cm^2/h, respectively. Subsequently, we normalized the release profiles for each formulation using the PTDR ReNo. This calculator is provided under Creative Commons License as well.

After normalization (Figure 11b), a burst release of 16% from Olfen® gel and 34% from Voltaren® Emulgel were observed. It is evident that the release behavior of diclofenac from both hydrogels was widely driven by drug solubility and that the emulsion system represents a minor influence on the release.

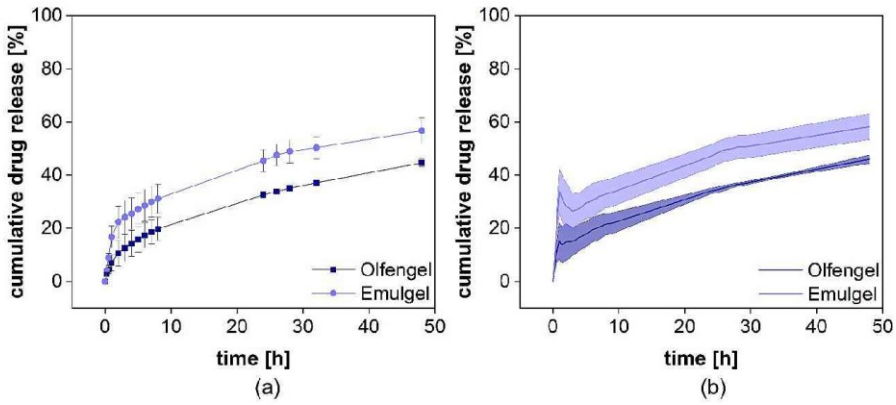

Figure 11. Cumulative release of two different diclofenac semisolid formulations. Measured diclofenac released into the acceptor compartment ((**a**), $n = 4$) and normalized release profile (**b**). Mean ± SD is shown.

4. Conclusions

Most dialysis-based performance assays demand a higher level of understanding from the operator. However, the requirements do not differ considerably from other dissolution tests. The selectivity of the separation method for the dissolved drug (e.g., by separating molecules with a specific molecular volume) and the separation time commonly have a strong impact on the release profile. Since most dialysis methods reported in previous research do not control hydrodynamics in the donor chamber and other influences, their limited reliability is not surprising. In the present investigation, we provide evidence for the reliability of a well-designed experimental setup, together with a dedicated mathematical methodology and documentation. To make it easier to comply with these high standards, we provide two computer models that can be customized for other dialysis-based release tests as well.

Supplementary Materials: The following are available online at https://www.mdpi.com/article/10.3390/pharmaceutics13122007/s1. Table S1: Commercial standards evaluated for testing the leakage of particles from the PTDR.

Author Contributions: Conceptualization, M.-P.M. and M.G.W.; software, M.-P.M., H.M., J.K. and E.F.; investigation, M.-P.M.; writing—original draft preparation, M.-P.M.; writing—review and editing, M.G.W.; funding acquisition, M.G.W.; supervision, M.G.W. All authors have read and agreed to the published version of the manuscript.

Funding: M.G.W. and H.M. were funded by the National University of Singapore and the Singaporean Ministry of Education (grant no. R-148-000-282-133, WBS-148-0000-297-114). M.G.W. and M.-P.M. were funded by the LOEWE initiative of the State of Hessen and the Hessen Modellprojekte grant no. 552/17-34.

Institutional Review Board Statement: Not applicable.

Informed Consent Statement: Not applicable.

Data Availability Statement: Not applicable.

Acknowledgments: The authors acknowledge Dirk Beilke, Björn Fähler and Pharma Test Apparatebau AG (Hainburg, Germany) for providing them with PTDR release cells.

Conflicts of Interest: E.F. is an employee of Eurofins PHAST Development GmbH & Co. KG. This relationship had no influence on the scientific data presented in this article. All other authors declare no conflict of interest.

Abbreviations

AAFE	absolute average fold error
AUC	area under the curve
BSA	bovine serum albumin
diclofenac-DEA	diclofenac diethylamine salt
DIMEC	Dialysis Membrane Permeation Calculator
DLS	dynamic light scattering
EV	extracellular vesicles
HPLC	High-performance liquid chromatography
HSA	human serum albumin
LOD	limit of detection
LOQ	limit of quantification
MWCO	molecular weight cut off
NIR	near-infrared light
PBS	phosphate-buffered saline
Ph. Eur.	European Pharmacopeia
PTDR	Pharma Test Dispersion Releaser
PTDR ReNo	PTDR release normalizer
PTFE	polytetrafluoroethylene
RC	regenerated cellulose
rpm	revolutions per minute
RRT	release response test
SD	standard deviation
SDS	sodium dodecyl sulfate
SEC	size exclusion chromatography
STELLA	Systems Thinking, Experimental Learning Laboratory with Animation
USP	United States Pharmacopeia
UV	ultraviolet light
Vis	visible light

References

1. D'Mello, S.R.; Cruz, C.N.; Chen, M.L.; Kapoor, M.; Lee, S.L.; Tyner, K.M. The evolving landscape of drug products containing nanomaterials in the United States. *Nat. Nanotechnol.* **2017**, *12*, 523–529. [CrossRef]
2. Marques, M.R.C.; Choo, Q.; Ashtikar, M.; Rocha, T.C.; Bremer-Hoffmann, S.; Wacker, M.G. Nanomedicines—Tiny particles and big challenges. *Adv. Drug Deliv. Rev.* **2019**, *151*, 23–43. [CrossRef]
3. Mast, M.P.; Modh, H.; Champanhac, C.; Wang, J.W.; Storm, G.; Kramer, J.; Mailander, V.; Pastorin, G.; Wacker, M.G. Nanomedicine at the crossroads—A quick guide for IVIVC. *Adv. Drug Deliv. Rev.* **2021**, 113829. [CrossRef]
4. Bunjes, H. Lipid nanoparticles for the delivery of poorly water-soluble drugs. *J. Pharm. Pharmacol.* **2010**, *62*, 1637–1645. [CrossRef]
5. Jung, F.; Nothnagel, L.; Gao, F.; Thurn, M.; Vogel, V.; Wacker, M.G. A comparison of two biorelevant in vitro drug release methods for nanotherapeutics based on advanced physiologically-based pharmacokinetic modelling. *Eur. J. Pharm. Sci.* **2018**, *127*, 462–470. [CrossRef] [PubMed]
6. Ashtikar, M.; Wacker, M.G. Nanopharmaceuticals for wound healing—Lost in translation? *Adv. Drug Deliv. Rev.* **2018**, *129*, 194–218. [CrossRef] [PubMed]
7. Zhao, Y.; Brown, M.B.; Jones, S.A. Pharmaceutical foams: Are they the answer to the dilemma of topical nanoparticles? *Nanomedicine* **2010**, *6*, 227–236. [CrossRef]
8. Salvioni, L.; Morelli, L.; Ochoa, E.; Labra, M.; Fiandra, L.; Palugan, L.; Prosperi, D.; Colombo, M. The emerging role of nanotechnology in skincare. *Adv. Colloid Interface Sci.* **2021**, *293*, 102437. [CrossRef] [PubMed]
9. Nothnagel, L.; Wacker, M.G. How to measure release from nanosized carriers? *Eur. J. Pharm. Sci.* **2018**, *120*, 199–211. [CrossRef]
10. Wacker, M.G.; Janas, C. Dialysis Cell for an In-Vitro Release Test Apparatus, Use of the Dialysis Cell and In-Vitro Release Test Apparatus. EP3047267A1, 17 September 2014.
11. Jablonka, L.; Ashtikar, M.; Gao, G.F.; Thurn, M.; Modh, H.; Wang, J.W.; Preuss, A.; Scheglmann, D.; Albrecht, V.; Roder, B.; et al. Predicting human pharmacokinetics of liposomal temoporfin using a hybrid in silico model. *Eur. J. Pharm. Sci.* **2020**, *149*, 121–134. [CrossRef]

12. Modh, H.; Fang, D.J.; Ou, Y.H.; Yau, J.N.N.; Kovshova, T.; Nagpal, S.; Knoll, J.; Wallenwein, C.M.; Maiti, K.; Bhowmick, S.; et al. Injectable drug delivery systems of doxorubicin revisited: In vitro-in vivo relationships using human clinical data. *Int. J. Pharm.* **2021**, *608*, 121073. [CrossRef] [PubMed]
13. Wallenwein, C.M.; Nova, M.V.; Janas, C.; Jablonka, L.; Gao, G.F.; Thurn, M.; Albrecht, V.; Wiehe, A.; Wacker, M.G. A dialysis-based in vitro drug release assay to study dynamics of the drug-protein transfer of temoporfin liposomes. *Eur. J. Pharm. Sci.* **2019**, *143*, 44–50. [CrossRef] [PubMed]
14. Jablonka, L.; Ashtikar, M.; Gao, G.; Jung, F.; Thurn, M.; Preuss, A.; Scheglmann, D.; Albrecht, V.; Roder, B.; Wacker, M.G. Advanced in silico modeling explains pharmacokinetics and biodistribution of temoporfin nanocrystals in humans. *J. Control. Release* **2019**, *308*, 57–70. [CrossRef] [PubMed]
15. Janas, C.; Mast, M.P.; Kirsamer, L.; Angioni, C.; Gao, F.; Mantele, W.; Dressman, J.; Wacker, M.G. The dispersion releaser technology is an effective method for testing drug release from nanosized drug carriers. *Eur. J. Pharm. Sci.* **2017**, *115*, 73–83. [CrossRef] [PubMed]
16. Gao, G.F.; Thurn, M.; Wendt, B.; Parnham, M.J.; Wacker, M.G. A sensitive in vitro performance assay reveals the in vivo drug release mechanisms of long-acting medroxyprogesterone acetate microparticles. *Int. J. Pharm.* **2020**, *586*, 119540. [CrossRef] [PubMed]
17. Gao, G.F.; Ashtikar, M.; Kojima, R.; Yoshida, T.; Kaihara, M.; Tajiri, T.; Shanehsazzadeh, S.; Modh, H.; Wacker, M.G. Predicting drug release and degradation kinetics of long-acting microsphere formulations of tacrolimus for subcutaneous injection. *J. Control. Release* **2021**, *329*, 372–384. [CrossRef]
18. Yu, M.; Yuan, W.; Li, D.; Schwendeman, A.; Schwendeman, S.P. Predicting drug release kinetics from nanocarriers inside dialysis bags. *J. Control. Release* **2019**, *315*, 23–30. [CrossRef]
19. Xie, L.; Beyer, S.; Vogel, V.; Wacker, M.G.; Mantele, W. Assessing the drug release from nanoparticles: Overcoming the shortcomings of dialysis by using novel optical techniques and a mathematical model. *Int. J. Pharm.* **2015**, *488*, 108–119. [CrossRef]
20. Zhang, Y.; Geißen, S.-U. In vitro degradation of carbamazepine and diclofenac by crude lignin peroxidase. *J. Hazard. Mater.* **2010**, *176*, 1089–1092. [CrossRef]
21. Chinese Pharmacopoeia Commission. *Chinese Pharmacoepia (Ch.P.)*, 10th ed.; Chinese Pharmacopoeia Commission: Beijing, China, 2015.
22. Smeraldi, J.; Ganesh, R.; Safarik, J.; Rosso, D. Statistical evaluation of photon count rate data for nanoscale particle measurement in wastewaters. *J. Environ. Monit.* **2012**, *14*, 79–84. [CrossRef]
23. Vysotskii, V.V.; Uryupina, O.Y.; Gusel'nikova, A.V.; Roldugin, V.I. On the feasibility of determining nanoparticle concentration by the dynamic light scattering method. *Colloid J.* **2009**, *71*, 739–744. [CrossRef]
24. Jung, F.; Thurn, M.; Krollik, K.; Li, D.; Dressman, J.; Alig, E.; Fink, L.; Schmidt, M.U.; Wacker, M.G. Sustained-release hot melt extrudates of the weak acid TMP-001: A case study using PBB modelling. *Eur. J. Pharm. Sci.* **2021**, *160*, 23–34. [CrossRef] [PubMed]
25. Jung, F.; Thurn, M.; Krollik, K.; Gao, G.F.; Hering, I.; Eilebrecht, E.; Emara, Y.; Weiler, M.; Gunday-Tureli, N.; Tureli, E.; et al. Predicting the environmental emissions arising from conventional and nanotechnology-related pharmaceutical drug products. *Environ. Res.* **2021**, *192*, 110219. [CrossRef] [PubMed]
26. Hansmann, S.; Miyaji, Y.; Dressman, J. An in silico approach to determine challenges in the bioavailability of ciprofloxacin, a poorly soluble weak base with borderline solubility and permeability characteristics. *Eur. J. Pharm. Sci.* **2018**, *122*, 186–196. [CrossRef] [PubMed]
27. Hansmann, S.; Darwich, A.; Margolskee, A.; Aarons, L.; Dressman, J. Forecasting oral absorption across biopharmaceutics classification system classes with physiologically based pharmacokinetic models. *J. Pharm. Pharmacol.* **2016**, *68*, 1501–1515. [CrossRef]
28. Janas, C.; Mostaphaoui, Z.; Schmiederer, L.; Bauer, J.; Wacker, M.G. Novel polymeric micelles for drug delivery: Material characterization and formulation screening. *Int. J. Pharm.* **2016**, *509*, 197–207. [CrossRef]
29. Wacker, M.G.; Lu, X.; Burke, M.; Nir, I.; Fahmy, R.; Zaidi, K. Testing the in-vitro product performance of nanomaterial-related drug products: View of the USP Expert Panel. *Pharmacop. Forum* **2021**, *47*, 1–14.
30. Bou-Abdallah, F.; Sprague, S.E.; Smith, B.M.; Giffune, T.R. Binding thermodynamics of Diclofenac and Naproxen with human and bovine serum albumins: A calorimetric and spectroscopic study. *J. Chem. Thermodyn.* **2016**, *103*, 299–309. [CrossRef]
31. Auler, J.; Espada, E.; Crivelli, E.; Quintavalle, T.B.G.; Kurata, A.; Stolf, N.; Issy, A.M.; Paschoa, O.E.D.; Danhof, M.; Breimer, D.; et al. Diclofenac plasma protein binding: PK-PD modelling in cardiac patients submitted to cardiopulmonary bypass. *Braz. J. Med. Biol. Res.* **1997**, *30*, 369–374. [CrossRef]
32. Wang, D.; Zhang, Y.; Liu, Y.-N.; Wang, J. Estimation of Binding Constants for Diclofenac Sodium and Bovine Serum Albumin by Affinity Capillary Electrophoresis and Fluorescence Spectroscopy. *J. Liq. Chromatogr. Relat. Technol.* **2008**, *31*, 2077–2088. [CrossRef]
33. European Directorate for the Quality of Medicines & Healthcare. *European Pharmacopeia (Ph. Eur.)*, 10th ed.; Council of Europe: London, UK, 2021.
34. Olejnik, A.; Goscianska, J.; Nowak, I. Active Compounds Release from Semisolid Dosage Forms. *J. Pharm. Sci.* **2012**, *101*, 4032–4045. [CrossRef] [PubMed]

Drug Delivery and Translational Research
https://doi.org/10.1007/s13346-022-01263-x

ORIGINAL ARTICLE

Encapsulation and release of hydrocortisone from proliposomes govern vaginal delivery

Marc-Phillip Mast[1,2] · Letícia Mesquita[3,4] · Kennard Gan[6] · Svetlana Gelperina[7] · José das Neves[3,4,5] · Matthias G. Wacker[6]

Accepted: 14 November 2022

Abstract

Topical preparations of hydrocortisone can be used for the anti-inflammatory treatment of the female genital area. Although the drug is a low-strength corticosteroid, systemic absorption and distribution of the drug are the most common safety risks associated with this therapy. In the current investigation, we elucidate the physicochemical properties of lipid-based drug carrier systems that govern the local bioavailability of hydrocortisone for intravaginal administration. For this purpose, we compared various proliposome formulations with a commercial cream. Depending on the availability of physiological acceptors, encapsulation and drug release from the lipid phase were found to be the most important drivers of drug bioavailability. The high permeability of hydrocortisone leads to rapid transport of the drug across the mucosal cell layer as indicated by experiments using HEC-1-A and CaSki cell monolayer models. Under sink conditions, differences in the release from the liposomes as determined in the Dispersion Releaser were almost negligible. However, under non-sink conditions, the drug release plateaued at levels corresponding to the encapsulation efficiency. After redispersion, all liposomal formulations performed better than the commercial drug product indicating that the encapsulation into the lipid phase is the main driver sustaining the release.

Keywords Vesicles · Liposomes · Nanocarrier · Drug delivery · In vitro dissolution · Permeability

✉ José das Neves
j.dasneves@i3s.up.pt

✉ Matthias G. Wacker
matthias.g.wacker@nus.edu.sg

Marc-Phillip Mast
marc-phillip.mast@itmp.fraunhofer.de;
mast@em.uni-frankfurt.de

[1] Fraunhofer Institute for Translational Medicine and Pharmacology ITMP, Theodor-Stern-Kai 7, 60596 Frankfurt/Main, Germany

[2] Goethe University, Max-Von-Laue-Straße 9, 60438 Frankfurt/Main, Germany

[3] i3S—Instituto de Investigação e Inovação em Saúde, Universidade do Porto, 4200-135 Porto, Portugal

[4] INEB—Instituto de Engenharia Biomédica, Universidade do Porto, Rua Alfredo Allen 208, 4200-135 Porto, Portugal

[5] IUCS—Instituto Universitário de Ciências da Saúde, Universidade do Porto, 4585-116 Gandra, Portugal

[6] Department of Pharmacy, Faculty of Science, National University of Singapore, 4 Science Drive 2, 117544 Singapore, Singapore

[7] D. Mendeleev University of Chemical Technology of Russia, Miusskaya pl. 9, 125047 Moscow, Russia

Abbreviations

ANOVA	Analysis of variance
β-CD	Methyl-β-cyclodextrin
C	Cholesterol
Caco-2	Carcinoma colon
CaSki	Human cervical carcinoma
CC_{50}	Half-maximal cytotoxic concentration
CE	Cellulose ester
DLS	Dynamic light scattering
DSC	Differential scanning calorimetry
EE%	Encapsulation efficiency
EPC	Egg phosphatidylcholine
f1	Difference factor
f2	Similarity factor
HBSS	Hank's Balanced Salt solution
HEC-1-A	Human endometrial adenocarcinoma
HPLC-UV	High-performance liquid chromatography with ultraviolet detection
LOD	Limit of detection
LOQ	Limit of quantitation
MWCO	Molecular weight cutoff
P_{app}	Apparent permeability coefficients
PDI	Polydispersity index

Published online: 30 December 2022

PER	Permeability enhancement ratio
PTDR	Pharma Test Dispersion Releaser
PTFE	Polytetrafluoroethylene
SPC	Soy phosphatidylcholine
sVSF	Simplified vaginal simulant fluid
SE	Standard error
SD	Standard deviation
TEER	Transepithelial electrical resistance
TEM	Transmission electron microscopy
US-FDA	United States Food and Drug Administration

Introduction

Topical formulations for the treatment of the vagina such as anti-infectives (e.g., for vulvovaginal candidiasis or bacterial vaginosis) or contraceptives (e.g., spermicides) are well-established. Vaginal delivery to achieve systemic absorption is less common, although some drugs (e.g., sexual hormones used for contraception or replacement therapy) can be extensively absorbed through the vaginal mucosa. Compared to the oral route of administration, the first-pass metabolism is avoided and systemic adverse reactions are typically reduced due to the lowered dose [1]. Currently, traditional formulation approaches including creams, gels, tablets, or foams are frequently used. They are easy to produce at a larger scale and often have high shelf life and stability. Still, these dosage forms may be uncomfortable for the patient due to a certain leakage or exhibit short residence times which affect the efficacy and patient compliance [2]. Novel vaginal delivery systems including nanoparticles, liposomes, or niosomes have been developed to overcome these issues [3, 4]. They exhibit improved distribution and a prolonged retention time at the site of action. Depending on their release characteristics, they are balancing the local and systemic drug concentrations leading to an optimized risk–benefit ratio [5, 6]. Regarding hydrocortisone which served as a model drug for this investigation, the clinical use to treat inflammation of the vaginal mucosa is certainly also affected by concerns of systemic side effects which are even more likely considering the structural similarities to steroid hormones that have excellent absorption behavior.

Liposomal carriers in particular have a long history of medical and non-medical use. Even before the approval of Doxil® by the United States Food and Drug Administration (US-FDA) in 1995, liposomal carriers were widely applied by the cosmetics industry globally [7]. They are composed of hollow spherical vesicles with at least one phospholipid bilayer. While hydrophilic drugs can be encapsulated in the aqueous compartment, lipophilic compounds are often integrated into the outer membrane. Liposomes are commonly prepared at the lab scale using the thin-film hydration method [8]. A thin film of phospholipids is created by the evaporation of the organic solvent used for the dissolution of the lipid phase. When mixed with water, hydration of the phospholipids leads to spontaneous self-assembly of vesicles [8]. The encapsulation efficiency (EE%) depends on the physicochemical properties of the drug substance as well as the type of phospholipids used for their preparation [9–12]. Additionally, the cholesterol content and further processing including the application of shear and extrusion steps impact their properties [10, 13]. Liposomes are commonly well-tolerated and have been used clinically since the 1990s. Their use for vaginal drug delivery is currently in pre-clinical research [2, 14, 15]. Their modification with biocompatible and mucoadhesive polymers may be performed to increase the residence time at the administration site [16].

Despite the aforementioned benefits, liposomes exhibit chemical and physical stability issues due to the oxidation and hydrolysis of phospholipids and the diffusion of drug molecules into the continuous phase [17]. This may result in a reduced EE% and aggregation of the vesicles [18, 19]. Proliposomes were designed to overcome these stability issues. Depending on the vehicle, they include proliposomes in solid dispersion [20, 21] or organic solution [22]. Sorbitol, mannitol, or cellulose particles are coated with a thin film of phospholipids to synthesize solid proliposomes. They can be produced using spray drying [23, 24], fluidized bed coating [13, 25, 26], film deposition on carrier method [27], and supercritical anti-solvent methods [28, 29]. Common administration routes of proliposomes include oral [30], transdermal [31], pulmonary [32], and vaginal delivery [33].

Hydrocortisone is a glucocorticoid with mild anti-inflammatory properties. It is currently used in the systemic and/or topical treatment of anaphylaxis, arthritis, dermatitis, asthma, or chronic obstructive pulmonary disease. The drug can further be used vaginally to treat vulvovaginal lichen planus or to reduce perineal pain after vaginal birth [34, 35]. The glucocorticoid exhibits poor aqueous solubility and high intestinal permeability [36].

Vaginal absorption of hydrocortisone in humans is not well-documented; however, animal data indicate extensive systemic exposure [37]. Of note, these observations were made when the drug was administered to rabbits using a 10% ethanolic solution and thus may not be representative of the human situation. Still, the vagina is a well-known absorption site of steroids. Topical delivery systems that delay the release could mitigate potential side effects such as a weakened immune response or headache. Also, delayed absorption could prolong the anti-inflammatory effect and even stronger glucocorticoids could be used.

Considering that local inflammation is the main indication for vaginal hydrocortisone therapy, we elucidated the physiological drivers of drug absorption from this administration site using different assay systems including drug release and permeation behavior. In this context, four new

proliposome formulations of hydrocortisone were prepared. They were characterized regarding their particle size, size distribution, EE%, and morphology after rehydration. Also, we used differential scanning calorimetry (DSC) to confirm the absence of crystalline hydrocortisone. Afterward, we used a semi-permeable membrane system to study the permeation of the drug and all four formulations across cell monolayer models that were shown relevant to vaginal drug delivery [38–42]. CaSki (human cervical carcinoma) and HEC-1-A (human endometrial adenocarcinoma) cell lines were used for these experiments. Additionally, we studied the drug release behavior from each formulation with and without maintaining sink conditions. For this study, the Pharma Test Dispersion (PTDR) Releaser technology was used [43, 44]. In this context, sink conditions refer to an experimental design in which the drug concentrations in each release experiment do not exceed at least one-third of the drug solubility in the donor compartment of the PTDR.

Materials and methods

Chemicals and materials

Spectra/Por® 6 cellulose ester (CE) dialysis membranes with a molecular weight cutoff (MWCO) of 50 kDa and a flat diameter of 28 mm were purchased from VWR International GmbH (Darmstadt, Germany). Hydrocortisone (> 98%), D-sorbitol (> 98%), cholesterol (C; > 99%), and methyl-β-cyclodextrin (β-CD) were purchased from Sigma-Aldrich (Taufkirchen, Germany). For liposome preparation, soy phosphatidylcholine (SPC) S100 and egg phosphatidylcholine (EPC) E80 were kindly gifted by Lipoid GmbH (Ludwigshafen, Germany). Ebenol® cream (Strathman GmbH & Co. KG, Hamburg, Germany) containing 0.5% hydrocortisone was purchased from a local pharmacy. It consists of carbomer, dimethicone, cetostearyl alcohol, water, glycerol, glycerol monostearate, potassium sorbate, medium-chain triglyceride, sodium edetate, octyl dodecanol, tromethamine, and oleyl oleate. All other chemicals were of analytical grade or equivalent and used as received. Hank's Balanced Salt solution (HBSS) and rat tail collagen type I were purchased from Thermo Fisher (Waltham, MA, USA). Ultra-pure water (Ultra Clear® system, Evoqua water technologies, Günzburg, Germany) was used in all experiments.

Manufacture of proliposomes

Initially, sorbitol powder within a particle size range of 90–180 µm was collected using two sieves with corresponding mesh sizes (WEPA Apothekenbedarf GmbH & Co. KG, Hillscheid, Germany). Afterward, the proliposomes were prepared by using a modified thin-film method. Therefore, phospholipids (250 mg) and hydrocortisone (15 mg) were dissolved in a chloroform–methanol mixture (8.25 mL; 4:1 (v/v)) in a 100-mL round-bottom flask. After adding sorbitol (2.5 g), the organic solvents were slowly evaporated under a vacuum using a Büchi Rotavapor R-114 (Büchi Labortechnik AG, Flawil, Schweiz). The resulting dry powder was carefully collected, and agglomerates were removed with a 180-µm sieve. Proliposomes with cholesterol were prepared by replacing 20 mol% of the lipid phase with cholesterol. Blank formulations were prepared similarly, without adding hydrocortisone.

Physicochemical characterization of proliposomes

Quantification of encapsulated hydrocortisone

The total amount of hydrocortisone (W_{total}) in the drug formulation was determined by high-performance liquid chromatography with ultraviolet detection (HPLC–UV). Briefly, each formulation (30 mg) was dissolved in 5 mL methanol and diluted before quantification. Afterward, the proliposomal formulation (50 mg) was hydrated with 1000 µL of ultrapure water. Before centrifugation (20,800 rcf, 15 min, 25 °C) using a Centrifuge 5430 R with an FA-45–30-11 rotor (Eppendorf AG, Hamburg, Germany), the liposomes were kept at room temperature for 30 min. The supernatant was appropriately diluted, and the amount of free hydrocortisone (W_{free}) was quantified. The EE% was calculated using Eq. 1:

$$EE\% = \frac{W_{total} - W_{free}}{W_{total}} \times 100\% \quad (1)$$

Dynamic light scattering

After preparing liposomal dispersions, the intensity mean diameter (z-average) and polydispersity index (PDI) of the proliposomal formulation were measured by dynamic light scattering (DLS) with a Malvern Zetasizer Nano-ZS (Malvern Panalytical Ltd., Malvern, UK) with a backscatter detector at an angle of 173°. The final dispersion was diluted 20-fold before the measurement. The attenuation was between 6 and 9 in all measurements. The same dispersion was also used to measure the zeta potential with a dip cell (Malvern Panalytical Ltd., Malvern, UK).

Electron microscopy

Proliposomal powder (30 mg) was mixed with 50 µL water for 1 min and further diluted with 950 µL water and again mixed for 1 min. The resulting dispersion (20 µL) was transferred to a coated copper grid. The liposomes were stained

with a 2% (m/v) uranyl acetate solution for 30 s and washed three times with water. Afterward, the characteristics of the liposomes were examined by transmission electron microscopy (TEM). A transmission electron microscope CM 12 (Philips, Amsterdam, Netherlands) equipped with a Gatan module 782 (ES 500 W) was used for this purpose.

Dynamic scanning calorimetry

The proliposomal formulations were characterized by dynamic scanning calorimetry (DSC). A DSC 6000 (PerkinElmer Inc., Waltham, MA, USA) equipped with an Intracooler II (PerkinElmer Inc.) was used. The measurement started at 20 °C and ended at 280 °C with a heating rate of 10 °C per minute. A constant nitrogen gas stream of 20.0 mL/min was maintained. Reference measurements were carried out with hydrocortisone, cholesterol, sorbitol, and all formulations. Each substance or formulation (5–15 mg) was weighed into 50-µL aluminum pans (PerkinElmer Inc.) prior to analysis.

Quantification of hydrocortisone

Hydrocortisone concentrations were quantified using a Chromaster high-performance liquid chromatography (HPLC) system (VWR Hitachi, Tokyo, Japan). An HPLC pump (5160), a column oven (5310), an autosampler (5260), and a UV–Vis detector (5420) were used. The mobile phase consisted of 54% (v/v) of methanol and 46% (v/v) of 0.1% (v/v) of trifluoroacetic acid in ultrapure water. Separation was carried out in a reversed-phase column (LiChroCART cartridge 125×4 mm packed with LiChrospher RP-18 silica gel, 5 µm, 100A, Merck KGaA, Darmstadt, Germany). The flow rate was set to 1 mL/min and a temperature of 35 °C was maintained over the run time of 9 min. The detection wavelength was 254 nm [45].

Samples were diluted with mobile phase and a volume of 40 µL was injected into the HPLC system. Linearity was demonstrated in the concentration range of 0.03–3 µg/mL. The limit of detection (LOD) and limit of quantitation (LOQ) were determined to be 8 and 26 ng/mL, respectively.

Drug solubility

A modified shake-flask method was used to determine the solubility of hydrocortisone in three different media. Briefly, an excess of the drug substance was suspended in a volume of 4 mL of each medium. The suspensions were stirred at 550 rpm in an incubator (INCU-Line® Standard IL 68R, VWR International GmbH, Darmstadt, Germany) at 37 °C for 24 h. Afterward, the solid excess was separated with a polytetrafluoroethylene (PTFE) syringe filter (13 mm diameter, 0.45 µm pore size, VWR International GmbH, Darmstadt, Germany) whereby the first 1 mL of the drug suspension was discarded to saturate the filters beforehand. The filtrates were diluted and analyzed by HPLC–UV. All experiments were performed in triplicate.

Cytotoxicity in HEC-1-A and CaSki cells

Proliposomes with and without hydrocortisone as well as pure hydrocortisone as a reference were tested for cytotoxicity using the resazurin reduction assay. The ability of cells to reduce resazurin provides a measure of mitochondrial metabolism, which is a marker of cell viability [46]. Human CaSki cervical and HEC-1-A endometrial cell lines were used as representative epithelial cell models of the female genital tract. CaSki and HEC-1-A cells were maintained in RPMI 1640 medium or McCoy's 5A medium, respectively, supplemented with 10% (v/v) fetal bovine serum, 100 U/mL penicillin, and 100 µg/mL streptomycin at 37 °C, 95% RH, and 5% CO_2. Genital cells were added to 96-well plates at a density of 5000 cells/well and incubated for 24 h. Cells were then incubated for 24 h with the different formulations at various concentrations in the range of 0.001–10 µg/mL, expressed as real or virtual hydrocortisone content (i.e., same amount of drug-free vesicles as in the case of drug-loaded vesicles). Culture medium and 1% (w/v) Triton X-100 were also tested as positive and negative controls, respectively. Finally, cells were washed twice with phosphate-buffered solution (pH 7.4) and incubated for 3 h with resazurin at a concentration of 10 µg/mL in the medium. Fluorescence from supernatants was measured at 590/530 nm and used to calculate the viability percentage. The obtained results were used to determine half-maximal cytotoxic concentration (CC_{50}) values using the log-logistic regression of viability vs. concentration data using Prism 8 (GraphPad, San Diego, CA, USA).

In vitro permeability experiments

CaSki and HEC-1-A cell monolayer models were used for testing drug permeability and cell association. Cells were acquired from ATCC (Manassas, VA, USA) and models have been described in detail previously [38, 39]. Briefly, cell monolayers were generated by seeding cells (3×10^5 cells/cm^2) on Millicell® cell culture membrane (Merck-Millipore, Darmstadt, Germany) inserts with 1 µm pore size and an area of 1.1 cm^2 that were pre-coated with rat tail collagen type I (10 µg/cm^2). Cells were maintained for 7–8 days in culture and the transepithelial electrical resistance (TEER) was determined periodically using an EVOM voltohmmeter with chopstick electrodes (World Precision Instruments, Sarasota, FL, USA). The medium was renewed every 2–3 days. Experiments were performed by removing the medium from apical and basolateral compartments and by replacing it with 500

µL of each sample dissolved/dispersed in HBSS and 1500 µL of plain HBSS, respectively. Samples were added at a concentration of 5 µg/mL (expressed in hydrocortisone content) based on the results obtained for cytotoxicity. Samples (500 µL) were collected from the basolateral compartments and replaced with fresh HBSS at 0.25, 0.5, 1, 2, 3, and 4 h. Medium from apical compartment and membrane supports containing cell monolayers were collected after the last time point. Cell monolayers were mixed with 1 mL acetonitrile in tubes and vortexed. Homogenates were then centrifuged, and supernatants were collected. TEER was monitored throughout the experiments. All samples were stored at − 20 °C until quantification.

Apparent permeability coefficients (P_{app}) were calculated from the drug levels measured in the basolateral compartment according to the following equation (Eq. 2):

$$P_{app} = \frac{Q}{ACt} \tag{2}$$

where Q is the total amount of permeated hydrocortisone, A is the permeation area, C is the initial drug concentration of hydrocortisone in the apical compartment at the beginning of the experiment, and t is the total time of the experiment [39]. The permeability enhancement ratio (PER) was additionally calculated by dividing P_{app} values when using drug-loaded formulations by P_{app} values of the plain drug for a given type of cell monolayer. Experiments were performed in triplicate.

Drug release using the pharma test dispersion releaser

All experiments were carried out with a commercial Dispersion Releaser system (Pharma Test Apparatebau AG, Hainburg, Germany) in a PTWS 120S dissolution apparatus II (Pharma Test Apparatebau AG, Hainburg, Germany) following the specifications of the USP. A mini vessel (250 mL) following the specifications of the Chinese Pharmacopeia [47] was used as the acceptor compartment. The vessels were filled with 120 mL of filtered and de-gassed (40 °C, 300 mbar, 30 min) medium. The membrane was pre-treated according to the instructions of the manufacturer, mounted around the donor chamber, and sealed with two O-rings. The volume of the donor compartment was 3.4 mL leading to a total volume of 123.4 mL in the final setup. The membrane around the donor chamber has a surface area of 10.95 cm^2 and a thickness of 0.008 cm.

Each vessel (acceptor compartment) was filled with a volume of 120 mL medium of simplified vaginal simulant fluid (sVSF) pH 4.2 [48]. When determining the membrane permeation rate constant, 4.5 mM of β-CD was added to maintain sink conditions. Also, hydrocortisone (1.25 mg) was dissolved in 3.4 mL of the medium and injected into the donor compartment. For release testing of proliposomes, the formulation (amount equivalent to 1.25 mg of hydrocortisone) was dispersed in the same amount of water. The liposomes spontaneously formed and were added to the donor chamber. Release medium was added to a total volume of 3.4 mL to avoid diffusion into the donor chamber. The dissolution tester operated at 37 ± 0.5 °C and 50 rpm. Samples (0.2 mL) were taken at 0.25, 0.5, 1, 2, 3, 4, 5, 6, 7, and 8 h, and the volume was replenished with fresh medium. For release experiments with Ebenol® cream, 250 mg semisolid formulation was weighed into the donor chamber and prefilled with 3 mL of medium. The release conditions were maintained as described above. All experiments were performed in triplicate. The difference factor (f1) and similarity factor (f2) were calculated for comparison of the release profiles.

Statistical analysis

One-way analysis of variance (ANOVA) was performed using Origin Pro (OriginLab, Northampton, MA, USA) to analyze the differences between the different formulations and free hydrocortisone. Tukey's HSD test was used for post hoc comparisons. Statistical significance was accepted for p values below 0.05.

Results and discussion

Four different proliposomal formulations of the model drug hydrocortisone were prepared to deliver the drug locally in the vaginal microenvironment. A commercial drug product, Ebenol® cream, and the drug substance were used as a comparison. To elucidate, the parameters affecting the exposure of the vagina to hydrocortisone, drug release, and permeability rate were taken into consideration. The proliposomes were prepared from SPC or EPC in the presence of 0 or 20 mol% of cholesterol. Sorbitol served as an inert carrier material during proliposome preparation. To exclude the presence of crystalline hydrocortisone in the drug formulations, they were further characterized by DSC. Additionally, after hydration of the proliposomes, their size, polydispersity index, and EE% were measured. The permeation of the various hydrocortisone drug formulations through a representative cell layer system was measured in CaSki (cervix carcinoma) and HEC-1-A (human endometrial adenocarcinoma) cells. To determine the drug release, we used the PTDR technology and a simplified vaginal simulant fluid (sVSF) under sink and non-sink conditions.

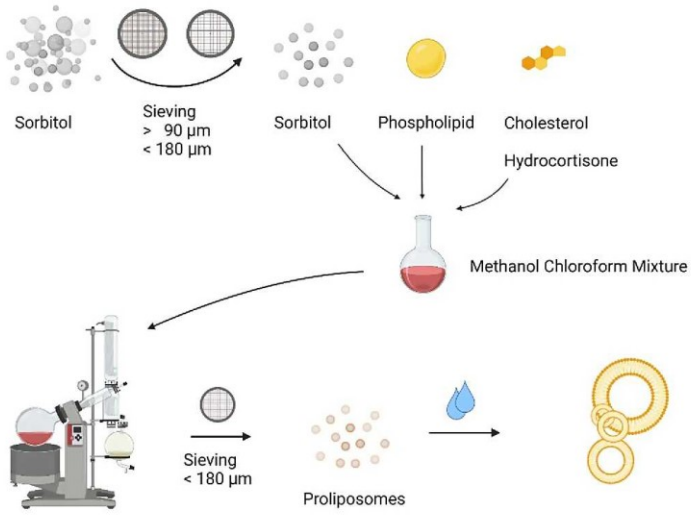

Fig. 1 Preparation of proliposomes by the coating of sorbitol with a thin film of phospholipids followed by hydration and formation of liposomes

Proliposome synthesis and physicochemical characterization

Liposomes are often used in the delivery of poorly soluble compounds such as hydrocortisone. At a smaller scale, liposomes can be prepared using the thin-film method through which vesicles assemble spontaneously after the hydration of phospholipids [8]. Proliposomes utilize an inert soluble carrier material such as sorbitol, mannitol, or sucrose. Once the proliposomes are exposed to water, the carrier dissolves fast and the phospholipids form the liposomal delivery system in situ. The preparation of these liposomes is presented in Fig. 1.

After hydration, the liposomes were characterized in terms of their size, PDI, and EE%. Results are summarized in Table 1. The vesicles were similar in size as indicated by their mean diameters. The addition of cholesterol only affected the size slightly when egg phosphatidylcholine (EPC) was used as the phospholipid component. Mean PDI values ranged from 0.437 to 0.534, indicating a broad size distribution. These values could be easily reduced to values below 0.3 by extrusion [49] but, however, would require additional processing post-hydration. Here, we specifically investigated the performance of a solid dosage form using in situ liposome formulation, which guarantees higher physical and chemical stability over time. Still, the PDI was within the measurable limits (below 0.7) [49]. The liposomes differed in their zeta potential depending on their phospholipid composition. SPC liposomes were slightly negatively charged ranging from −6 to −12 mV. Liposomes prepared with EPC featured even lower zeta potential values at about −34 mV (Table 1, $p<0.05$). The different purities of EPC and SPC (80% vs. 100%) may be responsible for the difference in charge. As indicated by earlier studies, negative liposomes are not strongly mucoadhesive due to the negatively charged mucin [3, 15]. More mucoadhesive materials tend to agglomerate in the presence of mucin leading to a faster clearance. The

Table 1 Physicochemical characteristics (particle size, PDI, zeta potential, encapsulation efficiency (EE%), and hydrocortisone content) of the four different proliposomal formulations. The values are expressed as mean±SD ($n=3$). The asterisk (*) denotes a significant difference ($p<0.05$) when compared with the formulation containing EPC

Formulation	Egg PC	Soy PC	Cholesterol (C)	Size (nm)	PDI	Zeta potential (mV)	EE% (%)	Drug conc. (%)
EPC	+			213±4	0.437±0.016	−34±3	20.4±1.9	0.33±0.02
EPC+C	+		+	230±9	0.426±0.014	−34±2	17.9±2.0	0.40±0.04
SPC		+		215±2	0.448±0.015	−6±1*	28.4±0.9*	0.52±0.06
SPC+C		+	+	213±4	0.534±0.130	−13±2*	24.5±2.3*	0.43±0.07

current drug delivery system forms a highly stable dispersion as required for topical delivery.

When added during preparation, cholesterol is embedded into the phospholipid bilayer of the liposomes and increases the rigidity of the membrane. Although there was no effect on size or size distribution, an effect on the EE% was expected. Hydrocortisone and cholesterol have very similar chemical structures; hence, both molecules are assumed to compete for the same site of interactions within the phospholipid bilayer. A slight but not significant reduction in the EE% was indeed observed for EPC liposomes. For SPC liposomes, the reduction of approximately 4% was significant ($p < 0.05$). The overall hydrocortisone content of the liposomal formulations ranged from 0.33 to 0.52%.

Morphological characterization of reconstituted proliposomes

The proliposomes were reconstituted in water and analyzed for morphological characteristics by TEM (see "Electron microscopy"). Liposomes of various sizes ranging from approximately 50 to 2500 nm were observed (see Fig. 2). The method allows the morphology of the liposomes to be studied in the dried state only. Even though the particle size of dried liposomes is often found to be smaller in TEM micrographs as compared to the hydrodynamic diameter observed by DLS, the staining procedure may also capture lipid-coated sorbitol particles. Hence, the presence of larger particles was an expected effect. A significant fraction of spherical vesicles confirms vesicle formation and supports findings made by DLS.

When using these liposomes for the delivery of hydrocortisone, the absence of crystalline drug is important. Hydrocortisone crystals would potentially be captured in the EE% and would be difficult to distinguish from the liposomal carrier. Hence, we conducted DSC measurements to investigate crystallinity.

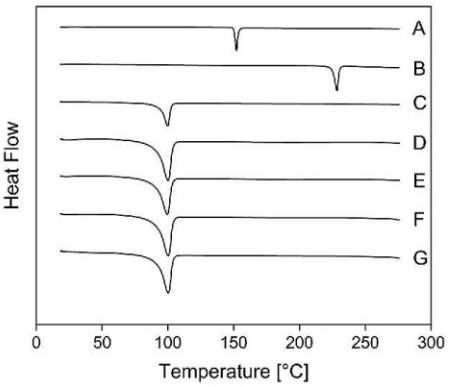

Fig. 3 Superimposed differential scanning calorimetry thermographs of cholesterol (**A**), hydrocortisone (**B**), sorbitol (**C**), and proliposomal formulations with EPC (D), EPC + C (E), SPC (F), and SPC + C (G)

Dynamic scanning calorimetry analysis of proliposomes

DSC analysis was conducted to investigate the physical state of hydrocortisone in the proliposomes (Fig. 3). Excipients used for the formulation were also measured separately. Sorbitol, cholesterol, and hydrocortisone exhibited sharp endothermic peaks at their corresponding melting points. The phase transition of cholesterol was measured at 151.6 °C while the melting point of hydrocortisone was observed at 228.1 °C (see Fig. 3A and B respectively). Sorbitol shows an endothermic peak at 99.9 °C that corresponds to the melting point of its gamma polymorph [50]. The enthalpy (ΔH) of the phase transition was 176.6 J/g (see Fig. 3C). This corresponds to previous investigations [50–52].

There was no indication of a phase transition at the melting points of cholesterol or hydrocortisone observed for

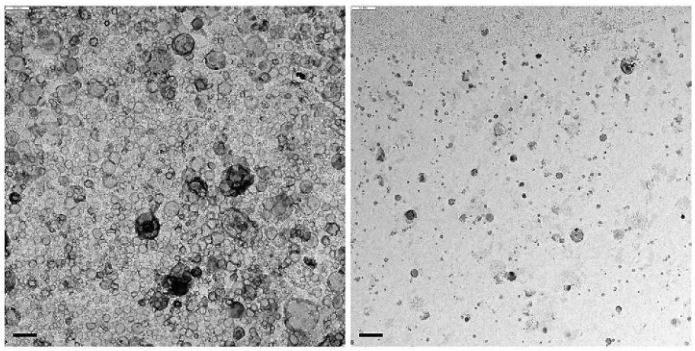

Fig. 2 TEM micrographs of selected proliposomal formulations SPC (left image) and SPC + C (right image). Both formulations contain hydrocortisone. The scale bar denotes 1000 nm (black bar in the bottom left corner)

any of the proliposomal formulations. Only the peak corresponding to sorbitol was reliably detected. This suggests that hydrocortisone was embedded into the phospholipid bilayer of the proliposomes. Furthermore, the high lipid content makes the presence of a large crystalline fraction unlikely. However, the sensitivity of the DSC method would still allow a residual fraction of hydrocortisone to occur in the crystalline state. When testing the physical mixture, hydrocortisone peaks were only observed for two preparations (EPC, EPC + C, data not shown).

ΔH of the sorbitol peak for the proliposomal formulations was reduced by about 17% from 144.9 to 149.8 J/g as compared to pure sorbitol with ΔH of 176.6 J/g. This could be due to an interaction of the phospholipids with the carrier sorbitol. Recrystallization during the evaporation process may have partially altered the polyol's physical state, namely its polymorphism [50]. Similar findings have also been observed when using mannitol for the production of proliposomes [53].

Drug solubility

The solubility of hydrocortisone in simplified vaginal simulant fluid (sVSF) provides more information on the rate-limiting steps during drug release from carrier systems. Commonly, liberation from liposomes is governed by the availability of suitable binding partners that solubilize the drug in its microenvironment. sVSF was used to measure the solubility at physiological core temperature (37 °C) [48]. The medium simulates the vaginal fluid of healthy women regarding pH (4.2), buffer capacity, and osmolality. As HBSS was used as a cell culture medium during the permeability experiments, hydrocortisone solubility in HBSS was studied as well. Hydrocortisone exhibited poor aqueous solubility which was independent of pH (Table 2). Considering that the phospholipids employed for this development are not affected by pH [54], a mechanism of release that is not influenced by the ionization can be assumed. Solubility at both acidic and near-neutral pH values was very similar (0.39 ± 0.02 mg/mL) and comparable to previous findings [55]. This allows the drug to remain completely dissolved during the cell viability and permeability studies. For release experiments in the PTDR, the solubility did not allow the testing under sink conditions (drug concentration remains below 33% of drug solubility). Therefore, cyclodextrins (β-CD) were added to the medium increasing the solubility to 1.46 ± 0.01 mg/mL (Table 2).

Table 2 Equilibrium solubility of hydrocortisone in three different media after 24 h. The values are expressed as mean ± SD ($n = 3$)

Medium	pH	Temperature	Hydrocortisone solubility (mg/mL)
Simplified vaginal simulant fluid (sVSF)	4.2	37.0 °C	0.39 ± 0.02
sVSF with 4.5 mM methyl-β-cyclodextrin	4.2	37.0 °C	1.46 ± 0.01
HBSS	7.3 ± 0.1	37.0 °C	0.39 ± 0.02

Cytotoxicity of proliposomal formulations

A cytotoxic effect of the formulations on the cell layers had to be excluded to measure permeability. Cytotoxicity was evaluated by the resazurin reduction assay using HEC-1-A and CaSki cell lines. Both cell lines model the female genital tract. The reconstituted liposomal formulations with and without hydrocortisone, as well as hydrocortisone alone, were incubated for 24 h up to concentrations of 10 µg/mL (expressed as real or virtual hydrocortisone content).

Both cell lines were not affected when exposed to hydrocortisone and most of the liposomal samples (Table 3 and Supplementary Material, Fig. S1). Except for the blank SPC + C proliposomes (at 10 µg/mL) in HEC-1-A cells, all formulations were able to maintain viability above 70% which is the typical minimal value for a compound or a formulation to be considered potentially safe [56].

Overall, these data suggest that formulations possess low cytotoxicity. Accordingly, hydrocortisone concentrations of 5 µg/mL were used during the permeability studies.

Liposome-mediated permeability of hydrocortisone

Two cell monolayer models based on CaSki or HEC-1-A immortalized cells were selected to study the epithelial permeability of hydrocortisone either in the free form or formulated as liposomes. TEER was monitored during cell monolayer formulation, as well as during permeability

Table 3 Cytotoxicity of hydrocortisone and proliposomal formulations with or without hydrocortisone (blank) to CaSki and HEC-1-A cells, CC_{50} values

Sample	CC_{50} (µg/mL)	
	CaSki	HEC-1-A
Hydrocortisone	> 10	> 10
EPC + C	> 10	> 10
EPC	> 10	> 10
SPC	> 10	> 10
SPC + C	> 10	> 10
Blank EPC + C	> 10	> 10
Blank EPC	> 10	> 10
Blank SPC	> 10	> 10
Blank SPC + C	> 10	8.2

experiments to monitor the cell barrier integrity (Supplementary Material, Figs. S2 and S3). Although provided from adjacent genital sites, both cell systems have been widely used as models of the cervicovaginal epithelium to study drug permeability. They provide an approximation of in vivo drug absorption [57, 58].

Hydrocortisone permeability was similar for both cell monolayer models and varied between 37 and 70% of the total drug amount after 4 h (Fig. 4). The permeated amount of hydrocortisone steadily increased and, in some cases, appeared to peak between 2 and 4 h. The permeability profiles were very similar for the free drug and the hydrated proliposomes ($p > 0.05$). This led to relatively similar calculated P_{app} values, as summarized in Table 4. The liposomes were able to maintain or only mildly increase the permeability of hydrocortisone (PER values varied between 1.0 and 1.8). Interestingly, P_{app} values obtained for hydrocortisone in the present study are in line, even if tendentially lower, to those reported previously in Caco-2 cell monolayers ($17.5 \pm 4.1 \times 10^{-6}$ cm^2/s) [59]. Alongside the report of Corbo et al. on the extensive systemic exposure to hydrocortisone after vaginal administration of the drug to ovariectomized rabbits, these data further support the high absorption of hydrocortisone through this route [37].

For both cell monolayer models, P_{app} values for SPC liposomes were apparently higher than those for EPC vesicles (Table 4). However, this observation was not significant. Two different phospholipids were used to prepare the proliposomes (soybean vs. egg). Their heterogeneous fatty acid composition could potentially lead to different interactions with the vaginal epithelial cells. This could explain the rank order observed in the permeability. Additionally, cholesterol was found to be involved in the membrane permeability of small molecules and solutes. It influences drug permeation through cell-based membranes of various cell lines [60, 61]. However, in this work, the addition of cholesterol to the proliposomal formulations did not change the permeability of hydrocortisone significantly.

To explain the outcome of the permeation experiment, the EE% should be considered. There is no significant difference between the permeation rates; however, the rank order of formulations reflects their encapsulation. During hydration, approximately 70–80% of the hydrocortisone remains in the continuous phase which would make it difficult to discriminate between formulations in the permeation assay. Still, the encapsulated fraction represents a small but interesting influence. Therefore, the release studies were likely to provide a better explanation of these observations.

Table 4 P_{app} values of hydrocortisone in the free form or formulated as liposomes across CaSki or HEC-1-A cell monolayers. Values are expressed as mean ± SD ($n = 3$). Mean PER values are included for proliposomal formulations

Sample	P_{app} (cm^2/s × 10^{-6})		PER	
	CaSki	HEC-1-A	CaSki	HEC-1-A
Hydrocortisone	9.9 ± 1.4	8.7 ± 1.3	-	-
EPC	9.6 ± 1.6	10.8 ± 0.2	1.0	1.2
EPC + C	16.6 ± 5.2	12.7 ± 0.1	1.7	1.5
SPC	11.0 ± 1.1	16.0 ± 7.3	1.1	1.8
SPC + C	10.3 ± 3.2	10.2 ± 3.3	1.0	1.2

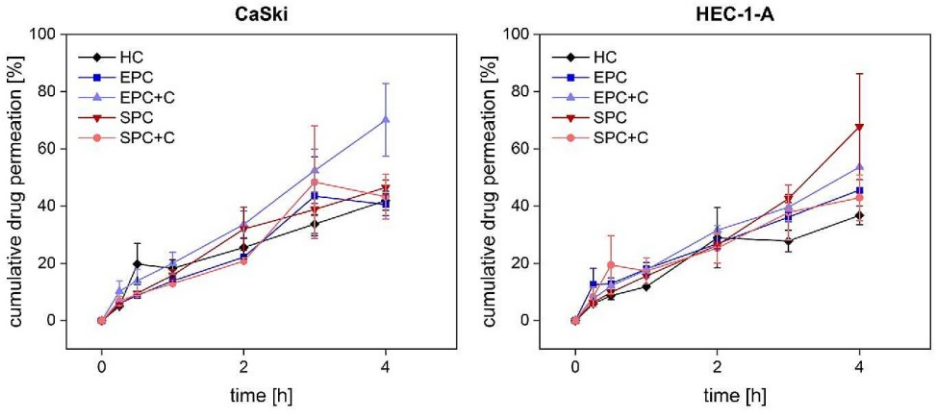

Fig. 4 Permeability profiles of hydrocortisone as either free drug or associated with proliposomal formulations in cell monolayers of CaSki (left side) and HEC-1-A (right side) cell lines. All values are expressed as mean ± SE ($n = 3$)

The hydrocortisone content in the cell monolayers was below the LOD. Thus, the amount becoming available could have reached a maximum of about 0.3% of the total dose. Noteworthy, other advantages can be advocated for the formulation strategy as well. For example, liposomal formulations applied in the vagina can establish adhesive interactions with the mucosal tissue and sustain drug residence at the site of absorption [33, 62]. Also, they can promote drug penetration, thus helping to reach deeper areas that also require anti-inflammatory action [63]. To quantify the influence of the encapsulated fraction, we investigated the release under sink and non-sink conditions.

Hydrocortisone release from liposomes

While the permeability experiment setup affords a cellular surface that requires both release and partitioning (into and out) of the cell layer to occur, the PTDR represents an aqueous environment where the acceptor phase is widely controlled by the medium composition. Hence, the release assay provides a higher resolution for the isolated release process and can be used to investigate the influences of a changing microenvironment. Also, in the PTDR setup, agitation of the donor compartment reduces the impact of the dialysis membrane on drug transport [43, 44]. The release from all four proliposome formulations and the permeation of hydrocortisone through the membrane were investigated. A commercial hydrocortisone cream, Ebenol®, was also used as a reference. When adding cyclodextrins to sVSF, all formulations performed similarly in terms of release behavior. Complete drug release was achieved within 4–6 h without any considerable differences in release rates (Fig. 5 left panel, $f1 < 15$ and $f2 > 50$). The cyclodextrins represent a suitable acceptor phase that attracts hydrocortisone molecules. At this elevated release rate, small differences cannot be discriminated.

In the absence of cyclodextrins, the solubility in sVSF gained more influence, and the rank order of the formulations could be established (Fig. 5 right panel). While proliposomes comprising EPC plateaued at approximately 82%, the total release from SPC liposomes reached 78–75%. The remaining non-released fraction matches the EE% for almost all drug formulations ("Proliposome synthesis and physicochemical characterization" section) except for SPC liposomes. The f1 and f2 values were calculated to qualify the similarity between the six release profiles under non-sink conditions. Here, we applied the f1 and f2 factors without reference to the US-FDA guideline on immediate release tablets which requires at least 85% release and 12 units to be tested. The coefficient of variation remains below 5% which is significantly lower than specified for immediate-release tablets. Also, in biorelevant medium, the second release phase is reached below 85% for some of the preparations. Setting a 10% average difference between two profiles ($f1 < 15$, $f2 > 50$) as the cutoff for a significant difference, the four proliposomal formulations were found to be similar. However, when the four proliposomal formulations were compared against HC and Ebenol® separately, the slower-releasing SPC and SPC + C formulations were found to be dissimilar to both HC and Ebenol®. Additionally, we

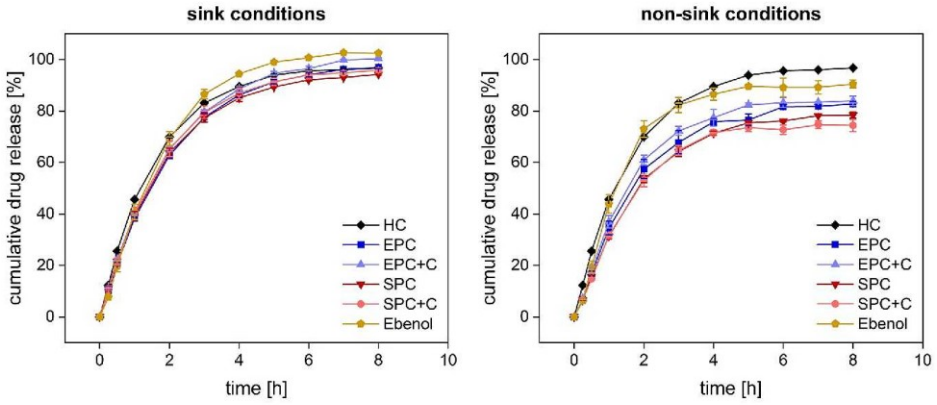

Fig. 5 Hydrocortisone release from proliposomes (EPC, EPC + C, SPC, and SPC + C formulations). Experiments were conducted under sink conditions with cyclodextrins as solubilizers (left) and under biorelevant non-sink conditions without cyclodextrins (right). Permeation of hydrocortisone through the membrane is indicated as HC for reference purposes (in both cases under sink conditions with cyclodextrins added). Values are expressed as mean ± SD ($n = 3$)

compared the 8-h values of the release profiles using Student's *t*-test ($p < 0.05$). Under sink conditions, there were no significant differences between the proliposomes and hydrocortisone. Under non-sink conditions, all formulations differed significantly from the hydrocortisone solution except for the Ebenol® cream.

Although more difficult to interpret due to the higher standard deviations, the same trends were observed in the permeability studies. EPC liposomes generally led to a faster permeation than SPC liposomes. The commercial cream did not delay the hydrocortisone release compared to the liposomal formulations and the release behavior is comparable to the hydrocortisone reference during the first 3 h. Afterward, the release plateaued at about 90% of the total drug amount. Because of their charge, these liposomes are not highly adhesive and are expected to moderately penetrate the upper mucus layer in which they may form a local depot [3, 15]. Combining the results of both, release and permeability experiments, the most important parameter involved in the performance of the proliposome is the EE%. It is mainly responsible for the fraction of hydrocortisone that undergoes a controlled release. Therefore, a higher EE% is likely to prolong the therapeutic effect.

Conclusions

Our experiments confirmed that the delivery of hydrocortisone from the proliposomes is strongly affected by drug solubility in the vaginal fluid and the encapsulation into the phospholipid bilayer of the vesicles. Hence, a higher EE% promotes sustained release and topical bioavailability. In this context, the high fluid volume in the PTDR should be considered. Even at this high volume, the differences between all formulation prototypes were apparent. Under physiological conditions, due to the much lower fluid volume available in the vagina, EE% would have an even stronger effect. Furthermore, the release behavior of the slowly-releasing SPC and SPC + C proliposomes was dissimilar to that of hydrocortisone and the commercial cream Ebenol®. Thus, SPC and SPC + C formulations are most likely to sustain the release. The high EE% is mainly responsible for an overall better performance than observed for the commercial product.

Supplementary Information The online version contains supplementary material available at https://doi.org/10.1007/s13346-022-01263-x.

Acknowledgements Marc-Phillip Mast acknowledges the State of Hessen for financial contributions to the LOEWE research center for Translational Medicine and Pharmacology (Frankfurt, Germany). Matthias G. Wacker acknowledges the Singaporean Ministry of Education (A-0004627-00-00) and the Resilience & Growth Fund of the National Research Foundation (A-0000065-09-00) for financial support. José das Neves acknowledges financing by Portuguese funds through FCT – Fundação para a Ciência e a Tecnologia/Ministério da Ciência, Tecnologia e Ensino Superior in the framework of the project "Institute for Research and Innovation in Health Sciences" (UID/BIM/04293/2019). This work was supported by the Ministry of Science and Higher Education of the Russian Federation (grant No. 075-15-2020-792, Unique identifier RF-190220X0031).

Author contribution Conceptualization: MPM, MGW; investigation: MPM, LM; writing—original draft preparation: MPM; writing—review and editing: MPM, KG, JdN, MGW, S.G.; funding acquisition: JdN, MGW; supervision: JdN, MGW, SG. All authors have read and agreed to the published version of the manuscript.

Funding All funding sources have been declared under Acknowledgements.

Availability of data and materials Materials are commercially available; data will be made available on request.

Declarations

Ethics approval Not applicable.

Conflict of interest The authors declare no competing interests.

References

1. das Neves J, Notario-Pérez F, Sarmento B. Women-specific routes of administration for drugs: a critical overview. Adv Drug Deliv Rev. 2021;176:113865.
2. Pavelić Ž, Škalko-Basnet N, Schubert R. Liposomal gels for vaginal drug delivery. Int J Pharm. 2001;219:139–49.
3. das Neves J, Amiji M, Sarmento B. Mucoadhesive nanosystems for vaginal microbicide development: friend or foe? WIREs Nanomed Nanobiotechnol. 2011;3:389–99.
4. Vanić Ž, Škalko-Basnet N. Nanopharmaceuticals for improved topical vaginal therapy: can they deliver? Eur J Pharm Sci. 2013;50:29–41.
5. Richardson JL, Whetstone J, Fisher AN, Watts P, Farraj NF, Hinchcliffe M, et al. Gamma-scintigraphy as a novel method to study the distribution and retention of a bioadhesive vaginal delivery system in sheep. J Control Release. 1996;42:133–42.
6. Vermani K, Garg S. The scope and potential of vaginal drug delivery. Pharm Sci Technol Today. 2000;3:359–64.
7. Patravale VB, Mandawgade SD. Novel cosmetic delivery systems: an application update. Int J Cosmet Sci. 2008;30:19–33.
8. Zhang H. Thin-film Hydration Followed by Extrusion Method for Liposome Preparation. In: D'Souza GGM, editor. Liposomes: Methods and Protocols. New York, NY: Springer New York 2017;17–22.
9. Batavia R, Taylor KMG, Craig DQM, Thomas M. The measurement of beclomethasone dipropionate entrapment in liposomes: a comparison of a microscope and an HPLC method. Int J Pharm. 2001;212:109–19.
10. Darwis Y, Kellaway IW. Nebulisation of rehydrated freeze-dried beclomethasone dipropionate liposomes. Int J Pharm. 2001;215:113–21.
11. Elhissi AMA, O'Neill MAA, Roberts SA, Taylor KMG. A calorimetric study of dimyristoylphosphatidylcholine phase transitions and steroid–liposome interactions for liposomes prepared by thin film and proliposome methods. Int J Pharm. 2006;320:124–30.
12. Shah H, Madni A, Rahim MA, Jan N, Khan A, Khan S, et al. Fabrication, in vitro and ex vivo evaluation of proliposomes and

liposomal derived gel for enhanced solubility and permeability of diacerein. PLoS ONE. 2021;16: e0258141.
13. Gala RP, Khan I, Elhissi AMA, Alhnan MA. A comprehensive production method of self-cryoprotected nano-liposome powders. Int J Pharm. 2015;486:153–8.
14. das Neves J, Nunes R, Machado A, Sarmento B. Polymer-based nanocarriers for vaginal drug delivery. Adv Drug Deliv Rev. 2015;92:53–70.
15. Pavelić Ž, Škalko-Basnet N, Filipović-Grčić J, Martinac A, Jalšenjak I. Development and in vitro evaluation of a liposomal vaginal delivery system for acyclovir. J Control Release. 2005;106:34–43.
16. Berginc K, Suljaković S, Škalko-Basnet N, Kristl A. Mucoadhesive liposomes as new formulation for vaginal delivery of curcumin. Eur J Pharm Biopharm. 2014;87:40–6.
17. Hunt CA, Tsang S. α-Tocopherol retards autoxidation and prolongs the shelf-life of liposomes. Int J Pharm. 1981;8:101–10.
18. Grit M, Crommelin DJA. Chemical stability of liposomes: implications for their physical stability. Chem Phys Lipid. 1993;64:3–18.
19. Wong M, Thompson TE. Aggregation of dipalmitoylphosphatidylcholine vesicles. Biochemistry. 1982;21:4133–9.
20. Payne NI, Ambrose CV, Timmins P, Ward MD, Ridgway F. Proliposomes: a novel solution to an old problem. J Pharm Sci. 1986;75:325–9.
21. Payne NI, Browning I, Hynes CA. Characterization of proliposomes. J Pharm Sci. 1986;75:330–3.
22. Perrett S, Golding M, Williams WP. A simple method for the preparation of liposomes for pharmaceutical applications: characterization of the liposomes. J Pharm Pharmacol. 1991;43:154–61.
23. Alves GP, Santana MHA. Phospholipid dry powders produced by spray drying processing: structural, thermodynamic and physical properties. Powder Technol. 2004;145:139–48.
24. Parhizkar E, Sadeghinia D, Hamishehkar H, Yaqoubi S, Nokhodchi A, Alipour S. Carrier effect in development of rifampin loaded proliposome for pulmonary delivery: a quality by design study. Adv Pharm Bull. 2022;12:336–45.
25. Chen C-M, Alli D. Use of fluidized bed in proliposome manufacturing. J Pharm Sci. 1987;76:419.
26. Kumar R, Gupta RB, Betegeri G. Formulation, characterization, and in vitro release of glyburide from proliposomal beads. Drug Delivery. 2001;8:25–7.
27. Singh N, Kushwaha P, Ahmad U, Abdullah M. Proliposomas: Una aproximación para el desarrollo de liposoma estables. Ars Pharmaceutica (Internet). 2019;60:231–40.
28. Xia F, Hu D, Jin H, Zhao Y, Liang J. Preparation of lutein proliposomes by supercritical anti-solvent technique. Food Hydrocoll. 2012;26:456–63.
29. Xia F, Jin H, Zhao Y, Guo X. Supercritical antisolvent-based technology for preparation of vitamin D3 proliposome and its characteristics. Chin J Chem Eng. 2011;19:1039–46.
30. Chu C, Tong S-s, Xu Y, Wang L, Fu M, Ge Y-r, et al. Proliposomes for oral delivery of dehydrosilymarin: preparation and evaluation in vitro and in vivo. Acta Pharmacol Sinica. 2011;32:973–80.
31. Kurakula M, Srinivas C, Kasturi N, Diwan PD. Formulation and evaluation of prednisolone proliposomal gel for effective topical pharmacotherapy. Int J Pharm Sci Drug Res. 2012;4:35–43.
32. Rojanarat W, Nakpheng T, Thawithong E, Yanyium N, Srichana T. Levofloxacin-proliposomes: opportunities for use in lung tuberculosis. Pharmaceutics. 2012;4:385–412.
33. Ning M-Y, Guo Y-Z, Pan H-Z, Yu H-M, Gu Z-W. Preparation and evaluation of proliposomes containing clotrimazole. Chem Pharm Bull. 2005;53:620–4.
34. Anderson M, Kutzner S, Kaufman RH. Treatment of vulvovaginal lichen planus with vaginal hydrocortisone suppositories. Obstet Gynecol. 2002;100:359–62.
35. Manfre M, Adams D, Callahan G, Gould P, Lang S, McCubbins H, et al. Hydrocortisone cream to reduce perineal pain after vaginal birth: a randomized controlled trial. MCN Am J Matern Child Nurs. 2015;40.
36. Lennernäs H, Skrtic S, Johannsson G. Replacement therapy of oral hydrocortisone in adrenal insufficiency: the influence of gastrointestinal factors. Expert Opin Drug Metab Toxicol. 2008;4:749–58.
37. Corbo DC, Liu J-C, Chien YW. Drug absorption through mucosal membranes: effect of mucosal route and penetrant hydrophilicity. Pharm Res. 1989;6:848–52.
38. das Neves J, Araújo F, Andrade F, Michiels J, Ariën KK, Vanham G, et al. In vitro and ex vivo evaluation of polymeric nanoparticles for vaginal and rectal delivery of the anti-HIV drug dapivirine. Mol Pharm. 2013;10:2793–807.
39. das Neves J, Sarmento B. Precise engineering of dapivirine-loaded nanoparticles for the development of anti-HIV vaginal microbicides. Acta Biomater. 2015;18:77–87.
40. Facchinatto WM, Galante J, Mesquita L, Silva DS, Martins dos Santos D, Moraes TB, et al. Clotrimazole-loaded N-(2-hydroxy)-propyl-3-trimethylammonium, O-palmitoyl chitosan nanoparticles for topical treatment of vulvovaginal candidiasis. Acta Biomater. 2021;125:312–21.
41. Grammen C, Augustijns P, Brouwers J. In vitro profiling of the vaginal permeation potential of anti-HIV microbicides and the influence of formulation excipients. Antiviral Res. 2012;96:226–33.
42. Notario-Pérez F, Galante J, Martín-Illana A, Cazorla-Luna R, Sarmento B, Ruiz-Caro R, et al. Development of pH-sensitive vaginal films based on methacrylate copolymers for topical HIV-1 pre-exposure prophylaxis. Acta Biomater. 2021;121:316–27.
43. Janas C, Mast MP, Kirsamer L, Angioni C, Gao F, Mantele W, et al. The dispersion releaser technology is an effective method for testing drug release from nanosized drug carriers. Eur J Pharm Sci. 2017;115:73–83.
44. Mast M-P, Modh H, Knoll J, Fecioru E, Wacker MG. An update to dialysis-based drug release testing - data analysis and validation using the Pharma Test Dispersion Releaser. Pharmaceutics. 2021;13:12.
45. Turpeinen U, Markkanen H, Välimäki M, Stenman UH. Determination of urinary free cortisol by HPLC. Clin Chem. 1997;43:1386–91.
46. Präbst K, Engelhardt H, Ringgeler S, Hübner H. Basic colorimetric proliferation assays: MTT, WST, and resazurin. In: Gilbert DF, Friedrich O, editors. Cell viability assays: methods and protocols. New York, NY: Springer New York. 2017;1–17.
47. Commission CP. Chinese Pharmacoepia (Ch.P.) 10th Edition. 2015.
48. Rastogi R, Su J, Mahalingam A, Clark J, Sung S, Hope T, et al. Engineering and characterization of simplified vaginal and seminal fluid simulants. Contraception. 2016;93:337–46.
49. Danaei M, Dehghankhold M, Ataei S, Hasanzadeh Davarani F, Javanmard R, Dokhani A, et al. Impact of particle size and polydispersity index on the clinical applications of lipidic nanocarrier systems. Pharmaceutics. 2018;10:2.
50. Nezzal A, Aerts L, Verspaille M, Henderickx G, Redl A. Polymorphism of sorbitol. J Cryst Growth. 2009;311:3863–70.
51. Khan I, Yousaf S, Subramanian S, Korale O, Alhnan MA, Ahmed W, et al. Proliposome powders prepared using a slurry method for the generation of beclometasone dipropionate liposomes. Int J Pharm. 2015;496:342–50.
52. Suitchmezian V, Jeß I, Näther C. Structural, thermodynamic, and kinetic aspects of the trimorphism of hydrocortisone. J Pharm Sci. 2008;97:4516–27.
53. Byeon JC, Lee S-E, Kim T-H, Ahn JB, Kim D-H, Choi J-S, et al. Design of novel proliposome formulation for antioxidant peptide, glutathione with enhanced oral bioavailability and stability. Drug Delivery. 2019;26:216–25.

54. Hazemoto N, Harada M, Suzuki S, Kaiho F, Haga M, Kato Y. Effect of phosphatidylcholine and cholesterol on pH-sensitive liposomes. Chem Pharm Bull (Tokyo). 1993;41:1003–6.
55. Naylor LJ, Bakatselou V, Dressman JB. Comparison of the mechanism of dissolution of hydrocortisone in simple and mixed micelle systems. Pharm Res. 1993;10:865–70.
56. Standardization IOf. ISO 10993–5:2009 Biological Evaluation of Medical Devices - Part 5: tests for in vitro cytotoxicity. Geneva, Switzerland. 2009.
57. Gorodeski GI. Estrogen increases the permeability of the cultured human cervical epithelium by modulating cell deformability. Am J Physiol Cell Physiol. 1998;275:C888–99.
58. Machado RM, Palmeira-de-Oliveira A, Gaspar C, Martinez-de-Oliveira J, Palmeira-de-Oliveira R. Studies and methodologies on vaginal drug permeation. Adv Drug Deliv Rev. 2015;92:14–26.
59. Heimbach T, Oh D-M, Li LY, Forsberg M, Savolainen J, Leppänen J, et al. Absorption rate limit considerations for oral phosphate prodrugs. Pharm Res. 2003;20:848–56.
60. Cao Z, Zhang X, Wang C, Liu L, Zhao L, Wang J, et al. Different effects of cholesterol on membrane permeation of arginine and tryptophan revealed by bias-exchange metadynamics simulations. J Chem Phys. 2019;150: 084106.
61. Zhang L, Bennett WFD, Zheng T, Ouyang P-K, Ouyang X, Qiu X, et al. Effect of cholesterol on cellular uptake of cancer drugs pirarubicin and ellipticine. J Phys Chem B. 2016;120:3148–56.
62. Ramanathan R, Jiang Y, Read B, Golan-Paz S, Woodrow KA. Biophysical characterization of small molecule antiviral-loaded nanolipogels for HIV-1 chemoprophylaxis and topical mucosal application. Acta Biomater. 2016;36:122–31.
63. Jøraholmen MW, Basnet P, Acharya G, Škalko-Basnet N. PEGylated liposomes for topical vaginal therapy improve delivery of interferon alpha. Eur J Pharm Biopharm. 2017;113:132–9.

6.3 Curriculum vitae

- entfernt **-**